Western Australian School of Mines (WASM): Minerals, Energy and Chemical Engineering

Progressive Damage Mechanism of Rocks Subjected to Cyclic Loading

Rashid Geranmayeh Vaneghi

This thesis is presented for the Degree of
Doctor of Philosophy
of
Curtin University

June 2020

DECLARATION

To the best of my knowledge and belief this thesis contains no material previously published by any other person except where due acknowledgment has been made.

This thesis contains no material which has been accepted for the award of any other degree or diploma in any university.

Signed:

Date: June 2020

Abstract

Rock materials are very complex. Understanding the behavior of rocks under specific loading is complicated as many factors contribute to their strength and deformation responses. Rock structures are usually loaded in one direction (uniaxial) or three directions (triaxial), monotonically or dynamically depending on the stress regime and changes in the stress state of surrounding areas due to excavation or other man-made activities. Rock behaves differently under different types of loading. Moreover, rock behavior depends on the rock type, which is governed by inherent rock-based variabilities such as mineralogy, grain size, and porosity. Consequently, separate analyses should be carried out for different rock types and different circumstances.

A specific type of loading, which is induced by certain natural and man-made activities, is cyclic/fatigue loading consisting of repeated loading–unloading cycles. Rock structures surrounding mine pillars, mine stopes and galleries in deep mining, road tunnels, and oil/gas storages might be subjected to this type of loading, either in the short term or the long term, due to seismic activities of earthquakes and volcanic activities as natural phenomena, and explosions, excavation, and vehicle transportation as man-made activities. Therefore, studying the responses of rock to these types of loading is necessary for the reliable design of structures.

The primary focus of this study was investigation of the cyclic strength and damage response of two completely mineralogically different rock types by conducting uniaxial compression experiments. Firstly, sources of variability in rock testing, which may lead to substantial scatter in the testing results, are discussed. Appropriate methods for categorization of rock samples are critically reviewed. Consequently, an inspection technique for identifying internal defects of rock samples and other measures to avoid or minimize sample-based or machine-based sources of variabilities is proposed. Secondly, different experimental testing scenarios were designed to explore the cyclic/fatigue behavior of rocks. The fatigue life, fatigue strength threshold, effect of loading history, damage progress and failure mechanisms are investigated throughout this research. The damage responses of the two rock types considered are discussed with regard to their microstructural differences. This allowed for a better understanding of fatigue behavior of granular and crystalline rock types.

The research indicates that ultrasonic measurements are a useful and accurate technique for pre-assessment of rock materials. These measurements can be used alongside thin section analysis and visual inspection for better categorization of rock

samples before testing. The cyclic/fatigue tests results indicate that the rock microstructure plays an important role in the damage response of rocks to this type of loading. Crystalline or hard rocks are found to be more vulnerable to fatigue damage than granular or soft rocks. This finding is a new insight into the fatigue behavior of rocks. It was also found that ultrasonic P-wave velocity measurement is a very appropriate tool to monitor damage progress during cyclic/fatigue loading. Observations made in this research also demonstrate that the failure mechanisms of the two considered rock types under cyclic loading are different from those under monotonic conditions, and vary not only due to their mineralogical differences, but also because of different conditions of the stress cycles. Greater lateral expansion is found to be the main response of rocks to cyclic/fatigue loading, and it is more evident for crystalline rocks than for granular rocks. Stress corrosion was found as another mechanism interacting with fatigue damage at cyclic/fatigue loading with high stress levels. The results of the current study are not only in good agreement with experimental works reported in the literature but also develop new insights to provide a deeper understanding of the dependency of the damage evolution of rock microstructures under cyclic loading.

Acknowledgements

First, I would like to sincerely thank Curtin University and all those who gave me this priceless opportunity to pursue PhD study at the Western Australian School of Mines (WASM).

I would also like to express my deepest gratitude to my research supervisors, Dr Mohammad Sarmadivaleh, Professor Arcady Dyskin, Dr Klaus Thoeni, and Dr Mostafa Sharifzadeh for their supervision and support. They have always been very supportive and approachable since they took the role of being my supervisors. They have always allocated time for me whenever I needed it and have provided me with great guidance and motivation until the end of my studies.

I extend my thanks to Professor Roger Thompson as previous chairperson and Dr Chunyan Fan as current chairperson of my research supervisory panel.

This research was financially supported by the Mining Research Institute of Western Australia (MRIWA) for the project M474 and Curtin University through the CSIRS scholarship. I owe my special thanks to these organizations for the scholarships and research financial support they provided me throughout my PhD studies. I also want to send my appreciation to my project managers at MRIWA, Dr Penny Atkins and Dr Charmaine de Witt, the Chief Executive Officer of MRIWA, Ms Nicole Roocke and all other MRIWA team members for their assistance and support.

I also appreciate the help of other friends and academic staff, including Professor Ernesto Villaescusa, Mr Pat Hogan, Dr Mohammad Ali Moridi, Dr Takahiro Funatsu, Mr Seyed Erfan Saberhosseini, Achola D. Okoth, Barnabas Kuek, Runhua Feng, Jimmy Li, and many others who shared knowledge. Karin Hosking provided professional proofreading assistance for selected chapters and published papers which is also highly appreciated.

Finally, a very special thank you to my family and my wife's family, who have been a constant support and have provided encouragement which helped me to pursue my higher education.

Dedication

I dedicate this thesis to:

My beloved wife Leila, who supported me through this journey and never doubted my ability to accomplish my goals, and her unconditional caring, love and motivation during the challenges of my whole life.

List of Publications

This doctoral thesis consists of the following individual papers that were published, accepted for publication, or are under review at the time of writing the thesis. The published paper 2 is re-printed in its published form in Appendix D.

1. Geranmayeh Vaneghi, R., Saberhosseini, S. E., Dyskin, A. V., Thoeni, K., Sharifzadeh, M., & Sarmadivaleh, M. (2020). Sources of variability in laboratory rock test results, under review.
2. Geranmayeh Vaneghi, R., Ferdosi, B., Okoth, A. D., & Kuek, B. (2018). Strength degradation of sandstone and granodiorite under uniaxial cyclic loading. Journal of Rock Mechanics and Geotechnical Engineering, 10(1). https://doi.org/10.1016/j.jrmge.2017.09.005, cited 15 times.
3. Geranmayeh Vaneghi, R., Thoeni, K., Dyskin, A. V., Sharifzadeh, M., & Sarmadivaleh, M. Strength and damage response of sandstone and granodiorite under different loading conditions of multi-stage uniaxial cyclic compression. Int J Geomech, n.d. https://doi.org/10.1061/(ASCE)GM.1943-5622.0001801.
4. Geranmayeh Vaneghi, R., Thoeni, K., Dyskin, A. V., Sharifzadeh, M., & Sarmadivaleh, M. (2020). Fatigue damage response of typical crystalline and granular rocks to uniaxial cyclic compression. Int J Fatigue, 138:105667. https://doi.org/https://doi.org/10.1016/j.ijfatigue.2020.105667.

Contents

List of Tables

List of Figures

Nomenclature

UCS	Uniaxial Compressive Strength
E	Young's modulus
ν	Poisson's ratio
ρ	Rock density
V_p	P-wave velocity
V_s	Shear wave (S-wave) velocity
f	Frequency
σ_{min}	Minimum applied stress
σ_{mean}	Mean applied stress
σ_{max}	Maximum applied stress
σ_a	Stress amplitude
σ_{p-p}	Peak to peak stress amplitude
σ_f	Stress at failure
σ_{mon}	Monotonic peak strength
σ_1	Major principal stress
σ_{ci}	Crack initiation stress threshold
σ_{cd}	Crack damage stress threshold
ε_r	Residual strain
$\Delta\varepsilon_r$	Differential residual strain
D_i	Damage variable at cycle *i*
CCL	Constant Cyclic Loading
SCL	Stepped Cyclic Loading
CI	Crack Initiation
CD	Crack Damage
SG	Strain Gauge
CT	Computational Tomography
Std. dev.	Standard deviation
LF	Loading Frame
LVDT	Linear Variable Differential Transformer
CAMSL	Cyclic Allowable Maximum Stress Levels

Chapter 1

Introduction

1.1. Background

The first question in designing structures in rock, such as underground openings, tunnels, rock pillars and foundations, is understanding the rock response to the applied stress state. The in-situ stress, which is due to gravitational stresses and/or tectonic stresses, is usually regarded as a static/hydrostatic stress. However, the stress state becomes much more complex when the rock is disturbed by activities such as excavation, blasting, or seismic events (Jaeger & Cook, 1980). Therefore, the structure is not always under a static/monotonic stress state. Some activities induce loading–unloading cycles. These activities vary depending on the excavation method, application of the rock structure, and geological conditions of the region under consideration. Some of these activities, such as earthquakes and volcanic activities, are natural but very low in frequency, almost unpredictable, and catastrophic. Other activities are man-made, such as explosions in mining and civil construction, excavation and backfilling in mining operations, and vehicle-induced vibrations. Therefore, structures including mine pillars, mine stopes and other underground openings in deep mining, mine tailings, traffic/haulage tunnels and roads, oil/gas storages are usually under a combination of static stresses and loading–unloading cycles, in essence. Figure 1.1 shows an example of structures which are prone to be affected by cyclic or dynamic loading, and rock engineering approaches related to this topic in which the effect of this type of loading is of great significance. In traffic and haulage tunnels/roads, rock masses surrounding these structures are subjected to loading–unloading cycles because of moving vehicles. Underground caverns, constructed to store oil, gas, or hydrocarbons, are under cyclic loading conditions because of loading during injection and unloading during discharge of the fluids/gases into or out of them. One consequence of these mining-induced seismic events is rockburst, which can result in unpredictable and catastrophic rock damage. The rock mass in the aforementioned areas is under coupled monotonic-cyclic conditions. The response to this type of loading is not fully understood and needs more detailed consideration.

The tendency of solid materials to fail under loading–unloading cycles, either in the short term or the long term, is known as “fatigue”. Depending on the conditions of the stress cycles and other factors, the mechanical properties and deformation responses of rocks change under cyclic processes. Damage accumulates gradually cycle after cycle as the cyclic loading proceeds and may result in the rock failure at a stress level lower than its monotonic strength. Hence, characterizing the mechanical properties and deformation behavior of rocks under cyclic loading conditions would help rock engineers to improve

their designs and, hence, provide more reliable and durable structures and avoid engineering disasters.

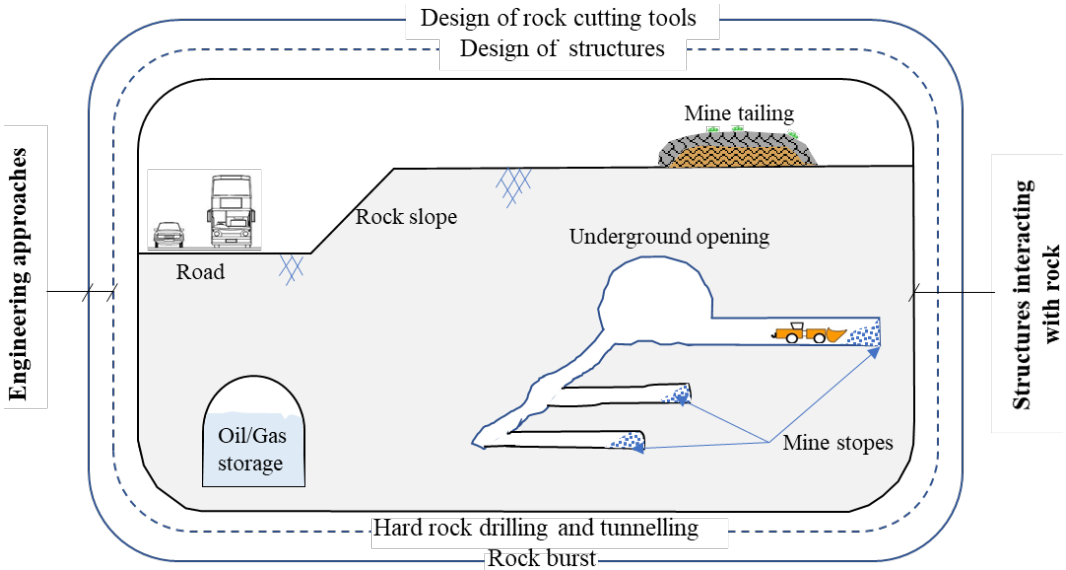

Figure 1.1. Schematic illustration of structures prone to cyclic dynamic loading and related issues in rock engineering.

Several factors affect the fatigue deformation responses of rocks and the number of cycles they sustain before failure. These factors are loading conditions (stress level, frequency, etc.), the rock type, or other testing conditions (Figure 1.2). Frequency, waveform, and stress level are specific to the cyclic loading conditions. However, anisotropy or heterogeneity of rock microstructure, saturation degree, and confinement are the factors which are usually considered in any experimental study of rock behavior in rock engineering. The rock damage would be different if any or all of these factors were to change. Therefore, it is clear that the rock damage response under coupled monotonic-cyclic conditions would be complicated and difficult to explore without focusing on important factors, instead of considering all affecting factors, for the sake of simplicity. Among these factors, rock type and conditions of stress cycles are the most significant ones.

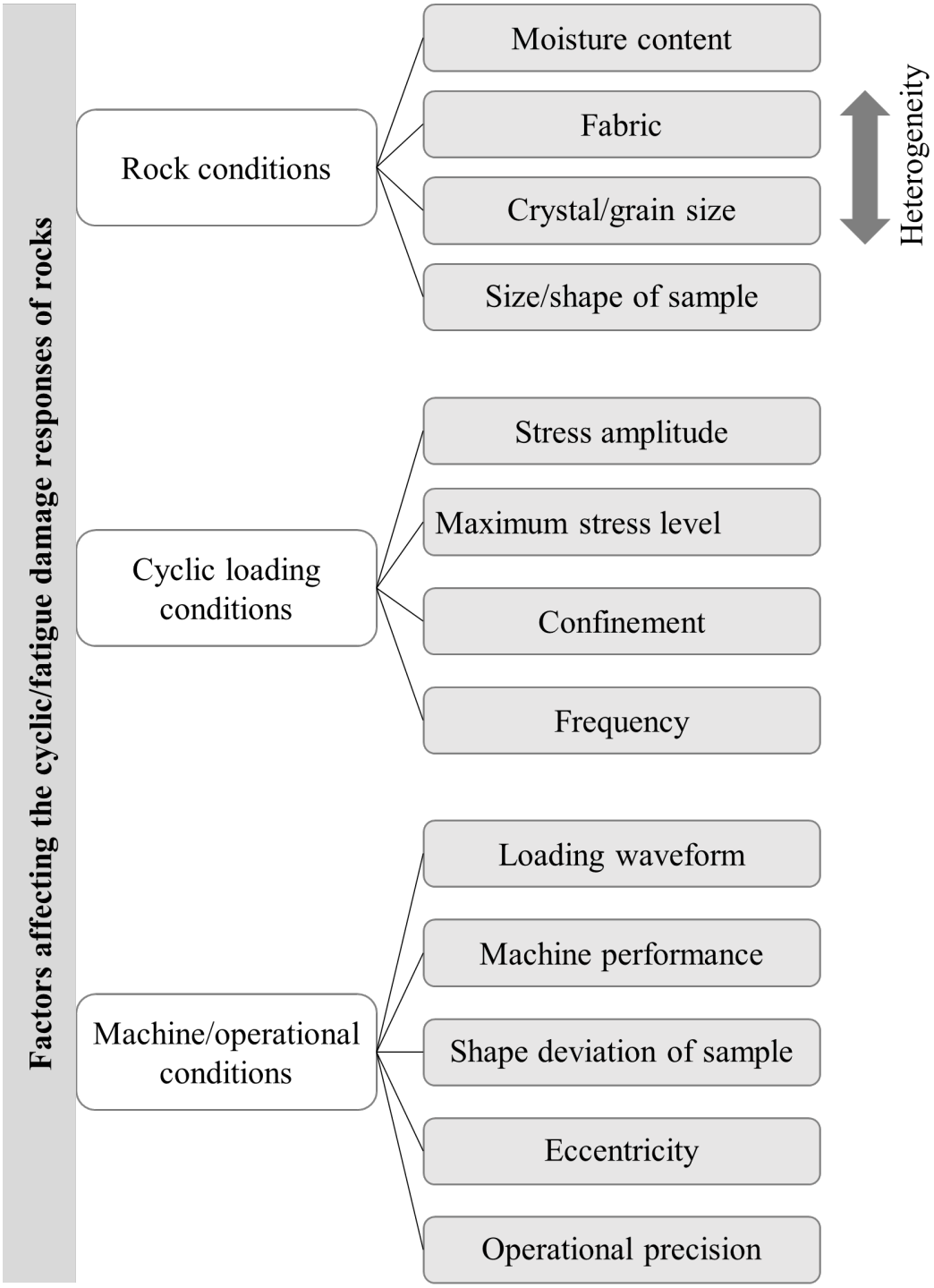

Figure 1.2. Chart showing the important factors affecting rock damage response under cyclic loading.

Quite a few researchers, especially in recent decades, have focused on this topic and investigated damage responses and degradation in mechanical parameters of rocks due to cyclic or fatigue loading. All studies related to cyclic loading of rocks are listed in Appendix A, considering the types of rock materials tested, types of tests and loading parameters, and fatigue limits and fatigue lives obtained. This area of investigation comes

back to early studies on cyclic behavior of rocks in mining (Attewell & Farmer, 1973; Burdine, 1963; Haimson, 1978) and is still ongoing (Li et al., 2019; Y. Zhang et al., 2019; Zhou et al., 2019), owing to technological developments and the invention of different measurement techniques. This issue has been investigated by implementing different types of experimental works, including uniaxial compression loading (Bagde & Petroš, 2005; Eberhardt et al., 1999), triaxial compression loading (Gatelier et al., 2002; Liu & He, 2012; Ma et al., 2013; Wang et al., 2013; Yang et al., 2015), indirect tensile tests (Erarslan et al., 2014; Erarslan et al., 2012a, 2012b; Erarslan, 2016; Ghamgosar et al., 2017; Wang et al., 2016), bending tests (Jamali et al., 2017; Cattaneo and Labuz, 2001), freeze–thaw or thermal cycles (Liu et al., 2015; Zhang et al., 2004), and wetting and drying cycles (Hale and Shakoor, 2003; Hua et al., 2017). It should be noted that the damage progress of rocks loaded under triaxial loading conditions was found to be favorably controlled by confining pressure since confinement reduces the initial anisotropy of the rocks by closing pre-existing microcracks along the axial direction. The fatigue limits of rocks would increase under high confinements. Therefore, rocks loaded under uniaxial compression loading or low confinements would show more susceptibility to the cyclic process (Brown & Hudson, 1973; Burdine, 1963; Gatelier et al., 2002; Ning et al., 2018; Rajaram, 1981; Song et al., 2013; Taheri et al., 2016). Different forms of cyclic loading path, either ramp waveform or sinusoidal waveform, have also been used for cyclic experiments (Figure 1.3). Depending on the aim of the cyclic test, researchers have carried out cyclic experiments in the form of constant cyclic loading (CCL), stepped cyclic loading (SCL) with either constant loading amplitude and mean stress level or increasing loading amplitude and mean stress level (Figure 1.4a), increasing ramp waveform (Figure 1.4b), damage stress mode (Figure 1.4c), and variable stress mode, which is a simplified form of seismic wave proposed by Liu et al. (2018).

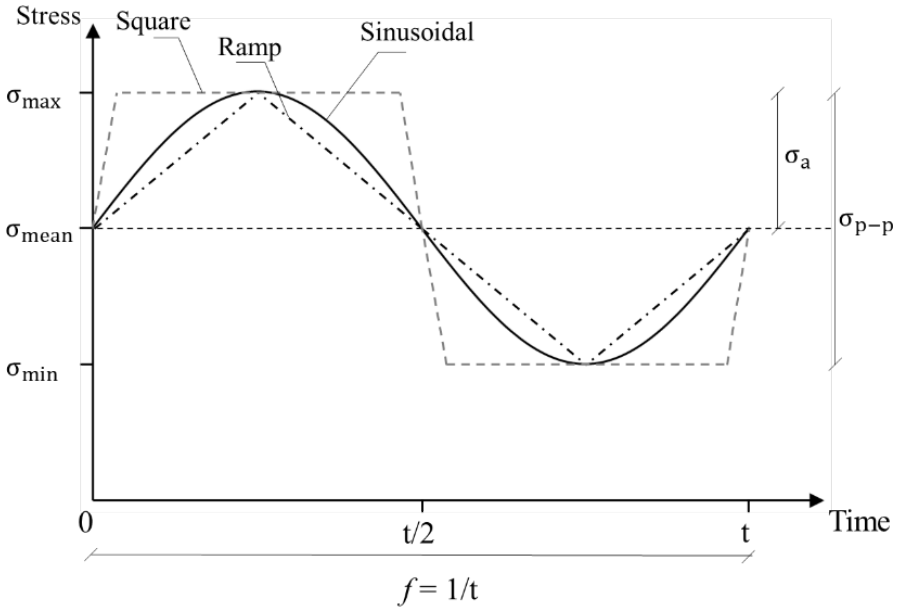

Figure 1.3. Different waveforms for stress cycles.

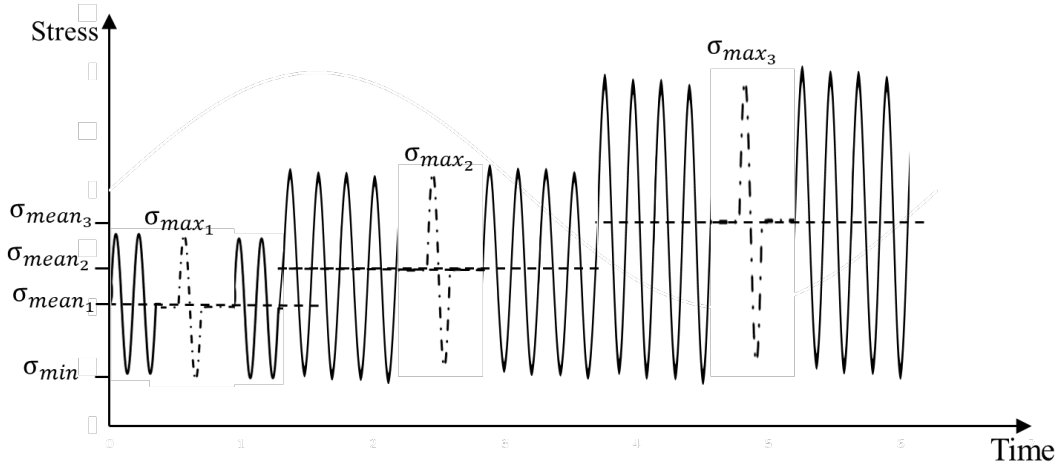

(a)

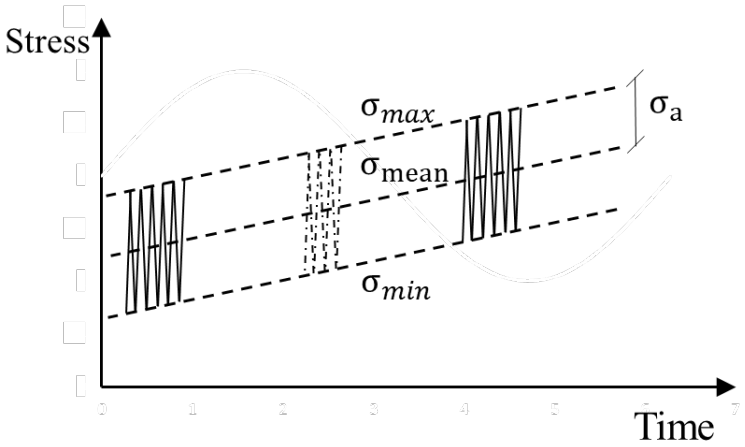

(b)

Figure 1.4 (continued on the next page).

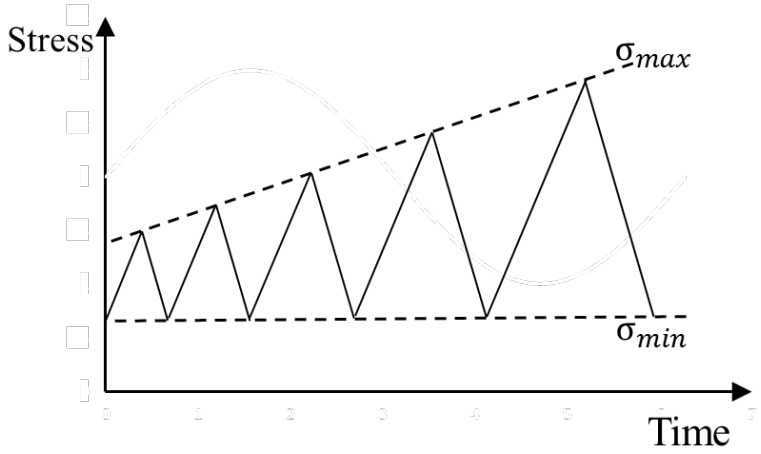

(c)

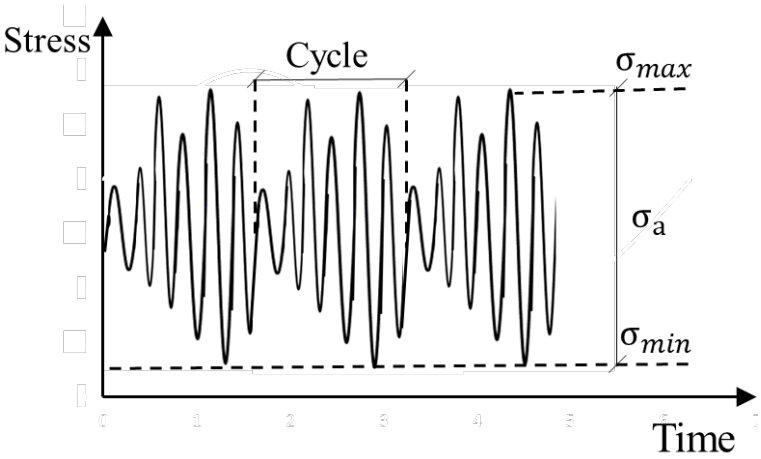

(d)

Figure 1.4 (continued from previous page). Stress paths with (a) constant or stepped cyclic loading, (b) ramp cycles with increasing mean stress, (c) damage-controlled cyclic test, and (d) variable modes of cycles used by researchers in experimental studies of cyclic loading.

In terms of the types of rocks tested under cyclic loading conditions, several research studies have been carried out on various rock types. Some of them have focused on the fatigue behavior of salt rocks to evaluate the stability of gas or oil storage caverns (Fan et al., 2016; Jiang et al., 2016; Ma et al., 2017; Voznesenskii et al., 2017; Wang et al., 2016). There is only very limited research that has used different rock types to explore the effect of rock microstructures on the fatigue damage response. For instance, one study compared the damage response of sandstone, tuff, marble, and granite under the fatigue process (Yamashita et al., 1999). It was found that the fatigue limits of rocks relate to their yielding stress levels. Artificial or intact rock samples with intermitted joint(s) were found to be more susceptible to cyclic loading than intact rocks without flaws, and the joint parameters

greatly affected their fatigue damage responses (Li et al., 2001; Li et al., 2003; Liu et al., 2017; Liu & Dai, 2018; Liu et al., 2017). Changes in tensile fatigue limits of crystalline and non-crystalline rocks under cyclic loading conditions were studied by Jamali Zavareh et al. (2017). This study found that weak minerals played an important role in the overall fatigue response of rocks. The brittleness of rocks was found to be a very important factor in the fatigue damage response. The crack density, induced by cyclic loading, was observed to be more noticeable in more brittle rocks compared with that in soft rocks, leading to the nucleation and propagation of large numbers of microcracks with greater energy in brittle rocks (Nejati & Ghazvinian, 2014). It was shown that the fatigue life of brittle onyx marble was shorter than that of soft limestone and sandstone. These studies were very limited in exploring the effect of cyclic loading on different rock materials since most of the rocks tested in their investigations either had very similar uniaxial compressive strength or they were only compared from specific perspectives. For instance, the fatigue strength limit of rocks was compared under tension, whereas rocks are usually under compression loading. These limitations have made it impossible to draw robust conclusions on the relationship between fatigue strength and damage response to rock microstructure.

Regarding the fatigue strength threshold or fatigue limit of sandstone and granite, there are a few research studies in which this subject has been investigated. Under uniaxial cyclic compression with different loading conditions, the fatigue limit of sandstone was reported to range from 0.65 to 0.87 (Burdine, 1963; Ray et al., 1999; Singh, 1989; Yamashita et al., 1999; Zhenyu & Haihong, 1990). The fatigue limit of granite rock has also been found in limited studies to vary between 0.60 and 0.80 (Akesson et al., 2004; Ishizuka et al., 1990; Rajaram, 1981; Yamashita et al., 1999). Although these studies attempted to determine the fatigue limits of these rocks under different cyclic loading conditions, there is no single study combining all individual results to reach a coherent understating of the difference between the fatigue limits of hard rocks and those of soft rocks, based on comprehensive experimental data, i.e. dependency of fatigue limits on rock microstructure.

The effects of cyclic loading conditions, including maximum stress level, loading amplitude, confining pressure, and loading frequency have also been investigated by many researchers. Higher maximum stress levels and loading amplitudes increase the damaging effect of cyclic loading, whereas a higher loading frequency or confinement was found to be in favor of rock loading capacity of rocks under cyclic loading conditions (Attewell &

Farmer, 1973; Burdine, 1963; Fuenkajorn & Phueakphum, 2010; Li et al., 2001; Liu & He, 2012; Ma et al., 2013; Momeni et al., 2015; Tien et al., 1990; Xiao et al., 2010). However, all or some of these loading conditions, simultaneously, affect the fatigue damage response of rocks and not much is known about which of them have greater damaging effects than others. This issue might be given different degrees of significance depending on the aim of the application. For instance, a higher stress level should be applied but very slowly (i.e. low loading frequency) to achieve higher efficiency from drilling tools or more homogenous fragmentation, while very strong rock support should be considered in loading conditions for stability of rock mass surrounding an excavation (Attewell & Farmer, 1973). It was also reported that the effect of loading frequency on the fatigue response of salt is lower than that of the maximum stress level and loading amplitude (Fuenkajorn & Phueakphum, 2010). On the other hand, it was observed that rock samples would more easily succumb under low frequency with high loading amplitude, rather than under high frequency with low loading amplitude (Attewell & Farmer, 1973). Therefore, it is difficult to reach to a general conclusion on this issue based on these limited studies. More specifically, the effect of loading frequency on the damage response of rocks is not fully understood.

Turning to the stress–strain behavior of rocks under cyclic loading, several investigations have revealed that the complete stress–strain curve of monotonic loading is a failure locus for cyclic loading and can be used as an indicator of the maximum allowable bound for rock deformation under cyclic loading in any loading path (Brown & Hudson, 1973; Guo et al., 2012; Haimson, 1978; Liu et al., 2018; Liu et al., 2017; Meng et al., 2016; Ning et al., 2018; Rajaram, 1981; Xiao et al., 2009). However, some scholars have questioned this finding in confined conditions by stating that differences between the maximum strain of rock under cyclic conditions and under monotonic compression increase with confining pressures (Brown & Hudson, 1973; Song et al., 2016). In other words, the susceptibility of rocks to cyclic loading decreases in confined conditions because the confining pressure leads to more ductile behavior of rocks in which the post-peak part of the stress–strain curve would be flatter compared with that of brittle behavior. So, the residual strength locus would not intersect if the cyclic loading stress level is less than the residual strength. It was also found that the complete stress–strain curve does not act as a failure locus for Brazilian cyclic loading (Wang et al., 2016). The damage evolution of rocks under cyclic loading conditions can be evaluated from the pattern of either stress–strain hysteresis loops or residual strain development throughout the cyclic

process. Three stages of loose–dense–loose and decelerating, steady, and accelerating were observed for the development of stress–strain hysteresis loops and irreversible strains cycles, respectively (Brantut et al., 2013; Chen et al., 2011; Fan et al., 2017; Guo et al., 2012; Jiang et al., 2009; Karakus et al., 2016; Liu et al., 2012; Liu et al., 2018; Liu et al., 2017; Ni, 2014; Taheri et al., 2016). This behavior was also reported for Brazilian cyclic loading (Wang et al., 2016). However, it was argued that the pattern of stress–strain hysteresis loops is not only different for hard and soft rocks (Liu et al., 2016) but also greatly depends on the loading conditions. For instance, the hysteresis loops of cyclic loading at higher loading levels are much looser than at lower loading levels, which indicates much higher plastic deformation under higher stress levels (Liu et al., 2014). In another study, it was discussed that the second phase of fatigue damage evolution accounts for a higher proportion of the whole fatigue process under high maximum stress levels, whereas the third or accelerating phase can rarely be seen (Xiao et al., 2009). Nevertheless, little is known about the damage evolution of rocks in extreme cases when both loading amplitude and maximum stress levels are high. Besides, some contradictory results have also been reported in which the cyclic damage was reported to evolve in a two-stage manner (Qiu et al., 2014). It was also revealed that as the loading frequency increases, the area under hysteresis loops, and in turn the energy loss, decreases (Ni, 2014). Moreover, there is still very little quantitative comparison of the evolution of axial and lateral deformations under cyclic loading conditions, despite limited research which attempted to demonstrate that the lateral deformation of rocks evolves more rapidly than axial deformation during cyclic loading (Rajaram, 1981; Zhenyu & Haihong, 1990). Therefore, there is still no definite explanation of why rocks show different patterns of damage evolution under cyclic loading and whether it relates to the rock microstructure and differs between the axial and lateral directions.

Failure mechanisms of rocks under cyclic loading conditions have been discussed in several studies (Haimson, 1978; Heap & Faulkner, 2008; Li et al., 1992; Li et al., 2017; Liu & He, 2012; Liu et al., 2012; Liu et al., 2017; Royer-Carfagni & Salvatore, 2000; Song et al., 2016). Grain breakage was found to be the main characteristic of cyclic loading on tuff (Erarslan and Williams, 2012a). In this regard, it was also argued that the creation of a large number of microcracks, rather than widening or propagation of a single microcrack, is the main effect of cyclic loading on tuff (Erarslan and Williams, 2012b). In another study, intergranular cracking and grain boundary loosening were found to be the dominant damaging phenomena in the first cycles of a cyclic compression test and crack

extension and crack coalescence usually occurred as the cyclic process approached the later and final stages (Haimson, 1978). On the other hand, Taheri et al. (2016) noted that rocks tend to show more brittle failure when they sustain a large number of cycles. It was also discussed that subcritical cracking is due to different behaviors of interlocked or cemented grains where there is no chemical environment (Erarslan, 2016), however it is unknown whether the subcritical cracking is purely a fatigue damage mechanism or if it interacts with other damage mechanisms, and whether or how these mechanisms change at higher stress levels. Turning to the effect of cyclic loading conditions, the effect of cyclic loading frequency and confining pressure on the failure mechanism of sandstone was studied by Liu and He (2012) and Liu et al. (2012). Under the same confining pressure, the localized band was wider at the higher loading frequency. Although each of these investigations is individually valuable and provides information about failure mechanisms of various rocks under cyclic loading, there is no single study providing sufficient evidence to clearly draw a conclusion on the failure mechanism of rocks and its relationship with loading conditions and microstructure.

Despite all these efforts, the nature of the fatigue damage response of rocks remains unclear and much less is known about the relation between the heterogeneity of rock microstructure and fatigue damage. The dependency of fatigue behavior of rocks on the loading frequency is unclear and there is no study in which this issue is unified or agreed upon by incorporating comprehensive data. Moreover, the failure modes of rocks underpinning their behavior under this particular loading have not been well studied and we still do not have agreed evidence verifying the available limited observations. The gaps in this research area, which this study seeks to bridge, are brought up later through research questions (c.f. Section 1.3).

1.2. Motivation

Despite the advent of new machines which are being used for the extraction of mineral ore bodies, drilling and blasting is usually taken as an economical method in most mining operations around the world. In this method, cyclic or dynamic loading is induced to the rock mass surrounding nearby structures of access galleries, mine pillars, mine stopes, tunnels, caverns, or even nearby buildings. All seismic activities impose this type of loading to the rock mass. This issue is also very important in the design of disc cutters for

tunnel boring machines (TBM) and Raise Boring Machines (RBM), which are commonly used for the excavation of tunnels and shafts in mining and civil construction.

Investigation of the strength response and damage evolution of rocks under cyclic loading, as the scope of this research, would be of great importance in these areas. A fundamental and experimental study of this topic can benefit rock engineering design in many aspects: (1) the peak strength and strain of rocks as main inputs in the design of a rock structure in any of abovementioned applications can be adjusted to deliver a well-engineered design, (2) it provides a comprehensive collection of data for the deformation responses and damage evolution of rocks under this type of loading, which would be of great value to researchers developing constitutive laws in theoretical and fundamental rock mechanics, and (3) it provides a foundation for time-dependent fracture mechanics analysis used in the design and estimation of the service life of drilling and cutting tools. Therefore, all these advantages help us to understand the mechanical response of different rock types to the cyclic or fatigue process in surface and underground excavations.

1.3. Research Questions and Objectives

1.3.1 Research questions

This thesis investigates the responses of rock materials to uniaxial cyclic compression loading. The following major questions are addressed in this research:

1. How do different rock types, in terms of strength, microstructure, and grain size, behave under cyclic compression loading? Which of the soft and granular or hard and crystalline rocks is more susceptible to this type of loading? What are the fatigue strength thresholds of soft and hard rocks?

2. How do cyclic loading conditions such as the stress amplitude, maximum level of stress cycles, and loading frequency affect the strength and deformation responses of crystalline and granular rocks under uniaxial compression loading?

3. What are the differences between failure mechanisms of soft/granular or hard/crystalline rocks under cyclic loading conditions and those under monotonic loading and how do they vary with the cyclic loading conditions?

1.3.2 Research objectives

As mentioned above, the core objective of this research is to enhance our understanding of rock fatigue and provide new insights to this research area. The main objectives of this research and the methodologies followed to achieve them are as follows:

- Conduct comprehensive laboratory experiments on two types of intact rocks to explore the effect of fatigue loading on rock materials. The experiments are performed on natural rock samples obtained from Australian outcrops. All experiments are performed under uniaxial compression loading with cycles in the form of sinusoidal signals.

- Provide a systematic understanding of how different rock types respond to cyclic loading conditions. Previous research has focused on specific rock types and there is no research merely investigating the fatigue response of different rocks under the same testing scenarios while keeping other variabilities constant. Two different rock types, one sandstone and one granite/granodiorite, which noticeably vary in terms of mineralogy, microstructure, and strength, were selected for this purpose to figure out the fatigue responses of rocks categorized between these two rocks or rocks that are very similar to them.

- Loading conditions of maximum stress level, amplitude, and frequencies significantly affect the fatigue responses of rocks. Another aim of this research is to evaluate the effect of these factors on the fatigue damage of rocks. Different loading paths of constant cyclic loading (CCL), increasing mean stress level or stepped cyclic loading (SCL) and multi-stage cyclic loading were designed for this purpose. Loading amplitude and stress level were kept constant throughout the constant cyclic loading (CCL) test until failure occurred. Mean stress level was increased to a higher value at stepped cyclic loading (SCL) without unloading the specimen, however, in multi-stage cyclic loading both mean stress level and loading amplitude were changed to a different level and specimen was unloaded completely after each stage. These different loading scenarios contribute to a better understating of the effect of cyclic loading history on the fatigue evolution of rocks. Different experimental scenarios also make it possible to find out which of these cyclic loading conditions has a stronger effect on rock fatigue.

- The number of cycles to failure, called fatigue life, of a rock under cyclic loading can be an indication of the service life of a rock structure. This research also seeks to investigate the variation in the fatigue lives of the selected rock types under different cyclic loading conditions. Cyclic tests are performed with different maximum stress levels, loading amplitudes, and frequencies to explore the effects of these testing parameters on fatigue life.

- Determine the fatigue strength threshold of tested rock types. The fatigue strength threshold is the main input for designing rock structures. The rock can sustain loading below this threshold under indefinite cycles without failure. Data from the literature, incorporated with the test results of the current study, will provide fatigue strength thresholds of these rock types which would be of great value for rock engineers.

- Analyze the deformation responses of rocks due to cyclic loading. The lateral and axial deformations of tested samples are measured using either linear variable differential transformers (LVDTs) or strain gauges. Any change in rock deformation as a response to cyclic loading is discussed throughout the experimental studies.

- Evaluate the damage evolution of tested rock types throughout the cyclic process by suitable techniques. The CT scanning, ultrasonic measurements, and a quantitative method will be either implemented or proposed for this aim to assess how damage evolves as the cyclic loading proceeds. Ultrasonic measurement can also be of great benefit in monitoring fatigue damage and categorizing rock samples. Damage evolution of tested rocks is evaluated by comparing the pattern of stress–strain hysteresis loops, difference in strain before failure, and residual strain during the cyclic stage, both in axial and lateral directions, considering microstructural differences of tested rocks. A damage variable is defined to quantify the development of fatigue, and to find out which of the loading conditions has a greater damaging effect and which of the granular/soft or crystalline/hard rocks show more damage evolution under the fatigue process.

- Compare the failure mechanisms of these rocks after monotonic tests with those tested under cyclic conditions. The failure modes of all tested samples will be analyzed visually after the tests. Based on these observations, it will be discussed how the failure modes of these rock types change if the loading conditions are changed and which of the loading conditions has a stronger effect on the failure modes. The results of this study allow us to identify the main damaging mechanism of rocks under loading–unloading processes.

1.4. Thesis structure

This thesis attempts to explore the strength and damage behavior of two mineralogically different rock types to cyclic processes through laboratory experiments. The experimental process, including tested rock types, test methods, and measurement techniques implemented in this research, is illustrated in Figure 1.5. This process considers equipment limitations and time constraints. Contents related to the testing procedure and testing equipment are partially repeated in each chapter due to the hybrid format of thesis. Figure 1.6 illustrates the relationship between the main body of the thesis with the key parameters investigated in each chapter. The quality of rock testing was improved in chapter 2 which was then used for experimental studies in other chapters. Each of chapters 3, 4, and 5 progressively bridged the gap and weakness identified in previous research and previous parts of current study and provided conclusive findings with more experimental data and observations (Figure 1.6). The effect of cyclic loading conditions (i.e. maximum level, amplitude, and frequency of stress cycles) on these parameters has been investigated throughout all the experiments conducted in this research.

This study was developed over time by identifying the sources of variabilities in rock testing and finding a way to have valid test results to study the research questions under different scenarios, answering the research questions aligned with the main questions of the research and bridging the gaps. The chapters of this thesis, which are individually presented in the form of peer-reviewed journal manuscripts, discuss the following content:

Chapter 2

Chapter 2 comprises systematic experimental work conducted on rock and aluminum samples to find the sources of variations in laboratory test results of rocks. This chapter discusses how we can improve the quality of rock testing and reduce scatter in test results. The findings of this chapter were later used to inspect, examine, and categorize the rock samples and testing equipment properly and accurately in order to achieve high-quality rock experiments throughout this research. The findings of this part of the study helped us to monitor the fatigue damage progress of rocks during cyclic loading, which is discussed in Chapter 4.

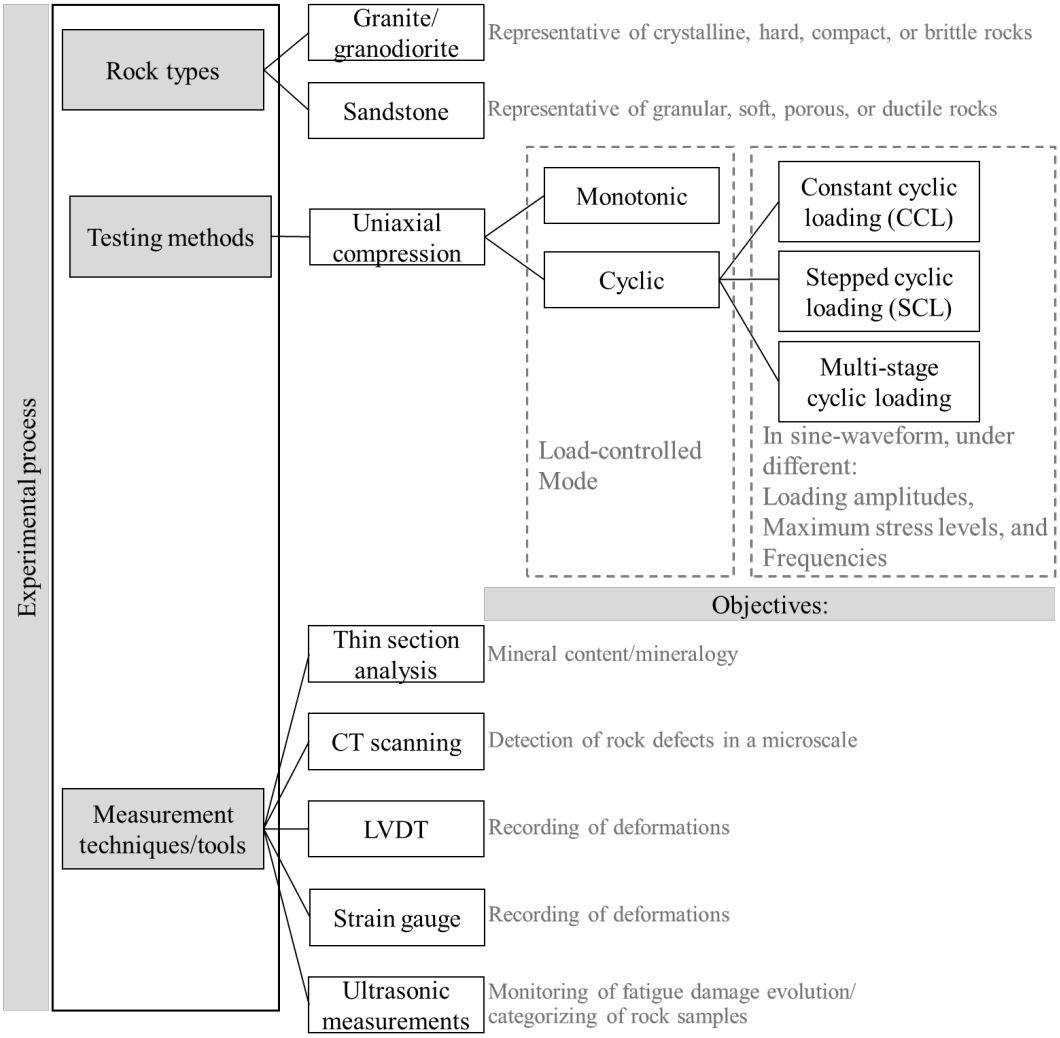

Figure 1.5. Experimental process implemented in this research.

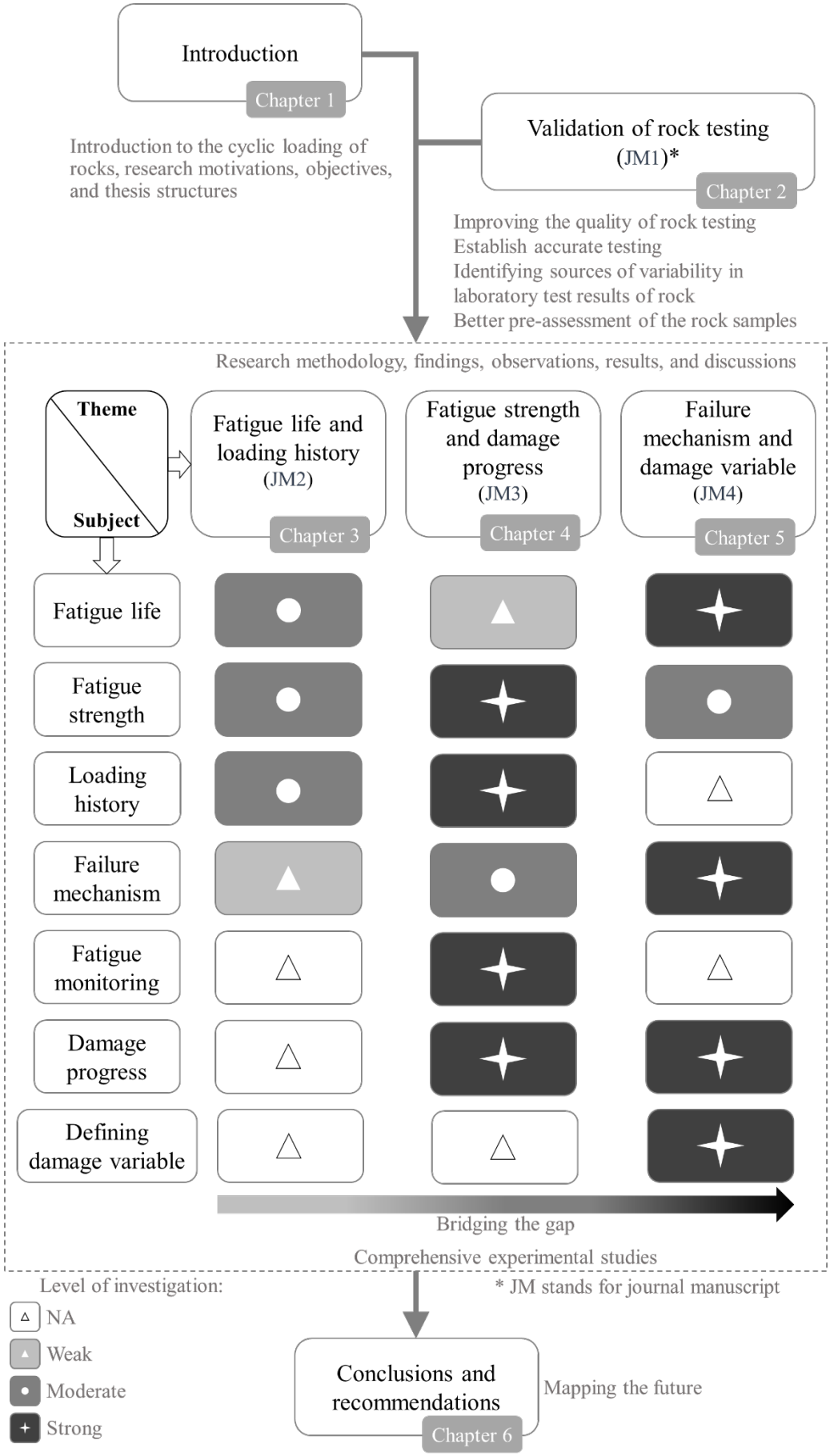

Figure 1.6. Flowchart of the thesis to investigate cyclic/fatigue responses of rocks.

Chapter 3

Chapter 3 presents the test results of cyclic loading experiments conducted on sandstone and granodiorite samples. This chapter provides an insight into the fatigue life and strength degradation of these two rock types under cyclic/fatigue loading. Cyclic tests have been performed under different loading paths of constant cyclic loading (CCL) and increasing mean stress level or stepped cyclic loading (SCL) which makes it possible to investigate the effect of the loading history on the strength degradation of tested rocks. This chapter also discusses the influence of the maximum applied stress level and the amplitude of stress cycles on the fatigue effect of rock samples. A preliminary comparison of failure modes of the tested rock samples under cyclic loading with those under monotonic conditions is also discussed in this chapter.

Chapter 4

Chapter 4 investigates the fatigue strength thresholds, fatigue damage progress and the technique implemented to monitor the damage development of selected granodiorite and sandstone samples under different cyclic loading conditions. The effect of loading history is also investigated, owing to the testing procedure of the multi-stage uniaxial cyclic compression loading, designed for this series of experiments. This chapter discusses the susceptibility of a crystalline rock such as granite/granodiorite and granular rock such as sandstone to the cyclic/fatigue damage process. The differences in stress–strain hysteresis loops, deformation response and residual fatigue damage of samples are also discussed with regard to microstructural differences in these rock types. This follows a comprehensive comparison of the failure modes of these samples under cyclic loading, not only with those under monotonic loading, but also when conditions of stress cycles are changed.

Chapter 5

Chapter 5 bridges the gaps in previous experimental studies in this research by conducting a comprehensive and systematic experimental investigation (cf. Figure 1.6). More than 70 monotonic and cyclic tests have been conducted under constant cyclic loading conditions to explore, in depth, the fatigue life, the strength and deformation response, and the damage evolution of sandstone and granite under cyclic/fatigue loading. It comprises a

focused analysis of the effect of loading frequency on the fatigue life of these rock types. This chapter provides a comparison of the lateral and axial damage development of rocks throughout the cyclic/fatigue process. It also discusses what probably interacts with actual fatigue damage at a high-stressed cyclic/fatigue loading. In addition, this chapter evaluates the failure mechanisms of these crystalline and granular rocks under cyclic conditions on a larger scale compared to the previous chapter and provides evidence for the main response of rocks to fatigue loading.

Chapter 6

The final chapter draws the conclusions of this research, outlines contributions of this study to the current state of knowledge and highlights recommendations for further research in this field.

References

Akesson, U., Hansson, J., & Stigh, J. (2004). Characterisation of microcracks in the Bohus granite, western Sweden, caused by uniaxial cyclic loading. *Engineering Geology*, *72*(1), 131–142. https://doi.org/https://doi.org/10.1016/j.enggeo.2003.07.001

Attewell, P. B., & Farmer, I. W. (1973). Fatigue behaviour of rock. *International Journal of Rock Mechanics and Mining Sciences & Geomechanics Abstracts*, *10*(1), 1–9. https://doi.org/https://doi.org/10.1016/0148-9062(73)90055-7

Bagde, M. N., & Petroš, V. (2005). Fatigue properties of intact sandstone samples subjected to dynamic uniaxial cyclical loading. *International Journal of Rock Mechanics and Mining Sciences*, *42*(2), 237–250. https://doi.org/https://doi.org/10.1016/j.ijrmms.2004.08.008

Brantut, N., Heap, M. J., Meredith, P. G., & Baud, P. (2013). Time-dependent cracking and brittle creep in crustal rocks: A review. *Journal of Structural Geology*, *52*, 17–43. https://doi.org/https://doi.org/10.1016/j.jsg.2013.03.007

Brown, E. T., & Hudson, J. A. (1973). Fatigue failure characteristics of some models of jointed rock. *Earthquake Engineering & Structural Dynamics*, *2*(4), 379–386. https://doi.org/10.1002/eqe.4290020407

Burdine, N. T. (1963). Rock Failure Under Dynamic Loading Conditions. *Society of Petroleum Engineers Journal*, *3*(01), 1–8. https://doi.org/10.2118/481-PA

Chen, Y., Watanabe, K., Kusuda, H., Kusaka, E., & Mabuchi, M. (2011). Crack growth in Westerly granite during a cyclic loading test. *Engineering Geology*, *117*(3), 189–197. https://doi.org/https://doi.org/10.1016/j.enggeo.2010.10.017

Eberhardt, E., Stead, D., & Stimpson, B. (1999). Quantifying progressive pre-peak brittle fracture damage in rock during uniaxial compression. *International Journal of Rock Mechanics and Mining Sciences*, *36*(3), 361–380. https://doi.org/https://doi.org/10.1016/S0148-9062(99)00019-4

Erarslan, N, Alehossein, H., & Williams, D. J. (2014). Tensile Fracture Strength of Brisbane Tuff by Static and Cyclic Loading Tests. *Rock Mechanics and Rock Engineering*, *47*(4), 1135–1151. https://doi.org/10.1007/s00603-013-0469-5

Erarslan, N, & Williams, D. J. (2012a). Investigating the Effect of Cyclic Loading on the Indirect Tensile Strength of Rocks. *Rock Mechanics and Rock Engineering*, *45*(3), 327–340. https://doi.org/10.1007/s00603-011-0209-7

Erarslan, N, & Williams, D. J. (2012b). The damage mechanism of rock fatigue and its relationship to the fracture toughness of rocks. *International Journal of Rock Mechanics and Mining Sciences*, *56*, 15–26. https://doi.org/https://doi.org/10.1016/j.ijrmms.2012.07.015

Erarslan, Nazife. (2016). Microstructural investigation of subcritical crack propagation and Fracture Process Zone (FPZ) by the reduction of rock fracture toughness under cyclic loading. *Engineering Geology*, *208*, 181–190. https://doi.org/https://doi.org/10.1016/j.enggeo.2016.04.035

Fan, J., Chen, J., Jiang, D., Chemenda, A., Chen, J., & Ambre, J. (2017). Discontinuous cyclic loading tests of salt with acoustic emission monitoring. *International Journal of Fatigue*, *94*, 140–144. https://doi.org/https://doi.org/10.1016/j.ijfatigue.2016.09.016

Fan, J., Chen, J., Jiang, D., Ren, S., & Wu, J. (2016). Fatigue properties of rock salt subjected to interval cyclic pressure. *International Journal of Fatigue*, *90*, 109–115. https://doi.org/https://doi.org/10.1016/j.ijfatigue.2016.04.021

Fuenkajorn, K., & Phueakphum, D. (2010). Effects of cyclic loading on mechanical properties of Maha Sarakham salt. *Engineering Geology*, *112*(1), 43–52. https://doi.org/https://doi.org/10.1016/j.enggeo.2010.01.002

Gatelier, N., Pellet, F., & Loret, B. (2002). Mechanical damage of an anisotropic porous rock in cyclic triaxial tests. *International Journal of Rock Mechanics and Mining Sciences*, *39*(3), 335–354. https://doi.org/https://doi.org/10.1016/S1365-1609(02)00029-1

Ghamgosar, M., Erarslan, N., & Williams, D. J. (2017). Experimental Investigation of Fracture Process Zone in Rocks Damaged Under Cyclic Loadings. *Experimental Mechanics*, *57*(1), 97–113. https://doi.org/10.1007/s11340-016-0216-4

Guo, Y., Yang, C., & Mao, H. (2012). Mechanical properties of Jintan mine rock salt under complex stress paths. *International Journal of Rock Mechanics and Mining Sciences*, *56*, 54–61. https://doi.org/https://doi.org/10.1016/j.ijrmms.2012.07.025

Haimson, B. C. (1978). Effect of Cyclic Loading on Rock. In M. Silver & D. Tiedemann (Eds.), *Dynamic Geotechnical Testing* (pp. 228–245). https://doi.org/10.1520/STP35679S

HALE, P. A., & SHAKOOR, A. (2003). A Laboratory Investigation of the Effects of Cyclic Heating and Cooling, Wetting and Drying, and Freezing and Thawing on

the Compressive Strength of Selected Sandstones. *Environmental and Engineering Geoscience*, *9*(2), 117–130. https://doi.org/10.2113/9.2.117

Heap, M. J., & Faulkner, D. R. (2008). Quantifying the evolution of static elastic properties as crystalline rock approaches failure. *International Journal of Rock Mechanics and Mining Sciences*, *45*(4), 564–573. https://doi.org/https://doi.org/10.1016/j.ijrmms.2007.07.018

Hua, W., Dong, S., Peng, F., Li, K., & Wang, Q. (2017). Experimental investigation on the effect of wetting-drying cycles on mixed mode fracture toughness of sandstone. *International Journal of Rock Mechanics and Mining Sciences*, *93*, 242–249. https://doi.org/https://doi.org/10.1016/j.ijrmms.2017.01.017

Ishizuka, Y., Abe, T., & Kodama, J. (1990). Fatigue Behaviour of Granite Under Cyclic Loading. *ISRM International Symposium*, p. 8. Retrieved from https://doi.org/

Jaeger, J. C., & Cook, N. G. W. (1980). Fundamentals of Rock Mechanics. *Geological Magazine*, *117*(4), 401. https://doi.org/DOI: 10.1017/S001675680003274X

Jamali, S., Hashemolhosseini, H., Baghbanan, A., Khoshkam, M., & Haghgouei, H. (2017). Evaluating Fatigue in Crystalline Intact Rocks under Completely Reversed Loading. *Geotechnical Testing Journal*, *40*(5), 789–797. https://doi.org/10.1520/GTJ20160250

Jiang, D., Fan, J., Chen, J., Li, L., & Cui, Y. (2016). A mechanism of fatigue in salt under discontinuous cycle loading. *International Journal of Rock Mechanics and Mining Sciences*, *86*, 255–260. https://doi.org/http://dx.doi.org/10.1016/j.ijrmms.2016.05.004

Jiang, X., Shu-chun, L., Yun-qi, T., Xiao-jun, T., & Xin, W. (2009). Acoustic emission characteristic during rock fatigue damage and failure. *Procedia Earth and Planetary Science*, *1*(1), 556–559. https://doi.org/https://doi.org/10.1016/j.proeps.2009.09.088

Karakus, M., Akdag, S., & Bruning, T. (2016). Rock Fatigue Damage Assessment by Acoustic Emission. *International Conference on Geomechanics, Geo-Energy and Geo-Resources*.

Li, G., Moelle, K. H. R., & Lewis, J. A. (1992). Fatigue crack growth in brittle sandstones. *International Journal of Rock Mechanics and Mining Sciences & Geomechanics Abstracts*, *29*(5), 469–477. https://doi.org/http://dx.doi.org/10.1016/0148-9062(92)92631-L

Li, N, Chen, W., Zhang, P., & Swoboda, G. (2001). The mechanical properties and a fatigue-damage model for jointed rock masses subjected to dynamic cyclical loading. *International Journal of Rock Mechanics and Mining Sciences*, *38*(7), 1071–1079. https://doi.org/http://dx.doi.org/10.1016/S1365-1609(01)00058-2

Li, Ning, Zhang, P., Chen, Y., & Swoboda, G. (2003). Fatigue properties of cracked, saturated and frozen sandstone samples under cyclic loading. *International Journal of Rock Mechanics and Mining Sciences*, *40*(1), 145–150. https://doi.org/http://dx.doi.org/10.1016/S1365-1609(02)00111-9

Li, T., Pei, X., Wang, D., Huang, R., & Tang, H. (2019). Nonlinear behavior and damage model for fractured rock under cyclic loading based on energy dissipation principle. *Engineering Fracture Mechanics*, *206*, 330–341. https://doi.org/https://doi.org/10.1016/j.engfracmech.2018.12.010

Li, X., Gong, F., Tao, M., Dong, L., Du, K., Ma, C., … Yin, T. (2017). Failure mechanism and coupled static-dynamic loading theory in deep hard rock mining: A review. *Journal of Rock Mechanics and Geotechnical Engineering*, *9*(4), 767–782. https://doi.org/https://doi.org/10.1016/j.jrmge.2017.04.004

Liu, E., & He, S. (2012). Effects of cyclic dynamic loading on the mechanical properties of intact rock samples under confining pressure conditions. *Engineering Geology*, *125*, 81–91. https://doi.org/http://dx.doi.org/10.1016/j.enggeo.2011.11.007

Liu, E., Huang, R., & He, S. (2012). Effects of Frequency on the Dynamic Properties of Intact Rock Samples Subjected to Cyclic Loading under Confining Pressure Conditions. *Rock Mechanics and Rock Engineering*, *45*(1), 89–102. https://doi.org/10.1007/s00603-011-0185-y

Liu, J., Xie, H., Hou, Z., Yang, C., & Chen, L. (2014). Damage evolution of rock salt under cyclic loading in unixial tests. *Acta Geotechnica*, *9*(1), 153–160. https://doi.org/10.1007/s11440-013-0236-5

Liu, M., & Liu, E. (2017). Dynamic mechanical properties of artificial jointed rock samples subjected to cyclic triaxial loading. *International Journal of Rock Mechanics and Mining Sciences*, *98*, 54–66. https://doi.org/http://dx.doi.org/10.1016/j.ijrmms.2017.07.005

Liu, Q., Huang, S., Kang, Y., & Liu, X. (2015). A prediction model for uniaxial compressive strength of deteriorated rocks due to freeze–thaw. *Cold Regions Science and Technology*, *120*, 96–107.

https://doi.org/https://doi.org/10.1016/j.coldregions.2015.09.013

Liu, X. S., Ning, J. G., Tan, Y. L., & Gu, Q. H. (2016). Damage constitutive model based on energy dissipation for intact rock subjected to cyclic loading. *International Journal of Rock Mechanics and Mining Sciences*, *85*, 27–32. https://doi.org/http://dx.doi.org/10.1016/j.ijrmms.2016.03.003

Liu, Y, Dai, F., Dong, L., Xu, N., & Feng, P. (2018). Experimental Investigation on the Fatigue Mechanical Properties of Intermittently Jointed Rock Models Under Cyclic Uniaxial Compression with Different Loading Parameters. *Rock Mechanics and Rock Engineering*, *51*(1), 47–68. https://doi.org/10.1007/s00603-017-1327-7

Liu, Yi, & Dai, F. (2018). A damage constitutive model for intermittent jointed rocks under cyclic uniaxial compression. *International Journal of Rock Mechanics and Mining Sciences*, *103*, 289–301. https://doi.org/https://doi.org/10.1016/j.ijrmms.2018.01.046

Liu, Yi, Dai, F., Fan, P., Xu, N., & Dong, L. (2017). Experimental Investigation of the Influence of Joint Geometric Configurations on the Mechanical Properties of Intermittent Jointed Rock Models Under Cyclic Uniaxial Compression. *Rock Mechanics and Rock Engineering*, *50*(6), 1453–1471. https://doi.org/10.1007/s00603-017-1190-6

Liu, Yi, Dai, F., Feng, P., & Xu, N. (2018). Mechanical behavior of intermittent jointed rocks under random cyclic compression with different loading parameters. *Soil Dynamics and Earthquake Engineering*, *113*, 12–24. https://doi.org/https://doi.org/10.1016/j.soildyn.2018.05.030

Liu, Yi, Dai, F., Xu, N., & Zhao, T. (2017). Cyclic flattened Brazilian disc tests for measuring the tensile fatigue properties of brittle rocks. *Review of Scientific Instruments*, *88*(8), 83902. https://doi.org/10.1063/1.4995656

Liu, Yi, Dai, F., Zhao, T., & Xu, N. (2017). Numerical Investigation of the Dynamic Properties of Intermittent Jointed Rock Models Subjected to Cyclic Uniaxial Compression. *Rock Mechanics and Rock Engineering*, *50*(1), 89–112. https://doi.org/10.1007/s00603-016-1085-y

Ma, Lin-jian, Liu, X., Wang, M., Xu, H., Hua, R., Fan, P., … Yi, Q. (2013). Experimental investigation of the mechanical properties of rock salt under triaxial cyclic loading. *International Journal of Rock Mechanics and Mining Sciences*, *62*, 34–41. https://doi.org/http://dx.doi.org/10.1016/j.ijrmms.2013.04.003

Ma, Linjian, Wang, M., Zhang, N., Fan, P., & Li, J. (2017). A Variable-Parameter Creep Damage Model Incorporating the Effects of Loading Frequency for Rock Salt and Its Application in a Bedded Storage Cavern. *Rock Mechanics and Rock Engineering*, *50*(9), 2495–2509. https://doi.org/10.1007/s00603-017-1236-9

Meng, Q., Zhang, M., Han, L., Pu, H., & Nie, T. (2016). Effects of Acoustic Emission and Energy Evolution of Rock Specimens Under the Uniaxial Cyclic Loading and Unloading Compression. *Rock Mechanics and Rock Engineering*, *49*(10), 3873–3886. https://doi.org/10.1007/s00603-016-1077-y

Momeni, A., Karakus, M., Khanlari, G. R., & Heidari, M. (2015). Effects of cyclic loading on the mechanical properties of a granite. *International Journal of Rock Mechanics and Mining Sciences*, *77*, 89–96. https://doi.org/http://dx.doi.org/10.1016/j.ijrmms.2015.03.029

Nejati, H. R., & Ghazvinian, A. (2014). Brittleness Effect on Rock Fatigue Damage Evolution. *Rock Mechanics and Rock Engineering*, *47*(5), 1839–1848. https://doi.org/10.1007/s00603-013-0486-4

Ni, X. H. (2014). Failure Characteristic of Granite under Cyclic Loading with Different Frequencies. *Applied Mechanics and Materials*, *638–640*, 1967–1970. Retrieved from https://doi.org/10.4028/www.scientific.net/amm.638-640.1967

Ning, J., Wang, J., Jiang, J., Hu, S., Jiang, L., & Liu, X. (2018). Estimation of Crack Initiation and Propagation Thresholds of Confined Brittle Coal Specimens Based on Energy Dissipation Theory. *Rock Mechanics and Rock Engineering*, *51*(1), 119–134. https://doi.org/10.1007/s00603-017-1317-9

Qiu, S.-L., Feng, X.-T., Xiao, J.-Q., & Zhang, C.-Q. (2014). An Experimental Study on the Pre-Peak Unloading Damage Evolution of Marble. *Rock Mechanics and Rock Engineering*, *47*(2), 401–419. https://doi.org/10.1007/s00603-013-0394-7

Rajaram, V. (1981). Mechanical Behavior of Granite Under Cyclic Compression. *International Conferences on Recent Advances in Geotechnical Earthquake Engineering and Soil Dynamics*, 11.

Ray, S. K., Sarkar, M., & Singh, T. N. (1999). Effect of cyclic loading and strain rate on the mechanical behaviour of sandstone. *International Journal of Rock Mechanics and Mining Sciences*, *36*(4), 543–549. https://doi.org/http://dx.doi.org/10.1016/S0148-9062(99)00016-9

Royer-Carfagni, G., & Salvatore, W. (2000). The characterization of marble by cyclic compression loading: experimental results. *Mechanics of Cohesive-Frictional*

Materials, *5*(7), 535–563. https://doi.org/10.1002/1099-1484(200010)5:7<535::AID-CFM102>3.0.CO;2-D

Sara, C., & F., L. J. (2001). Damage of Marble from Cyclic Loading. *Journal of Materials in Civil Engineering*, *13*(6), 459–465. https://doi.org/10.1061/(ASCE)0899-1561(2001)13:6(459)

Singh, S. K. (1989). Fatigue and strain hardening behaviour of graywacke from the flagstaff formation, New South Wales. *Engineering Geology*, *26*(2), 171–179. https://doi.org/http://dx.doi.org/10.1016/0013-7952(89)90005-7

Song, H., Zhang, H., Fu, D., & Zhang, Q. (2016). Experimental analysis and characterization of damage evolution in rock under cyclic loading. *International Journal of Rock Mechanics and Mining Sciences*, *88*, 157–164. https://doi.org/http://dx.doi.org/10.1016/j.ijrmms.2016.07.015

Song, R., Yue-ming, B., Jing-Peng, Z., De-yi, J., & Chun-he, Y. (2013). Experimental investigation of the fatigue properties of salt rock. *International Journal of Rock Mechanics and Mining Sciences*, *64*, 68–72. https://doi.org/http://dx.doi.org/10.1016/j.ijrmms.2013.08.023

Taheri, A., Royle, A., Yang, Z., & Zhao, Y. (2016). Study on variations of peak strength of a sandstone during cyclic loading. *Geomechanics and Geophysics for Geo-Energy and Geo-Resources*, *2*(1), 1–10. https://doi.org/10.1007/s40948-015-0017-8

Taheri, A., Yfantidis, N., Olivares, C., Connelly, B., & Bastian, T. (2016). *Experimental Study on Degradation of Mechanical Properties of Sandstone Under Different Cyclic Loadings BT - Experimental Study on Degradation of Mechanical Properties of Sandstone Under Different Cyclic Loadings*.

Tien, Y. M., Lee, D. H., & Juang, C. H. (1990). Strain, pore pressure and fatigue characteristics of sandstone under various load conditions. *International Journal of Rock Mechanics and Mining Sciences & Geomechanics Abstracts*, *27*(4), 283–289. https://doi.org/http://dx.doi.org/10.1016/0148-9062(90)90530-F

Voznesenskii, A. S., Krasilov, M. N., Kutkin, Y. O., Tavostin, M. N., & Osipov, Y. V. (2017). Features of interrelations between acoustic quality factor and strength of rock salt during fatigue cyclic loadings. *International Journal of Fatigue*, *97*, 70–78. https://doi.org/https://doi.org/10.1016/j.ijfatigue.2016.12.027

Wang, W., Wang, M., & Liu, X. (2016). Study on Mechanical Features of Brazilian Splitting Fatigue Tests of Salt Rock. *Advances in Civil Engineering*, *2016*(Article

ID 5436240), 10. Retrieved from https://doi.org/10.1155/2016/5436240

Wang, Z., Li, S., Qiao, L., & Zhao, J. (2013). Fatigue Behavior of Granite Subjected to Cyclic Loading Under Triaxial Compression Condition. *Rock Mechanics and Rock Engineering*, *46*(6), 1603–1615. https://doi.org/10.1007/s00603-013-0387-6

Xiao, J.-Q., Ding, D.-X., Jiang, F.-L., & Xu, G. (2010). Fatigue damage variable and evolution of rock subjected to cyclic loading. *International Journal of Rock Mechanics and Mining Sciences*, *47*(3), 461–468. https://doi.org/http://dx.doi.org/10.1016/j.ijrmms.2009.11.003

Xiao, J.-Q., Ding, D.-X., Xu, G., & Jiang, F.-L. (2009). Inverted S-shaped model for nonlinear fatigue damage of rock. *International Journal of Rock Mechanics and Mining Sciences*, *46*(3), 643–648. https://doi.org/http://dx.doi.org/10.1016/j.ijrmms.2008.11.002

Yamashita, S., Sugimoto, F., Imai, T., Namsrai, D., Yamauchi, M., & Kamoshida, N. (1999). The Relationship Between the Failure Process of the Creep Or Fatigue Test And of the Conventional Compression Test On Rock. *9th ISRM Congress*. Paris, France: International Society for Rock Mechanics and Rock Engineering.

Yang, S.-Q., Ranjith, P. G., Huang, Y.-H., Yin, P.-F., Jing, H.-W., Gui, Y.-L., & Yu, Q.-L. (2015). Experimental investigation on mechanical damage characteristics of sandstone under triaxial cyclic loading. *Geophysical Journal International*, *201*(2), 662–682. https://doi.org/10.1093/gji/ggv023

Zhang, S., Lai, Y., Zhang, X., Pu, Y., & Yu, W. (2004). Study on the damage propagation of surrounding rock from a cold-region tunnel under freeze–thaw cycle condition. *Tunnelling and Underground Space Technology*, *19*(3), 295–302. https://doi.org/https://doi.org/10.1016/j.tust.2003.11.011

Zhang, Y., Feng, X.-T., Zhang, X., Wang, Z., Sharifzadeh, M., & Yang, C. (2019). A Novel Application of Strain Energy for Fracturing Process Analysis of Hard Rock Under True Triaxial Compression. *Rock Mechanics and Rock Engineering*, *52*(11), 4257–4272. https://doi.org/10.1007/s00603-019-01868-8

Zhenyu, T., & Haihong, M. (1990). An experimental study and analysis of the behaviour of rock under cyclic loading. *International Journal of Rock Mechanics and Mining Sciences & Geomechanics Abstracts*, *27*(1), 51–56. https://doi.org/https://doi.org/10.1016/0148-9062(90)90008-P

Zhou, H. W., Wang, Z. H., Wang, C. S., & Liu, J. F. (2019). On Acoustic Emission

and Post-peak Energy Evolution in Beishan Granite Under Cyclic Loading. *Rock Mechanics and Rock Engineering*, *52*(1), 283–288. https://doi.org/10.1007/s00603-018-1614-y

Chapter 2

Sources of variability in laboratory rock test results[1]

[1] This chapter has been submitted for publication as a journal article in an international journal as:

Geranmayeh, V. R., Saberhosseini, S. E., Dyskin, V. A., Thoeni, K., Sharifzadeh, M., & Sarmadivaleh, M. (2019), Sources of variability in laboratory rock test results, under review.

ABSTRACT

Appropriate rock characterization is beneficial in providing a reliable judgment on rock properties which is crucial for the design process of rock engineering applications. However, it can be difficult to obtain consistent mechanical parameters due to substantial variations in rock properties. In this research, uniaxial compression tests of dolerite samples collected from a gold mine in Western Australia showed substantial scatter in the results. Rock categorization based on the P-wave velocities is as accurate as the thin section analysis, which suggests that they can be used together to get a more accurate initial understanding of the rock types before any laboratory testing. The quality of sample preparation and rock–machine interaction greatly affect the test results. For instance, non-parallelness of loading platens can lead to considerable scatter of the testing results, which would be perceived as rock variability. It is suggested that the current testing standards should be modified towards a better control of the loading machine performance and equipment precision. Finally, the possibility of pre-existing microcracks in rock, neither detected by the thin section analysis nor by the ultrasonic measurement, must be examined by the CT scanning as they can affect the test results. This study will enhance our knowledge about the sources of variability in laboratory test results of rock which is essential for obtaining reliable data.

2.1. Introduction

Rock material is very complex and requires a precise and meticulous identification of its physical and mechanical properties. Valid inspection, examination and testing methods are needed in order to gain such an understanding of rock characterization. It is essential for a rock mechanics engineer to have accurate and comprehensive information about the rock material for design and for dealing with engineering challenges of rock structures. Thanks to the technological developments and invention of new testing devices, rock characterization methods have been changed and developed remarkably within the last decades. However, some uncertainties still exist about the rock characterization since there are several variability sources affecting its behavior. Some of these variabilities are associated with the rock itself such as lithology, microstructural features, porosity, water content and how much and how long

it has been under the stress and weathering conditions. Other factors are the scale as well as the testing and examination conditions.

Different sources of variability have been considered by Hadjigeorgiou & Harrison (2011). These are associated with the data collection, rock testing methods, equipment precision, and in some cases inappropriate methods implemented in numerical analysis. Furthermore, another type of variability or uncertainty, called systematic uncertainty, also becomes noticeable when the data obtained from the laboratory scale is used for rock engineering designs at in-situ scale (Duzgun et al., 2002). More recently, different sources of uncertainties specifically integrated in practical application of slope stability analysis have been defined and reviewed in an investigation by Abdulai and Sharifzadeh (2019).

The variability sources differ in different stages of the laboratory tests. As illustrated in Figure 2.1, the variability in test results may stem from different sources before the experiment, during the sample preparation, during the testing itself, and finally during the data analysis. Therefore, the variability sources could be inherent (rock-based), sample-based, machine-based, or statistical. The effect of these sources during each stage, individually, may not be significant, but the effects of these sources are cumulative with noticeable interaction effects.

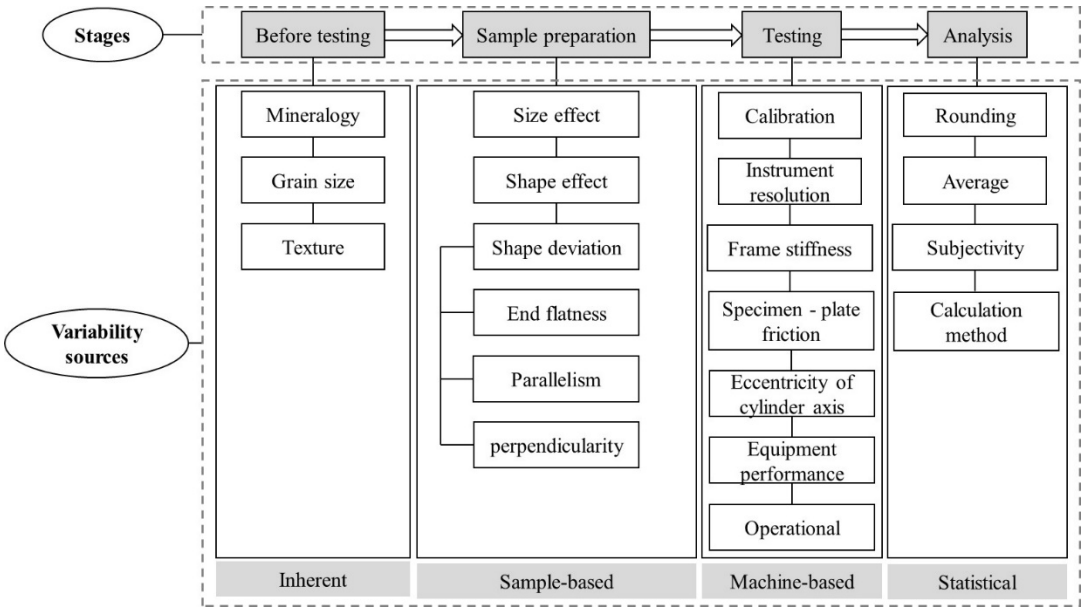

Figure 2.1. Different sources of variabilities for the rock laboratory test results.

To date, several studies have attempted to investigate the effect of the variability on rock strength. In these studies, the uncertainties in the estimation of shear strength of the rock discontinuities have been quantified using the probabilistic approach (Duzgun et al., 2002). The contributions of the uncertainty sources coming from the measurements of the sample dimensions, flatness, parallelism, rounding, calibration, and resolution of the instruments and transducers in the determination of the unconfined compressive strength of rocks were also analyzed (Kuhinek et al., 2011). It was found that these variabilities contribute to less than 1% of the uncertainty of the uniaxial compressive strength (UCS) for the rocks with more than 118 MPa of the UCS values. Similarly, it was pointed out that the scattering in the rock UCS values showed a decreasing trend with an increase in the rock strength so the stronger rocks should give very close test data (Rohde & Feng, 1990). There have also been some attempts to determine the minimal number of samples needed to reduce uncertainties in the rock mechanical properties obtained from the tests (Gill et al., 2005; Ruffolo & Shakoor, 2009).

The effect of the sample shape (Liang et al., 2016; Xu & Cai, 2017) and size on the rock strength has been studied by many researchers (Labuz & Biolzi, 2007; Masoumi et al., 2017; 2017; 2016; Tsur-Lavie & Denekamp, 1982), whereas it has been pointed out that there are still potential avenues for further investigation in this area (Roshan et al., 2016). Prakoso and Kulhawy (2011) investigated the correlation between rock strength and the sample diameter and moisture content. The effect of the sample cross-sectional shape on its strength was investigated both numerically and experimentally. It was shown that the sample cross-sectional shape had minor effect on its peak strength while noticeably affecting the post-peak behavior. Interestingly, it was shown that a square prism specimen was stronger than a cylinder specimen with the same height to diameter (or height to width) ratio (Xu & Cai, 2017). More recently, the sample height to diameter ratio and cross section were shown to control the rock mechanical properties and damage thresholds (Du et al., 2019).

The effect of sample shape deviations including the sample end flatness, parallelism, and perpendicularity on the rock UCS was also investigated (Nikolić et al., 2018; Štambuk et al., 2015). It was reported that the parallelism of the ends and the sample axis perpendicularity do not considerably affect the UCS value, whereas the effect of the end flatness could be significant. The acceptable tolerance of the end flatness, however, has been optimized to be 60% higher than specified in the existing standards

(Štambuk et al., 2015). The sample end preparation was reported to greatly affect the uniaxial compressive strength of concrete specimens and the degree of this influence depends upon the thickness of the machine end caps (Carino, 1994).

There were also some attempts to address the machine-based variabilities (Brady, 1971; Gao et al., 2018; Hemami & Fakhimi, 2014; Hudson et al., 1972; Xu & Cai, 2017). For instance, the effect of insert materials on the elastic behavior of rock samples under the axial compression was investigated by Brady (Brady, 1971), who suggested that the low-modulus inserts should be avoided in such testing. This was also discussed in another investigation (Hudson et al., 1972), as well as the advances in rock testing machine technologies which was a great step forward in rock testing. The loading frame–rock sample interaction was also studied numerically, considering the effect of any variation of sample dimension, end platen friction, and the loading frame stiffness on the rock strain response (Gao et al., 2018). Friction between the rock sample ends and the loading platens was found to control the size effect of the rock samples under compressive test, indicating that the size effect would be negligible if the end friction is removed (Hemami & Fakhimi, 2014). Obviously, the end frictional effect decreases in rock samples with high aspect ratio (Gao et al., 2018).

All these factors are usually checked at the first stages of the experiments. However, not enough attention has been paid to address the effect of such variabilities on the final laboratory test results. It seems that more considerations should be taken into account beyond the ordinary visual inspections of the rock samples and checking the existing controlling instructions of the rock testing equipment. Using experiments on rock and aluminum samples of equal dimensions, this paper discusses some sources of variability that could potentially cause scatter of the UCS values.

Inherent variabilities of rock such as mineralogy, grain size, and texture are the first parameters commonly determined by the microscopic examinations. The testing conditions and rock–machine interaction will be considered as the other source of variability; these are usually presumed to be the same for all tests. However, they may differ from one rock type to another, and can depend on the other testing conditions as well. So, this study seeks to explain why and how these parameters should be checked if such scattered test data is obtained. It should be noted that the variability due to the data analysis, calibration, instrument resolution, frame stiffness, sample–loading platen friction, sample size effect and shape effect are not considered in this study since some

of them (like the size and shape effects) are not supposed to be important for these experiments, while other factors were consistent throughout all conducted tests.

This paper also discusses the importance of additional examinations that need to be considered for any rock testing to have valid design parameters. This implies the necessity of having a good controlling guideline, which is discussed later in this paper considering the main sources and effects of variability on the uniaxial strength. Different examination techniques were used for this purpose to find out the reasons and the inherent sources or external factors behind the obtained scattering of the UCS values. Both quantitative and qualitative approaches are used in this paper to address this issue – which is of great importance in a rock testing applicable to all mining, petroleum and geotechnical engineering fields.

The sample preparation and the uniaxial compressive strength results for the tested rock samples are presented in Section 2.3. Section 2.3 discusses the examination of the rock inherent variability and the categorizations based on the results of the measurements. Section 2.4 describes the control tests carried out to assess the testing conditions and the reasons for such external factors to be checked before rock testing. The effect of testing condition, specifically loading platen defects, on the test results is numerically investigated in Section 2.5. Section 2.6 discusses the CT scan technique as a useful tool to check for pre-existing micro-cracks. Finally, conclusions are provided in Section 2.7.

2.2. Rock testing

2.2.1. Sample preparation

Dolerite rock cores have been collected from the Enterprise gold mine located northwest of Kalgoorlie, Western Australia. This mine is hosted within the Ora Banda district mainly dominated by the late Archaean lithology and mafic sequences. A sequence of the Siberia Komatiite and ultramafic as the base rocks, the Big Dick Basalt, Cashmans Sedimentary Horizon, Bent Tree and Victorious Basalts and the Black Flag Sediments from bottom to top have formed the main local geology of this region. The main host rock of this deposit is the layered mafic dolerite sill intruding the above-mentioned rock domains (Norton Gold Fields, 2012).

After visual inspection of the rock cores, 88 dolerite samples have been prepared, with 50.5 mm in diameter and a length to diameter ratio of L/D>2, and with similar visual mineralogy (Figure 2.2). All these specimens were taken from adjacent core trays. The average density of these samples was 2,958 kg/m3. The rock samples have been prepared according to ASTM D4543-08 and ISRM 1979 (ASTM D4543-08, 2008b; ISRM, 1979a). Reasonable efforts have been made to prepare the samples with the flatness to satisfy the closest tolerance specified by these relevant standards. However, the best flatness obtained for these samples after several times of grinding was less than 0.004 inches (102 μm) while it should have been less than 0.001 inches (25 μm) according to the mentioned standards (Figure 2.3). The required flatness for these samples could not be achieved by the grinding machine used. This is mainly because of the hard minerals within the rock texture inter-grown with other minerals with different hardness. The grinding wheel or component misalignment might also have affected the grinding precision. It is usually more difficult to get the desired flatness for hard rocks than it is for soft rocks. In the next sections, the effect of the end flatness on the obtained results will be discussed.

Figure 2.2. Dolerite samples prepared for the UCS testing.

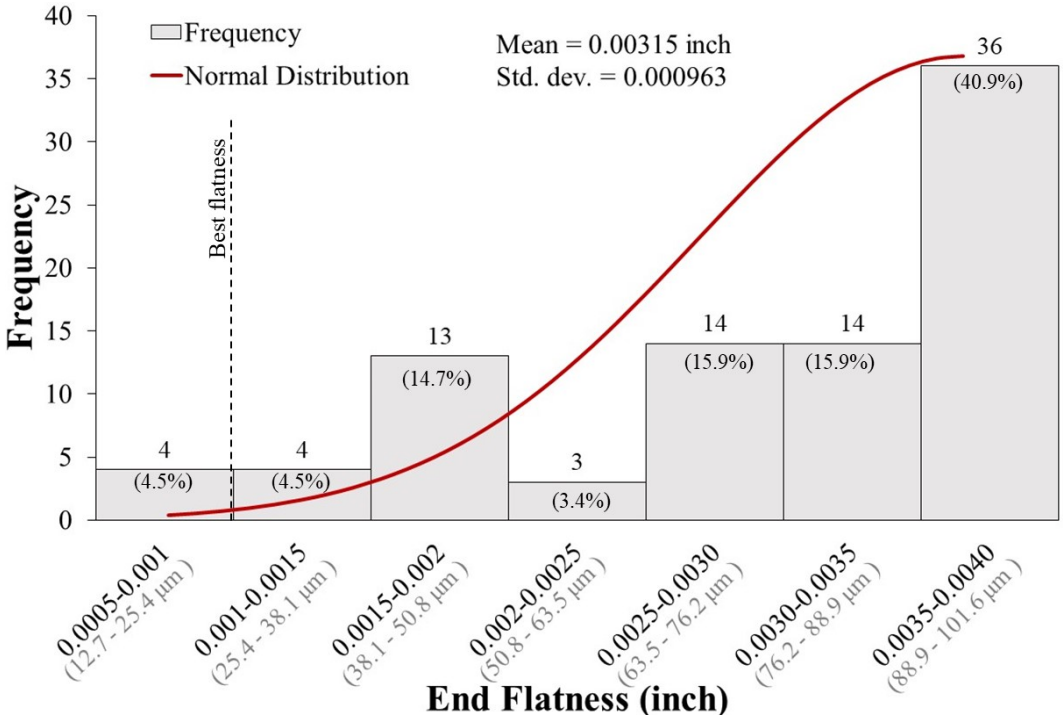

Figure 2.3. The obtained flatness range and its normal cumulative distribution curve for the dolerite samples, Std. dev. stands for standard deviation.

2.2.2. Unconfined compression tests

Five samples were selected for the uniaxial compression testing to obtain a statistically representative value for UCS. These samples were first checked to ensure that they did not have any visible defects. Their textures were then visually inspected based on their appearances in terms of differences in their textures, grain sizes, and colors in general. A uniaxial testing machine of 600–700 kN/mm stiffness, with a computer-controlled axial actuator, was used for this test. The data were captured by a PC connected to the testing system. The deformation of the samples was recorded using two rosette strain gauges attached on the middle of the two sides of the sample surface opposite to each other. Each strain gauge recorded both horizontal and vertical strains. A data logger with nonlinearity of 0.1% frequency of sampling was used for strain data recording.

Table 2.1 gives information about the rock samples, obtained UCS, and a classification made on the tested rock samples simply based on their visible textures. These samples were classified into different groups (4, 5, and 1) based on judgments a geologist usually makes during the rock core selection for the experimental testing. The stress–strain curves for these tests are shown in Figure 2.4. As can be seen, the

measured values of the UCS of the tested samples are greatly scattered from 86 MPa to 315 MPa, with almost 270% difference. The samples failed at totally different peak stresses even though they were of the same visual categories. By taking samples UCT-1, UCT-2 and UCT-3 for instance, their obtained UCS differ by about 60% although they all belong to the same category (rock type 4). So, it is not clear why a strong rock, such as dolerite, produces such a scatter of UCS values, while it usually has very few flaws, which are the main sources of such discrepancy. This is against reported results (Rohde & Feng, 1990) which indicate that measured UCS values for stronger rocks should be very close, with only small deviations from the mean value. It should be noted that the samples have a small difference in heights but by no means could this difference affect the UCS by 270%. Hence, it is concluded that other factors must influence the results and possible factors are discussed in the next sections.

Table 2.1. Unconfined Compressive Strength (UCS) of the tested samples.

Sample No.	Height(mm)	UCS (MPa)	Category*
UCT-1	102.08	138.49	4
UCT-2	106.16	85.9	4
UCT-3	102.93	135.97	4
UCT-4	102.33	314.86	5
UCT-5	107.78	267.86	1
Average = 188.6 MPa, Std. dev.= 97.53			

* The samples were visually categorized based on their visible textures

2.3. Examination of rock inherent variabilities

As already mentioned, rock inherent variability is one of the main sources of uncertainty in rock engineering and is linked to the rock type (Hadjigeorgiou & Harrison, 2011). Since rock materials differ in their mineralogy, grain size, and texture, the degree of uncertainty and variability would also be different for each rock type. Therefore, heterogeneous and anisotropic rocks would need more examinations, compared to the relatively homogenous and isotropic rocks in order to get reliable design-based data. In this section, the inherent variability of the collected rock samples has been estimated by microscopic examination of thin sections and the analysis of the measured pulse velocities (i.e. ultrasonic testing), to assess whether and how the variability in microstructure affected the uniaxial compression test results. For this

purpose, the rock samples are categorized based on their inherent parameters obtained by the two techniques explained hereafter.

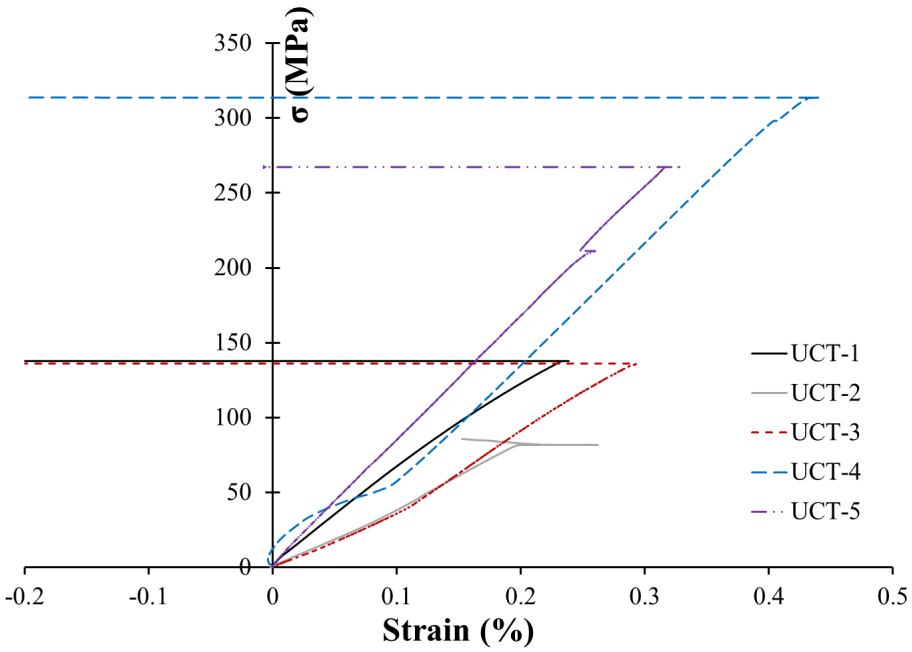

Figure 2.4. Stress–strain curves for the uniaxial compressive tests on dolerite samples.

2.3.1. Thin section analysis

Determination of the rock minerals, its micro-fractures, alterations, grain size, and fabric, usually characterized by analyzing a thin section of rock sample, is very helpful for the model analysis and practical purposes of the mechanical behavior of rocks (ISRM, 1979b). To this end, 8 samples were randomly selected covering all visually categorized rock types (Figure 2.5). Some of these sections were selected from the rock pieces/cores as close as possible to the tested rock samples. The first three samples (R1–R3) are peridotite (base of dolerite sill) and the other five (R4–R8) are dolerite. The samples have all been recrystallized to greenschist metamorphic assemblages with various alteration of chlorite, epidote, and carbonate. The analysis shows the variation in the mineral assemblages of the samples. The main rock type is dolerite sills, which in the Goldfields region of Western Australia are differentiated with the ultramafic or peridotite bases graded into typical dolerite assemblages of clinopyroxene and plagioclase. Quartz becomes part of the mineralization as differentiation proceed but is

only minor (~5%) in some samples and partly inter-grown with feldspar. Figure 2.6 shows some images from the thin section analysis of these samples in cross polarized light (XPL).

Figure 2.5. Eight rock samples selected for the thin section analysis.

It should be mentioned that within the dolerite sills in the Goldfields, the grain size can vary from very fine-grained (margins of dolerite body) to coarse-grained in the core of the body. The grain size is a function of temperature during crystallization and alteration. Table 2.2 shows the full rock name, grain size and classification of the analyzed thin section samples. As can be seen, those samples visually categorized as rock type 4 are “Chlorite/Chlorite-carbonate altered peridotite” and those categorized as rock type 1 are “Epidote-Chlorite altered quartz dolerite”. What can be clearly seen in this table is the similarity between the rock types. Rock types 1 and 4 are visually similar as they are in alteration, explored from the thin section analysis. On the other hand, while rock types 1 and 5 are visually distinguishable, they have the same alteration and are categorized microscopically the same (“Epidote-Chlorite altered quartz dolerite”). Taken together, this comparison indicates that the visual inspection and judgment by a professional geologist or rock engineer could be questionable and is not always accurate and needs more examinations and analysis.

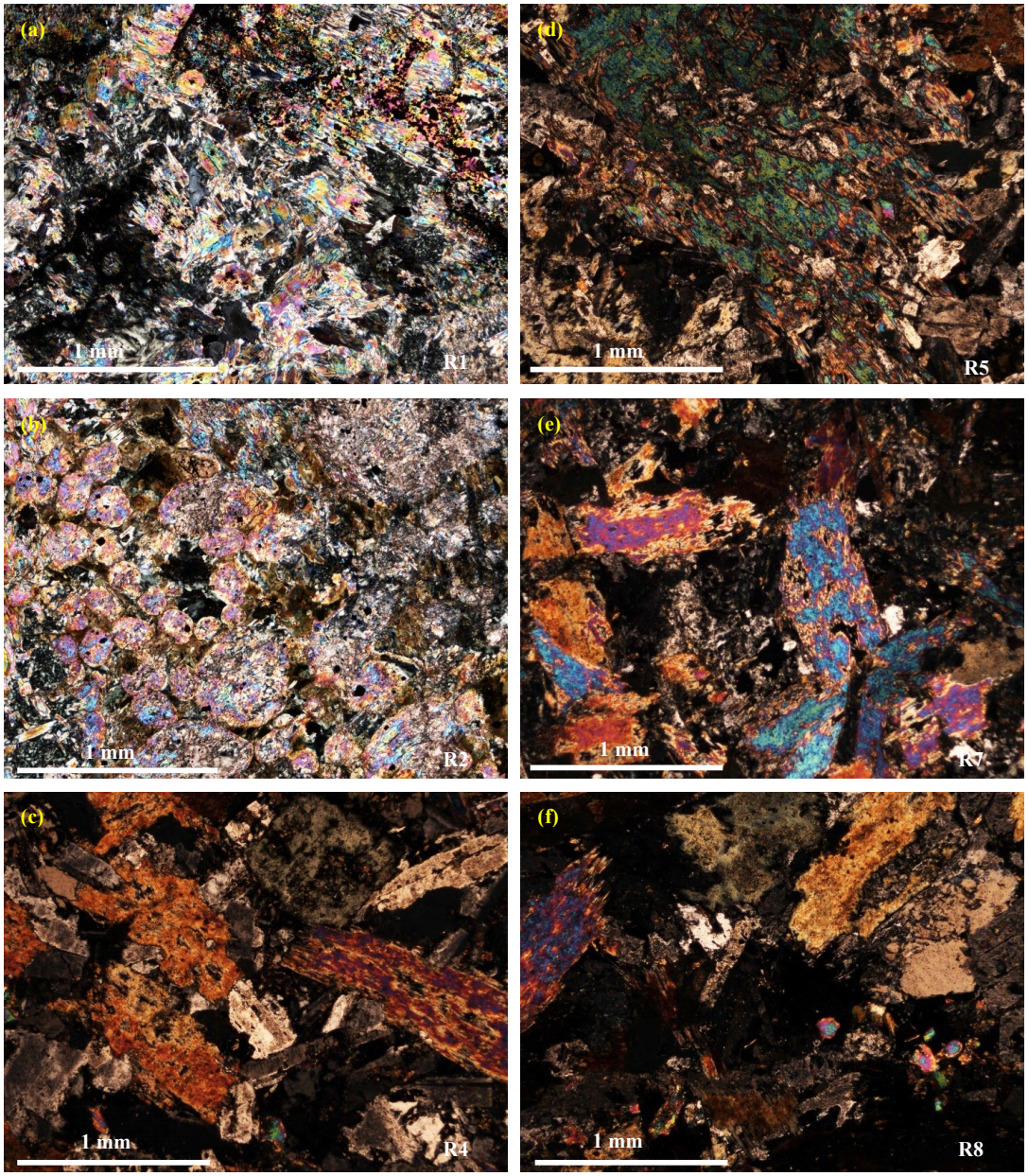

Figure 2.6. Photomicrographs of thin sections of tested rock samples: (a) R1: the rounded forms preserved are former clinopyroxene and / or olivine crystals partially or totally enclosed in coarser grained pyroxene (now altered to fibrous amphibole-tremolite); (b) R2: a poikilitic texture where medium-grained former pyroxene encloses finer grained, rounded pyroxene and/or olivine, (c) R4: the interlocking texture of plagioclase and former clinopyroxene, now replaced by actinolite; (d) R5: medium-grained former pyroxene encloses finer grained plagioclase laths; (e) R7: a dolerite texture is defined by interlocking columnar plagioclase (dirty brown color due to alteration) and prismatic clinopyroxene; (f) R8: a dolerite texture of altered plagioclase and pyroxene dominates the sample. Patches of chlorite and epidote are present. Irregular patches of quartz are partly intergrown with the feldspar, in cross polarized light (XPL).

With respect to the uniaxial strength of the rock samples, as can be seen in Table 2.2, rock type 4 ("Chlorite /Chlorite-carbonate altered peridotite") resulted in a UCS value in the range of 86 MPa to 139 MPa (UCT-1, UCT-2, and UCT-3), while rock types 1 and 5 (categorized microscopically as "Epidote-chlorite altered quartz dolerite"), resulted in a very high value of UCS, higher than 267 MPa (UCT-4 and UCT-5). Although rock types 1 and 5 showed mineralization of quartz, a question arises as to whether a minor quartz mineralization or minor difference in alteration sequence could change the rock mechanical properties to vary by almost 270%. Turning to the samples of R2 and R3, categorized as the same rock type, the UCS for rock samples close to them (UCT-2 and UCT-3) differ almost 60% from each other. The questions raised by this comparison are how a rock engineer can make sure that the difference in mechanical properties of rock, visually similar and identical, could be due to differences in mineralization; and whether there is another factor affecting the obtained data. How should a rock engineer or geologist analyze the rock samples to have valid rock parameters for the design? In the next section, the available rock samples were investigated in terms of their ultrasonic elastic parameters to see whether the major factor affecting the results can be determined and whether their classifications made by the ultrasonic results match the microscopic classification.

Table 2.2. The full rock name and classification, grain size and quartz content of the rock samples after thin section analysis and comparison with the visual categorization.

Sample No.	Visual category	Full rock name and classification	Grain size (mm)	Quartz content	Tested sample	UCS (MPa)
R1	4	Chlorite altered peridotite	<1	-	UCT-1	138.49
R2	4	Chlorite-carbonate altered peridotite	<1	-	UCT-2,3	135.97, 85.9
R3	4	Chlorite-carbonate altered peridotite	<1	-	UCT-2,3	135.97, 85.9
R4	1 or 3	Chlorite-epidote altered dolerite	<2	-	-	-
R5	4	Chlorite-epidote altered dolerite	<1	-	-	-
R6	1	Epidote-chlorite altered quartz dolerite	<1	~2-5%	-	-
R7	1	Epidote-chlorite altered quartz dolerite	<1	~5%	UCT-5	267.86
R8	5	Epidote-chlorite altered quartz dolerite	<1	~5%	UCT-4	314.86

2.3.2. Ultrasonic parameters

Ultrasonic wave velocity measurements are popular for non-destructive testing (NDT) of rocks as it is relatively cheap, quick, simple, and easy to implement. This testing was conducted on 78 dolerite samples to both determine their dynamic elastic constants and potentially categorize them into different distinguishable groups for further experiments and to compare this classification with that based on the thin section analysis. The P-wave (longitudinal wave) and S-wave (shear wave) velocities have been recorded in this testing according ASTM D2845-08 (ASTM, 2008a). A high-frequency ultrasonic test system with a digital waveform display was used for these experiments. It includes a signal generator, oscilloscope, and data acquisition unit and other components, the same as most commercially available ultrasonic test systems. Two different pairs of sensors (transducers) were used for measuring the waves. V103-RM and V153-RM transducers from OLYMPUS – both with a nominal frequency of 1.0 MHz and nominal element size of 13 mm – were used to record the compression and shear wave velocities, respectively.

Some measurements and verifications have been taken for determination of travel time, delay time and positioning of transducers to ensure the validity of this experiment on the tested samples, according to ASTM and ISRM standards (ASTM, 2008b; Aydin, 2014). Some of these measurements include using clippers for coaxial positioning of two sensors normal to the sample's end surfaces, applying coupling medium (silicone grease) between the sample surfaces and each transducer to improve the energy transmission, and applying a small seating force again for better energy transmission.

The P-wave velocity measurements have been conducted in both vertical (normal to the end surfaces of the samples) and diametrical (horizontal across the diameter or normal to the lateral dimension of the sample) directions. Three measurements have been conducted in three different points in each direction (3 in vertical and 3 in diametrical). As illustrated in Figure 2.7, all three measurements in each direction approximately resulted in the same P-wave arrival times (measured by the time of the first break, Figure 2.7) and, hence, they have been averaged for further analysis. Almost all vertical P-wave velocities vary by less than 2% from their average values except for two cases of which a crack is visible on the sample surface. Therefore, generally speaking, it can be concluded that the samples are isotropic since all velocities vary by less than 2% from their average values according to ASTM D2845-08 (ASTM, 2008a).

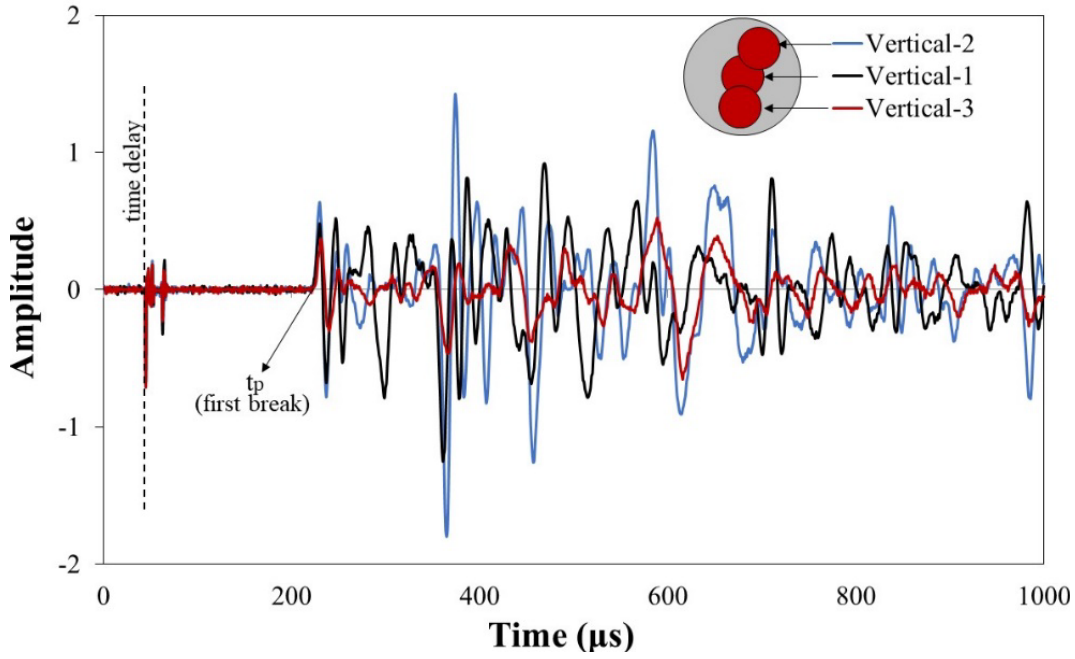

(a)

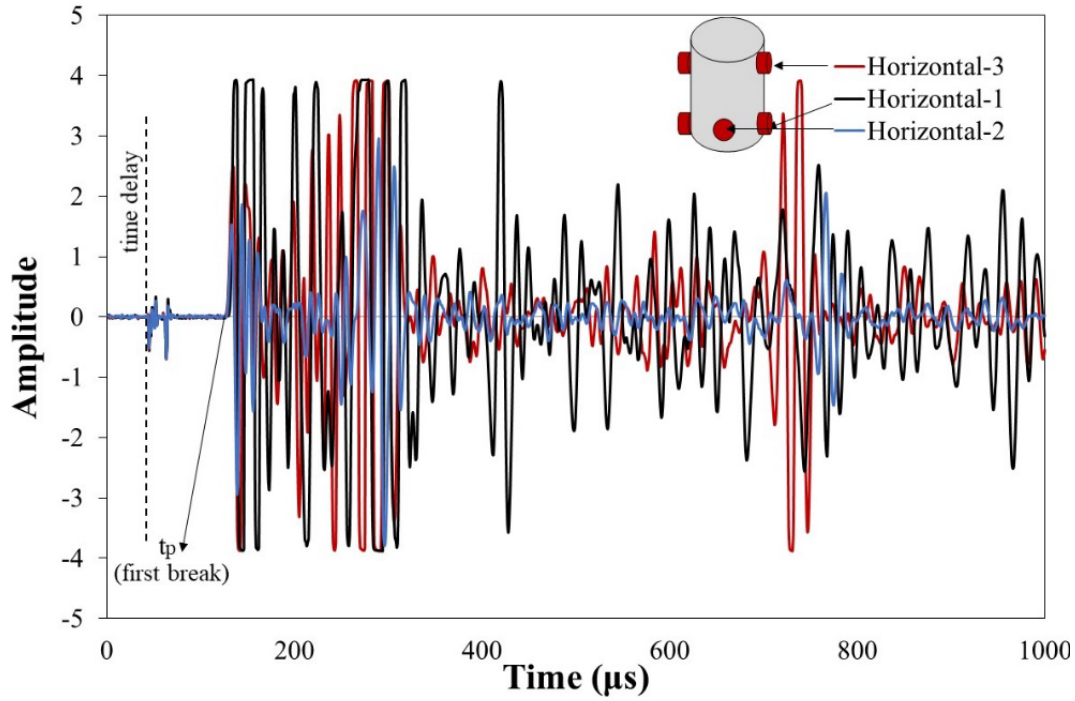

(b)

Figure 2.7. Two examples of P-wave records. The arrival times were recorded by the time of first break: (a) vertical (axial) directions; (b) diametrical (horizontal) directions.

The S-wave velocity measurements have been conducted twice along the axial direction of the samples (normal to the sample ends). For the first measurement, both transducers were attached onto the sample end surfaces aligned parallel to each other (on the identical phase known hereafter as S-Phase-0). For the second measurement, one of the transducers was rotated almost 90 degrees to make a change in the phase of its wave arrival time, hereafter known as S-Phase-1 (Figure 2.8). The S-Phase-0 velocities were taken as the representative shear velocities because this measurement is very sensitive to the direction of the transducers and operational error which is more likely in S-Phase-1 direction. Figure 2.9 shows the values for vertical P-wave velocities and S-Phase-0 shear velocities for all tested samples. The average P-wave and S-wave velocities were determined with 6160 and 3530 m/s, respectively, for this rock type. The results are very similar to what has been reported for dolerite rocks in Western Australia in another investigation (Adams & Dentith, 2018).

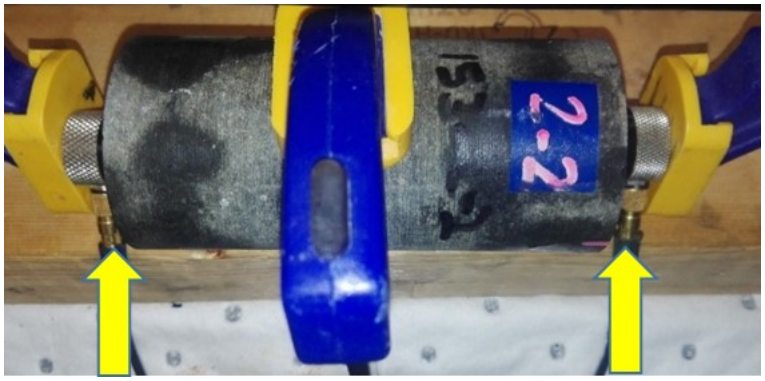

(a)

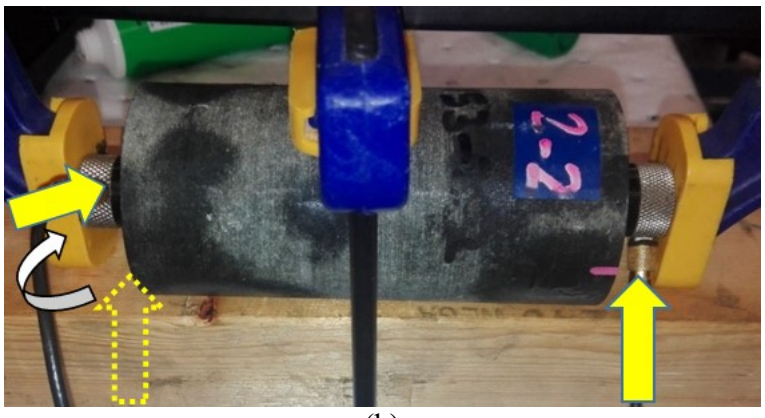

(b)

Figure 2.8. S-wave velocity measurement in a) Phase-0 mode and b) Phase-1 mode along the sample axis.

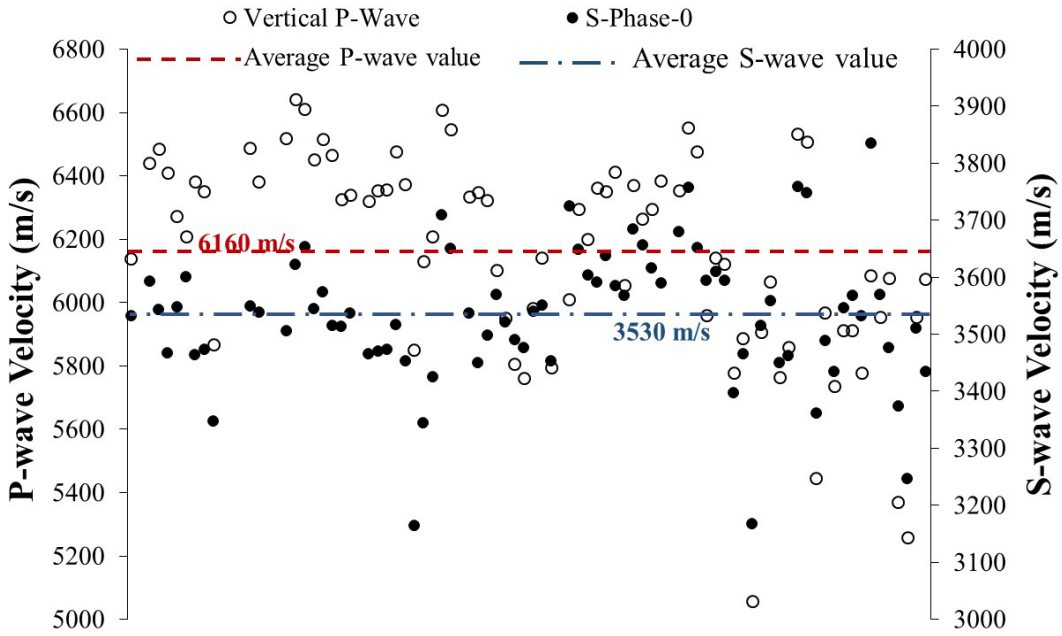

Figure 2.9. Shear wave velocities for Phase-0 and vertical P-wave velocities of all tested samples.

Two ultrasonic dynamic elastic constants of Young's modulus and Poisson's ratio were calculated from the measured compression (P-wave) and shear wave (S-wave) velocities. The dynamic Elastic Young's modulus and Poisson's ratio are calculated from the following equations (ASTM, 2008a):

$$E = \left[\rho V_s^2 (3V_p^2 - 4V_s^2)/(V_p^2 - V_s^2)\right] \quad (2.1)$$

$$\nu = \rho\left(V_p^2 - 2V_s^2\right) \quad (2.2)$$

Here E is the dynamic Young's modulus, ν is the Poisson's ratio, V_p is the P-wave velocity, V_s is the S-wave velocity and ρ is the rock density. Figure 2.10 shows the values calculated for the dynamic Young's modulus and Poisson's ratio for all samples. The average dynamic Young's modulus and Poisson's ratio were determined as 92.45 GPa and 0.25, respectively, for this rock type, however the scatter is considerable.

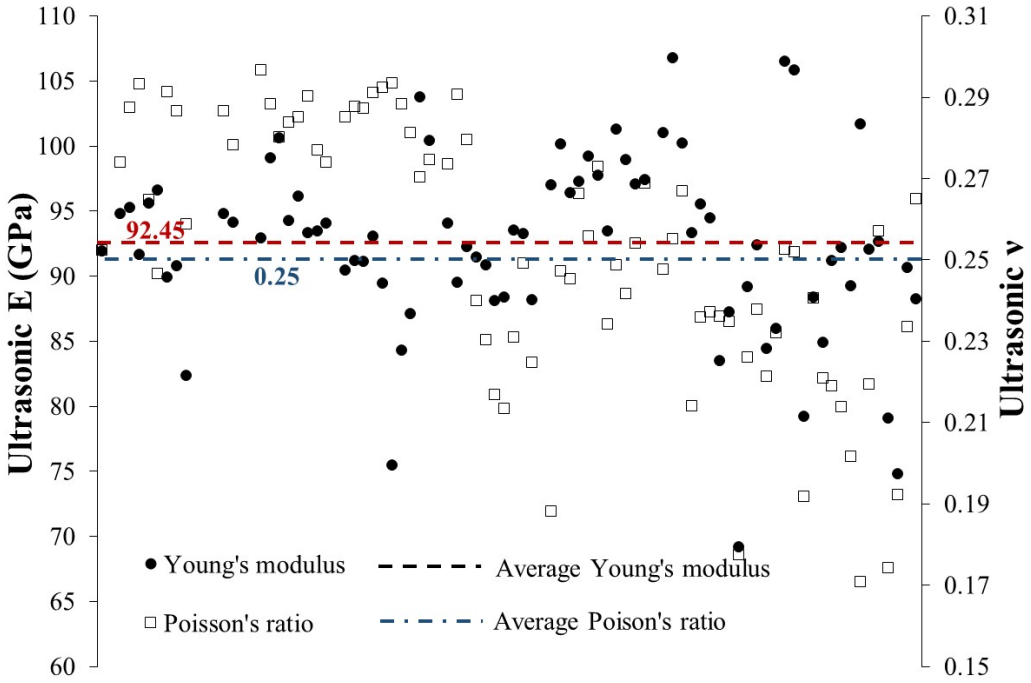

Figure 2.10. Determined dynamic Young's modulus and Poisson's ratio of the rock samples.

As already mentioned, an initial objective of the ultrasonic measurements was to classify the available rock samples into different groups based on the obtained data. The data for the P-wave velocities and the Young's modulus were selected for this purpose. Scott's normal reference rule (Scott, 2010) was used to categorize rock samples based on the P-wave velocities and Young's modulus. In this method, the bin width (or category) is determined according to the equation below:

$$\text{Bin width} = (3.5\times\sigma)/\sqrt[3]{n} \qquad (2.3)$$

where σ is the standard deviation of the data (either the wave velocities or Young's modulus) and n is the number of values in the data source. The histograms plotted from this method are illustrated in Figure 2.11. As can be seen from this figure, generally four rock types can be assigned for all rock samples. These four groups, A, B, C and D can be described as:

A: very strong dolerite,

B: strong dolerite,

C: medium strong dolerite

D: weak dolerite (or with microcracks)

The ultrasonic parameters of the samples of the thin section analysis (R1 to R8) are approximated from the ultrasonic measurements of samples which were cut adjacent to them. For instance, the P-wave velocity of R4 was considered to be 5900 m/s based on the P-wave velocity measured from the sample that had been cut from the adjacent rock piece. Then, the classification based on the thin section analysis can be compared with that of the ultrasonic measurement. This comparison is shown in Table 2.3. It is apparent from this table that there is an agreement between these categories and rock types determined from the thin section analysis and the P-wave velocities. For instance, as can be seen in this table, R1, R2, and R3 belong to the same category based on both this section analysis and P-wave measurements. It should be mentioned that this comparison is between thin section analysis and P-wave velocity measurements not visual category as it has been questioned as subjective in previous sections.

It should be noted that this will not be true for the rock categorization based on the Young's modulus, since Young's modulus is calculated from both P-wave and S-wave, whereas the S-wave measurements are very sensitive to the testing and operational conditions. Therefore, it could be said that the P-wave velocity measurements can be used to categorize rock samples for further analysis. This is very advantageous because the ultrasonic test is less expensive, simpler, and quicker than the thin section analysis. Having the ultrasonic parameters of the rock samples, a geologist, rock engineer or lab technician would be able to both have a good idea about the mechanical properties of the rock samples and use these, along with the thin section analysis, to better categorize the rock types. A similar comparison has been drawn on the samples used for the compression tests (Table 2.4). What can be clearly seen in this table is the similarity between visual category, the range of UCS, and category based on the P-wave velocity measurement for the fractured samples. This is evident in the case of those samples (UCT-1, UCT-2, and UCT-3), visually categorized as rock type 4, which failed at the same range of UCS between 86 MPa and 139 MPa, and also belong to the same group "B" based on the P-wave velocity measurements. However, there is an inconsistency between the results. Taken the UCT-4 sample, for example, it failed at a high value of stress (315 MPa), while the rock samples near to it resulted relatively in low value of P-wave velocity. This contradiction indicates that there might be other factors affecting the UCT results, of which the rock–machine interaction will be discussed in the next section.

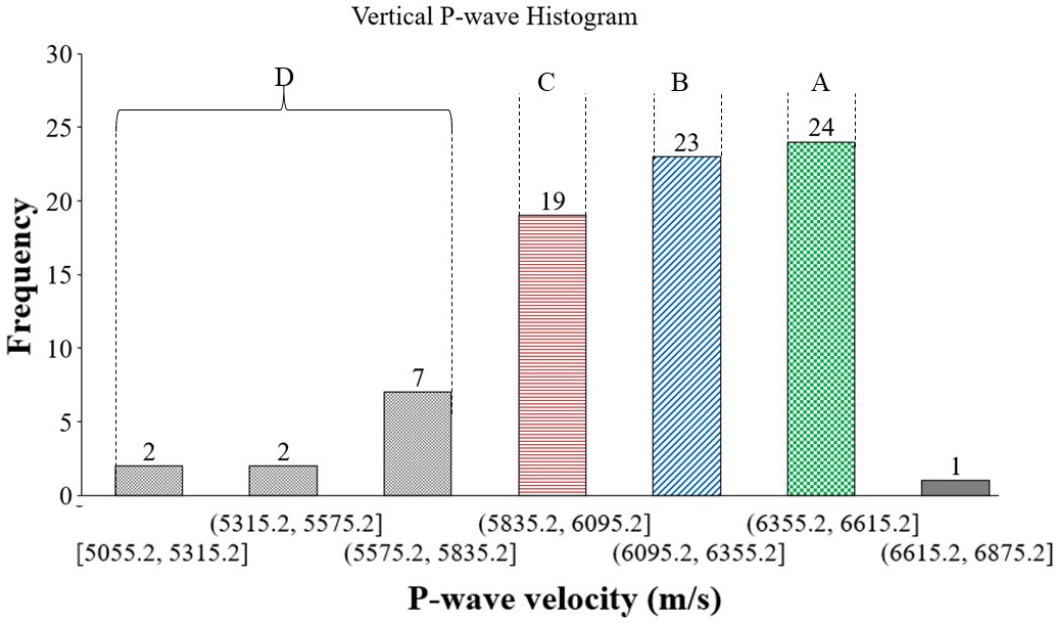

(a)

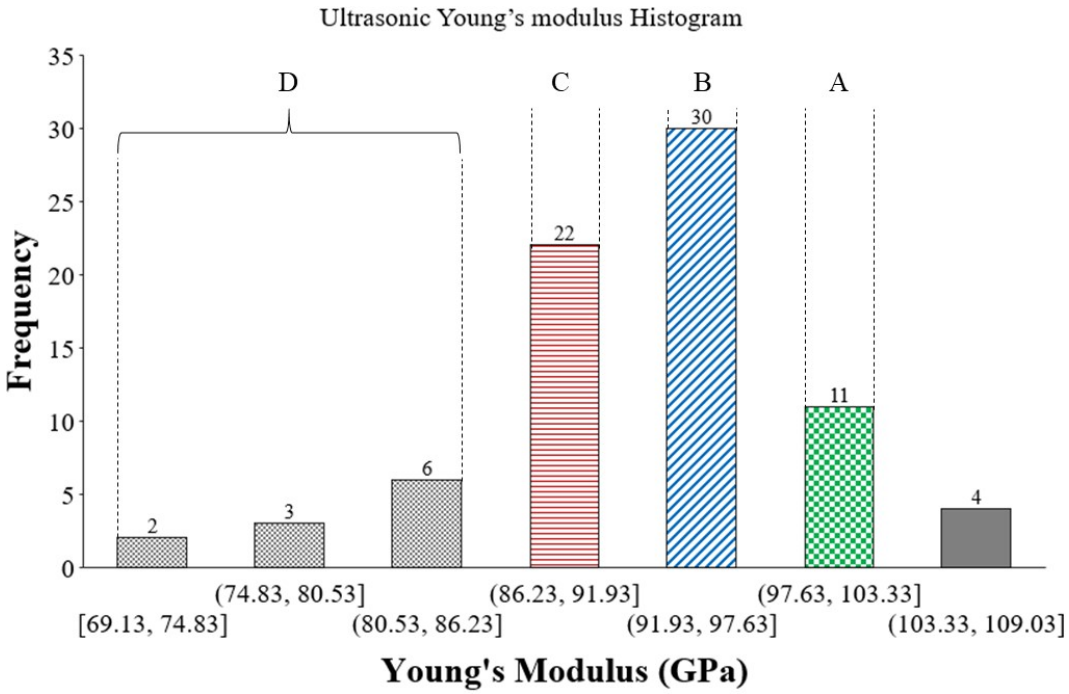

(b)

Figure 2.11. Histograms showing four main groups of tested rock samples based on (a) P-wave velocities and (b) dynamic Young's modulus.

Table 2.3. Comparison between rock type categories based on the ultrasonic measurements and thin section analysis.

Sample No.	Visual category	Full rock name and classification	P-wave velocity		Ultrasonic Young's Modulus	
			(m/s)	Class	(GPa)	Class
R1	4	Chlorite altered peridotite	≈6400	A	≈94	B
R2	4	Chlorite-carbonate altered peridotite	≈6400	A	≈94	B
R3	4	Chlorite-carbonate altered peridotite	≈6600	A	≈100	A
R4	1/3	Chlorite-epidote altered dolerite	≈5900	C	≈87	C
R5	4	Chlorite-epidote altered dolerite	≈5900	C	≈91	C
R6	1	Epidote-chlorite altered quartz dolerite	≈5350	D	≈79	D
R7	1	Epidote-chlorite altered quartz dolerite	≈6120	B	≈94	B
R8	5	Epidote-chlorite altered quartz dolerite	≈5800	D	≈88	C

Table 2.4. Comparison between the visual category, UCS and category determined from the ultrasonic measurements of the rock samples failed under unconfined compressive test.

Sample No.	UCS (MPa)	Visual Category	P-wave velocity		Ultrasonic Young's Modulus	
			(m/s)	Class	(GPa)	Class
UCT-1	138.49	4	≈6150	B	≈92	B
UCT-2	85.9	4	≈6350	B	≈94	B
UCT-3	135.97	4	≈6350	B	≈94	B
UCT-4	314.86	5	≈6000	C	≈96.5	B
UCT-5	267.86	1	≈6370	A	≈99	A

Note: The P-wave velocities and dynamic Young's modulus values of these samples are approximated from those of nearest samples.

2.4. Testing conditions

As already mentioned, all factors which might affect the testing results should be checked to obtain valid data required for a reliability-based design. Inherent variability and testing conditions can both affect the results of a physical or mechanical testing. The inherent variability which come from different physical parameters of the testing material is somehow unavoidable but still needs precise examination. The effect of these parameters has been checked throughout the previous section. However, it is dubious whether the scatter observed in the rock UCS data is a direct consequence of the inherent variability or not.

The variability due to the testing conditions could form another source of variability of the obtained mechanical properties. Among the possible sources, the sample-based variability coming from the shape deviation and machine-based variability coming from the equipment performance and the operational errors are discussed herein. In order to check these variabilities, a solid material with homogenous structure should be selected for testing in which the inherent variability is not of concern or otherwise ignorable. The testing variability could come from the shape deviation of the testing sample including flatness of its ends, perpendicularity, and parallelism related to the inaccuracy of the sample preparation, size effect pertinent to the different aspect ratio of the tested samples, or the loading machine performance. For samples with the same aspect ratios, the shape deviation and machine performance would be the remaining sources of variability affecting the test results. To check these types of variability, aluminum samples, as a standard medium with approximately homogenous structure, were selected for the control testing.

The test samples are fabricated by extrusion using 6061-T6 aluminum alloy, according to the Australian/New Zealand Standard: AS/NZS 1664.1 AS/NZS (1997) (AS/NZS, 1997). The samples are 39.96 mm in diameter with a L/D ratio of 2.0. Sixteen tests have been carried out on these samples with details outlined in Table 2.5. It should be noted that two strain gauges were attached on each sample on different positions, as specified in Table 2.5. Two axial and two lateral strains were recorded during each test. Samples were loaded within the elastic limit up to a maximum load level as described in Table 2.5. For repeatability of the obtained data, some tests have been conducted on the same sample. Two different loading frames were used for these tests to check the variabilities attributed to the accuracy and performance of the loading machine.

2.4.1. The effect of sample shape deviation

According to the standards, there are strict requirements for the preparation of a rock sample to determine its mechanical properties. The effect of shape deviation including flatness, perpendicularity, and parallelism of the prepared sample on the mechanical properties have already been investigated (Hawkes & Mellor, 1970; Hoskins et al., 1968; Štambuk et al., 2015). According to these investigations, the effects of the parallelism and perpendicularity of the rock sample on its UCS would be negligible. However, the end surface flatness can be a critical parameter and needs more assessment. The effect of the end flatness on rock mechanical properties, including the UCS, is more evident for hard rocks. This is shown in Figure 2.12 in which a big dependency of stronger rock like granite on the sample end surface texture variation (flatness) can be clearly seen. The end preparation has been shown to affect the uniaxial compressive strength of concrete by 6% for stronger samples, whereas the samples with low strength showed lower sensitivity to the quality of end flatness (Carino, 1994). The unground rock samples have lower strength compared to the ground and flat samples (Fukui et al., 2005). It was also reported that the rock failure mechanism could be changed from splitting failure to shear failure in unconfined compression test because of the end effect (Gao et al., 2018). These all indicate that the sample end flatness could greatly affect the mechanical properties of rocks. The flatness tolerance specified by the ASTM D4543-08 (ASTM, 2008b), is about 0.001 inch (25 μm), which is difficult to achieve, especially for hard rocks. Some attempts have been made to optimize the flatness tolerance. However, these attempts have only used a small data sample and were limited to only some rock types. There is, therefore, a promising avenue for further research in this area to answer the question of how and to what extent the surface end flatness affects the mechanical properties of rocks covering all rock types and probably to optimize or change the sample preparation requirements.

Table 2.5. Descriptions of the tests conducted on the aluminum samples.

Test No. (A-)		3	4	5	6	7	7-1	8	8-1	9	9-1	10	10-1	11	11-1	12	12-1
Sample No.		3	4	5	5	7	7	7	7	7	7	7	7	7	7	8	8
Loading Type	Static	✓	✓	-	-	✓	✓	✓	✓	✓	✓	✓	✓	✓	✓	✓	✓
	Cyclic	-	-	✓	✓	-	-	-	-	-	-	-	-	-	-	-	-
Loading Frame (LF)	"1"	✓	✓	✓	✓	✓	✓	-	-	-	-	-	-	✓	✓	✓	✓
	"2"	-	-	-	-	-	-	✓	✓	✓	✓	✓	✓	-	-	-	-
Max Load	kN	313	338	250	264	310	310	358	381	300	300	300	309	240	250	300	300
	MPa	250	270	200	210	248	248	285	303	240	240	240	245	190	200	240	240
Loading Rate	MPa / sec	0.1	0.1	0.1	0.1	0.1	0.1	-	-	-	-	-	-	0.1	0.1	0.1	0.1
	kN / min	-	-	-	-	-	-	7.5	7.5	7.5	7.5	7.5	7.5	-	-	-	-
	Hz	-	-	1	1	-	-	-	-	-	-	-	-	-	-	-	-
No. of strain gauges		2	2	2	2	2	2	2	2	2	2	2	2	2	2	2	2
Position of strain gauges	Top	-	-	-	-	SG-1				SG-2				SG-1			
	Middle	✓	✓	✓	✓	-				-				-			
	bottom	-	-	-	-	SG-2				SG-1				SG-2			
Remarks on strain gauges		Middle and opposite sides				Top and bottom on the same side											
Other Remarks		With spherical platens											Without spherical platens				

Notes: (1): Test N-1 was the same as Test-N while the sample turned 180 degrees with respect to the Test-N, N is the test number;
(2): SG stands for the strain gauge.

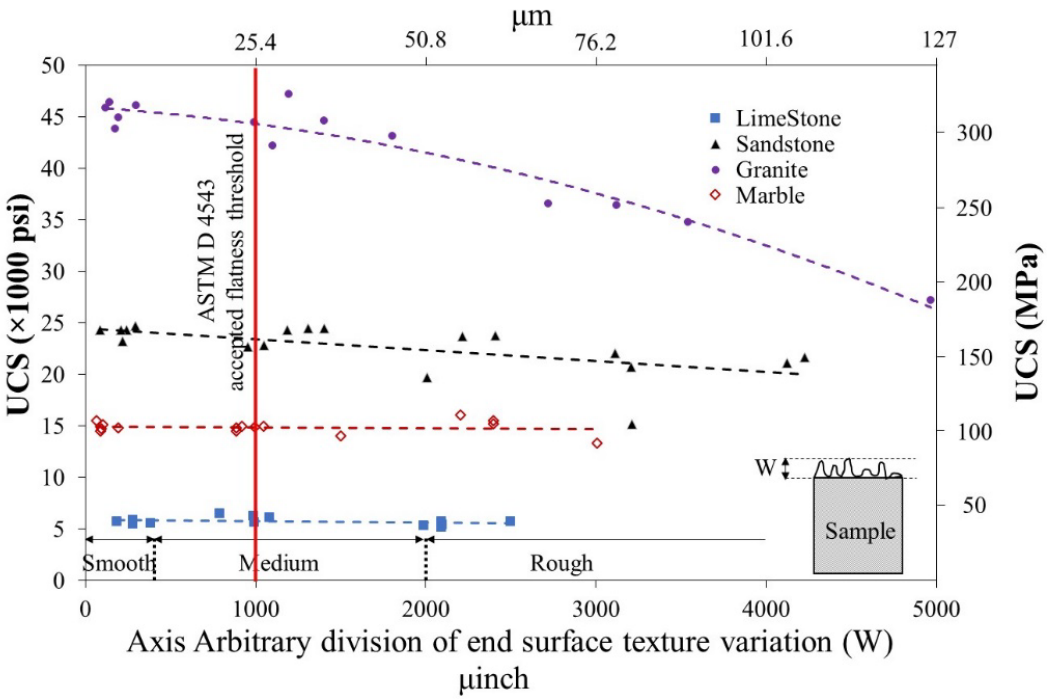

Figure 2.12. Effect of the sample end surface texture variation (flatness- W) on the UCS of rock, showing great dependency of hard rocks on the sample end flatness compared to weak rocks (modified after Hoskins & Horino (1968) and Štambuk et al. (2015)).

In this study, aluminum samples were ground almost flat with flatness less than 0.0005 in (<10 µm) using high-quality machinery to avoid the variation resulting from the non-flatness of the samples. On the other hand, the inherent variability of these samples is ignorable since the aluminum alloy used is approximately homogenous with stable properties. Therefore, any difference in the results of the UCS tests conducted on these samples could be attributed to either testing conditions (excluding shape deviation because all samples are flat with the same aspect ratio) or the loading machine performance. For this purpose, four tests (numbers 3 to 6) have been conducted either in quasi-static (monotonically loaded up to a stress level) or cyclic loading (loaded monotonically up to a stress level, unloaded again and then underwent repetitive loading-unloading stages under a constant frequency). The tests aimed to investigate: a) correctness and precision of the testing procedure (i.e. operation errors) and b) whether there is any unusual behavior related to the loading frame or not. Therefore, if the deformation responses of these tests match each other, it will show that the testing conditions and machine performance are quite satisfactory and the inconsistency in the UCS results of the tested rock samples could be caused by either the rock inherent

variability or inconsistent end surface flatness. Otherwise, it could be said that the testing conditions play a part in the inconsistency of the obtained UCS data of rock together with the inherent variability.

The strain gauge readings of these tests showed inconsistency in the deformation response of tested samples even for the same flat and homogenous sample. As can be seen in Figure 2.13, the strain recorded by SG-1 (strain gauge attached on the middle of the sample facing the front side of the machine) showed a noticeable difference from the strain recorded by SG-2 (strain gauge facing the back side of the machine) for all these four tests. This difference is about 20% for tests A-3 and A-6 (Table 2.6). Such huge differences indicate that the loading machine performance or the testing condition can be a source of variability of the test results. For further evaluations, tests A-7 and A-7-1 (with strain gauges attached on the same side of the sample at equal distances from its top and bottom) have been conducted on the same sample to see whether this discrepancy comes from the uneven loading of the sample or inconsistency in the strain gauge installation. It should be noted that test A-7-1 was conducted on the same sample (sample 7) while it was turned 180 degrees to check the loading condition of two sides of the loading frame. For these tests, the top and bottom axial strain gauges again showed different results – with 8.7% and 3.6% differences for the tests A-7 and A-7-1, respectively (Table 2.6). The top strain gauge (for test A-7 facing the front of the frame, and for test A-7-1 facing the back of the loading frame) showed 20% difference in recorded strain after the test. This amount was 10% for the bottom strain gauge. Hence, one side of the samples deforms more than the other side. This could be because of either uneven loading of the frame or tilting of the loading bar with respect to the sample end surfaces. It should be noted that the sample and strain gauge installation were identical for these two tests. Another conclusion is that the scatter data obtained for the UCS of the rock samples is not necessarily related to the shape deviation or rock inherent variabilities, as the loading machine also plays a role in the scatter of the results.

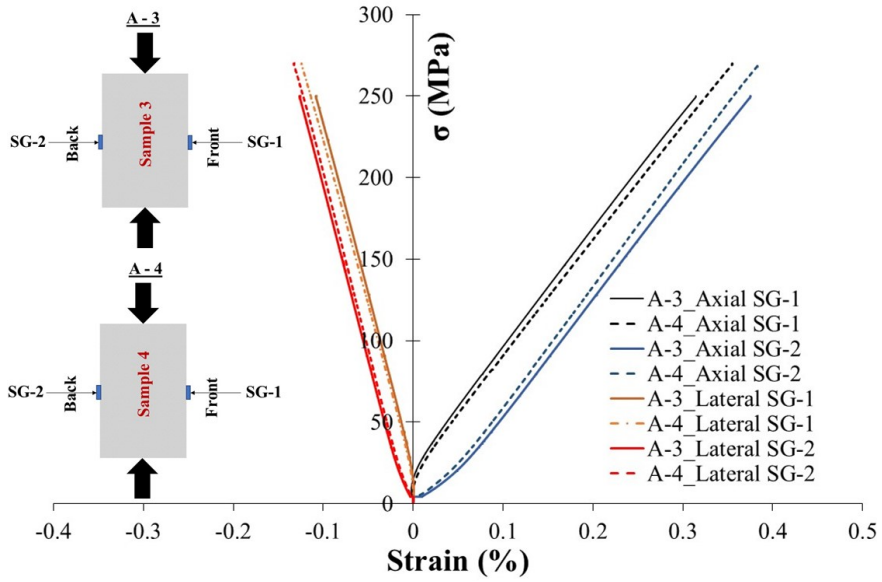

(a)

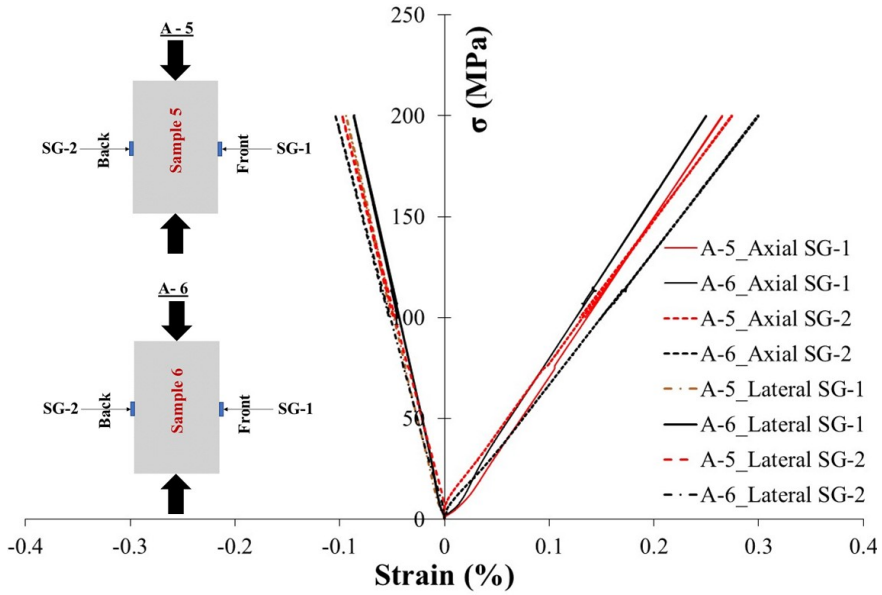

(b)

Figure 2.13. Stress–strain response of tests number: (a) 3, 4, and (b) 5, and 6, conducted on the aluminum samples.

Table 2.6. Comparison of axial strains recorded by strain gauges attached on different points of the aluminum samples.

Test number(A-)	Axial strains recorded by gauges attached on						Difference (%)	@Stress (MPa)	Strain gauges				Other Remarks		
	Top		Middle		Bottom				Top	Middle	Bottom	Position			
	Front	Back	Front	Back	Front	Back									
3	-	-	✓	✓	-	-	19.3	250	-	✓	-	Middle and opposite sides	With spherical platens	LF1	
4	-	-	✓	✓	-	-	9.1								
3 and 4	-	-	✓	-	-	-	4.7								
3 and 4	-	-	-	✓	-	-	4.3								
5	-	-	✓	✓	-	-	3.4	200							
6	-	-	✓	✓	-	-	19.8								
7	✓	-	-	-	✓	-	8.7	245	SG-1	-	SG-2	Top and bottom on the same side			
7-1	-	✓	-	-	-	✓	3.6								
7 and 7-1	✓	✓	-	-	-	-	20								
7 and 7-1	-	-	-	-	✓	✓	10								
8	✓	-	-	-	✓	-	5.5	280							
8-1	-	✓	-	-	-	✓	5.4								
8 and 8-1	✓	✓	-	-	-	-	0.6								
8 and 8-1	-	-	-	-	✓	✓	10								
9	✓	-	-	-	✓	-	10.1	238	SG-2	-	SG-1			LF2	
9-1	-	✓	-	-	-	✓	4.8								
9 and 9-1	✓	✓	-	-	-	-	39.6								
9 and 9-1	-	-	-	-	✓	✓	46.7								
10	✓	-	-	-	✓	-	0.8	238					Without spherical platens		
10-1	-	✓	-	-	-	✓	4.9								
10 and 10-1	✓	✓	-	-	-	-	33.5								
10 and 10-1	-	-	-	-	✓	✓	41.2								
11	✓	-	-	-	✓	-	1.2	190	SG-1	-	SG-2			LF1	
11-1	-	✓	-	-	-	✓	0.13								
11 and 11-1	✓	✓	-	-	-	-	>80								
11 and 11-1	-	-	-	-	✓	✓	>80								
12	✓	-	-	-	✓	-	1.8	240							
12-1	-	✓	-	-	-	✓	1.4								
12 and 12-1	✓	✓	-	-	-	-	>40								
12 and 12-1	-	-	-	-	✓	✓	>40								

Notes: (1): Test A-N-1 was the same as A-N while the sample turned 180 degrees with respect to the A-N, N is any number,
(2): Differences are calculated for the axial strains only, and
(3): SG stands for the strain gauge and LF stands for the Loading Frame.
(4): Tests on aluminum are named with A-N format such A-12, A-5, etc.

2.4.2. Loading machine performance

Further analysis of the test results carried out by the loading frame "1" (LF1) indicates that the back side of the samples showed higher strain than the front side. It was found that this behavior is characteristic of almost all tests carried out by this loading frame on both rock and aluminum samples (Figure 2.14 and Figure 2.15). All these comparisons can be seen in Table 2.6. This issue was also numerically investigated which will be discussed in Section 2.5. For better assessment of the testing conditions, another loading frame ("LF2") was chosen to repeat these tests to check the observed

behavior. Two tests (tests A-8 and A-8-1) with the same procedure taken during tests A-7 and A-7-1 were conducted on the same sample (No. 7) in order to avoid any change in strain gauge installation and the sample itself. The results showed that the strain recorded by the top strain gauge still differs about 5.5% from the bottom one (Table 2.6). However, their differences are lower than what have been recorded for tests A-7 and A-7-1 (8.7%). The top strain gauges for these two tests showed almost the same readings with less than 0.6% error throughout the tests, while it was more than 20% for tests A-7 and A-7-1 carried out by loading frame "1" (LF1). This could be an indication of the better performance of LF2. The bottom strain gauges for these two tests (tests A-8 and A-8-1), however, showed the same differences as recorded in tests A-7 and A-7-1 (10%). Tests A-8 and A-8-1 have been repeated with the same sample inverted so that SG-2 is at the top and SG-1 is at the bottom to see if the platens on the bottom or the spherical seat on the top contribute to the different results. These two tests were named tests A-9 and A-9-1 (Table 2.5). No improvement has been observed and there was still mismatch between the strains. The strains recorded by the bottom and top strain gauges still showed ≥40% differences (refer to differences for tests A-9 and A-9-1 in Table 2.6).

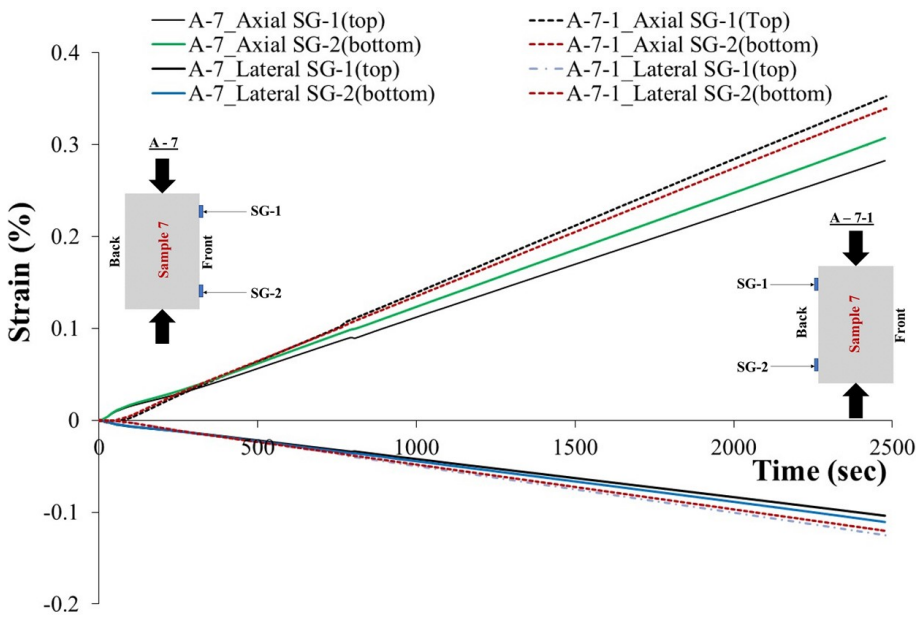

Figure 2.14. Strain development of test A-7 and test A-7-1 conducted on the same aluminum sample by the loading frame LF1, showing more deformation recorded by the strain gauges facing the back of the loading frame compared to when they are facing the front of the loading frame.

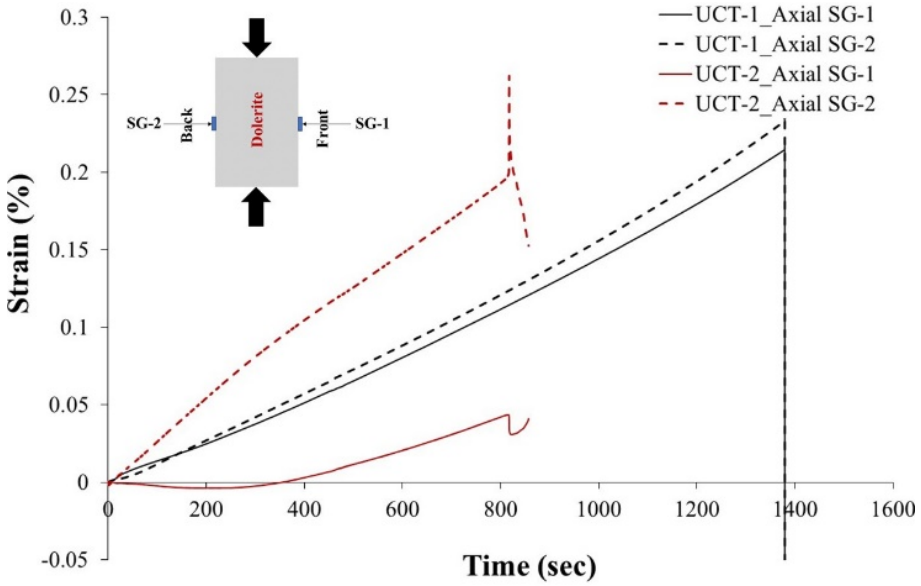

(a)

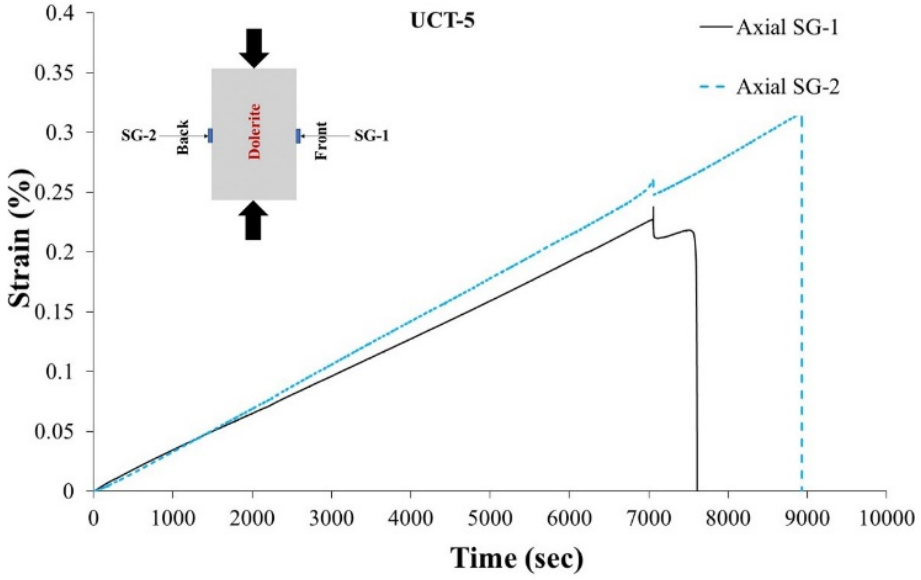

(b)

Figure 2.15 (continued on the next page).

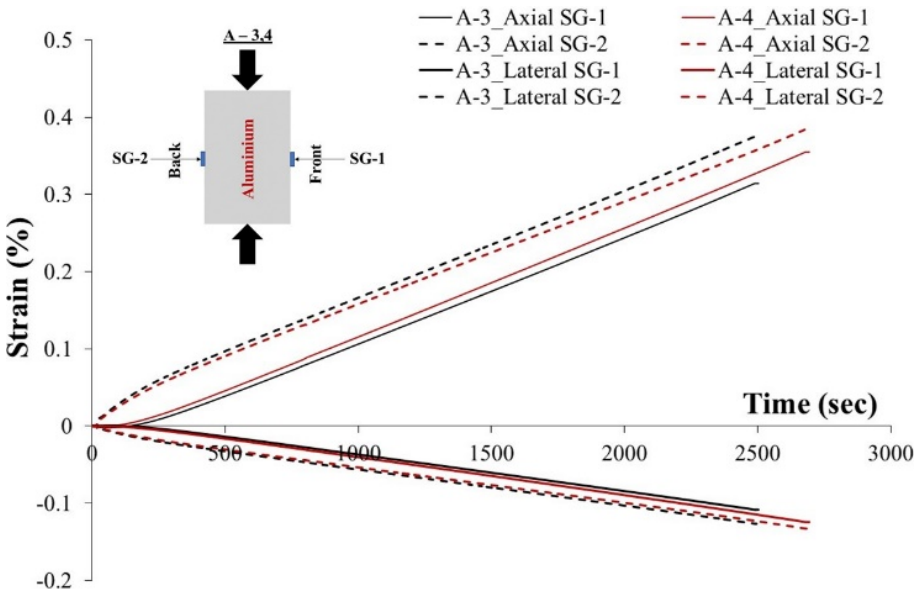

(c)

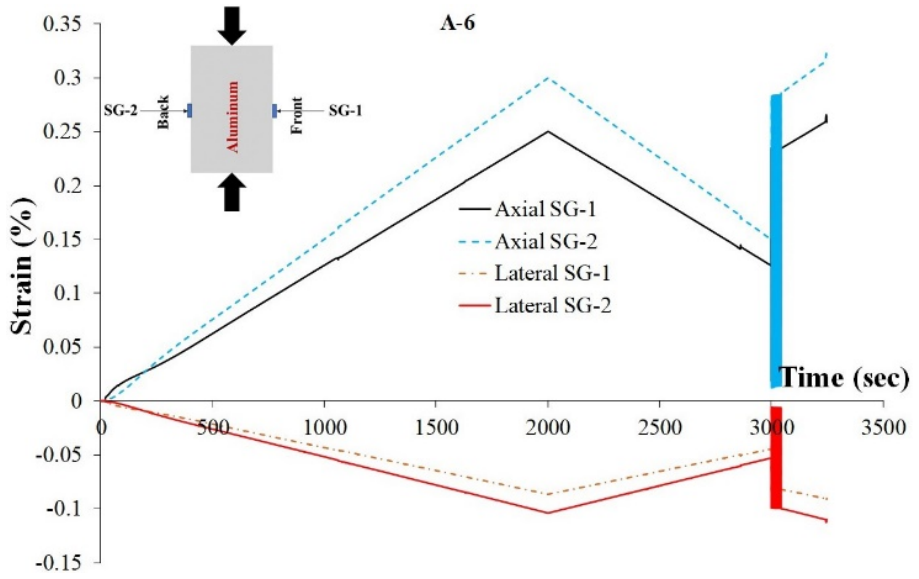

(d)

Figure 2.15 (continued from previous page). Strain curves of the tests: (a) UCT-1 and UCT-2 on Dolerite samples; (b) UCT-5 on Dolerite sample; (c) tests A-3 and A-4 on aluminum samples; (d) Test A-6 on aluminum sample, conducted by the loading frame LF1, indicating more strain recorded by the strain gauges facing the back of the loading frame compared when they are facing the front of the loading frame.

Although the best effort has been made to centralize the sample, the platens and spherical seats with respect to the loading frame and one another, the effect of spherical

seats on the observed strain behavior was unclear. For this purpose, six more tests have been conducted with both loading frames using flat loading platens instead of the spherical ones between the sample end and the loading frame. As can be seen from Table 2.6, the results revealed a good agreement between the strain data of the top and bottom strain gauges for all these six tests (tests A-10 to A-12-1). The strain curves of tests A-10 and A-11-1 are shown in Figure 2.16, for example. However, the comparison between recordings of the top strain gauges (for example the top strain gauge of test A-10 with the top strain gauge of test A-10-1) with each other and the bottom strain gauges with each other for all these tests, on the other hand, still showed a poor agreement and huge differences (33.5% and 41.2% for the top and bottom strain gauges, respectively, see Table 2.6).

Detailed analysis of data for tests A-11 to A-12-1 conducted by loading frame LF1 revealed another observation. As can be seen in Figure 2.17, there is mismatch between the measurements of the top and bottom strain gauges in both tests A-11 and A-12 (when the strain gauges face the front of the machine), whereas, for samples turned 180 degrees (the strain gauges face the back of the machine) for tests A-11-1 and A-12-1, all strain measurements are quite the same. The consistency in the last obtained data reveals that both the testing procedure and strain gauge installation were quite accurate and there was no variability because of the operation error and eccentricity of the cylinder axis. On the other hand, it also indicates that the spherical platens might be a source of variability in the obtained rock testing results and can induce non-uniform loading on the sample. It is despite the fact that the spherical platens are especially used to compensate the variations in the parallelism of the sample's ends and to transmit the axial load uniformly. In summary, these observations show that although both loading frames were calibrated and the testing procedure was the same for all conducted tests, the machine performance itself and precision of its attached equipment greatly affects the testing condition and in turn rock laboratory test results. In the next section, this finding will be verified through numerical analysis.

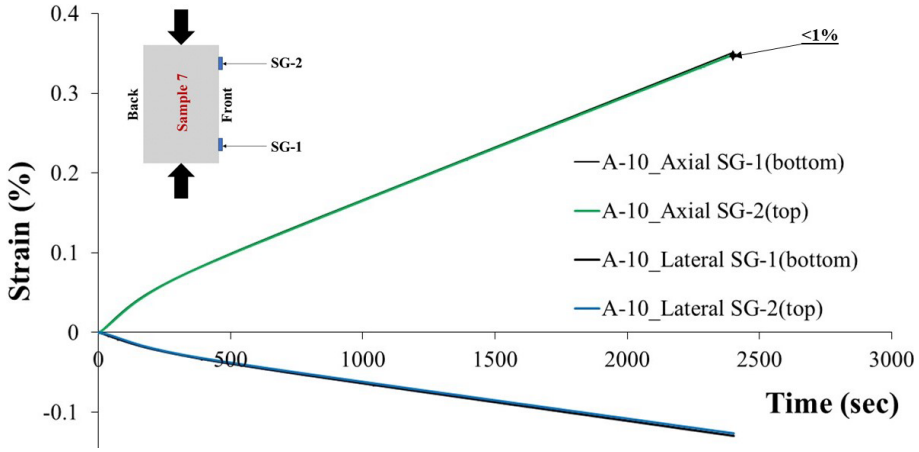

(a)

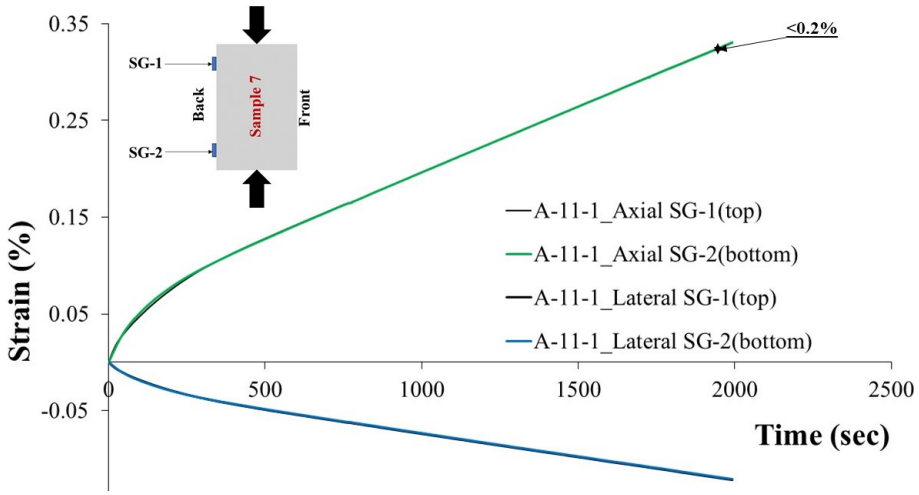

(b)

Figure 2.16. Strain curves obtained in the loading frames with flat loading platens: (a) test A-10; (b) test A-11-1, conducted with loading fame LF2 and LF1, respectively. Good agreement is seen between the strain recordings of top strain gauges with the bottom ones when the straight platens were used instead of the spherical platens between the sample end and loading frame.

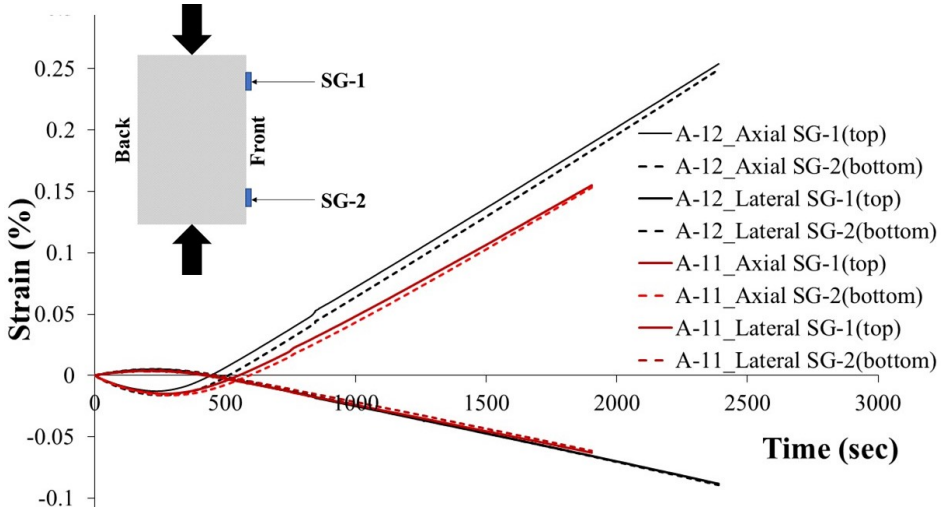

(a)

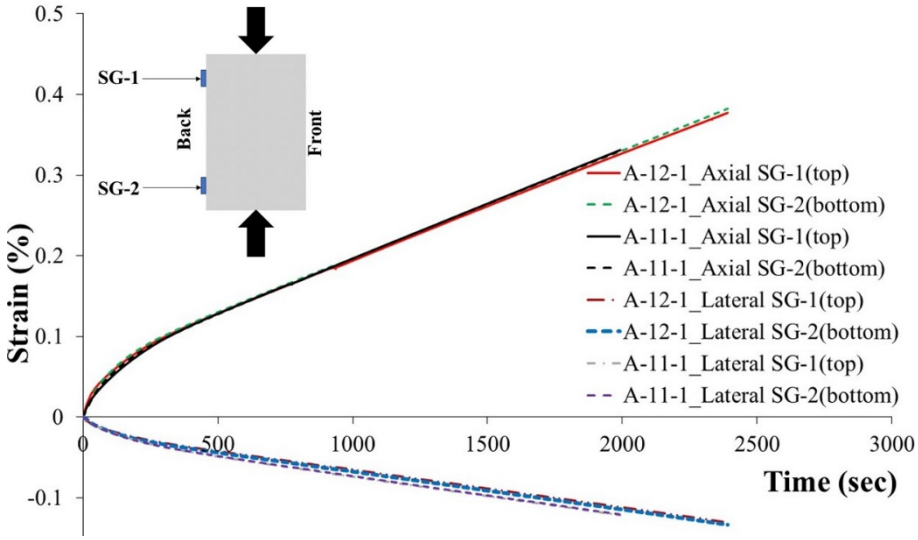

(b)

Figure 2.17. Comparison between strain developments of the top and bottom strain gauges when they are facing (a) the front (test A-11 and A-12); (b) the back ((tests A-11-1 and A-12-1) of loading frame LF1, conducted without spherical platens.

2.5. Numerical Analysis

In order to explore the effect of testing conditions on the obtained results, Finite Element Method (FEM) simulations have been carried out using ABAQUS3D 6.14 (ABAQUS, 2014). For this purpose, two tests, A-11 and A-11-1, were taken as targets of this simulation. The aim of this numerical analysis was to find the effects of misalignment, non-axiality or other factors that affect the experimental measurements.

The parameters of the generated model, dimensions, and material properties are listed in Table 2.7. Two contact interfaces were defined at the top and bottom of the sample with normal and tangential properties. The pressure-overclosure behavior of the normal contact elements was considered as a hard contact during the numerical analysis. The bottom bar of the model was fixed in 3 directions (x, y, and z). The top plate of the model was fixed in 2 directions (x and y). A constant uniform pressure of 54.125 MPa is applied on the surface of the cylindrical plate to induce the same loading condition as in the experiments. The lateral surfaces of the cylindrical sample were free of load. The loading rate throughout the test was the same as in the experiments. The element type C3D8 is considered for mesh generation which is defined as Continuum 3 Dimensional 8 Nodal elements. 1918 3D elements were considered for the analysis (Figure 2.18). Firstly, an ideal condition in which sample and the loading platens are in direct contact with each other with neither non-axiality nor misalignment was simulated to obtain the strain development throughout the test. Then, back analysis was undertaken in which the top plate and bottom bar were either tilted or moved with respect to the aluminum sample to see the effects of these defects on the strain results and to reproduce the actual strain data of tests A-11 and A-11-1.

This numerical analysis shows that the transition (movement of the center of either top plate or bottom bar with respect to the center of the sample, i.e. eccentricity) does not affect the strain curves of the aluminum sample throughout the test if its end surfaces are in complete contact with the top platen and bottom bar. On the other hand, the strain curves are very sensitive to the misalignment of the top plate and bottom bar. A very small angular change of touching end surfaces of these two components with respect to the sample (tilt) greatly affects the overall trend and results of the strain development of the sample.

Table 2.7. Different components of the model generated for numerical analysis in ABAQUS, dimensions, and the material properties.

	Diameter (mm)	Height (mm)	E (GPa)	ν
Aluminum Sample	39.96	77.1	70	0.33
Top cylindrical steel plate	75	39.72	200	0.27
Bottom steel bar	54	54	200	0.27

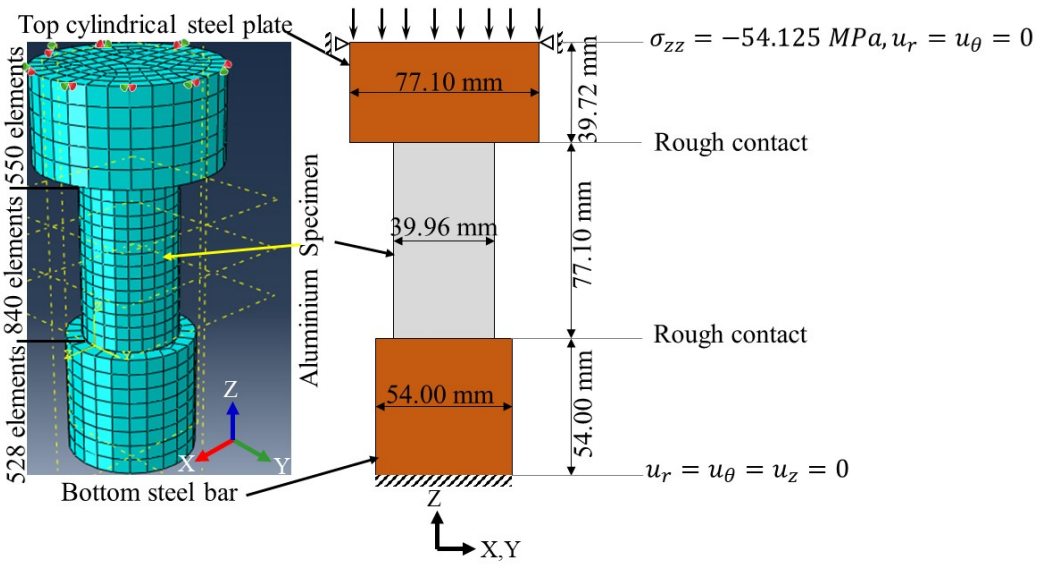

(a) (b)

Figure 2.18. Numerical uniaxial compressive test set-up for the aluminum sample: (a) FEM model; (b) sample and platen dimensions with boundary conditions. Rough contact is a contact on which all relative sliding movement between two surfaces is prevented by specifying an infinite coefficient of friction.

This model has been run with different tilt angles to reproduce the experimental results. Finally, a tilt angle of the plate of 0.106° was selected as an angle in which the numerical result is in good agreement with the experimental data. The axial and lateral strain contours of the sample after this simulation can be seen in Figure 2.19. It should be mentioned that the top plate and bottom bar have been tilted from the right side (View A in Figure 2.19) of the model and a gap between them and the sample has been created on the left side of the model (View b in Figure 2.19). So, the strain results of the right side and left side of the model were compared with the experimental data of tests A-11-1 and A-11, respectively. Four measurement points of the model were exactly on the same points where the strain gauges were installed (Figure 2.19). The strain development of the numerical model was compared with the experimental data in Figure 2.20. What stands out in this figure, is the curves of the strain obtained in the numerical simulation with 0.106° tilt of the top plate and bottom bar which are the same as in the experiments. This is more obvious when the experimental and numerical data are compared with that of the ideal condition simulated numerically. The final strains of the numerical simulations differ by less than 8% from that of the experiments which are acceptable. This difference could be because of the operational errors during the

experiments in turning the sample 180° or installation of the strain gauge in an identical distance from the top and bottom. It can, therefore, be concluded that the discrepancy in the results, compared to an ideal condition, is mainly due to the misalignment or tilt of the top and bottom plate with respect to the sample.

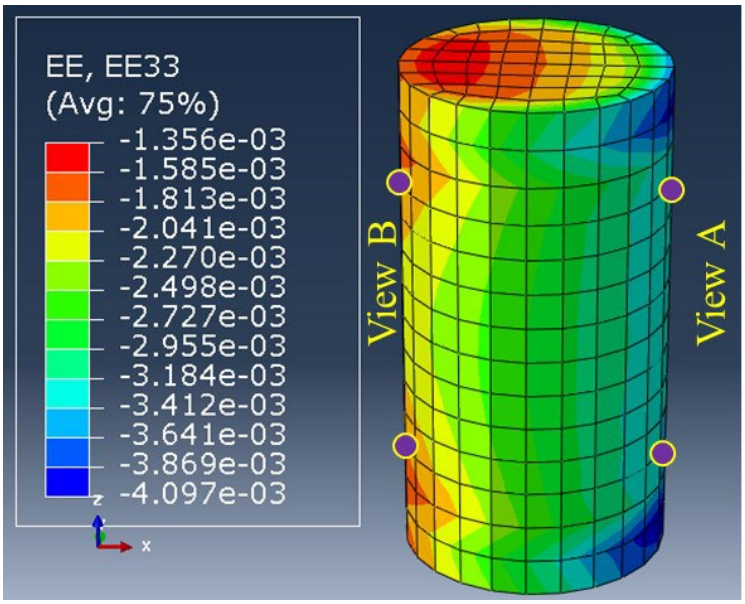

(a)

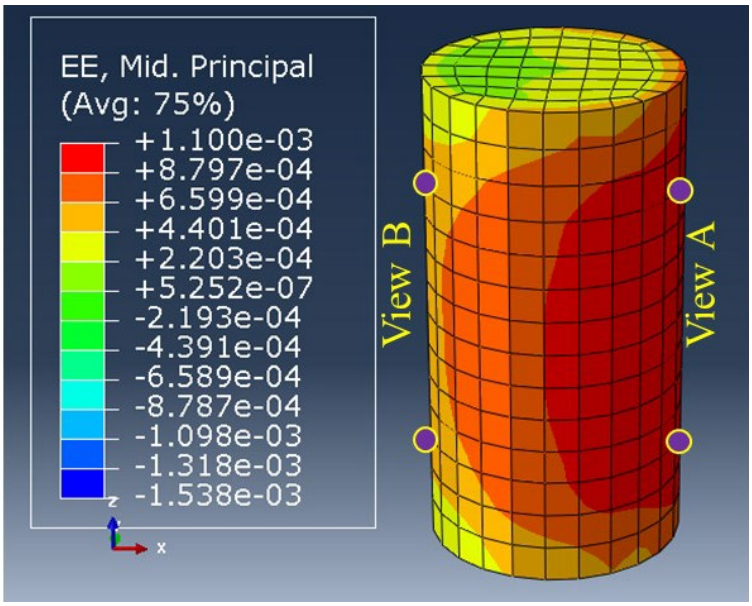

(b)

Figure 2.19. Results of the FEM modelling: the axial (a) and lateral (b) strain contours of the aluminum sample with 0.106° angular tilt of the top plate and bottom bar with respect to the sample; four measurement points are also shown.

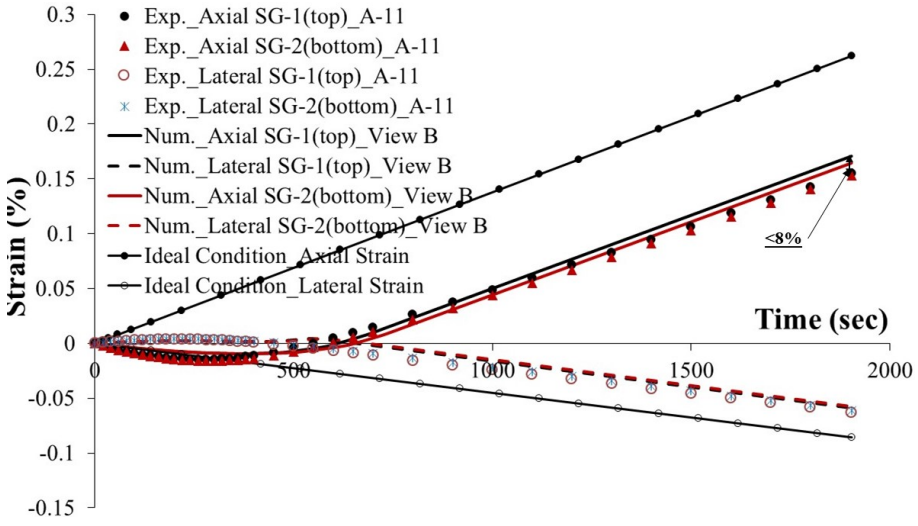

(a)

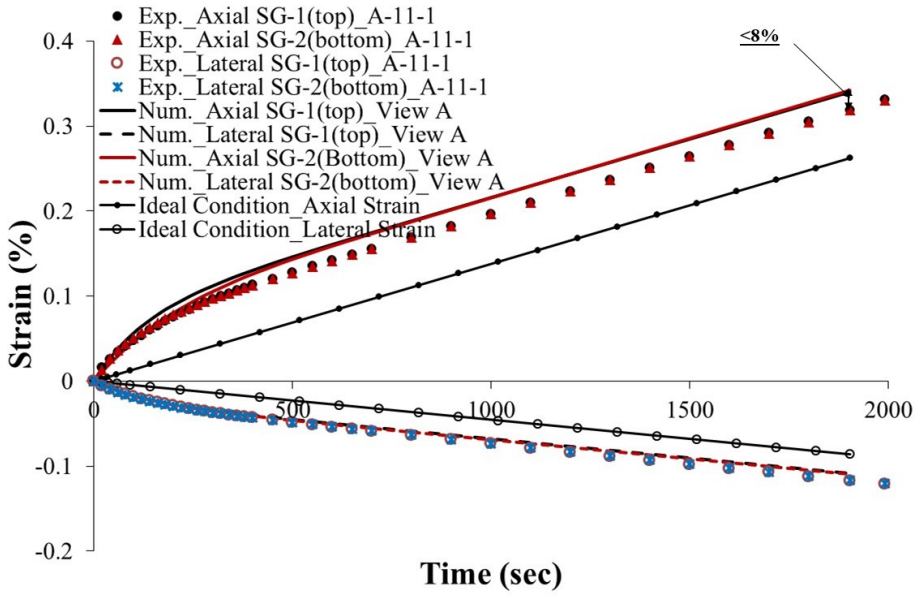

(b)

Figure 2.20. Comparison of the strain curves obtained from the numerical simulations in both ideal conditions and with misalignment with the experimental data for (a) test A-11 and (b) test A-11-1. Exp. and Num. stand for Experimental and Numerical, respectively.

This numerical simulation strongly proves that a minor defect or inadequate precision of the equipment setup can affect the experimental results. This finding clearly explains that testing conditions are of great importance and as such they need to be carefully examined.

Therefore, it is concluded that some modifications need to be made to the relevant standards to address the required precision and performance of the testing equipment before the commencement of any rock testing. Such probable guidelines would not only minimize the operational errors, but also assure an experimentalist that the rock testing equipment is sufficiently accurate to carry out a test and to obtain valid data.

2.6. Pre-existing microcracks

In the previous sections, it was presumed that either the inherent rock properties or the testing conditions might affect the obtained test results. There might also be other factors like pre-existing micro-cracks which cannot be considered as an inherent feature, however, they can be formed either during the mineralization due to temperature and pressure gradient or during the operational activities of core taking and sample preparation. Such microstructural features and initial damage can noticeably affect the laboratory test results (Eberhardtv et al., 1998; Pakzad et al., 2018). In this study, the Computational Tomography (CT), as an NDT technique, was used to characterize some of the rock (dolerite) samples. Even qualitatively, the CT can provide useful information about the invisible rock features like cracks, heterogeneity, and change in lithology. This test showed that there might be some pre-existing micro-cracks inside the rock samples which can neither be detected by the thin section analysis since it might be outside the sections taken for this analysis nor by the ultrasonic measurements because of the insufficiently wide frequency band of the transducers used for the purpose. It should also be mentioned that it is almost impossible to detect such tiny cracks visually. For example, an inclined tiny crack was detected inside a dolerite sample, while it has neither been detected visually nor through the ultrasonic test. As shows in Figure 2.21, this crack starts from the bottom of the sample and extends almost toward the middle. This crack could greatly affect the strength properties of the rock sample. Therefore, CT scanning is an excellent tool to detect invisible rock features required to be explored for better understanding of rock behavior.

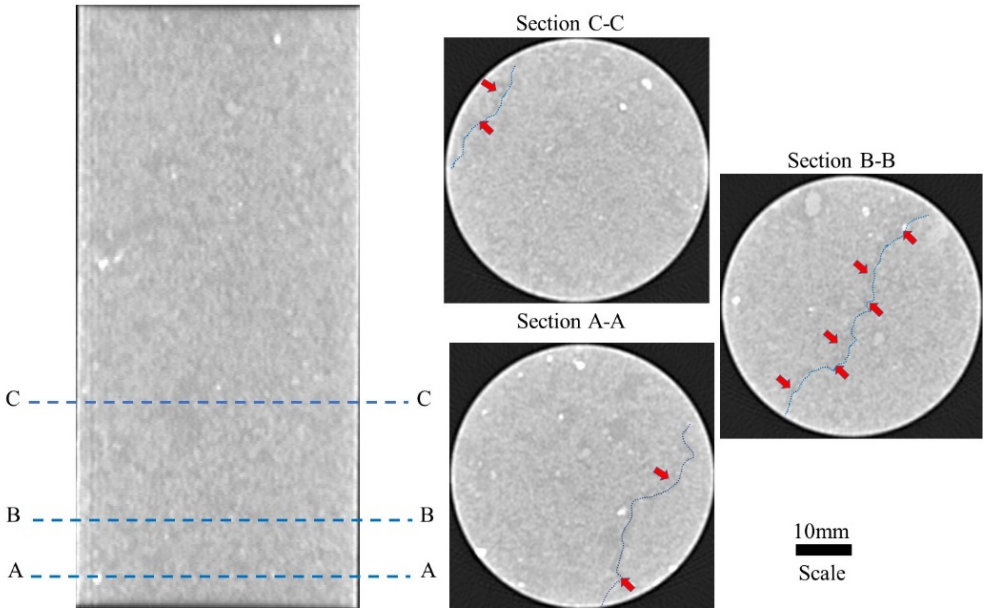

Figure 2.21. CT scan slices for a dolerite sample showing a tiny pre-existing microcrack inside the sample.

2.7. Conclusions

This study set out to explore the affecting factors behind the variations in UCS results for dolerite rock samples. Another objective of this study was to see the difference between the rock sample categorizations made, based on the inherent parameters, including mineralogy and ultrasonic elastic constants. Although these categorizations are trivial and by no means new, the integration of this technique with others (e.g. cross-checking between the categorization based on visual inspection, thin section analysis and ultrasonic measurement) may provide new insights. This will be beneficial for an experimentalist to categorize a set of real samples from the field. In general, it seems that in any rock engineering project, the rock samples selected for the experimental analysis need precise examinations rather than simply visual inspections. These examinations include but are not limited to analyzing the inherent properties such as mineralogy and ultrasonic elastic constants. The ultrasonic measurement of P-wave velocity has been found to be a straightforward and quick way of having a proper estimation of the mechanical properties of rock samples. The rock categorization based on the ultrasonic P-wave velocities has been determined to be as accurate as the thin

section analysis, which suggests that they can be used together to get a more accurate preliminary evaluation of the rock types before carrying out any experimental tests.

It has been found that, among all variability sources investigated, the test results were affected by the sample shape deviation, mineralogical differences due to the different kinds of the alterations, and testing conditions. The rocks' inherent variability is unavoidable since rocks vary in spatial and time domain, however, the variability because of the sample preparation could be at least reduced to an acceptable level. Here, we raise the possibility that the existing standard for the sample preparation, specially the end flatness, might not be good enough. An FEM analysis was implemented to check the effect of the testing conditions – specifically the loading plate deviation – and it has been found that the tilt/misalignment of the top plate and bottom steel bar with respect to the sample was the main reason of the discrepancies in the results. Therefore, the testing condition and loading machine performance have been found to act as hidden factors often not seen but affecting the laboratory test results. It seems that the standards for rock sample preparation and test instructions need to be modified to answer the questions of how and to what extent they can affect the laboratory tests results for all types of rock testing. More research could provide such information to establish a greater degree of test accuracy – this could include conducting comprehensive tests on different rock types considering the effect of sample shape deviation, especially the end flatness, the loading frame precision, the design and setup considerations of the spherical seats. Therefore, control tests with minimal variation in sample preparation, using a homogenous fabricated medium alongside the back analysis using FEM, are highly recommended to improve the loading quality.

The spherical seats also need to undergo quality control to monitor the change in deformational behavior of the sample, by conducting some tests with and some tests without them. The interface friction between the spherical seats themselves and between the sample and loading platens should also be reduced. Using lubricants, which has been recommended by the relevant standards, might help but it does not remove the sample-platen friction and the end effect completely. This has also been addressed in other investigations (Xu et al., 2017). Using hydraulic spherical seats instead of the mechanical ones could be of assistance.

Finally, it has been emphasized that while it is almost impossible to identify pre-existing microcracks either visually or through the thin section analysis and even the ultrasonic measurements, they may play a considerable role in rock test results. The CT

scanning technique would allow experimentalists to detect such defects inside the rock samples. It is recommended that this technique to be included into the relevant standards as an accurate way for pre-assessment of the rock samples.

Improving the quality of rock testing and reducing the scatter of the results will improve our understanding of the mechanics of rock deformation and failure and will assist in avoiding large scale rock failures.

Acknowledgements

This research was funded by both the Curtin Strategic International Research Scholarship (CSIRS) and Mining Research Institute of Western Australia (MRIWA) scholarship. The support provided by both institutions is highly acknowledged. The authors also would like to thank the departments of Mining and Metallurgical Engineering and Petroleum Engineering of Western Australian School of Mines (WASM), Curtin University for the provided laboratory facilities. We are thankful to Prof. Ernesto Villaescusa and Pat Hogan for their supports throughout the laboratory experiments. The collaborations of the Norton Gold Fields company in providing rock cores and the Commonwealth Scientific and Industrial Research Organization (CSIRO) of the Western Australia in providing access to a CT scanner are also highly appreciated. The third author would also like to acknowledge the support from the Australian Research Council through project DP190103260.

References

ABAQUS. (2014). Abaqus 6.14: analysis user's manual. *Dassault Syste`mes Simulia Corp, Providence*.

Abdulai, M., & Sharifzadeh, M. (2019). Uncertainty and Reliability Analysis of Open Pit Rock Slopes: A Critical Review of Methods of Analysis. *Geotechnical and Geological Engineering*, *37*(3), 1223–1247. https://doi.org/10.1007/s10706-018-0680-y

Adams, C., & Dentith, M. (2018). Defining Petrophysical Properties of Ultramafic and Mafic Rocks In Terms of Alteration. *ASEG Extended Abstracts*, *2018*(1), 1–8. https://doi.org/10.1071/ASEG2018abW9_4F

AS/NZS. (1997). Aluminum Structures Part 1: Limit State Design, Australian/New Zealand Standard AS/NZS 1664.1:1997. *Standards Australia*. Sydney, Australia: Standards Australia.

ASTM. (2008a). ASTM D2845-08, Standard Test Method for Laboratory Determination of Pulse Velocities and Ultrasonic Elastic Constants of Rock (Withdrawn 2017). *ASTM International*. Retrieved from www.astm.org

ASTM. (2008b). *ASTM D4543-08, Standard Practices for Preparing Rock Core as Cylindrical Test Specimens and Verifying Conformance to Dimensional and Shape Tolerances*. Retrieved from https://doi.org/10.1520/D4543-08

Aydin, A. (2014). Upgraded ISRM Suggested Method for Determining Sound Velocity by Ultrasonic Pulse Transmission Technique. *Rock Mechanics and Rock Engineering*, *47*(1), 255–259. https://doi.org/10.1007/s00603-013-0454-z

Brady, B. T. (1971). Effects of inserts on the elastic behavior of cylindrical materials loaded between rough end-plates. *International Journal of Rock Mechanics and Mining Sciences & Geomechanics Abstracts*, *8*(4), 357–369. https://doi.org/https://doi.org/10.1016/0148-9062(71)90047-7

Carino, N. J. (1994). Effects of Testing Variables on the Strength of High-Strength (90 Mpa) Concrete Cylinders. *Special Publication*, *149*. https://doi.org/10.14359/4176

Du, K., Su, R., Tao, M., Yang, C., Momeni, A., & Wang, S. (2019). Specimen shape

and cross-section effects on the mechanical properties of rocks under uniaxial compressive stress. *Bulletin of Engineering Geology and the Environment*. https://doi.org/10.1007/s10064-019-01518-x

Duzgun, H. S. B., Yucemen, M. S., & Karpuz, C. (2002). A probabilistic model for the assessment of uncertainties in the shear strength of rock discontinuities. *International Journal of Rock Mechanics and Mining Sciences*, *39*(6), 743–754. https://doi.org/https://doi.org/10.1016/S1365-1609(02)00050-3

Eberhardt, E., Stead, D., Stimpson, B., & Read, R. S. (1998). Identifying crack initiation and propagation thresholds in brittle rock. *Canadian Geotechnical Journal*, *35*(2), 222–233. https://doi.org/10.1139/t97-091

Fukui, K., Okubo, S., & Terashima, T. (2005). Electromagnetic Radiation from Rock During Uniaxial Compression Testing: The Effects of Rock Characteristics and Test Conditions. *Rock Mechanics and Rock Engineering*, *38*(5), 411–423. https://doi.org/10.1007/s00603-005-0046-7

Gao, M., Liang, Z., Li, Y., Wu, X., & Zhang, M. (2018). End and shape effects of brittle rock under uniaxial compression. *Arabian Journal of Geosciences*, *11*(20), 614. https://doi.org/10.1007/s12517-018-3957-9

Gill, D. E., Corthésy, R., & Leite, M. H. (2005). Determining the minimal number of specimens for laboratory testing of rock properties. *Engineering Geology*, *78*(1), 29–51. https://doi.org/https://doi.org/10.1016/j.enggeo.2004.10.005

Hadjigeorgiou, J., & Harrison, J. P. (2011). Uncertainty and Sources of Error in Rock Engineering. *12th ISRM Congress*, p. 5. Retrieved from https://doi.org/

Hawkes, I., & Mellor, M. (1970). Uniaxial testing in rock mechanics laboratories. *Engineering Geology*, *4*(3), 179–285. https://doi.org/https://doi.org/10.1016/0013-7952(70)90034-7

Hemami, B., & Fakhimi, A. (2014). Numerical Simulation of Rock-Loading Machine Interaction. *48th U.S. Rock Mechanics/Geomechanics Symposium*, p. 7. Retrieved from https://doi.org/

Hoskins, J. R., Horino, F. G., & States., U. (1968). *Effect of end conditions on determining compressive strength of rock samples* (p. 22 p.). p. 22 p. Retrieved from file://catalog.hathitrust.org/Record/005980245

Hudson, J. A., Crouch, S. L., & Fairhurst, C. (1972). Soft, stiff and servo-controlled

testing machines: a review with reference to rock failure. *Engineering Geology*, *6*(3), 155–189. https://doi.org/https://doi.org/10.1016/0013-7952(72)90001-4

ISRM. (1979a). *SM for Determining the Uniaxial Compressive Strength and Deformability of Rock Materials*.

ISRM. (1979b). *Suggested Method for Petrographic Description of Rocks*.

Kuhinek, D., Zorić, I., & Hrženjak, P. (2011). Measurement Uncertainty in Testing of Uniaxial Compressive Strength and Deformability of Rock Samples. *Measurement Science Review*, *11*(4), 112–117. https://doi.org/https://doi.org/10.2478/v10048-011-0021-2

Labuz, J. F., & Biolzi, L. (2007). Experiments with rock: Remarks on strength and stability issues. *International Journal of Rock Mechanics and Mining Sciences*, *44*(4), 525–537. https://doi.org/https://doi.org/10.1016/j.ijrmms.2006.09.005

Liang, C. Y., Zhang, Q. B., Li, X., & Xin, P. (2016). The effect of specimen shape and strain rate on uniaxial compressive behavior of rock material. *Bulletin of Engineering Geology and the Environment*, *75*(4), 1669–1681. https://doi.org/10.1007/s10064-015-0811-0

Masoumi, H., Arefi, A., Hagan, P., Roshan, H., & Sharifzadeh, M. (2017). An Improvement to Unified Size Effect Law for Intact Rock. *51st U.S. Rock Mechanics/Geomechanics Symposium*, p. 6. Retrieved from https://doi.org/

Masoumi, H., Roshan, H., & Hagan, P. C. (2017). Size-Dependent Hoek-Brown Failure Criterion. *International Journal of Geomechanics*, *17*(2), 4016048. https://doi.org/10.1061/(ASCE)GM.1943-5622.0000706

Masoumi, H., Saydam, S., & Hagan, P. C. (2016). Unified Size-Effect Law for Intact Rock. *International Journal of Geomechanics*, *16*(2), 4015059. https://doi.org/10.1061/(ASCE)GM.1943-5622.0000543

Nikolić, M., Karavelić, E., Ibrahimbegovic, A., & Miščević, P. (2018). Lattice Element Models and Their Peculiarities. *Archives of Computational Methods in Engineering*, *25*(3), 753–784. https://doi.org/10.1007/s11831-017-9210-y

Norton Gold Fields. (2012). *ENTERPRISE OPEN CUT MINE MINING PROPOSAL PADDINGTON GOLD PTY LTD*. Retrieved from

https://nortongoldfields.com.au/wp-content/uploads/2018/02/Enterprise-Mining-Proposal.pdf

Pakzad, R., Wang, S., & Sloan, S. (2018). Numerical Study of the Failure Response and Fracture Propagation for Rock Specimens with Preexisting Flaws under Compression. *International Journal of Geomechanics*, *18*(7), 4018070. https://doi.org/10.1061/(ASCE)GM.1943-5622.0001172

Prakoso, W. A., & Kulhawy, F. H. (2011). Effects of Testing Conditions on Intact Rock Strength and Variability. *Geotechnical and Geological Engineering*, *29*(1), 101–111. https://doi.org/10.1007/s10706-010-9356-y

Rohde, J., & Feng, H. (1990). Analysis of the variability of unconfined compression tests of rock. *Rock Mechanics and Rock Engineering*, *23*(3), 231–236. https://doi.org/10.1007/BF01022955

Roshan, H., Masoumi, H., & Hagan, P. C. (2016). On Size-Dependent Uniaxial Compressive Strength of Sedimentary Rocks in Reservoir Geomechanics. *50th U.S. Rock Mechanics/Geomechanics Symposium*, p. 6. Retrieved from https://doi.org/

Ruffolo, R. M., & Shakoor, A. (2009). Variability of unconfined compressive strength in relation to number of test samples. *Engineering Geology*, *108*(1), 16–23. https://doi.org/https://doi.org/10.1016/j.enggeo.2009.05.011

Scott, D. W. (2010). Scott's rule. *Wiley Interdisciplinary Reviews: Computational Statistics*, *2*(4), 497–502. https://doi.org/10.1002/wics.103

Štambuk Cvitanović, N., Nikolić, M., & Ibrahimbegović, A. (2015). Influence of specimen shape deviations on uniaxial compressive strength of limestone and similar rocks. *International Journal of Rock Mechanics and Mining Sciences*, *80*, 357–372. https://doi.org/https://doi.org/10.1016/j.ijrmms.2015.10.008

Tsur-Lavie, Y., & Denekamp, S. A. (1982). Comparison of size effect for different types of strength tests. *Rock Mechanics*, *15*(4), 243–254. https://doi.org/10.1007/BF01240592

Xu, Y., & Cai, M. (2017). Numerical study on the influence of cross-sectional shape on strength and deformation behaviors of rocks under uniaxial compression. *Computers and Geotechnics*, *84*, 129–137. https://doi.org/https://doi.org/10.1016/j.compgeo.2016.11.017

Xu, Y. H., & Cai, M. (2017). Influence of Loading System Stiffness on Post-peak Stress–Strain Curve of Stable Rock Failures. *Rock Mechanics and Rock Engineering*, *50*(9), 2255–2275. https://doi.org/10.1007/s00603-017-1231-1

Xu, Y. H., Cai, M., Zhang, X. W., & Feng, X. T. (2017). Influence of end effect on rock strength in true triaxial compression test. *Canadian Geotechnical Journal*, *54*(6), 862–880. https://doi.org/10.1139/cgj-2016-0393

Chapter 3

Strength degradation of sandstone and granodiorite under uniaxial cyclic loading[1]

[1] This chapter has been published in *Journal of Rock Mechanics and Geotechnical Engineering* as:

Geranmayeh Vaneghi, R., Ferdosi, B., Okoth, A. D., & Kuek, B. (2018). Strength degradation of sandstone and granodiorite under uniaxial cyclic loading. Journal of Rock Mechanics and Geotechnical Engineering, 10(1). https://doi.org/10.1016/j.jrmge.2017.09.005, **Cited 15 times**, and reprinted with permission in Appendix D.

ABSTRACT

Change in mechanical properties of rocks under static loading has been widely studied and documented. However, the response of rocks to cyclic loads is still a much-debated topic. Fatigue is the phenomenon when rocks under cyclic loading fail at much lower strength as compared to those subjected to the monotonic loading conditions. A few selected cored granodiorite and sandstone specimens have been subjected to uniaxial cyclic compression tests to obtain the unconfined fatigue strength and life. This study seeks to examine the effects of cyclic loading conditions, loading amplitude and applied stress level on the fatigue life of sandstone, as a soft rock, and granodiorite, as a hard rock, under uniaxial compression test. One aim of this study is to determine which of the loading conditions has a stronger effect on rock fatigue response. The fatigue response of hard rocks and soft rocks is also compared. It is shown that the loading amplitude is the most important factor affecting the cyclic response of the tested rocks. The more the loading amplitude, the shorter the fatigue life, and the greater the strength degradation. The granodiorite specimens showed more strength degradation compared to the sandstone specimens when subjected to cyclic loading. It is shown that failure modes of specimens under cyclic loadings are different from those under static loadings. More local cracks were observed under cyclic loadings especially for granodiorite rock specimens.

3.1. Introduction

In situ rock is basically subjected to monotonic and cyclic or dynamic loadings. A proper and detailed understanding of how the mechanical properties of rock change when subjected to different loading scenarios is required for the safe and proper design and construction of civil, mining and geotechnical engineering structures such as underground openings, tunnels, rock pillars, foundations and for better understanding of other related operations such as drilling and blasting. Cyclic loadings are generated by seismic events, earthquakes, blasting, repetitive loadings and explosions which affect either surface or underground rock structures (Figure 3.1). As shown in Figure 3.1, the stability of an underground excavation (openings like tunnels, galleries, caverns and shafts) is not only controlled by rock microstructures, geological features and in situ stress state, but also by the type of loading which could be static or dynamic. The

period of cyclic loading, its frequency and stress level are important factors which govern the influence of cyclic loading on a rock body. Hence, the mechanical properties of rock under cyclic or dynamic loading should be different from those under static loading condition.

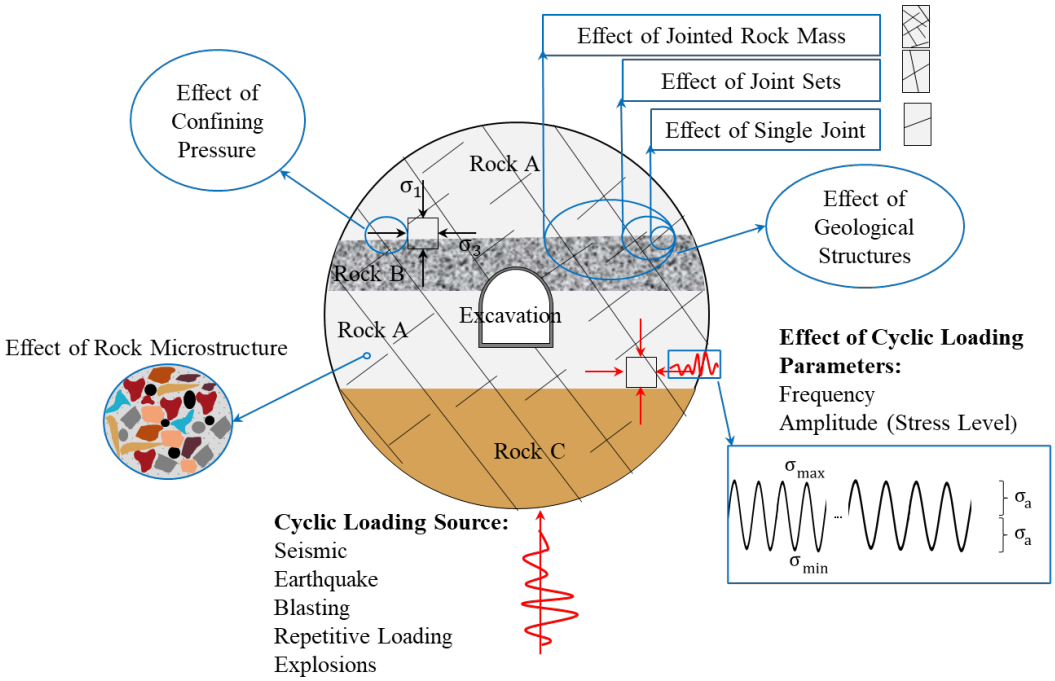

Figure 3.1. Typical schematic view of rock cyclic problems and their important factors in underground excavation design as well as other common influencing factors. σ_1 and σ_3 are the major and minor principal stresses, respectively; and σmin, σmax, and σa are the minimum stress, maximum stress, and loading amplitude stress levels, respectively, during a cyclic loading.

It has been widely acknowledged that a rock structure subjected to cyclic loading often fails prior to reaching its designed stress level or bearing capacity of its static uniaxial compressive strength (UCS). The mechanism is widely referred to as “fatigue” (Eberhardt et al., 1998). Fundamental rock structures, as mentioned above, are often subjected to cyclic loadings and their mechanical strengths experience degradation along with the loading period. Therefore, the effects of cyclic loading on stability and serviceability of rock structures cannot be neglected.

From the literature review, it was found that some researchers focused on the variation and degradation of intact or jointed rock properties under uniaxial and triaxial cyclic loadings and some others investigated the fatigue damage mechanism. It was first reported by Burdine (1963) that the pore pressure and confinement affected the

cyclic response of sandstone, and rock fatigue strength decreased and increased at high pore pressure and confinement, respectively. Attewell & Farmer (1973) also examined the strength degradation of concrete, mortar and rock under cyclic loading. They revealed that the fatigue strengths of their tested materials decreased up to 50%-70% compared to the static strength. Prost (1988) investigated the effect of pre-existing joints in Pikes Peak granite and Dakota sandstone on the crack initiation and propagation under compression-tension cyclic loading. He reported that the rocks generally failed at low number of cycles when loaded under higher stress levels and loading amplitudes. Macro tests conducted by Singh (1989) also concluded that cyclic loadings led to progressive weakening of rocks and in particular showed that there was a remarkable drop in the UCS of rocks following cyclic loading.

Zhenyu & Haihong (1990) attempted to correlate the experimental data of fatigue life to the mechanical properties of a rock specimen. They developed a constitutive equation to explain the stress-strain curves for cyclic loading. However, there is no single validated rule to describe the cyclic loading behavior of a rock. The equation developed by Zhenyu & Haihong (1990) only gives a best fit under given conditions.

The effects of cyclic loading and strain rate on the uniaxial strength of sandstone were studied by Ray et al. (1999). They reported that the degradation of rock strength is noticeable at higher maximum stress levels. According to their results, the axial failure strain was also relatively higher at higher stress levels.

Bagde and Petroš (2005a) reported that the fatigue strength and Young's modulus of sandstone decreased and increased, respectively, with the loading frequency. Bagde and Petroš (2005b) reported that the loading machine showed sensitivity to high loading amplitude applied at high loading frequency, and found that the real applied loading amplitude was remarkably lower than the target loading amplitude. Bagde and Petroš (2005c) also revealed that the cyclic dynamic responses are different under different loading waveforms and loading rates. The sine waveform was found to have a stronger dynamic effect than a ramp (triangle) waveform. It was reported that damage accumulates most rapidly under square waveforms (Gong & Smith, 2003); however, it is purely of academic interest. Because the loading rate of a square waveform is theoretically infinite in a quarter of a cycle, its dynamic effect is similar to an impact load (Xiao et al., 2008). The effects of loading amplitude and frequency on the strength degradation and deformation behavior of rocks under uniaxial cyclic compression were also studied by Bagde and Petroš (2009). They reported that the microstructure, texture

and quartz content of the rock specimens affect the fatigue strength and cyclic dynamic response. It was found that the microfracturing is the main cause of fatigue failure.

Different damage variables used to examine the damage evolution under cyclic loading were discussed by Xiao et al. (2010; 2009) . When the permanent strain is plotted against the number of cycles, it was observed that the three-stage inverted S-shaped model is well capable of describing the whole process of fatigue damage development. The curve can be divided into three phases. The shape of the curve is dependent on the rock properties and magnitude of stress applied to the rock. The three phases may be associated with the three stages that a crack undergoes, i.e. crack initiation, stable propagation and unstable propagation (Xiao et al., 2009). Bastian et al. (2014) conducted uniaxial and triaxial cyclic compressive tests on Hawkesbury sandstone to examine the variation in its mechanical properties under cyclic loading conditions. Rapid evolution of damage was observed as unloading initiation stress and unloading amplitude increased. The variations of mechanical parameters and failure mechanism of Lac du Bonnet granite under uniaxial cyclic loading were discussed by Ghazvinian (2015). He described the relationship between the critical stress thresholds (crack initiation and crack damage thresholds) and the fatigue damage pattern during the cyclic process. Taheri et al. (2016) also studied the change in mechanical properties of the Hawkesbury sandstone during various cyclic loading conditions using uniaxial and triaxial compression tests. They reported that the unstable crack propagation was observed at approximately 65% of the cumulative axial strain.

To date, most of previous works attempted to evaluate the change in mechanical properties of rocks under different cyclic loading conditions. Few studies, however, have addressed the question: Which of the maximum stress level and loading amplitude has a stronger cyclic effect? Moreover, the cyclic response of soft rocks and hard rocks is not fully understood. As mentioned previously, the fatigue behavior of hard rocks such as granodiorite and soft rocks such as sandstone, which are very common rocks in most rock structures, was always of great importance. The cyclic behaviors of these two kinds of rocks under constant frequency but with varying loading stress amplitude and stress level are presented in this study.

3.2. Experimental set-up

3.2.1. Rock Specimens

Among the intrusive rocks, granite and granodiorite are the most common and frequently encountered ones in most underground mining activities. In addition, as a result of the high strength of granitic rock, it is also widely used in the construction industry. Sandstone is also bedrock for rock structures and its behavior is different from a hard rock like granodiorite. The rock specimens were obtained from sandstone and Gosford granite/granodiorite outcrops quarry in New South Wales, Australia. Petrographic thin section analysis shows that granodiorite is weakly altered coarse-grained leucocratic holocrystalline and it contains anhedral quartz (20%-30%), orthoclase (~20%), subhedral, zoned plagioclase (20%-30%) and medium-grained flakes biotite (~10%). Sandstone is fine-grained and well-sorted and dominated by sub-rounded to angular quartz (~80%). The matrix material consisting of clay and sericite accounts for around 10% of the specimen. The intergranular porosity of this sandstone is approximately 10%. Photographs of the analyzed specimens from these two rock types in cross polarized light (XPL) are shown in Figure 3.2. The typical specimens of granodiorite and sandstone are shown in Figure 3.3. The densities of tested sandstone and granodiorite specimens were 2204 kg/m^3 and 2524 kg/m^3, respectively.

Specimens were available in two sizes: regular size with diameter of about 54 mm and height of 131 mm and small size with diameter of 42 mm and height of 102 mm. Seven (five small-size and two regular-size) specimens of granodiorite and seven (four small-size and three regular-size) of sandstone were tested to determine their UCS values. The sandstone specimens were oven-dried for 24 h so as to eliminate any moisture present therein. Since the average water content was determined to be very low (equal to 0.3%), the effect of water content on the obtained results was neglected.

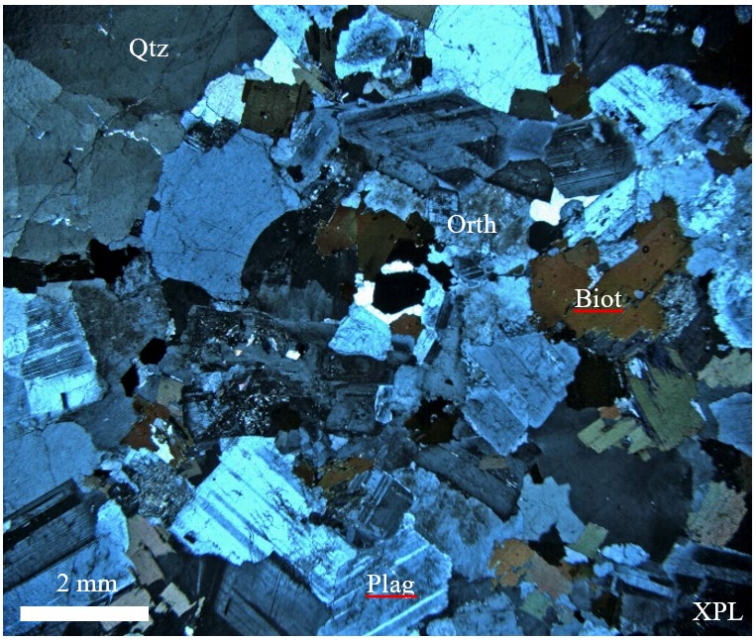

(a)

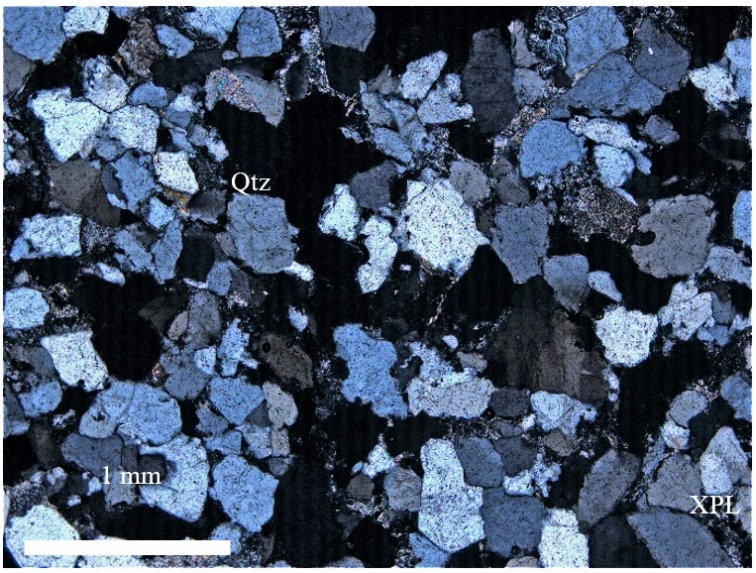

(b)

Figure 3.2. Photomicrographs of (a) granodiorite and (b) sandstone in XPL. Qtz, Plag, Orth and Biot stand for quartz, plagioclase, orthoclase and biotite, respectively.

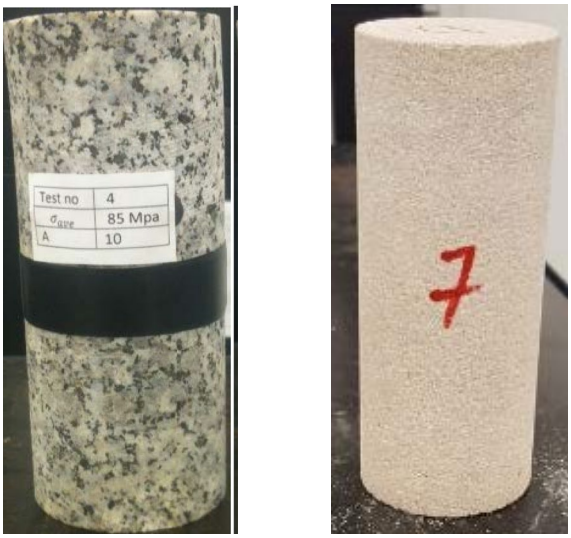

(a) (b)

Figure 3.3. Typical specimens of (a) granodiorite and (b) sandstone before testing.

3.2.2. Equipment

The tests were done using a GCTS uniaxial testing system UCT 1000, as shown in Figure 3.4. The machine is fitted with a computer-controlled axial actuator and can load a specimen by controlling the loading rate or strain rate. The UCT 1000 is capable of both dynamic and static tests, and the data obtained from the tests were collected automatically using PC-based software.

The specimens were loaded using a servo-controlled loading machine. The linear variable differential transformers (LVDTs) were used for simultaneous readings of axial, radial and volumetric strains. UCS values for all specimens were recorded for analysis.

3.2.3. Methodology

Some laboratory tests have been performed through use of uniaxial cyclic loading to investigate the mechanical fatigue behaviors of the tested rocks. The granodiorite and sandstone specimens, used for cyclic loading, were in the same size as those used for monotonic uniaxial compression loadings.

Uniaxial monotonic compression tests were conducted on both rock types. The average UCS for the tested specimens was used as the guiding maximum possible strength of the rock and to define the maximum stress level of cyclic loading. Table 3.1

shows the average UCS for regular- and small-size granodiorite and sandstone specimens. The stress-strain curves of uniaxial tests on small-size specimens are illustrated in Figure 3.5. It should be mentioned that post-peak part of these curves are not correct as all samples failed suddenly at peak stresses.

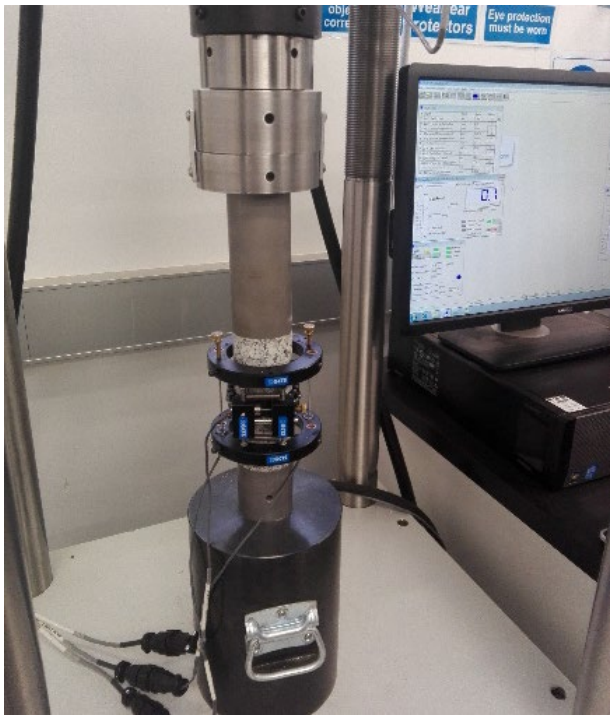

(a)

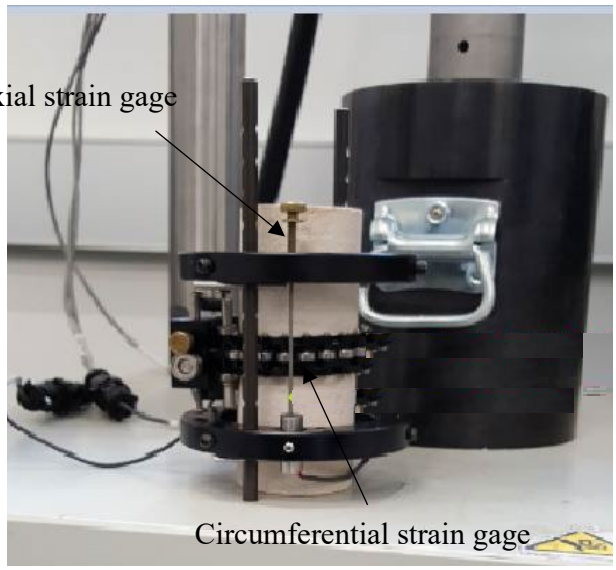

(b)

Figure 3.4. (a) Machine set-up and (b) LVDTs configuration to measure the axial and radial deformations.

The uniaxial cyclic tests were carried out in a stress control mode. The loading waveform was sine waveform which has already been found to have a stronger dynamic effect than a ramp (triangle) waveform (Bagde & Petroš, 2005c). The loading amplitudes were varied yet frequency was kept constant at 1 Hz. Two types of cyclic loadings were considered in these uniaxial cyclic tests. These two types were constant mean stress level or constant cyclic loading (CCL), and increasing mean stress level or stepped cyclic loading (SCL). The cyclic loading path with respect to time is illustrated schematically in Figure 3.6.

The CCL was designed to examine the effects of loading amplitude and the maximum stress level on fatigue strength. The regular-size specimens were tested under a CCL condition while the testing for the small-size specimens was done in a SCL manner.

Table 3.1. Average UCS of small- and regular-size granodiorite and sandstone specimens.

Rock type	Specimen No.*	UCS (MPa)	Average UCS (MPa)
Sandstone	St.-R-1	35.6	36.2
	St.-R-2	35.3	
	St.-R-3	37.6	
	St.-S-1	43.76	44
	St.-S-2	52.11**	
	St.-S-3	45.21	
	St.-S-4	42.95	
Granodiorite	G-R-1	116.71	120
	G-R-2	123.25	
	G-S-1	86.7	105.1
	G-S-2	103	
	G-S-3	124.6	
	G-S-4	103.3	
	G-S-5	107.7	

* St.: Sandstone; G: Granodiorite; R: regular-size specimen; S: small-size specimen.

** This specimen was not considered in the calculation of average UCS, since its strength seems to be quite different to the approximate strength values obtained for the three specimens.

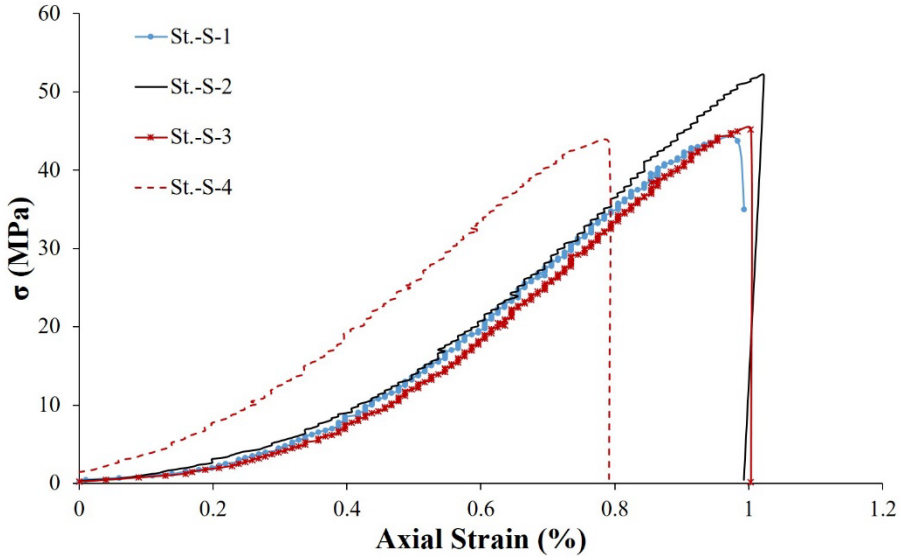

(a)

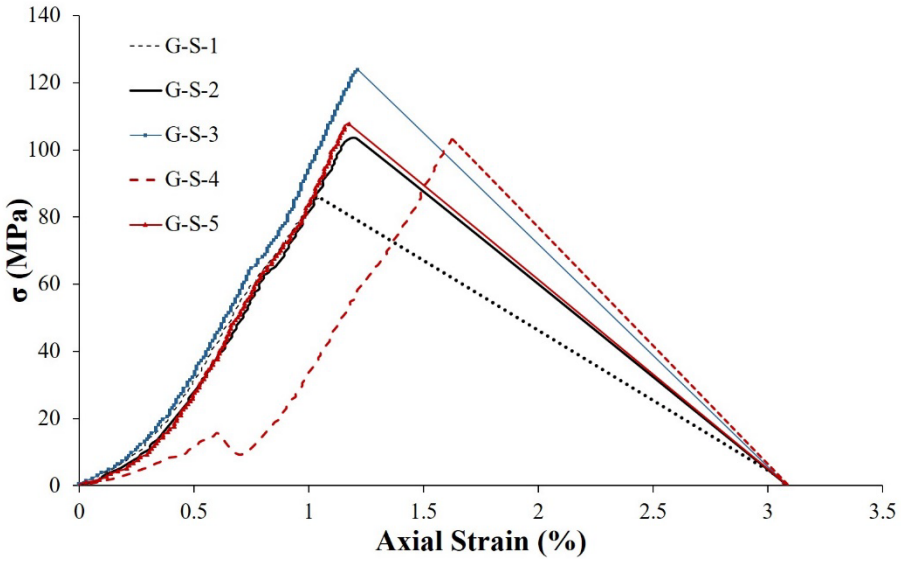

(b)

Figure 3.5. Stress-strain curves for monotonic uniaxial compression tests conducted on small-size (a) sandstone and (b) granodiorite specimens.

Under SCL conditions, the loading amplitude was kept constant whereas the maximum stress level was increased step by step. These tests were designed to find the fatigue stress of the tested rocks and to explore the effect of maximum stress level on the fatigue strength. For the SCL tests, the initial mean stress was set and the specimen loaded at a set amplitude for a specific time *t*. If no failure occurred, the mean stress was raised and the amplitude was kept constant and again the loading was done for another period of time *t*. This step-wise increase of mean stress was done up to the

failure point. The maximum stress level was set as 75%-90% of static strength (UCS) for the granodiorite specimens and 85%-97% of UCS for the sandstone specimens. The amplitude stresses were set as 3-8 MPa and 5-10 MPa in cyclic tests conducted on sandstone and granodiorite specimens, respectively. The specimen was axially loaded up to the mean stress level (the average of the maximum and minimum stress levels, σ_{mean}) in the load control mode with loading rates of approximately 1 kN/s and 0.23 kN/s for regular- and small-size sandstone specimens and 3.3 kN/s and 0.23 kN/s for regular- and small-size granodiorite specimens, respectively. Since the results of the cyclic tests on regular specimens were somewhat scattered, the loading rate on small-size specimens was set relatively low. However, for the cyclic tests, it was attempted to set the loading rate of the initial loading to be the same as that of the uniaxial monotonic tests.

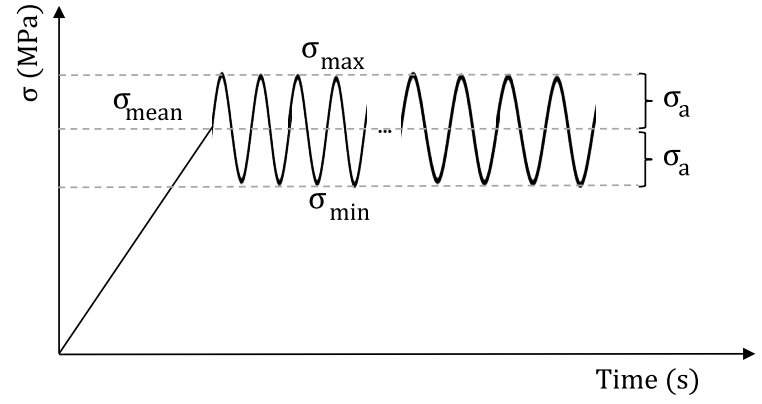

(a)

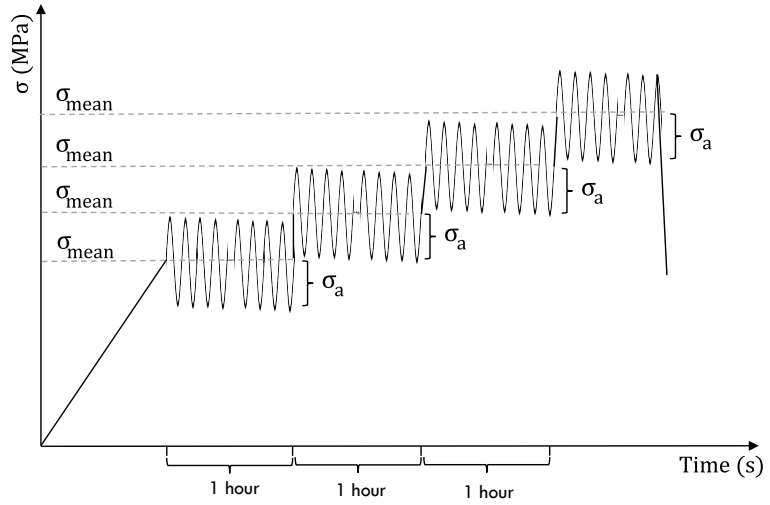

(b)

Figure 3.6. Schematic illustration of cyclic loading path with (a) CCL and (b) SCL.

3.3. Results and discussion

The effects of the maximum stress level and loading amplitude on fatigue life and strength degradation of the tested rocks were investigated by uniaxial cyclic tests. As mentioned earlier, two types of cyclic loadings with constant mean stress level, named CCL, and increasing mean stress level cyclic loading, named SCL, were considered in these tests. Table 3.2 shows the experimental scheme and obtained results of uniaxial compression cyclic tests for both granodiorite and sandstone specimens. It is noteworthy that some specimens (St.-R-9, G-R-3 and G-R-4) were reloaded when they did not fail after a large number of cycles during the first loading path of CCL tests. Therefore, the results for specimens St.-R-10, G-R-5 and G-R-6 were used to analyze the effect of cyclic loading history on their fatigue response. Although these three specimens were loaded at a higher mean stress level for the second time, they were put into the CCL category.

Characteristics of all SCL paths are detailed in Table 3.3. As can be seen, in all SCL, the loading amplitudes (σ_α) were constant yet the mean stress levels were varied. According to this table, the mean stress level and loading amplitude of specimen St.-S-5, for instance, were set to 34.5 MPa and 3 MPa, respectively, for the first step. Then the specimen would be loaded for up to 30 min (1800 cycles). If it did not fail, the test would continue for another 1800 cycles within the second step in which the mean stress level would be increased to 37 MPa under the same loading amplitude (3 MPa). This procedure would be continued up to the failure point of the specimen.

Figure 3.7 shows the stress-strain curves for the cyclic tests carried out on regular- and small-size specimens of granodiorite and sandstone. It should be mentioned that post-peak parts of these curves are not correct as all samples failed suddenly at peak stresses. As displayed in Figure 3.7a, the sandstone specimens St.-R-5, St.-R-6, St.-R-8 and St.-R-10 failed at 30.92 MPa, 30.89 MPa, 32.84 MPa and 33.84 MPa, respectively. Figure 3.7b also presents that specimens St.-S-5, St.-S-6 and St.-S-7, which were loaded under 3 MPa, 5 MPa and 6 MPa, failed at 39.47 MPa, 38.03 MPa and 35.69 MPa, respectively. The greater the loading amplitude, the lower the fatigue strength. The regular-size granodiorite specimens G-R-5, G-R-6 and G-R-7 failed at 85.09 MPa, 102.4 MPa and 93.11 MPa, respectively (Figure 3.7c). The small-size granodiorite specimens (G-S-6 and G-S-7), as illustrated in Figure 3.7d, failed at 83.33 MPa and 79.4 MPa, respectively. These two specimens failed at the first step of SCL

even though it was planned to load them under different stress levels during the fatigue process. The results are explained in detail in the following sections.

Table 3.2. Experimental scheme of uniaxial compression cyclic tests for both granodiorite and sandstone specimens.

Rock type	Specimen No.	Loading type	σ_{min} (MPa)	σ_{mean} (MPa)	σ_{max} (MPa)	σ_{max}/UCS (%)	σ_a (MPa)	σ_f (MPa)	σ_f/UCS (%)	Number of cycles	Remarks
Sandstone	St.-R-4	CCL	20	25	30	83.3	5				Not failed after 2 h
	St.-R-5		24	29	34	94.4	5	30.92	85.9	65	
	St.-R-6		26	29	32	88.8	3	30.89	85.8	12	
	St.-R-7		18	26	34	94.4	8				Failed before cyclic loading starts
	St.-R-8		18	26	34	94.4	8	32.84	91	71	
	St.-R-9		20	26	32	88.8	6				Not failed after 2 h
	St.-R-10		24	29	35	97.2	6	33.84	94	449	Continued on specimen St.-R-9
	St.-S-5	SCL	31.5	34.5	37.5	85.2	3	39.47	89.7	2153	Failed on the second step
	St.-S-6		27.5	32.5	37.5	85.2	5	38.03	86.4	1930	Failed on the second step
	St.-S-7		25.5	31.5	37.5	85.2	6	35.69	81.1	470	Failed on the first step
Granodiorite	G-R-3	CCL	80	85	90	75	5				Not failed after 1 h
	G-R-4		84	89	94	78.3	5				Not failed after 2 h
	G-R-5		79	89	99	82.5	10	85.09	71	331	Continued on specimen G-R-3
	G-R-6		86	96	106	88.3	10	102.4	85.3	217	Continued on specimen G-R-4
	G-R-7		81.5	89	96.5	80.41	7.5	93.11	77.6	7	
	G-S-6	SCL	70	77.5	85	81	7.5	83.33	79.3	9	Failed on the first step
	G-S-7		65	75	85	81	10	79.4	75.6	191	Failed on the first step

Table 3.3. Detail of loading path for specimens loaded under SCL tests.

Rock type	Specimen No.	Step	σ_{mean} (MPa)	σ_a (MPa)	Loading sequence
Sandstone	St.-S-5	1	34.5	3	Loading for 30 min. If no failure, increase mean stress to 37 MPa
		2	37		Loading for 30 min. If no failure, increase mean stress to 39 MPa
		3	39		Loading for 30 min. If no failure, increase mean stress to 41 MPa
		4	41		Loading for 30 min. If no failure, stop test.
	St.-S-6	1	32.5	5	Loading for 30 min. If no failure, increase mean stress to 35 MPa
		2	35		Loading for 30 min. If no failure, increase mean stress to 37 MPa
		3	37		Loading for 30 min. If no failure, increase mean stress to 39 MPa
		4	39		Loading for 30 min. If no failure, stop test.
	St.-S-7	1	31.5	6	Loading for 30 min. If no failure, increase mean stress to 34 MPa
		2	34		Loading for 30 min. If no failure, increase mean stress to 36 MPa
		3	36		Loading for 30 min. If no failure, increase mean stress to 38 MPa
		4	38		Loading for 30 min. If no failure, stop test.
Granodiorite	G-S-6	1	77.5	7.5	Loading for 1 h. If no failure, increase mean stress to 82.5 MPa
		2	82.5		Loading for 1 h. If no failure, increase mean stress to 87.5 MPa
		3	87.5		Loading for 1 h. If no failure, increase mean stress to 92.5 MPa
		4	92.5		Loading for 1 h. If no failure, increase mean stress to 122.5 MPa
		5	112.5		Loading for 1 h. If no failure, stop the test.
	G-S-7	1	75	10	Loading for 1 h. If no failure, increase mean stress to 80MPa
		2	80		Loading for 1 h. If no failure, increase mean stress to 85 MPa
		3	85		Loading for 1 h. If no failure, increase mean stress to 90 MPa
		4	90		Loading for 1 h. If no failure, increase mean stress to 110 MPa
		5	110		Loading for 1 h. If no failure, stop the test

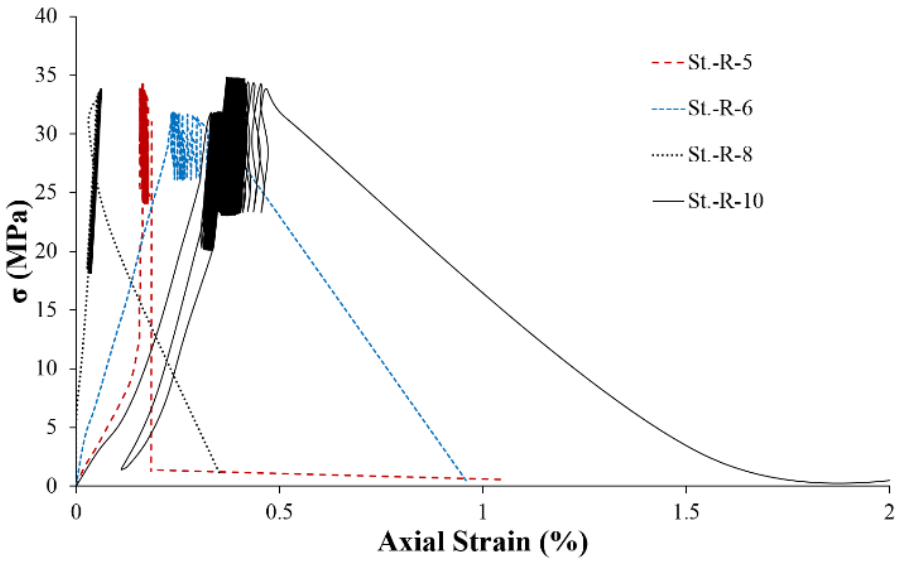

(a)

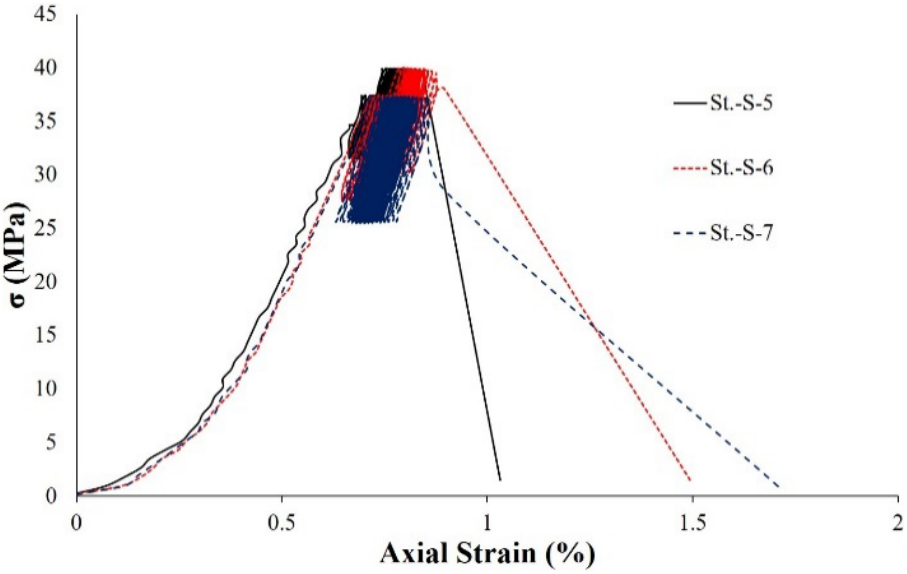

(b)

Figure 3.7 (continued on the next page).

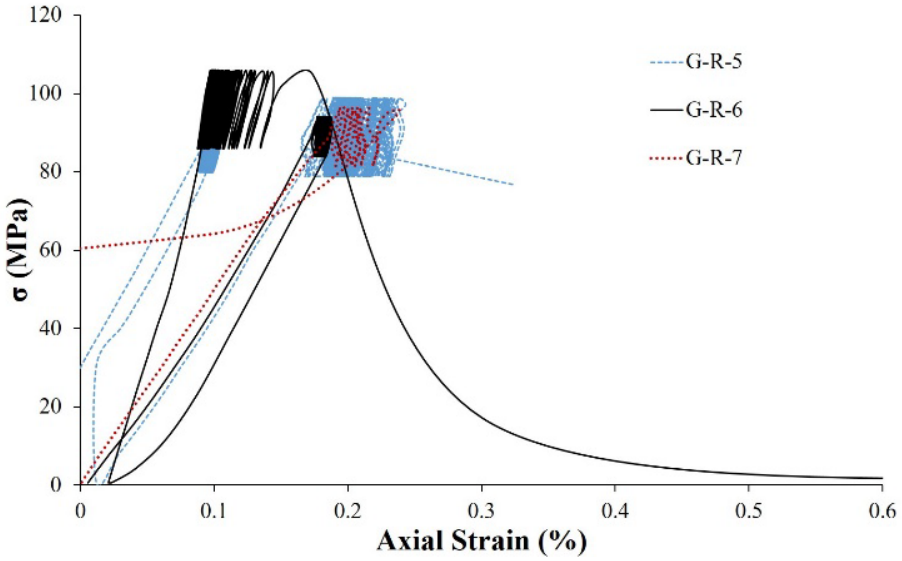

(c)

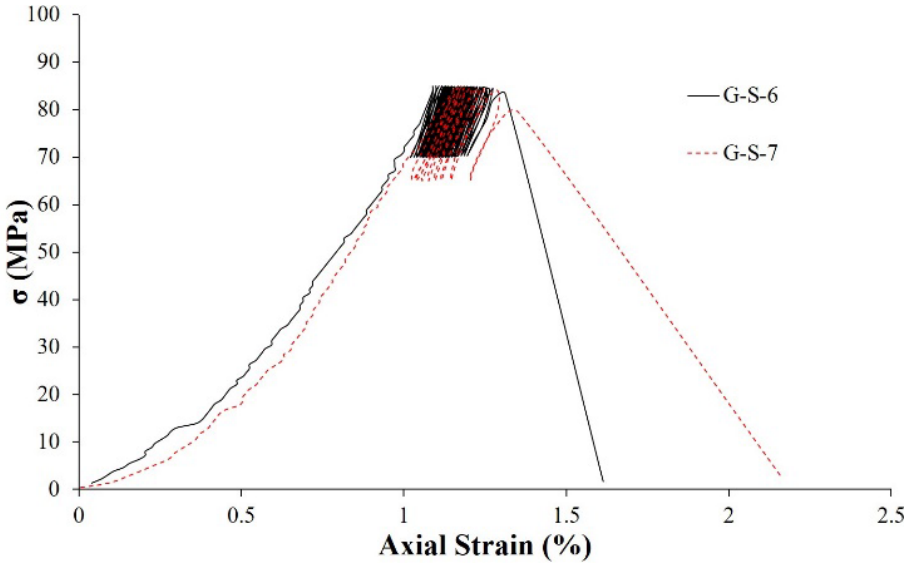

(d)

Figure 3.7 (continued from previous page). Stress-strain curves for uniaxial cyclic tests conducted on (a) regular- and (b) small-size sandstone specimens, and (c) regular- and (d) small-size granodiorite specimens.

3.3.1. Effect of maximum stress level

The analysis of fatigue behavior of specimens as well as strength characteristics under various maximum stress levels has been carried out. In Table 3.2, the maximum stress

levels were inadequate to influence the fatigue behavior of some rock specimens, either for granodiorite or sandstone.

As can be found in Table 3.2, the sandstone specimens St.-R-4 and St.-R-9 did not fail even after a large number of cycles when they were loaded under the maximum stress levels of 30 MPa (83.3% of UCS) and 32 MPa (88.8% of UCS), respectively. This is also observed during the cyclic tests on small-size sandstone specimens, St.-S-5 and St.-S-6, under the maximum stress levels of 85.2% of UCS (37.5 MPa) during the first step of SCL path. As the maximum stress level exceeded 90% of UCS, all sandstone specimens failed and fatigue life decreased as well. The specimens St.-S-5 and St.-S-6, as can be seen in Table 3.2, yielded when the applied maximum stress level increased to 91% of UCS (40 MPa) during the second step of SCL. The effect of the maximum stress level on strength degradation of specimens St.-R-5 and St.-R-8 were more noticeable. They failed just after 65 cycles and 71 cycles (shorter fatigue life), respectively, since they were loaded under a higher maximum stress level of 94.4% of UCS (34 MPa).

Comparing the results of specimens St.-R-4 and St.-S-6 with St.-R-5, under the same loading amplitude of 5 MPa, it can be seen that the fatigue life of specimens decreased as the maximum stress level increased. The specimen St.-R-5 failed after 65 cycles under a maximum stress level of 34 MPa (94.4% of UCS), whereas both specimens St.-R-4 and St.-S-6 did not fail under the maximum stress of 83.3% and 85.2% of UCS, respectively, even after a large number of cycles.

A similar result was also obtained for granodiorite specimens. Specimens G-R-3 and G-R-4 did not fail after 1 h (about 3600 cycles) and 2 h (about 7200 cycles) of loading under the maximum stress levels of 90 MPa (75% of UCS) and 94 MPa (78.3% of UCS), respectively, however they failed when the maximum stress levels increased to 82.5% and 88.3% of UCS (results of G-R-5 and G-R-6), respectively. The fatigue life and strength (σ_f) of specimen G-S-7 under a maximum stress level of 85 MPa (81% of UCS) were compared with those of G-R-5 and G-R-6 under higher maximum stress levels of 99 MPa and 106 MPa (82.5% and 88.3% of UCS), respectively. It was found that the loading history had a great effect on cyclic response even though the loading amplitude was equal to 10 MPa for all specimens. Since G-R-5 and G-R-6 failed under a larger number of cycles compared to G-S-7, the strain-hardening behavior is clear, because they have already been loaded under cyclic conditions and experienced the fatigue process. As can be seen, specimen G-R-6, which had already been loaded under

the maximum stress level of 78.3% of UCS, failed after 217 cycles, while specimen G-R-5, which had already experienced loading under a maximum stress level of 75% of UCS, failed after 313 cycles. Thus it can be stated that when a rock experienced a higher loading level at previous loading stages, yet less than the fatigue stress threshold, a shorter fatigue life would be resulted.

A similar finding was also reported by other researchers. According to Singh (1989) and Momeni et al. (2015), the rock material tends to fail at a low number of cycles and has a shorter fatigue life as the maximum stress level increases (Figure 3.8). As can be seen in Figure 3.8, when the maximum stress level exceeded 90% of monotonic compressive strengths of granodiorite and graywacke, they failed at a number of cycles less than 200. Whereas when the graywacke, for instance, was loaded at 88% of UCS, it sustained more than 6000 cycles. It can be concluded that every rock material has a strength threshold, named as fatigue strength, and the rock fails at a low number of cycles when the maximum stress level is more than this threshold, if other testing conditions remain constant. Thus the maximum applied stress level is of great importance in assessing the mechanical parameters of rock and design of any structure which will be operated under a cyclic loading condition.

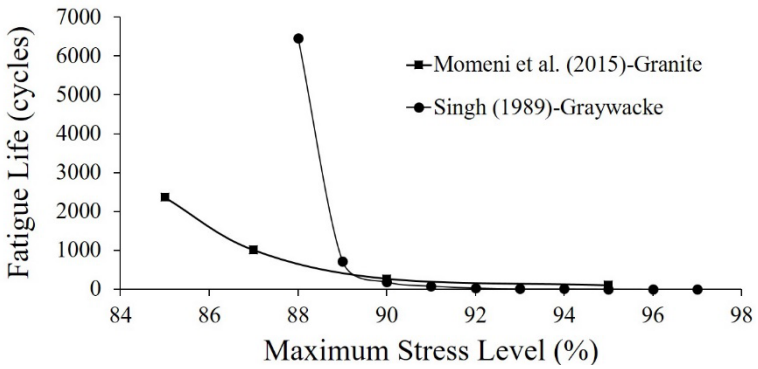

Figure 3.8. Effect of the maximum stress level on fatigue life of granodiorite and graywacke. Data obtained from Singh (1989) and Momeni et al. (2015) under loading frequency of 1 Hz.

3.3.2. Effect of loading amplitude

Amplitude is a key factor when analyzing the cyclic loading, as it is an indicator of how much the maximum and minimum stresses vary from the mean stress and it also determines the values expected for the maximum stress reached. Even with a slightly

lower initial loading stress, the specimens subjected to higher magnitudes of amplitude failed sooner than those under low amplitudes.

Comparing the fatigue life and strength of small-size sandstone specimens, St.-S-5 and St.-S-6, under the same maximum stress level, it is clear that the fatigue life and strength of sandstone decreased as the loading amplitude increased from 3 MPa to 5 MPa. Specimen St.-S-5 with loading amplitude of 3 MPa failed after 2153 cycles during the second stage of SCL when the maximum stress level was 40 MPa. Specimen St.-S-6, whereas, with loading amplitude of 5 MPa, failed after 1930 cycles during the second stage of SCL when the maximum stress level was 40 MPa. The fatigue strength of specimen St.-S-6 loaded under a higher loading amplitude was 38.03 MPa (86.4% of UCS), lower than that of specimen St.-S-5, which was 39.47 MPa (89.7% of UCS).

Comparing the fatigue life and strength of specimen St.-S-7 with those of specimens St.-S-5 and St.-S-6, it suggests that the effect of loading amplitude is stronger than that of the maximum stress level. Specimen St.-S-7 loaded under a maximum stress level of 85.2% of UCS with higher loading amplitude of 6 MPa failed during the first step of SCL, after just 470 cycles (shorter fatigue life) and lower fatigue stress (81.1% of UCS) compared to St.-S-5 and St.-S-6 that did not fail during the first step (at the same maximum stress level of 85.2% of UCS). These two specimens failed during the second stage when the maximum stress level increased to 91% of UCS. Thus it can be concluded that the rock would more easily yield at a lower maximum stress level with higher loading amplitude than at a high maximum stress level with low loading amplitude. This finding, however, needs to be validated by more experimental data. The importance of loading amplitude has also been stated by Attewell and Farmer (1973) when they compared the cyclic response of rocks under different loading amplitudes and frequencies. They believed that failure of rock occurs more easily at low-frequency dynamic stress with higher amplitude than at high-frequency dynamic stress with low loading amplitude.

As can be found in Table 3.2, if the fatigue strengths of granodiorite specimens G-S-6 and G-S-7 are compared, the fatigue strength of G-S-6 with loading amplitude of 7.5 MPa was 83.33 MPa (79.3% of UCS) compared to that of 79.4 MPa (75.6% of UCS) for G-S-7 with higher loading amplitude of 10 MPa.

The effect of loading amplitude on fatigue life was also reported by Singh (1989), He et al. (2016) and Taheri et al. (2016). The more the loading amplitude, the shorter the fatigue life. As shown in Figure 3.9, the graywacke specimens sustained 10,189

cycles under loading amplitude of 50 MPa, while they failed at 287 cycles when the loading amplitude increased to 83 MPa (Singh, 1989). As illustrated in this figure, this trend was also reported by He et al. (2016) and Taheri et al. (2016) for their tested sandstone specimens. The sandstone specimens were loaded more than 100 cycles under loading amplitude of 40 MPa, whereas they failed just after 2 cycles as the loading amplitude increased to 47 MPa (Taheri et al., 2016). The sandstone specimens tested by He et al. (2016) showed a similar result. Specimens sustained loading up to 233 cycles when the loading amplitude was less than 10 MPa, while they failed after 20 cycles when the loading amplitude was more than 60 cycles.

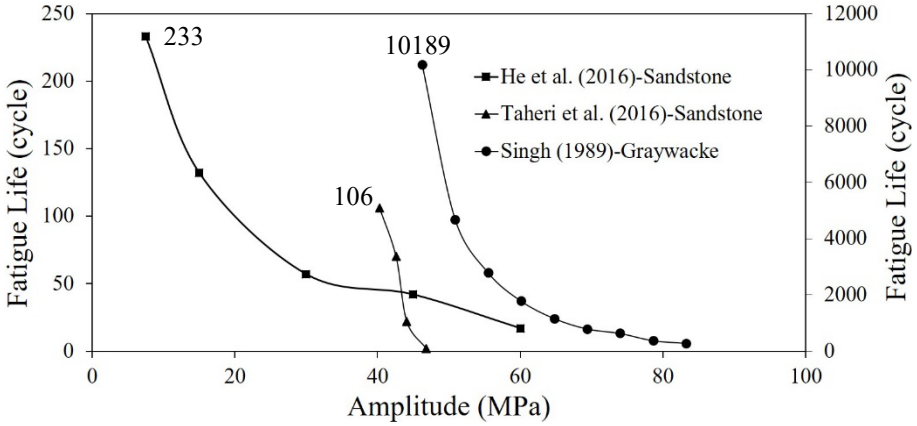

Figure 3.9. Effect of loading amplitude on fatigue life of rock material under cyclic loading. Data obtained from Singh (1989), He et al. (2016) and Taheri et al. (2016).

3.3.3. Fatigue strength

The fatigue strength of the tested rocks can be determined from the results discussed above. As previously mentioned, each type of rock has a strength threshold at which it can sustain loading under a large number of cycles if the loading level is less than this threshold. According to Table 3.2 and based on the discussion in previous sections, the fatigue strengths of sandstone and granodiorite specimens can be taken as 90% and 80% of their UCS values, respectively. Thus the fatigue strengths of regular- and small-size sandstone specimens are 32 MPa and 40 MPa, respectively. These amounts were found equal to be 96 MPa and 85 MPa for regular- and small-size granodiorite, respectively.

Based on the fatigue strengths of sandstone and granodiorite, it can be concluded that the fatigue strength of hard rocks is relatively lower than that of soft rocks. Thus

the brittle rocks are more prone to be weakened under cyclic loading than ductile rocks. The more brittle the rock, the more the strength degradation, and the less the fatigue strength.

3.3.4. Failure modes of the tested rock specimens

Damage mechanism was always an interesting topic to figure out how solid materials fail by fracturing and cracking. Identifying crack development through laboratory tests would improve our understanding of the real failure process in practice (Eberhardt, 1998). The failure modes of the tested sandstone and granodiorite specimens are presented in Figure 3.10. As can be seen in this figure, there were more fractured planes observed on both sandstone and granodiorite specimens after cyclic loading compared to static loading tests. The main shearing plane (named 1) is accompanied by axial tensile cracks (named 2) for both specimens under cyclic loading. More tensile splitting cracks were observed under a cyclic loading condition. Since the granodiorite rock is more brittle, there was more powder on the fracture planes after the cyclic tests, which is an indication of fatigue failure. This pattern was also observed by Wang et al. (2013). Similar failure modes for sandstone specimens under triaxial monotonic and cyclic tests were also reported by Liu et al. (2011; 2012) and Yang et al. (2015).

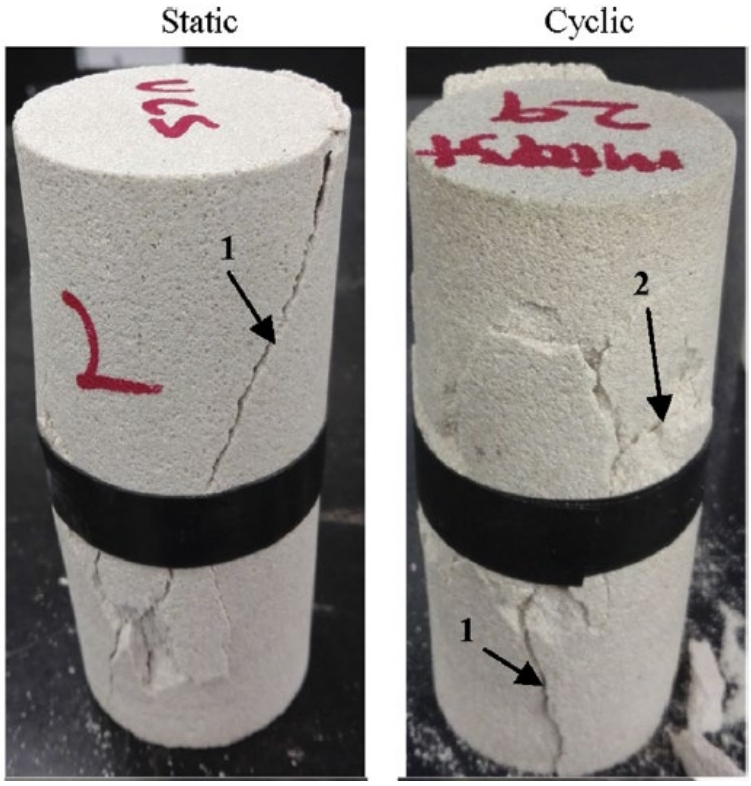

(a)

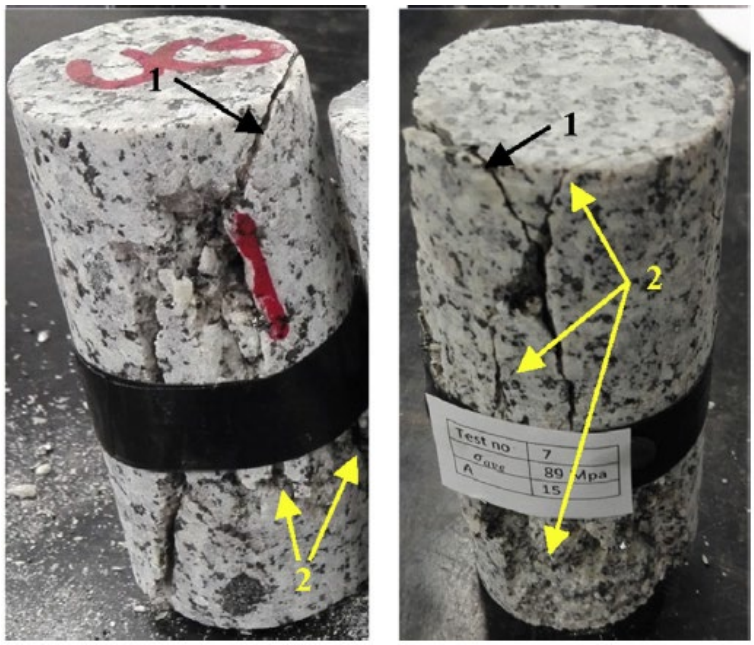

(b)

Figure 3.10. Failure modes of tested (a) sandstone and (b) granodiorite specimens under static and cyclic loadings. Cracks named 1 are shearing cracks and the ones named 2 are axial tensile cracks.

3.3.5. Rock nonhomogeneity and response to cyclic loadings

During laboratory testing of granodiorite and sandstone specimens subjected to uniaxial cyclic loadings, there were some disparities observed in the fatigue failure of rock specimens. Some specimens developed immediate failure and premature yielding though the loading amplitude was minimal and the maximum stresses were not significantly high. However, a few specimens have shown no yielding or axial strain and lateral strain as a result of dynamic deformation failure. One significant observation noted is that fatigue characteristics are dependent on geological condition, in situ stress and depth of core extraction as well as chemical composition of the rock microstructure formation. The unlikely variability in cyclic failure is an obvious heterogeneity of the rock specimens due to changes in in situ stress distribution, which might have altered the mechanical properties of the intact rock, i.e. strength, deformability and especially permeability initiated due to development of network of stress relief cracks. These conditions could have created stress corrosion phenomena and plenty of weakening mechanical actions, i.e. weak strain bonds around the crack tips thus facilitating crack propagation at lower stress levels.

Moreover, the perceived nonhomogeneity is a result of microscale heterogeneity of the rock specimens. It is believed that the presence of microstructures has created an additional dimension on the nonhomogeneous specimen. There is room for expansion of one or more individual micro-fractures into cleavage fractures (splitting/extension mode) and a dramatic drop of load-bearing capacity to abrupt failure.

3.4. Conclusions

The main objectives for this study were to investigate the effects of loading amplitude and stress on the mechanical properties of sandstone and granodiorite and to understand how the cyclic response differs from soft rock of sandstone to hard rock of granodiorite. From the conducted tests and obtained results, the following conclusions were drawn:

(1) The increasing mean stress level tests (SCL path) provides a decent way to not only explore the effect of the maximum stress level and loading amplitude on cyclic response of rocks but also to investigate the effect of loading history on their fatigue behavior.
(2) The fatigue life decreased with an increase in the maximum stress level if the cyclic loading amplitude remained constant.
(3) The decreases in the fatigue life and strength were evident with increasing loading amplitude.
(4) The effect of loading amplitude is stronger than that of the maximum stress level. The rock would more easily yield at a lower maximum stress level with higher loading amplitude than at high maximum stress level with lower loading amplitude.
(5) The fatigue strength of hard/brittle rocks seems to be less than that of soft/ductile rocks. The more brittle the rock, the more the strength degradation, and the less the fatigue strength.
(6) It is observed that more local cracks are formed after cyclic loading tests compared to static loading tests.

Further experimental work, however, is required to be carried out to validate that the loading amplitude has more cyclic effect than the maximum stress level. Different rock types are suggested to be tested under cyclic loading to precisely explore the difference between fatigue response of hard rocks and soft rocks. It would also be interesting to assess the effects of rock fabric and its heterogeneity on the fatigue response.

Conflict of interest

The authors wish to confirm that there are no known conflicts of interest associated with this publication and there has been no significant financial support for this work that could have influenced its outcome.

Acknowledgements

We would like to express our sincere gratitude to Department of Mining Engineering and Metallurgical Engineering of Western Australian School of Mines (WASM), Curtin University for the provided laboratory equipment at Geomechanics laboratory, Mining Research Institute of Western Australia (MRIWA) for the financial support and also special appreciation to Dr. Takahiro Funatsu for his technical support to undertake the laboratory tests.

References

Attewell, P. B., & Farmer, I. W. (1973). Fatigue behaviour of rock. *International Journal of Rock Mechanics and Mining Sciences & Geomechanics Abstracts*, *10*(1), 1–9. https://doi.org/https://doi.org/10.1016/0148-9062(73)90055-7

Bagde, M N, & Petroš, V. (2005a). Fatigue properties of intact sandstone samples subjected to dynamic uniaxial cyclical loading. *International Journal of Rock Mechanics and Mining Sciences*, *42*(2), 237–250. https://doi.org/https://doi.org/10.1016/j.ijrmms.2004.08.008

Bagde, M N, & Petroš, V. (2005b). The Effect of Machine Behaviour and Mechanical Properties of Intact Sandstone Under Static and Dynamic Uniaxial Cyclic Loading. *Rock Mechanics and Rock Engineering*, *38*(1), 59–67. https://doi.org/10.1007/s00603-004-0038-z

Bagde, M N, & Petroš, V. (2005c). Waveform Effect on Fatigue Properties of Intact Sandstone in Uniaxial Cyclical Loading. *Rock Mechanics and Rock Engineering*, *38*(3), 169–196. https://doi.org/10.1007/s00603-005-0045-8

Bagde, Manoj N, & Petroš, V. (2009). Fatigue and dynamic energy behaviour of rock subjected to cyclical loading. *International Journal of Rock Mechanics and Mining Sciences*, *46*(1), 200–209. https://doi.org/https://doi.org/10.1016/j.ijrmms.2008.05.002

Bastian, T. J., Connelly, B. J., Olivares, C. S., Yfantidis, N., & Taheri, A. (2014). Progressive damage of Hawkesbury sandstone subjected to systematic cyclic loading. *Mining Education Australia – Research Projects Review*.

Burdine, N. T. (1963). Rock Failure Under Dynamic Loading Conditions. *Society of Petroleum Engineers Journal*, *3*(01), 1–8. https://doi.org/10.2118/481-PA

Eberhardt, E. B. (1998). *Brittle rock fracture and progressive damage in uniaxial compression* (University of Saskatchewan). Retrieved from http://hdl.handle.net/10388/etd-10212004-001228

Eberhardt, E., Stead, D., Stimpson, B., & Read, R. S. (1998). Identifying crack initiation and propagation thresholds in brittle rock. *Canadian Geotechnical Journal*, *35*(2), 222–233. https://doi.org/10.1139/t97-091

Ghazvinian, E. (2015). *Fracture Initiation and Propagation in Low Porosity Crystalline Rocks: Implications for Excavation Damage Zone (EDZ)*

Mechanics (Queen's University). Retrieved from http://hdl.handle.net/1974/13715

Gong, M., & Smith, I. (2003). Effect of Waveform and Loading Sequence on Low-Cycle Compressive Fatigue Life of Spruce. *Journal of Materials in Civil Engineering*, *15*(1), 93–99. https://doi.org/10.1061/(ASCE)0899-1561(2003)15:1(93)

He Ning;, M. L., & chen Caihui, Y. Z. (2016). Strength and Fatigue Properties of Sandstone under Dynamic Cyclic Loading. *Shock and Vibration*, *2016*, 8. https://doi.org/https://doi.org/10.1155/2016/9458582

Liu, EnLong, He, S., Xue, X., & Xu, J. (2011). Dynamic Properties of Intact Rock Samples Subjected to Cyclic Loading under Confining Pressure Conditions. *Rock Mechanics and Rock Engineering*, *44*(5), 629–634. https://doi.org/10.1007/s00603-011-0151-8

Liu, Enlong, Huang, R., & He, S. (2012). Effects of Frequency on the Dynamic Properties of Intact Rock Samples Subjected to Cyclic Loading under Confining Pressure Conditions. *Rock Mechanics and Rock Engineering*, *45*(1), 89–102. https://doi.org/10.1007/s00603-011-0185-y

Momeni, A., Karakus, M., Khanlari, G. R., & Heidari, M. (2015). Effects of cyclic loading on the mechanical properties of a granite. *International Journal of Rock Mechanics and Mining Sciences*, *77*, 89–96. https://doi.org/http://dx.doi.org/10.1016/j.ijrmms.2015.03.029

Prost, G. L. (1988). Jointing at rock contacts in cyclic loading. *International Journal of Rock Mechanics and Mining Sciences & Geomechanics Abstracts*, *25*(5), 263–272. https://doi.org/http://dx.doi.org/10.1016/0148-9062(88)90003-4

Ray, S. K., Sarkar, M., & Singh, T. N. (1999). Effect of cyclic loading and strain rate on the mechanical behaviour of sandstone. *International Journal of Rock Mechanics and Mining Sciences*, *36*(4), 543–549. https://doi.org/http://dx.doi.org/10.1016/S0148-9062(99)00016-9

Singh, S. K. (1989). Fatigue and strain hardening behaviour of graywacke from the flagstaff formation, New South Wales. *Engineering Geology*, *26*(2), 171–179. https://doi.org/http://dx.doi.org/10.1016/0013-7952(89)90005-7

Taheri, A., Yfantidis, N., Olivares, C., Connelly, B., & Bastian, T. (2016). *Experimental Study on Degradation of Mechanical Properties of Sandstone Under Different Cyclic Loadings BT - Experimental Study on Degradation of Mechanical Properties of Sandstone Under Different Cyclic Loadings*.

Wang, Z., Li, S., Qiao, L., & Zhao, J. (2013). Fatigue Behavior of Granite Subjected to Cyclic Loading Under Triaxial Compression Condition. *Rock Mechanics and Rock Engineering*, *46*(6), 1603–1615. https://doi.org/10.1007/s00603-013-0387-6

Xiao, J.-Q., Ding, D.-X., Jiang, F.-L., & Xu, G. (2010). Fatigue damage variable and evolution of rock subjected to cyclic loading. *International Journal of Rock Mechanics and Mining Sciences*, *47*(3), 461–468. https://doi.org/http://dx.doi.org/10.1016/j.ijrmms.2009.11.003

Xiao, J.-Q., Ding, D.-X., Xu, G., & Jiang, F.-L. (2009). Inverted S-shaped model for nonlinear fatigue damage of rock. *International Journal of Rock Mechanics and Mining Sciences*, *46*(3), 643–648. https://doi.org/http://dx.doi.org/10.1016/j.ijrmms.2008.11.002

Xiao, J., Ding, D., Xu, G., & Jiang, F. (2008). Waveform effect on quasi-dynamic loading condition and the mechanical properties of brittle materials. *International Journal of Rock Mechanics and Mining Sciences*, *45*(4), 621–626. https://doi.org/http://dx.doi.org/10.1016/j.ijrmms.2007.07.025

Yang, S.-Q., Ranjith, P. G., Huang, Y.-H., Yin, P.-F., Jing, H.-W., Gui, Y.-L., & Yu, Q.-L. (2015). Experimental investigation on mechanical damage characteristics of sandstone under triaxial cyclic loading. *Geophysical Journal International*, *201*(2), 662–682. https://doi.org/10.1093/gji/ggv023

Zhenyu, T., & Haihong, M. (1990). An experimental study and analysis of the behaviour of rock under cyclic loading. *International Journal of Rock Mechanics and Mining Sciences & Geomechanics Abstracts*, *27*(1), 51–56. https://doi.org/https://doi.org/10.1016/0148-9062(90)90008-P

Chapter 4

Strength and damage response of sandstone and granodiorite under different loading conditions of multi-stage uniaxial cyclic compression[1]

[1] This chapter has been published in *International Journal of Geomechanics* as a journal article of:

Geranmayeh Vaneghi R, Thoeni K, Dyskin VA, Sharifzadeh M, Sarmadivaleh M. Strength and damage response of sandstone and granodiorite under different loading conditions of multi-stage uniaxial cyclic compression. Int J Geomech n.d. https://doi.org/10.1061/(ASCE)GM.1943-5622.0001801.

ABSTRACT

Understanding the strength and deformation response of hard and soft rocks under cyclic loading is very important for assessing fatigue in rock engineering structures. The effect of cyclic loading on rocks is different and more complex than that of monotonic loading. In this paper, the deformation and strength response of two mineralogically and microstructurally different rocks, sandstone and granodiorite, have been investigated by conducting multi-stage uniaxial cyclic compression loading tests. It is shown that these two rocks behave differently under cyclic loading mainly because of their microstructures. The stress–strain hysteresis loops of sandstone samples showed three phases of development, while there were two phases for the granodiorite samples. The fatigue strength threshold of granodiorite as hard rock is shown to be less than that of sandstone as soft rock. Residual lateral strain develops faster than residual axial strain during the cyclic stages. Axial and lateral strain after each step of loading, as well as residual strain, showed an increasing trend with maximum stress levels and loading amplitude. We discuss how rock damage develops in a rapid manner in lower loading frequencies and find that rock damage propagation can be assessed by ultrasonic measurement. The failure modes of the rock samples were also evaluated. We found that the damage mechanism of rocks under cyclic loading is highly dependent on loading frequency. In addition, the failure modes of the two rock types under cyclic loading differ not only from those under the monotonic conditions but also from those under different loading conditions. This study contributes to a deeper understanding of the deformation response and damage evolution of hard rocks and soft rocks under fatigue processes.

4.1. Introduction

Rock engineering structures such as traffic/haulage roads, mine and road tunnels, pressure tunnels, mine stopes, caverns, oil/gas storages and waste repositories are subjected to cyclic loading. Repetitive loading–unloading cycles cause rocks to deform and fail differently than when they undergo monotonic loading conditions. Cyclic loading can be induced by any repetitive loading–unloading activities, such as earthquakes (Haimson, 1978; Taheri et al., 2016) and blasting (Li et al., 2017; Sun et al., 2017) as high-frequency seismic events, traffic, slow injection and discharge of gas

(Fan et al., 2016; Ma et al., 2013; Roberts et al., 2015), oil (Wang et al., 2013), and hydrocarbons (Voznesenskii et al., 2017) in underground storages and even inflation and deflation of volcanic edifices (Kendrick et al., 2013) as low-frequency seismic events. An underground tunnel, for instance, might be at risk of instability, e.g., due to induced vibration from the repetitive loading of blasts in nearby galleries, or earthquakes (Figure 4.1), if the mechanical behavior of the surrounding rock mass at such conditions has not been properly assessed. The tunnel boundary is subjected to a biaxial state of stress since radial stress is zero after excavation. As biaxial loading requires the use of a true triaxial loading frame the fatigue response of rock structures under uniaxial compression has recently received attention in the field of fundamental rock mechanics.

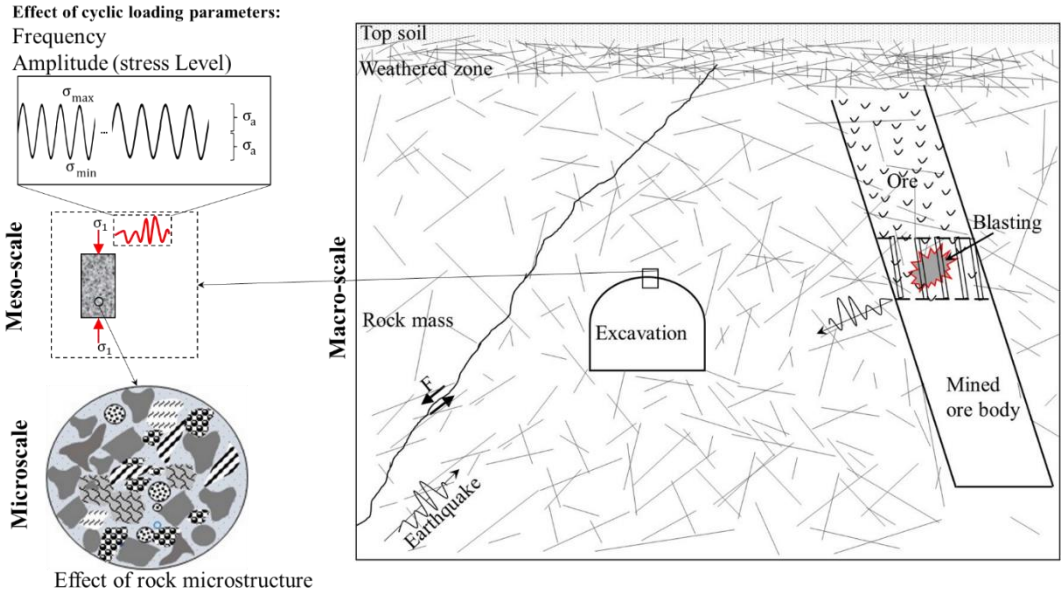

Figure 4.1. Schematic view of an underground opening under cyclic loading due to the effect of nearby blasting and earthquakes as well as other factors, shown in different scales, governing its stability (rock types, rock microstructure, and loading parameters). σ_1, σ_{max}, σ_{min}, and σ_a are the major principal stress around the tunnel boundary, maximum, minimum stress, and stress amplitude of the cyclic loading, respectively.

Previous research has established that the strength of rocks decreases by 30 to 50% under cyclic loading compared to monotonic strength (Attewell & Farmer, 1973; Bagde & Petroš, 2005a). On the other hand, rocks may also show hardening behavior, depending on the rock type and loading conditions (Singh, 1989; Taheri et al., 2016).

Loading parameters including the maximum stress level, loading amplitude, and loading frequency affect the strength and damage response of rocks under cyclic loading. The effect of stress levels on the fatigue strength of rocks has been investigated experimentally (Ma et al., 2013; Momeni et al., 2015; Ray et al., 1999; Singh, 1989). The experiments show that the higher the maximum applied stress, the greater the reduction in the fatigue strength of rocks. Loading amplitude has also been found to be an important factor affecting the fatigue response of rocks (Bagde & Petroš, 2009; He et al., 2016; Liu et al., 2018; Singh, 1989; Taheri et al., 2016). The strength degradation of rock loaded under a low stress level with high cycling amplitude is more than when it is loaded under a higher stress level with a lower cycling amplitude (Geranmayeh Vaneghi et al., 2018). There have also been attempts to address the effect of loading frequency on the deformation and strength of rocks (Attewell & Farmer, 1973; Bagde & Petroš, 2005a; Fuenkajorn & Phueakphum, 2010; Liu & He, 2012; Liu et al., 2012; Xiao et al., 2009). However, the dependence of fatigue strength and deformation on loading frequency is still not clear. The deformation response of rocks under cyclic loading is another complex problem since it is noticeably affected by loading parameters. For instance, it has been observed that axial strain at failure increases dramatically with an increase in the maximum stress level in cyclic loading (Ray et al., 1999). On the other hand, some rocks loaded under cyclic condition show hardening behavior (Ma et al., 2013; Taheri et a., 2016). However, as pointed out by Cerfontaine and Collin (2018) very little is known about the deformation response of rocks under this type of loading. Also, the damage mechanism that underpins this behavior is not fully understood and is limited to specific observations (Fan et al., 2016; Liu & He, 2012; Liu et al., 2017; Liu et al., 2018).

The types of behavior are different in soft and hard rocks. In particular, the failure mechanism is greatly dependent on the microstructure, quartz content, and porosity of the rock (Peng & Yang, 2018). Rock type and texture play a significant role in the deformation behavior of rocks under different loading scenarios. Sedimentary rocks such as sandstone, which is known as a porous rock, show different deformation and failure responses compared to compact rocks such as granite with completely interlocked grains and with no initial porosity (Potyondy, 2012). This difference is very important since these rock types are usually the common host rocks for surface and

underground excavations and are often used in building and construction (Ludovico-Marques et al., 2012). The deformation behavior of soft rocks and hard rocks under monotonic loading has been comprehensively studied. However, the deformation response of these rock types has never been compared under cyclic or fatigue processes. It seems that there is no systematic understanding of how rock materials behave under cyclic loading. This topic is in early stages of investigation and the need for more experimental data obtained from cyclic tests on different rock types is clear.

This study seeks to explore how two different rock types behave under multi-stage cyclic loading. The rock types considered are granodiorite and sandstone, representing a typical crystalline hard rock and comparably soft porous rock, respectively. The stress–strain relationship during different loading steps of these two mineralogically different rocks is compared and discussed in detail in Section 4.3.1. The effect of the maximum stress level, stress amplitude, and loading frequency on fatigue strength or post-cyclic peak strength and strain of these rocks has also been analyzed, compared, and generalized by incorporating more data from the literature (Section 4.3.2 to Section 4.3.4). The residual axial and lateral strains of individual loading stages of consecutive cycles are also compared with each other in Section 4.3.5. We discuss how different evolution responses of residual axial and lateral strain during cyclic steps relate to the damage mechanism of these rocks. This issue is also analyzed and validated by comparing the P-wave and S-wave velocities obtained from ultrasonic measurement carried out on the samples before each loading step (Section 4.3.6). Finally, a comparison of the failure modes under monotonic and cyclic loading is presented and discussion on how loading conditions influence different failure modes is provided (Section 4.3.7).

4.2. Experimental methodology

4.2.1. Rock samples

Two different rock types, a fine-grained sandstone (S) and a weakly altered coarse-grained granodiorite (G), acquired from outcrops in New South Wales, Australia, are used for this investigation. The mineral content of these rocks, determined from microscopic thin section analysis, is presented in Table 4.1. Figure 4.2 shows

photomicrographs of thin sections of the tested samples. The average density of the granodiorite and sandstone samples was determined to be 2670 kg/m^3 and 2168 kg/m^3, respectively. The water content of the samples was negligible in this investigation (0.11% for the granodiorite and 0.37% for the sandstone) and all samples were dried before testing.

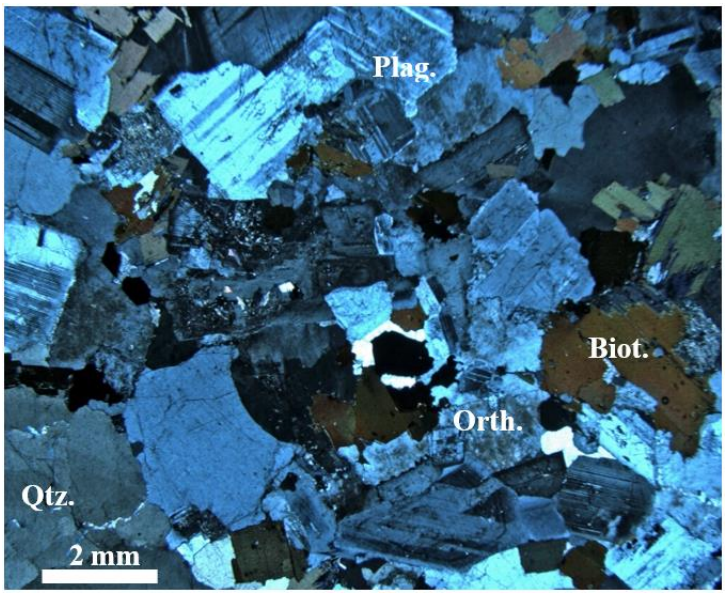

(a)

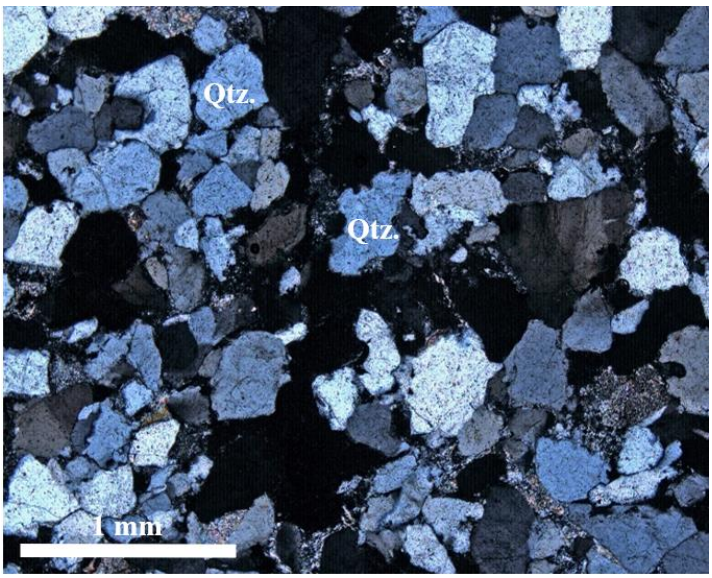

(b)

Figure 4.2. Photomicrographs of thin sections of two representative samples in cross polarized light (XPL): (a) granodiorite, and (b) sandstone, Qtz., Orth., Biot., and Plag. stand for Quartz, orthoclase, biotite, and plagioclase, respectively.

Table 4.1. Description of mineral components of the tested samples.

Sample name	Mass content of mineral components and average grain size				Description
	Quartz	Alkali feldspar (orthoclase)	plagioclase	biotite	
Fine-grained, well sorted *sandstone* (arenite)	80% (<1 mm)	-	-	-	~80% sub-rounded to angular quartz, ~10% clay and sericite, Intergranular porosity of ~10%, coatings of thin brown to black rim of iron-oxide around the grains and rare presence of grains of tourmaline, zircon and flakes of muscovite
Weakly altered *granodiorite*	~30% (4–5 mm)	~20% (3–4 mm)	~20-30% (2–3 mm)	~10% (1–2 mm)	Contains anhedral quartz and medium-grained flakes of biotite partially altered with chlorite

Altogether 17 sandstone samples and 7 granodiorite samples, all in a cylindrical shape with diameter of about 42 mm and length to diameter ratio of L/D = 2.4–2.5, were prepared according to ASTM D4543-08 and ISRM 1979 (ASTM, 2008b; Bieniawski & Bernede, 1979). Self-aligning spherical seats lubricated with grease were used to remove the effect of ample end flatness by minimizing the interface friction between the spherical seats themselves and the sample-platen contact and for uniform distribution of the stress on the sample end surface. Some samples of granodiorite and sandstone are shown in Figure 4.3.

(a)

(b)

Figure 4.3. Samples used in the experiments: (a) granodiorite and (b) sandstone.

4.2.2. Testing Equipment

A GCTS loading machine (UTC-1000 with compression loading capacity of 1000 kN and stiffness of 600–700 kN/mm) was used for the uniaxial monotonic and cyclic tests (Figure 4.4a). This frame is equipped with an electro-hydraulic closed-loop digital servo control system enabling smooth loading at any test stage under both load- and strain-controlled modes. Two rosette strain gauges with 10 mm in length and 120 Ω resistance were fitted on each sample (middle of the sample and opposite to each other) in order to record the axial and lateral strains (Figure 4.4b). A high-frequency ultrasonic measurement system with a data acquisition unit, oscilloscope, and signal generator was used for ultrasonic measurement of the compression (P) and shear wave (S) travel time (Figure 4.4c). The P-wave and S-wave ultrasonic data were measured using two different pairs of V103-RM and V153-RM transducers from OLYMPUS, respectively. The nominal element size and nominal frequency of these transducers is 13 mm and 1.0 MHz, respectively. Figure 4.4d shows these sensors attached on both ends of a sample during ultrasonic measurement.

4.2.3. Test procedure

Cyclic loading tests under different stress amplitudes (σ_a), maximum stress levels (σ_{max}), and loading frequencies (*f*) were conducted on the rock samples to investigate the effect of loading conditions on deformation and strength. The average uniaxial compression strength (UCS) of the samples was used to set the maximum stress level of the cyclic tests. The average UCS of the granodiorite and sandstone rock samples was measured to be 106.2 MPa and 41.7 MPa, respectively. The same load rate (0.1 MPa/s) was used for all tests. It should be noted that the average UCS of both samples was calculated from UCS values of small-size samples of the same material reported in Table 1 taken from another study (Geranmayeh et al., 2018) and the UCS values of 35.1 MPa and 112 MPa, obtained for samples of G-7 and S-17, respectively.

The cyclic stages were conducted under sinusoidal waveform type. This waveform has been found to have a larger dynamic effect on the deformation response of rocks than the triangle ramp waveform (Bagde & Petroš, 2005c; Xiao et al., 2008; Zhenyu & Haihong, 1990). Multi-stage cyclic tests were carried out under different steps;

ultrasonic measurement and Computational Tomography (CT) were conducted before each loading stage (Figure 4.5). The stress path for each step of the test is shown in Figure 4.6. CT was used as a non-destructive technique to scan the samples in order to assess quality before the loading tests and to check for any microcrack development inside the rock samples after each loading step. A Siemens SOMATOM X-ray CT device with energy beam of 140 kV/500mAs was used for this purpose.

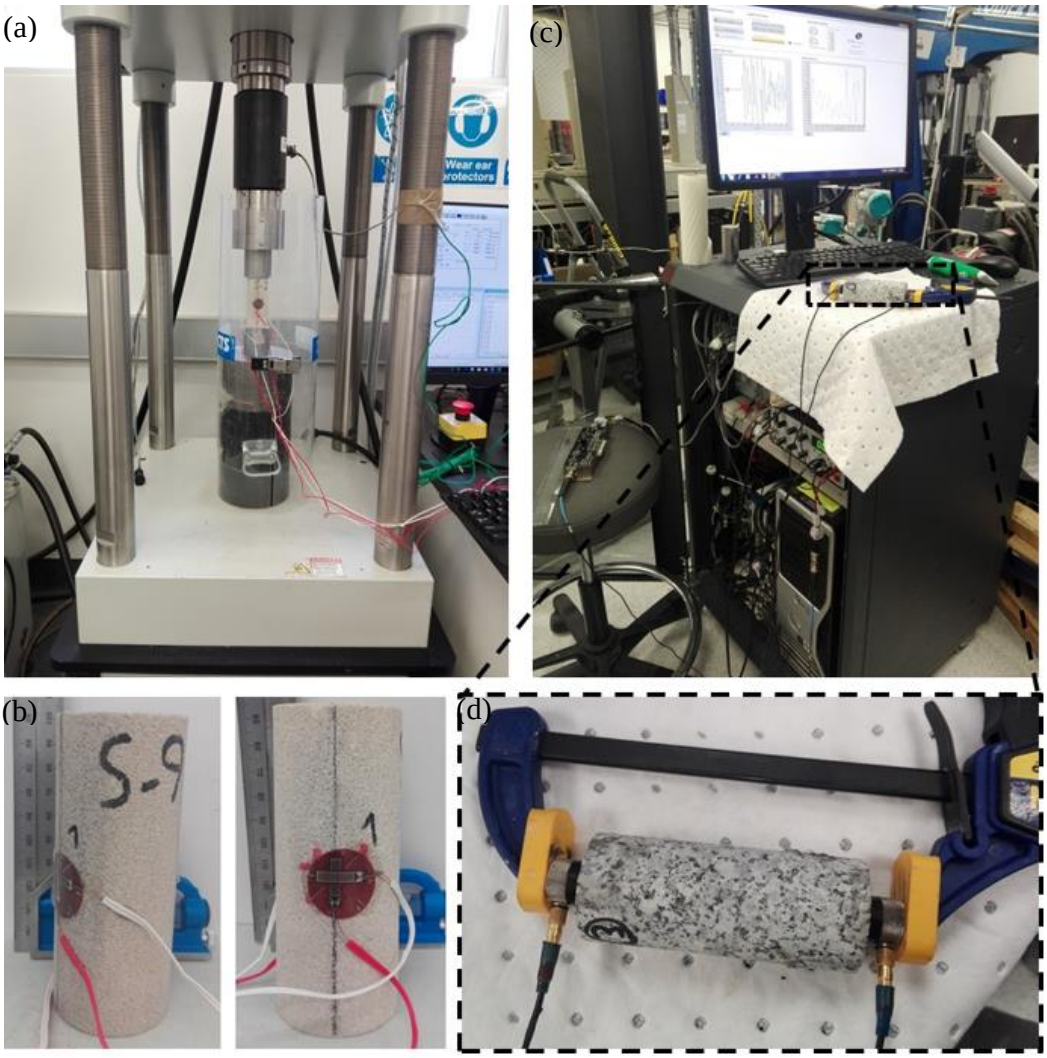

Figure 4.4. Testing equipment: (a) UCT-1000 uniaxial compression test frame, (b) two rosette strain gauges attached on two sides of the sample, (c) ultrasonic measurement system, and (d) ultrasonic transducers during measurement.

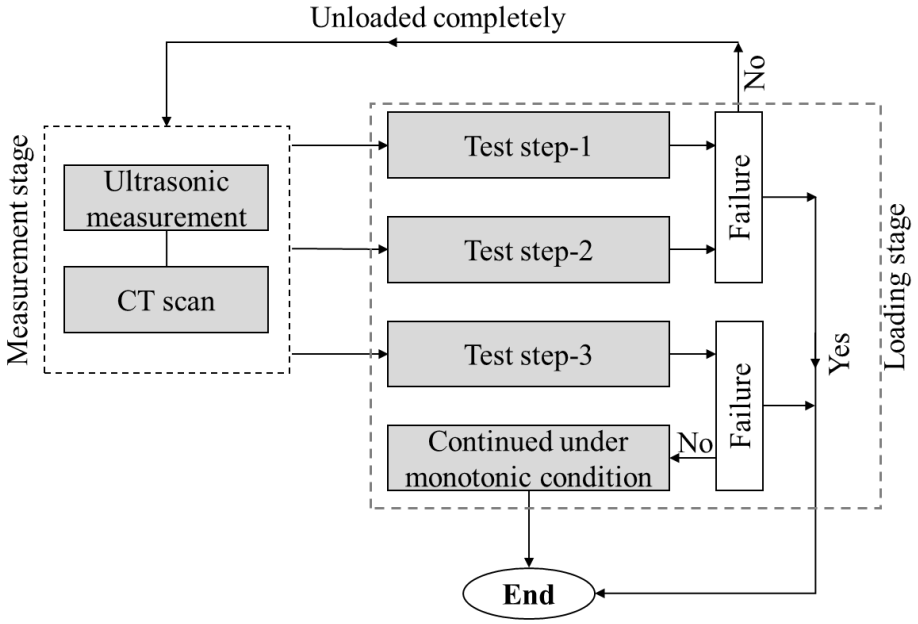

Figure 4.5. Flow chart representing the testing steps of the multi-stage cyclic loading tests conducted on samples.

Table 4.2 shows the loading setup for all tested samples. The cyclic tests were carried out under loading frequencies of 0.05, 0.1 and 1 Hz. The stress amplitudes were set to 10, 15, and 35 MPa for the granodiorite and 3, 5, 6, and 10 MPa for the sandstone samples. The maximum stress level was kept constant at 80% of $UCS_{ave.}$ for the cyclic tests of the granodiorite samples, except for sample G-3, whereas it was set at 84, 90 and 96% of $UCS_{ave.}$ for the cyclic tests of the sandstone samples. The minimum stress level was set above 42 MPa and 15 MPa for the granodiorite and sandstone samples, respectively. The minimum stress level of sample G-6 was set low (15 MPa) in order to study the effect of high loading amplitude on the cyclic behavior of the granodiorite samples. All the cyclic tests were conducted between the minimum stress level equal to or above the crack initiation stress threshold σ_{ci} (which generally occurs around 40% of the peak uniaxial compression strength (Brace et al., 1966; Martin & Chandler, 1994)), and the uniaxial peak strength. This helped in investigating the effect of loading and unloading on unstable crack growth within the samples.

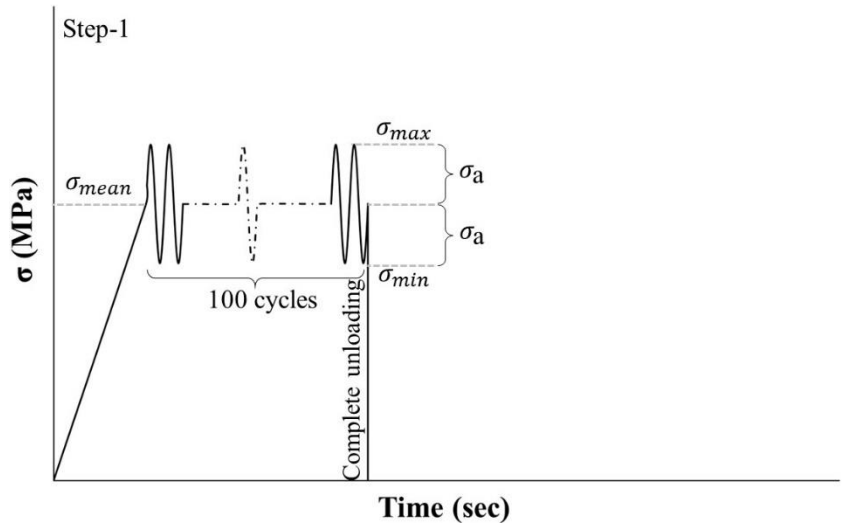

(a)

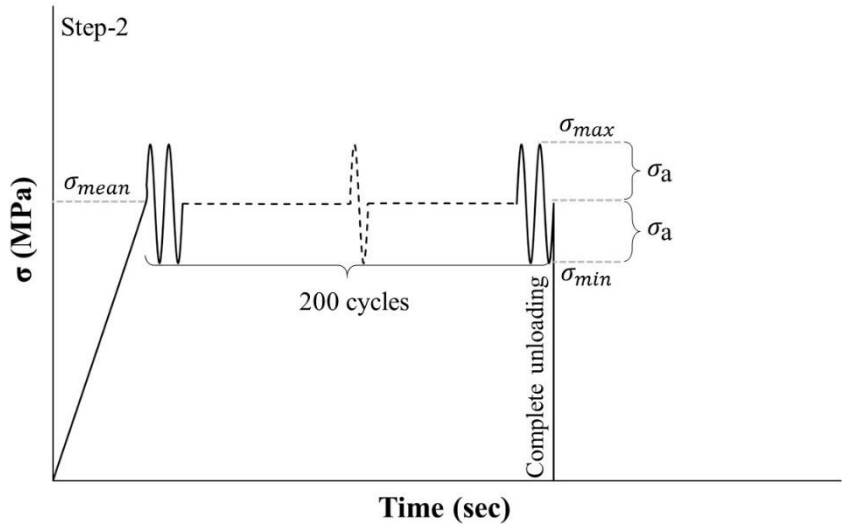

(b)

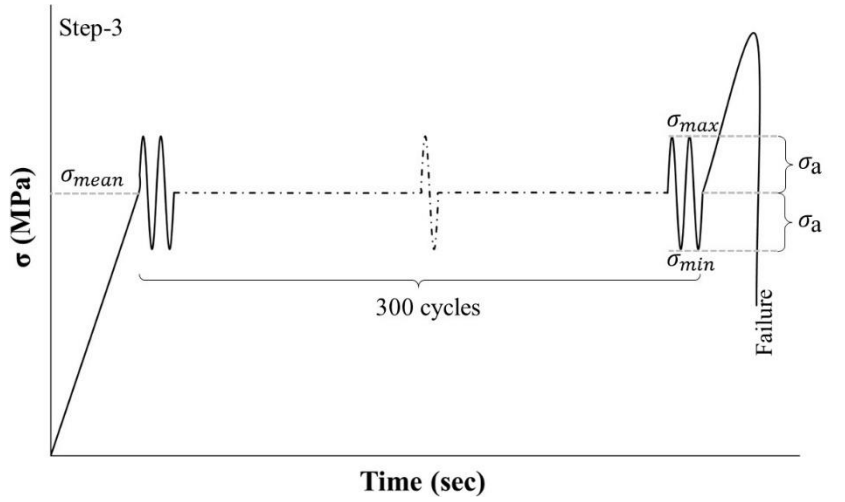

(c)

Figure 4.6. Schematic stress path for (a) step-1, (b) step-2, and (c) step-3 of the multi-stage cyclic loading test.

Table 4.2. Loading setup for the multi-stage cyclic tests on the granodiorite (G) and sandstone (S) samples.

	Sample No.	Frequency (Hz)	σ_{min} (MPa)	σ_{mean} (MPa)	σ_{max} (MPa)	σ_{max}/UCS (%)	σ_a (MPa)
Granodiorite	G-1	1	65	75	85	80	10
	G-2	0.05	65	75	85	80	10
	G-3 [a]	0.1	60	75	90	85	15
	G-4	0.05	55	70	85	80	15
	G-5	0.1	65	75	85	80	10
	G-6	0.05	15	50	85	80	35
	G-7	monotonic loading					
Sandstone	S-1	1	25.5	31.5	37.5	90	6
	S-2	0.05	25.5	31.5	37.5	90	6
	S-3	1	17.5	27.5	37.5	90	10
	S-4	0.05	17.5	27.5	37.5	90	10
	S-5	1	30	35	40	96	5
	S-6	0.05	30	35	40	96	5
	S-7 [b]	1	34	37	40	96	3
	S-8	0.05	34	37	40	96	3
	S-9	1	15	25	35	84	10
	S-10	0.05	15	25	35	84	10
	S-11	0.05	30	35	40	96	5
	S-12 [c]	1	30	35	40	96	5
	S-13	1	17.5	27.5	37.5	90	10
	S-14	1	17.5	27.5	37.5	90	10
	S-17	monotonic loading					

[a]G-3 was loaded under monotonic condition up to 75 MPa in step-0 then unloaded completely → step-1 → step-2 to failure
[b]S-7 stopped at the 30th cycle during step-1
[c]S-12 was loaded under monotonic conditions up to 34 MPa in step-0 then unloaded completely → step-1 → step-2 to failure

4.3. Results and discussion

4.3.1. Overall stress–strain behavior

The effects of maximum stress levels, loading frequency, and loading amplitude during cyclic loading on the strength and deformation response of tested rock samples have been investigated throughout these experimental tests. The samples underwent cyclic loading of 100 cycles at first step, then were unloaded completely and the test was

repeated for a second and third time for 200 cycles and 300 cycles, respectively, until failure happened. If the sample did not fail during these steps, step-3 continued under monotonic conditions until failure. Table 4.3 summarizes the failure steps, the number of cycles (fatigue life if failure occurs), and stress levels depending on the different loading scenarios considered in this study. Some scenarios were repeated on other samples when the test was unsuccessful (e.g. S-13, S-14, S-3). The results of those successful tests are discussed hereafter.

Table 4.3. Results of the multi-stage uniaxial cyclic compression tests conducted on sandstone and granodiorite samples.

Step	Sample No.	σ_f (MPa)	σ_f/UCS_{ave} (%)	Number of cycles	Final strain (%)[a]		Remarks
					Axial	Lateral	
1		-	-	100	0.185	-0.037	
2	G-1	-	-	200	0.198	-0.083	
3		123.6	116	300	0.287	-0.324	Failed at monotonic stage after Step-3
1	G-2	-	-	100	0.189	-0.049	
2		80.0	75	17	0.192	-0.744	Failed during Step-2
0		-	-	-	0.190	-0.110	
1	G-3		-	100	0.201	-0.087	
2		113.5	107	200	0.258	-0.492	Failed at monotonic stage after Step-3
1		-	-	100	0.176	-0.049	
2	G-4			200	0.180	-0.094	
3		112.1	106	300	0.218	-0.101	Failed at monotonic stage after Step-3
1		-	-	100	0.188	-0.217	
2	G-5		-	200	0.188	-0.101	
3		116.3	109	300	0.225	-0.351	Failed at monotonic stage after Step-3
1	G-6	83.5	79	33	0.288	-0.538	Failed during Step-1
1	S-1[b]	-	-	100	0.213	-0.126	-
1	S-2[b]	-	-	100	0.561	-0.329	-
1	S-3[b]	-	-	100	0.207	-0.104	-
1	S-4	-	-	100	0.250	-0.162	
2		36.6	88	1	0.310	-0.283	Failed during Step-2
1	S-5	32.6	78	0	0.362	-0.365	Failed during monotonic stage of Step-1
1	S-6	34.9	84	0	0.208	-0.152	Failed during first unloading cycle of Step-1
1	S-7	-	-	30	0.216	-0.142	Stopped at 30th cycle
2		34.5	83	0	0.030	0.016	Failed before the first cycle of Step-2
1	S-8	39.2	94	5	0.026	-0.039	Failed during Step-1
1	S-9	-	-	100	0.170	-0.101	
2		31.4	75	117	0.076	-0.073	Failed during Step-2
1	S-10	34.3	82	2	0.345	-0.436	Failed during Step-1
1	S-11	39.7	95	18	0.249	-0.427	Failed during Step-1
1	S-13	33.8	81	4	0.387	-0.371	Failed during Step-1
1	S-14	35.8	86	8	0.432	-0.510	Failed during Step-1

[a] Final strain here is the strain when a test was finished, regardless of failure or the end of the cycles.
[b] These samples broke during test setup of Step-2, hence only results for Step-1 are available.

Figure 4.7 shows the stress–strain curves for samples G-1, G-2, G-3, G-4, S-7, and S-14. The values of both axial and lateral strains were the average values recorded by two strain gauges attached on the middle of the samples. The recordings of both strain gauges have been analyzed to avoid any variation in the results stemming from equipment precision, sample shape deviation, or operational variability (cf. chapter 2)

What stands out in the stress–strain curves presented in Figure 4.7 is the increase in both lateral and axial strain during the monotonic loading stages with test steps Step-1, Step-2 and Step-3 (cf. Figure 4.6). Those samples which did not fail at previous steps experienced more axial and lateral strain during successive steps (Table 4.3). This can clearly be seen in some of the stress–strain curves of both granodiorite and sandstone samples (Figure 4.7d and Figure 4.7e). This finding clearly indicates the effect of loading history on cracking and damage evolution of the rock samples. The difference in strain levels between two consecutive steps during the monotonic stages is related to cracking and unstable crack growth since the samples had already been loaded at a stress level above the crack initiation stress threshold (σ_{ci}) during the previous step. This is the irreversible and permanent strain that rocks usually show under loading–unloading history, in contrast to perfectly elastic materials for which permanent strain is ignorable after complete unloading (Eberhardt et al., 1999). The increase in strain following the test steps was more noticeable for the sandstone samples than the granodiorite specimens. This can be seen by comparing the difference in strains marked in Figure 4.7d and Figure 4.7e. This observation indicates that the effect of previous loading, either cyclic or monotonic, on crack/damage development in sandstone was more noticeable than that in granodiorite. Pore collapse followed by transgranular cracking of the sandstone samples resulted in more deformation than the crack closure, and new intergranular or intragranular crack initiation/extension in interlocked grains of granodiorite samples. However, it should be noted that this greatly depends on the stress level applied.

From the stress–strain curves in Figure 4.7 and Figure 4.8, it can be seen that the hysteresis loops for the sandstone and granodiorite samples showed different patterns. Hysteresis loops for most rock types under cyclic testing usually develop according to the three-phase law of loose–dense–loose (Taheri et al., 2016; Taheri et al., 2017; Tien et al., 1990; Wang et al., 2016; Xiao et al., 2009). However, this pattern may vary depending on loading conditions and rock types. Hysteresis loops for soft rocks follow

the three-phase law in which irreversible strains accumulate rapidly during the first cycles followed by a stable incremental rate during the dense or second phase, and finally by an accelerated rate in strain accumulation recognizable by a loose pattern of the stress–strain curves approaching failure. On the other hand, hysteresis loops for hard rocks follow a dense pattern throughout the test followed by a sudden loose phase near failure. Therefore, the loose phase in strain accumulation during the first cycles is barely visible for hard crystalline rocks like granodiorite. This can be clearly seen from comparison of the stress–strain curves in Figure 4.7 and Figure 4.8. The first loose pattern of hysteresis loops is noticeable for sandstone, while it is generally dense for granodiorite throughout the test until failure, with a sudden expansion of the hysteresis loops. This result reflects the difference in deformation response and fracture mechanism of these different rock types.

Comparing the hysteresis loops of the axial and lateral strains reveals another interesting feature. The lateral strain for both sandstone and granodiorite samples develops rapidly at a greater rate of increase than the axial strain. This can be seen from the expansion and overall slope of the stress–strain hysteresis loops illustrated in Figure 4.8. The expansion of the lateral strain hysteresis loops is more than that of the axial strain. As also shown in Figure 4.8, the overall slope of the stress–lateral strain hysteresis loops is higher than that of the axial strain. Apparently, the reason for this difference is the gradual development of large dilatant cracks oriented parallel to the loading direction; their opening creates strongly increasing lateral strain (dilatancy). This could also be due to the closure of microcracks aligned perpendicular or at an angle with respect to the loading direction, during loading–unloading stages of the cyclic process. This observation, which has also been reported in another study (Zhenyu & Haihong, 1990), causes more extension of the lateral deformation and in turn a looser pattern of stress–strain hysteresis loops of the lateral strain than of the axial strain. What is surprising here is that this deformation response is more obvious for stress–strain hysteresis loops of the sandstone samples (cf. Figure 4.7c with Figure 4.7e and Figure 4.8a with Figure 4.8b). This is because of the difference in the number of microcracks in these two rock types due to their microstructures. Grains in sandstone as a porous rock is sutured along narrow contacts which could deboned at lower stresses even before the actual mechanical loading (for instance during core taking etc.). Therefore, probably the greater number of pre-existing microcracks in sandstone, because of its

voids and relatively weak cementation, resulted in greater dilatancy and lateral expansion compared to the granodiorite, which has larger interlocked grains and a relatively lower number of dilatant microcracks.

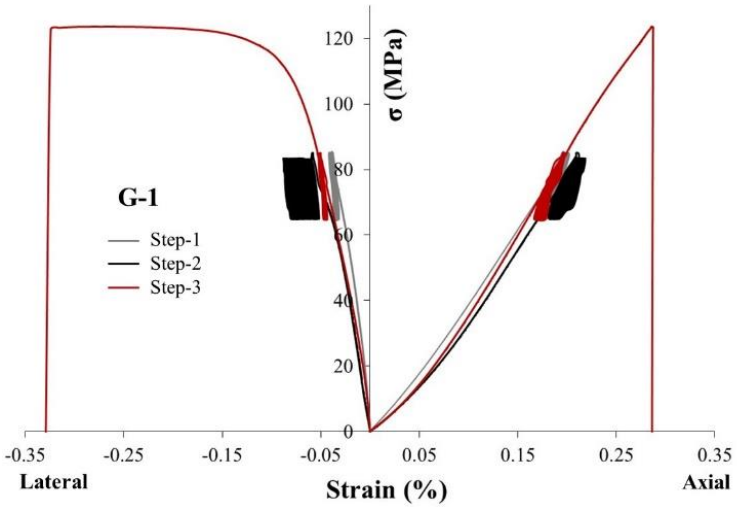

(a)

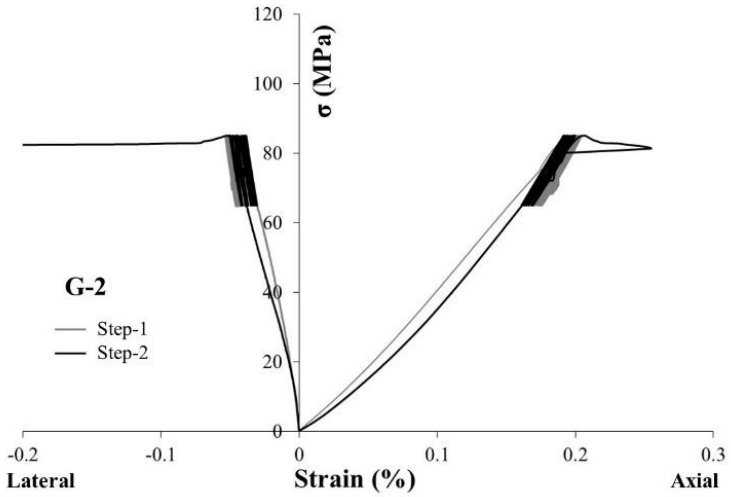

(b)

Figure 4.7 (continued on the next page).

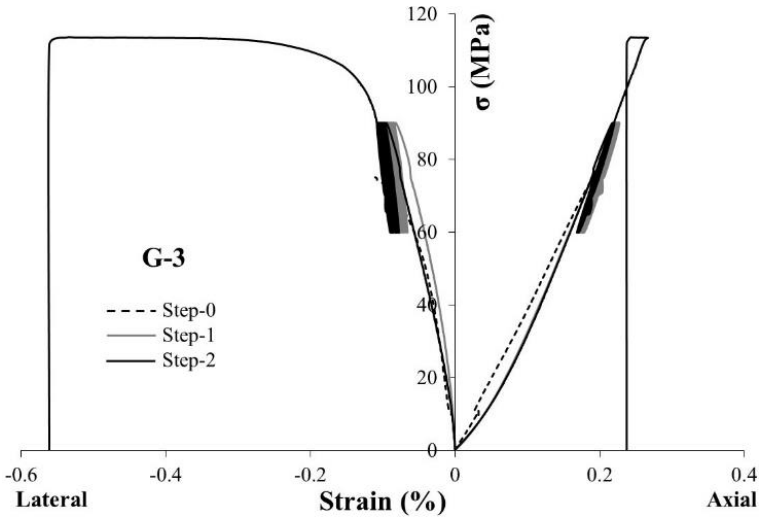

(c)

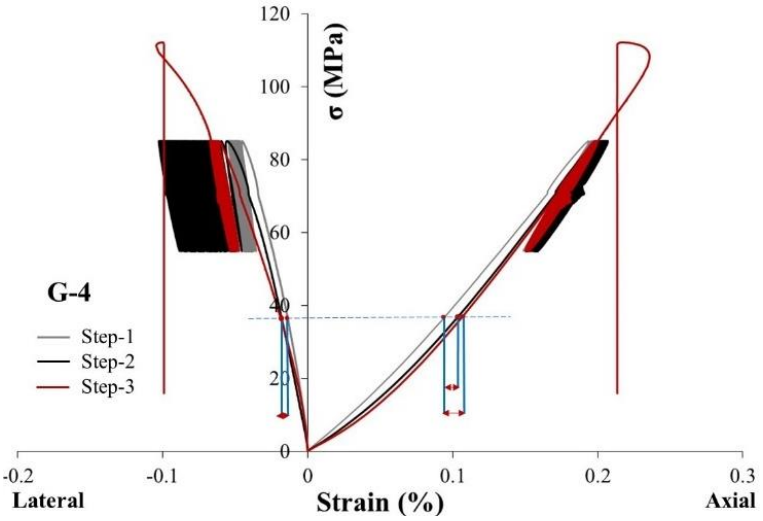

(d)

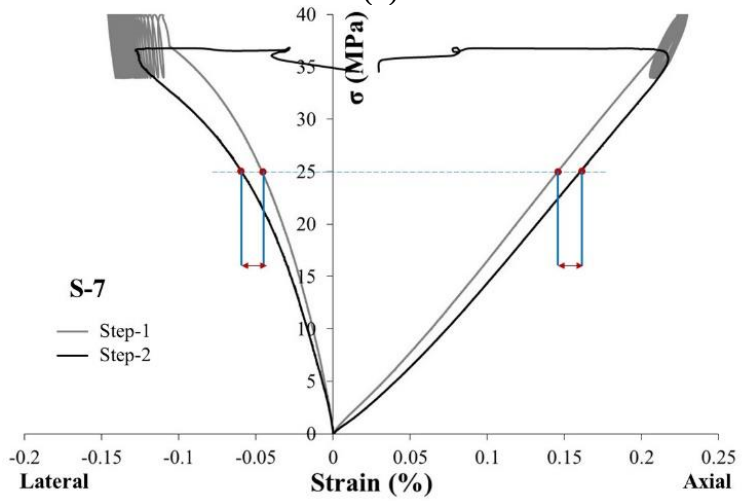

(e)

Figure 4.7 (continued on the next page).

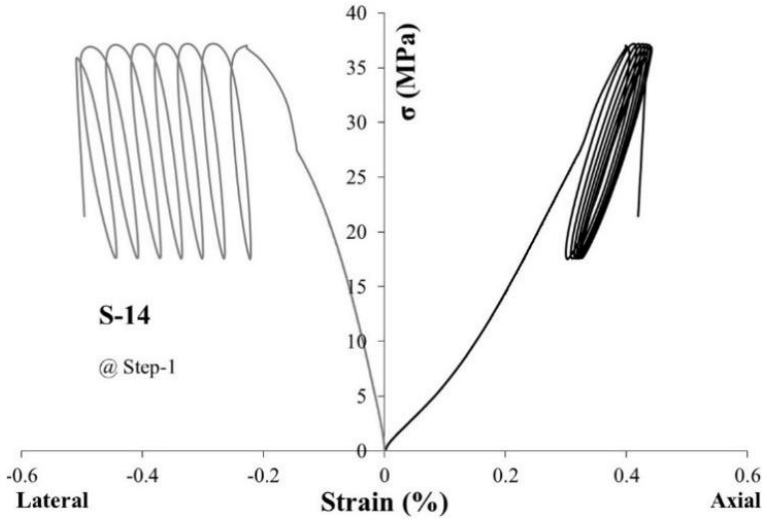

(f)

Figure 4.7 (continued from previous pages). The stress–strain curves of the multi-stage uniaxial cyclic compression tests for granodiorite: (a) G-1, (b) G-2, (c) G-3, (d) G-4, and sandstone: (e) S-7, and (f) S-14, samples.

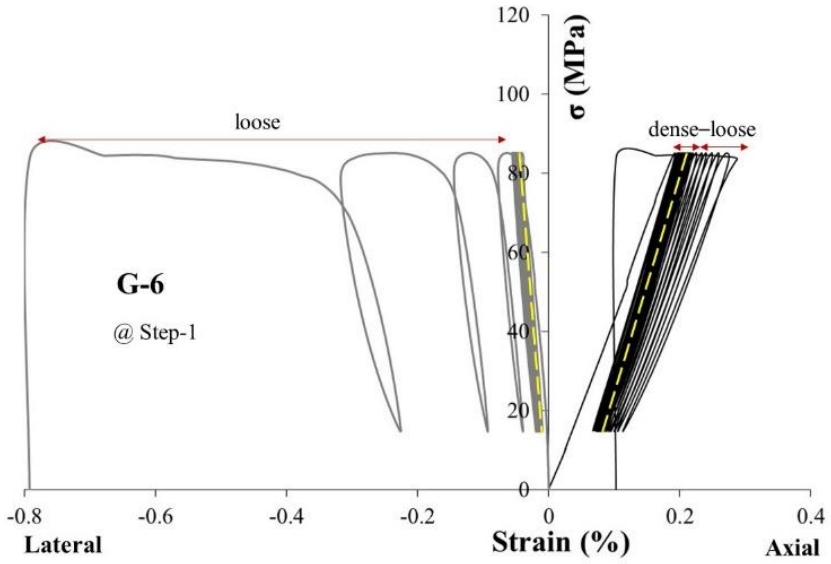

(a)

Figure 4.8 (continued on the next page).

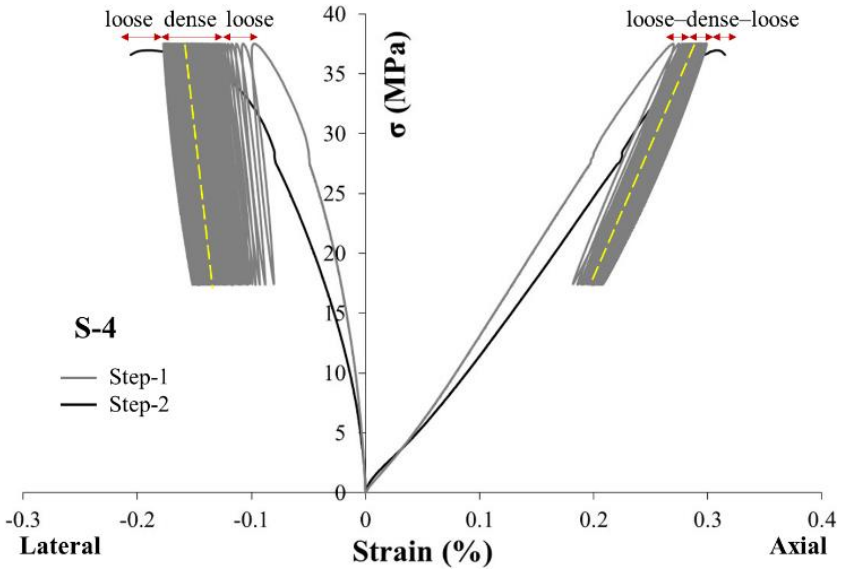

(b)

Figure 4.8 (continued from previous page). The stress–strain curves of the multi-stage uniaxial cyclic compression tests: (a) granodiorite sample of G-6, and (b) sandstone sample of S-4, showing different patterns for hysteresis loops of two different rock types throughout the cyclic test.

4.3.2. The effect of maximum stress levels

The effect of maximum stress levels on fatigue strength or post-cyclic peak strength and deformation can be considerable. For instance, sample G-3 loaded under a maximum stress level of 90 MPa (85% of UCS) and loading amplitude of 15 MPa showed larger strains and less peak strength than sample G-5, loaded under a maximum stress level and loading amplitude of 85 MPa (80% of UCS) and 10 MPa, respectively (Table 4.3). The axial and lateral strain increased with an increase in the applied maximum stress level and loading amplitude. The axial and lateral strain for sample G-3 were determined to be 0.258% and 0.492%, respectively, compared with 0.225% and 0.351% recorded for sample G-5. A similar response was also observed for the sandstone samples. Samples S-13 and S-14, both loaded under a maximum stress level of 37.5 MPa (90% of UCS) and loading amplitude of 10 MPa, failed at greater axial and lateral strain and fewer cycles, compared to sample S-9 loaded under the same loading amplitude but with lower maximum stress of 35 MPa (84% of UCS), which failed during the second loading step (step-2) under a higher number of cycles (117

during the second step and 217 in total). Samples S-13 and S-14 failed during loading step-1 and experienced greater strain, whereas sample S-9 did not fail during step-1 and experienced less axial and lateral strain. This is illustrated in Figure 4.9 in which the strain for these samples during loading step-1 is compared. Samples S-13 and S-14 failed at a lower number of cycles (4 and 8 cycles during step-1, respectively), compared with sample S-9. Therefore, it can be concluded that the higher the maximum stress level, the greater the axial and lateral deformation and the shorter the fatigue life. This result, which has also been reported in other studies (Geranmayeh et al., 2018; Ma et al., 2013; Ray et al., 1999; Singh, 1989), is consistent and independent of the rock type.

Comparison of the residual axial strain of these samples at unloading points (valley points) of the cyclic stages revealed another interesting detail. Residual axial strain accumulates rapidly at higher maximum stress levels. This is shown in Figure 4.10. Independent of the values of the initial strain before the start of the cyclic stage, the difference $\Delta\varepsilon_r$ between strain at the first cycle and strain at the last cycle, N = 100, was greater for samples loaded under a higher maximum stress level. This value was determined to be 0.015% for S-9, loaded under a lower maximum stress level, compared with 0.018%, 0.248%, and 0.117% for S-3, S-13, and S-14, respectively. This behavior was also observed for the granodiorite samples during loading step-1. Sample G-3, loaded under a higher maximum stress level, experienced greater $\Delta\varepsilon_r$ of 0.007% compared with that of G-5 (0.004%), loaded under the lower maximum stress level and loading amplitude. From Figure 4.10a, it can be seen that strain accumulation during the second phase of fatigue development (II) is more noticeable for the sample loaded under a higher maximum stress level. This indicates that sample G-3, for example, loaded under a greater maximum stress level, deformed relatively more during the second phase than G-5. Therefore, the slope of the second phase of both axial and lateral strains showed an increasing trend with an increase in the maximum stress level. This result, which has also been reported by others (Gong & Smith, 2003; Guo et al., 2012; Liu & Liu, 2017; Momeni et al., 2015), supports the idea that microcracks develop at a higher rate at higher maximum stress levels.

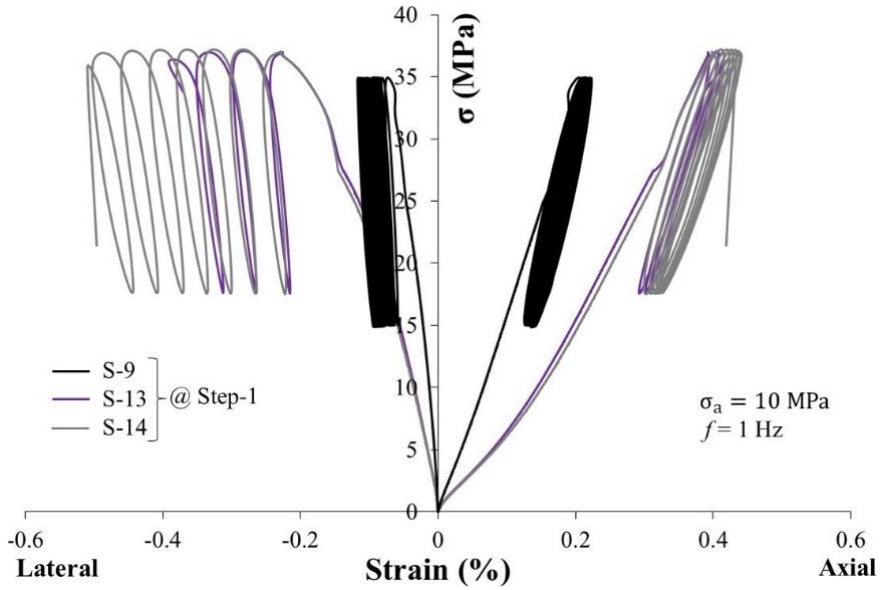

Figure 4.9. The stress–strain curves for the sandstone samples during step-1 under loading amplitude of 10 MPa, loading frequency of 1 Hz, and maximum stress of 85% of UCS for S-9 and 90% of UCS for S-13 and S-14.

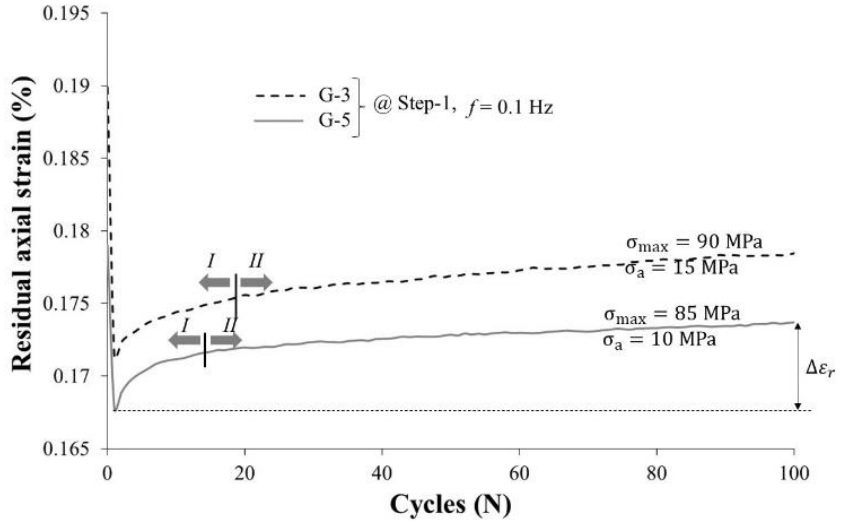

(a)

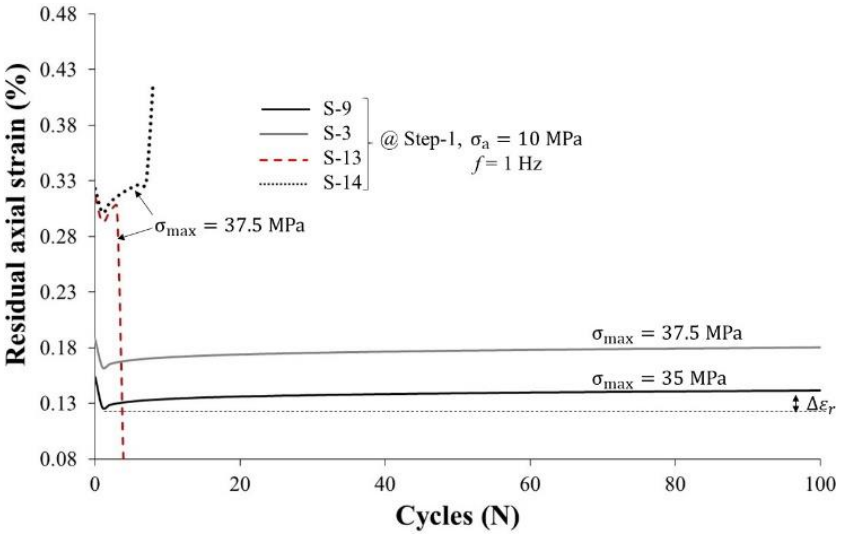

(b)

Figure 4.10. Comparison of the residual axial strains for: (a) granodiorite samples of G-3 and G-5, and (b) sandstone samples of S-3, S-9, S-13, and S-14.

Turning now to the fatigue strength threshold at which the rock can sustain loading and unloading under indefinite cycles without failure, this limit is different for these two rock types. Fatigue strength is defined as the maximum stress at which a rock can be cyclically loaded for a large number of cycles without failure (Schijve, 2008; Vutukiri et al., 1978). Hence, the relevant fatigue life of the sample will be infinite for that stress level. Generally, plotting the stress ratio of the maximum stress level of cyclic loading to monotonic peak strength ($\sigma_{max}/\sigma_{mon}$) against the number of cycles, termed as S–N plot, is a meaningful representation of fatigue strength and fatigue life.

Figure 4.11 illustrates the S–N curve for the sandstone and granite or granodiorite rocks of the current experiments and other published research (Burdine, 1963; Geranmayeh et al., 2018; Hardy, 1970; Ishizuka et al., 1990; Momeni et al., 2015; Nejati & Ghazvinian, 2014; Rajaram, 1981; Scholz & Koczynski, 1979; Singh, 1989; Taheri et al., 2016; Xiao et al., 2010; 2011; Yamashita et al., 1999; Zhenyu & Haihong, 1990). As can be seen, there is a downward trend in the data, despite the noticeable scatter around the regression line, plotted for all data on the semi-log axes. The equation for the regression line obtained and the standard deviation of data for both rock types are also shown on Figure 4.11. This trend confirms the abovementioned statement that the greater the stress ratio, the shorter the fatigue life. Moreover, the difference between the fatigue strength threshold of sandstone, as a relatively soft rock, and granite/granodiorite, as a hard rock, can be clearly identified from the S–N curve. This threshold ranges from 0.75 to 0.9 of monotonic peak strength for sandstone and 0.65 to 0.80 for granite/granodiorite. These thresholds can be used as the reference fatigue limits for these two rock types but they may vary depending on loading conditions. It should be noted that a million cycles have been considered here to be sufficient for most rock engineering applications. These findings support the idea that the fatigue strength threshold of soft and ductile rocks is higher than that of hard and brittle rocks (Geranmayeh et al., 2018). Therefore, it can be assumed that hard rocks are more susceptible to cyclic loading, compared to soft rocks, and their strength degradation under cyclic loading is more pronounced. As can also be seen in this figure, the Cyclic Allowable Maximum Stress Levels (CAMSL) of these rock types are determined based on experimental data. For instance, for a medium-cycle event (≈100–10000 cycles) such as mine haulage roads, sandstone would not fail under the cyclic conditions if the maximum stress level did not exceed 80% of its monotonic strength. The CAMSLs determined can be used as rough stress levels for design purposes in both practical applications and experimental studies.

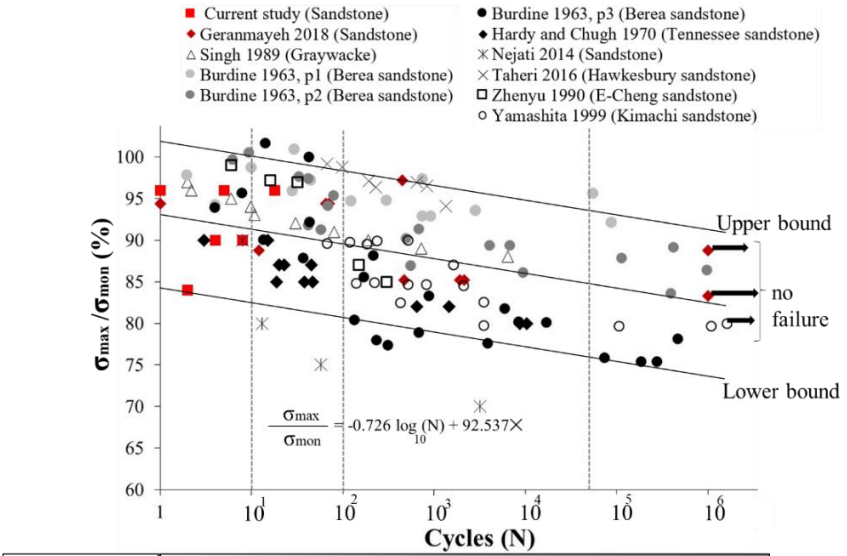

Cycle number	Low	Medium	High	
Examples	Oil/gas discharge	Earthquake	Traffic	Blasting / Rock Cutting
CAMSL	<90%	<85%	<80%	<75% Fatigue

(a)

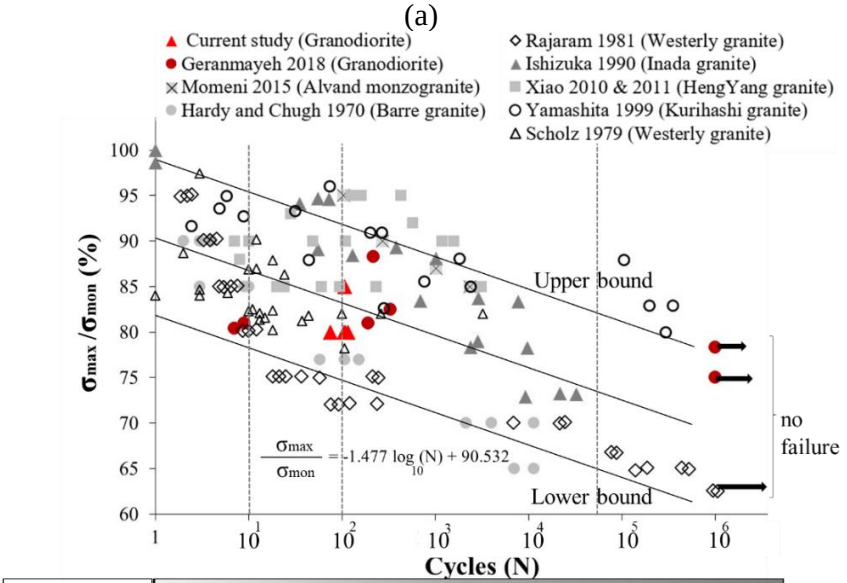

Cycle number	Low	Medium	High	
Examples	Oil/gas discharge	Earthquake	Traffic	Blasting / Rock Cutting
CAMSL	<80%	<75%	<70%	<65% Fatigue

(b)

Figure 4.11. S–N curves for: (a) sandstone, and (b) granite/granodiorite samples, tested cyclically under constant loading amplitude of uniaxial / triaxial compression (Burdine, 1963; Geranmayeh Vaneghi et al., 2018; Hardy, 1970; Ishizuka et al., 1990; Momeni et al., 2015; Nejati & Ghazvinian, 2014; Rajaram, 1981; Scholz & Koczynski, 1979; Singh, 1989; Taheri et al., 2016; Xiao et al., 2010, 2011; Yamashita et al., 1999; Zhenyu & Haihong, 1990); CAMSL stands for Cyclic Allowable Maximum Stress Level.

4.3.3. The effect of cycling amplitude

The cycling amplitude, defined as half of the algebraic difference between maximum and minimum stress levels, greatly affects the strength degradation of rock under cyclic loading conditions (He et al., 2016; Singh, 1989; Taheri et al., 2016). Comparing the fatigue life and strain of samples G-2, G-4, and G-6, all tested under the same maximum stress level, shows that sample G-6, loaded under a higher loading amplitude of 35 MPa, failed during step-1 after 33 cycles at a shorter fatigue life compared with other samples that sustained loading for step-2 and even step-3 of the test steps (Figure 4.12a). The axial and lateral strain of sample G-6 were greater than those of samples G-2 and G-4 during step-1 (Table 4.3). Therefore, damage develops more rapidly at higher loading amplitudes. This is clearly shown in Figure 4.13a, in which samples G-6 and G-4 resulted in more $\Delta\varepsilon_r$ of lateral strain during step-1 than sample G-2, loaded under a relatively lower loading amplitude. Similarly, samples S-13 and S-14 loaded under a loading amplitude of 10 MPa failed at a shorter fatigue life during step-1, compared with sample S-1 under a lower loading amplitude of 6 MPa, which sustained loading during this step (Figure 4.12b). As can be seen in this figure, the stress–strain hysteresis loops for the samples under higher loading amplitude show a wider pattern compared to those for a lower loading amplitude. The residual lateral strain also increases more rapidly for samples S-13 and S-14 with higher loading amplitudes (Figure 4.13b). These results are consistent with the literature confirming that damage accumulation is more evident at higher loading amplitudes (Gong & Smith, 2003; He et al., 2016) and the higher the loading amplitude, the shorter the fatigue life (Geranmayeh et al., 2018; He et al., 2016; Liu et al., 2018; Singh, 1989; Xiao et al., 2010). The ratio of stress amplitude to monotonic strength (σ_a/σ_{mon}) against the number of cycles, obtained from the literature and this study, is plotted in Figure 4.14. The curves fitted for each individual data in this figure all generally show a decreasing trend in fatigue life with an increase in loading amplitude or σ_a/σ_{mon} ratio, regardless of the test type and other loading conditions.

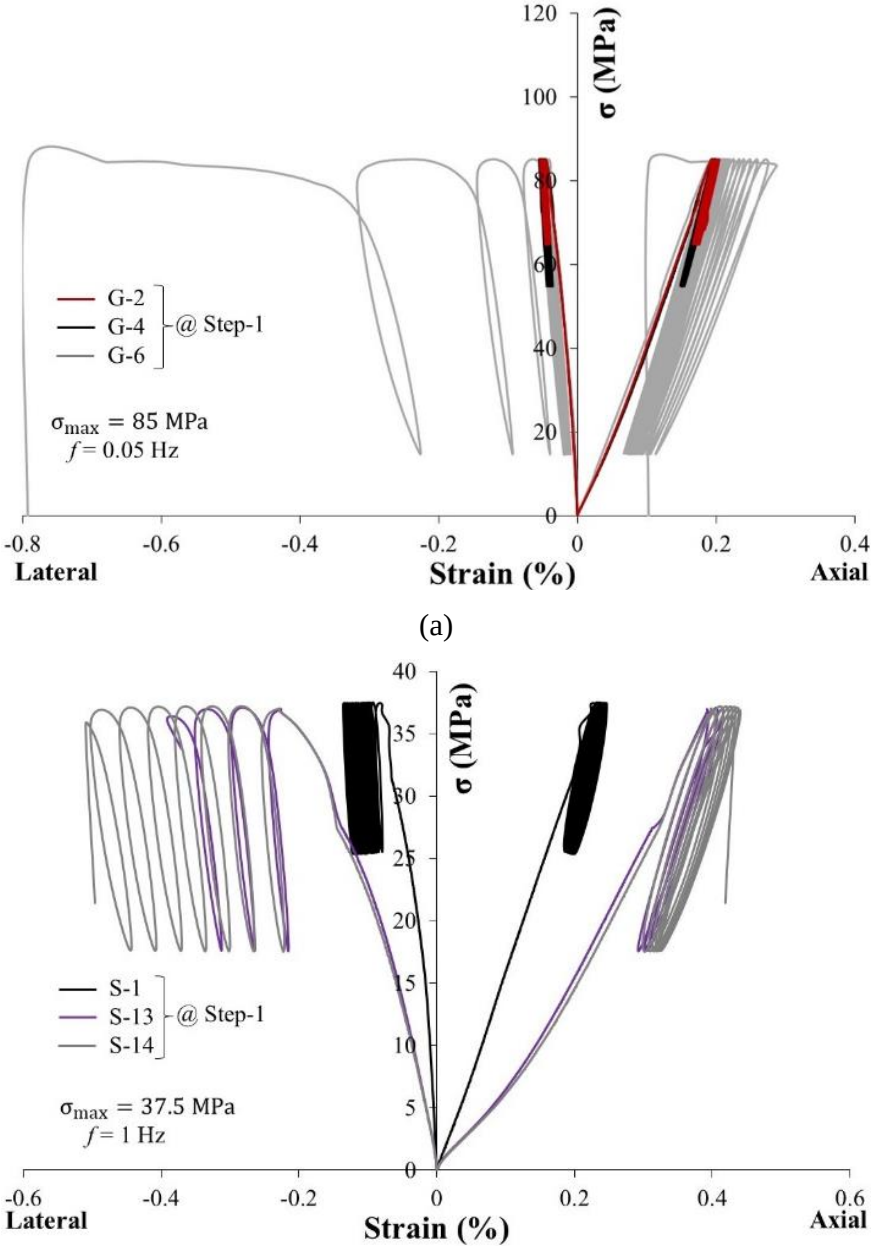

Figure 4.12. Stress–strain curves for: (a) granodiorite samples of G-2, G-4, and G-6, and (b) sandstone samples of S-1, S-13, and S-14 during step-1.

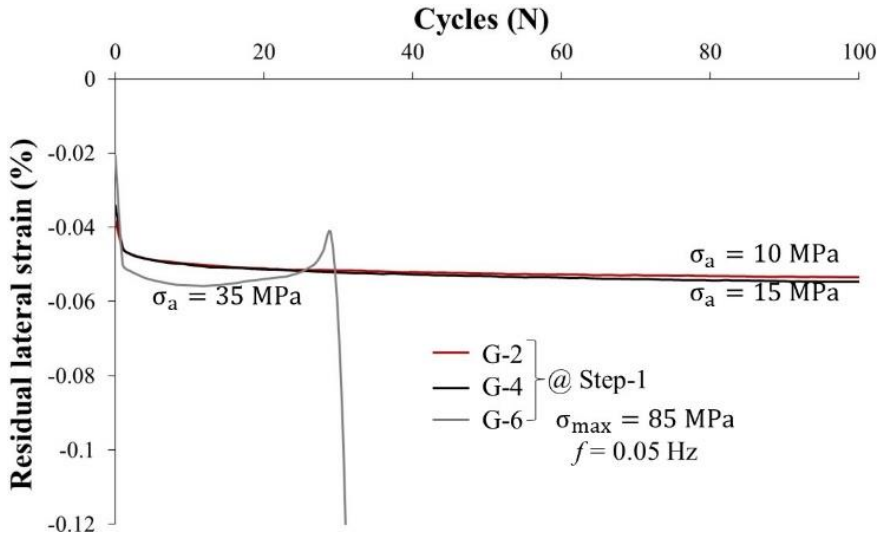

(a)

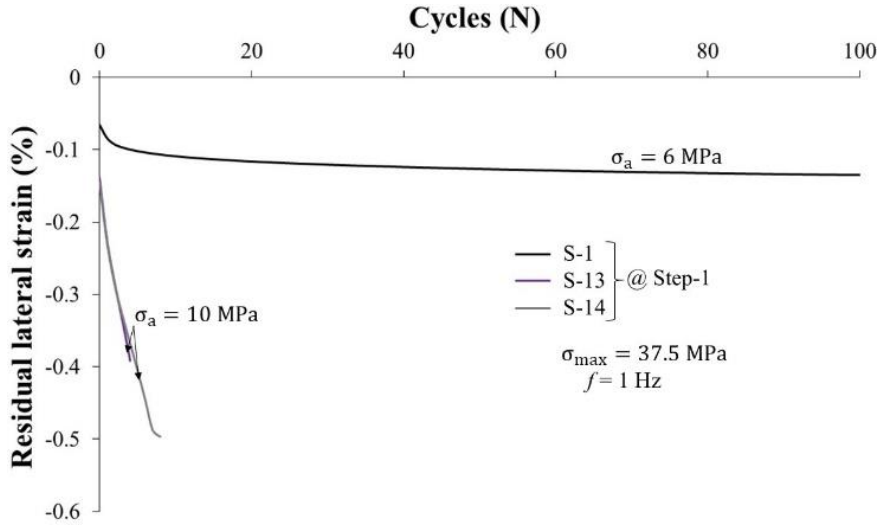

(b)

Figure 4.13. Comparison of residual lateral strain for: (a) granodiorite samples of G-2, G-4, and G-6, and (b) sandstone samples of S-1, S-13, and S-14 during step-1.

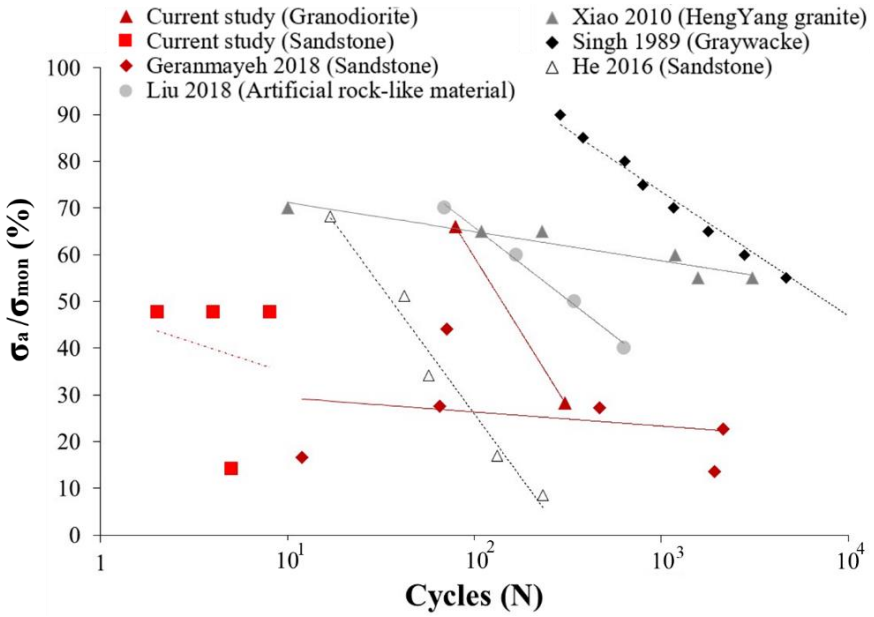

Figure 4.14. The ratio of stress amplitude to monotonic strength of some rocks, tested cyclically under different loading conditions.

4.3.4. The effect of loading frequency

The effect of loading frequency on the strength and fatigue deformation of rocks is complicated since cyclic testing under high loading frequencies is very sensitive to the performance of loading machines, especially when the applied loading amplitude is high (Bagde & Petroš, 2005b). On the other hand, most cyclic tests so far have been carried out at low frequencies since most mining and civil related structures are exposed to low-frequency events. Based on the literature, there is no clear trend relating loading frequency to fatigue strength and fatigue life at high loading frequencies (Bagde & Petroš, 2009; He et al., 2016; Ishizuka et al., 1990). However, there is a direct relationship between loading frequency, fatigue strength and fatigue life at low frequencies of usually less than 1 Hz. Comparison of the test results of samples G-2, G-5, and G-1, all loaded under the same maximum stress of 85 MPa and loading amplitude of 10 MPa, and loading frequencies of 0.05, 0.1 and 1.0 Hz respectively, shows that fatigue life increases with loading frequency. Sample G-2 failed at the second loading step (step-2) and totally sustained 117 loading cycles, whereas samples G-5 and G-1 did not fail during the cycle stages, each achieving fatigue lives of more than 600 cycles. The failure strength of these samples also showed an increasing trend

with loading frequency. Sample G-2 failed at 80.0 MPa while the failure stress levels for samples G-5 and G-1, both tested at a relatively higher loading frequency, were 116.33 MPa and 123.6 MPa, respectively. Those samples that were loaded at higher frequencies failed at greater axial and lateral strains (Table 4.3). Similarly, sample S-7 under 1 Hz sustained loading for more than 30 cycles and final axial and lateral strains of 0.216% and -0.142%, respectively, during step-1, compared with S-8 with 0.05 Hz that failed at the 5^{th} cycle with smaller final axial and lateral strains of 0.026% and -0.039%, respectively (Table 4.3).

The residual strains showed a decreasing trend with increasing loading frequency. The development of residual axial strain during step-1 is shown in Figure 4.15 for samples loaded under the same stress level but at different frequencies. A closer comparison of the $\Delta\varepsilon_r$ values indicates that residual strain develops rapidly at low loading frequencies. Therefore, it could be concluded that the evolution of damage during cyclic loading becomes slower at higher loading frequencies. In other words, microcracks do not have enough time to propagate at higher loading frequencies. In contrast, microcracks can develop more easily at low loading frequencies since the loading is applied slowly and there is enough time for nucleation of new microcracks and propagation and branching of existing cracks. This could also explain why the samples loaded at higher loading frequencies sustained greater final axial and lateral strain.

In Figure 4.15a and Figure 4.15b, it can be seen that residual fatigue development in the sandstone samples was greater than that of the granodiorite samples. This finding relates to the microstructure of these two rock types, in which the almost homogenous grain cluster of the sandstone allows uniform crack propagation, whereas the irregular orientation of the grain boundaries of the interlocked hard grains of granodiorite restrain the initiation and propagation of cracks. Hence, this finding could be another reflection of the ductile behavior of sandstone and brittle behavior of hard granodiorite rock.

Another interesting finding is that lateral strain accumulation is greater than that of axial strain during cyclic loading. Comparing $\Delta\varepsilon_r$ in Figure 4.15b and Figure 4.15c shows that the development of lateral strain is almost double the development of axial strain. This difference was more evident in the case of low loading frequencies. This finding clearly indicates that lateral strain is irrecoverable and why the expansion of

stress–lateral strain hysteresis loops is wider than that for axial strain (cf. Section 4.3.14.3.1).

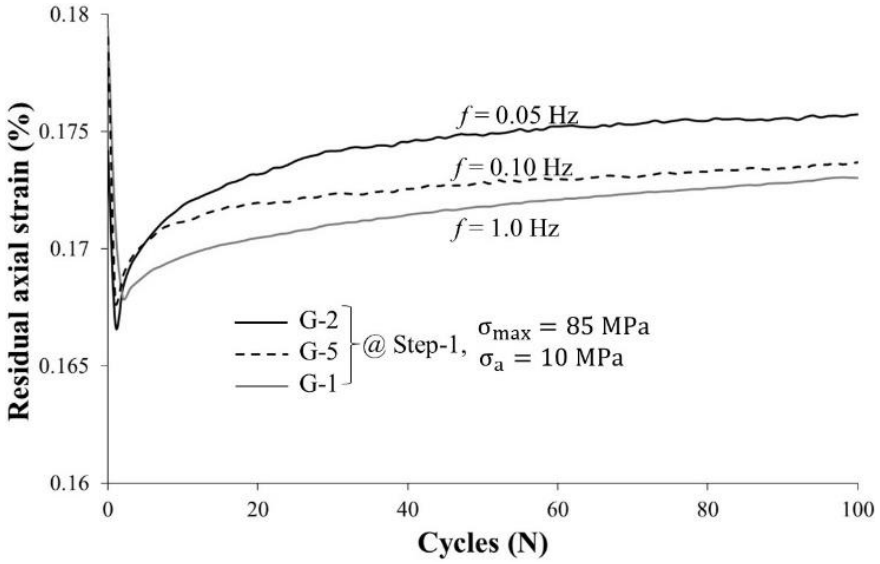

(a)

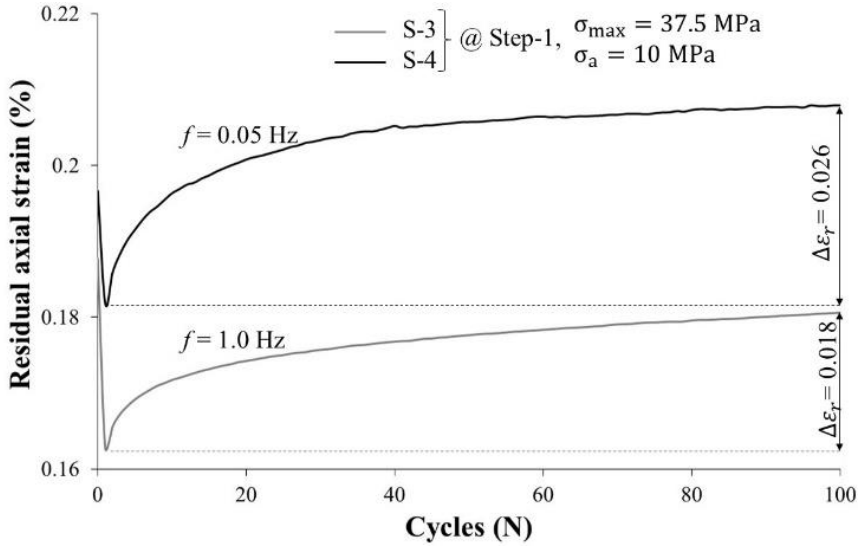

(b)

Figure 4.15 (continued on the next page).

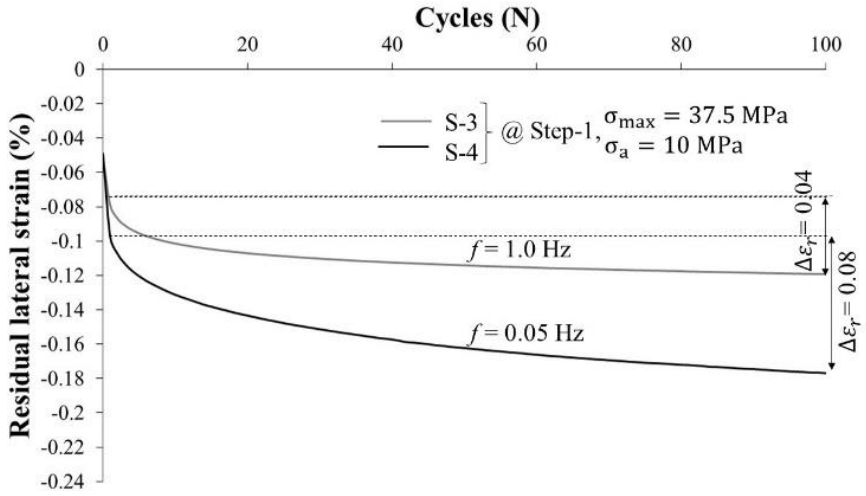

(c)

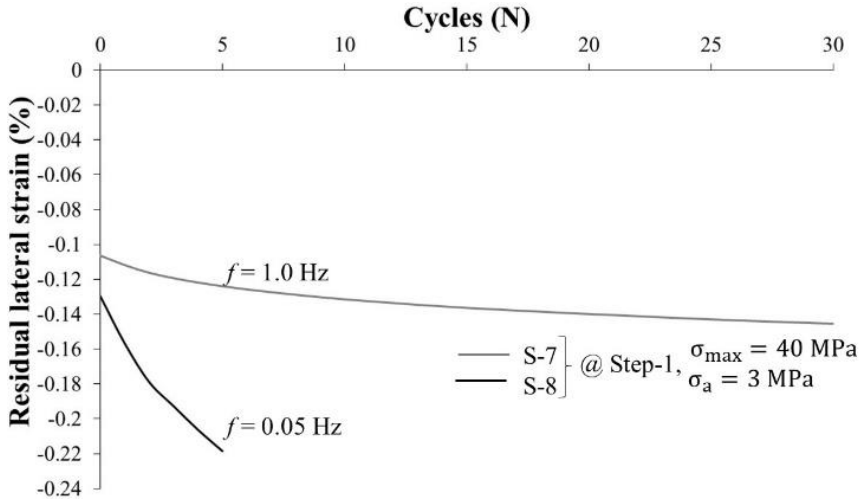

(d)

Figure 4.15 (continued from previous page). Comparison of residual strain for: (a) granodiorite samples G-2, G-5, and G-1, and (b), and (c) sandstone samples S-3, and S-4, and (d) sandstone samples S-7, and S-8, during step-1.

4.3.5. Variation in residual strain

Residual strain, usually determined at valley or peak points of a cycle and gradually accumulating as cycles approach fatigue failure, is taken as irreversible deformation and an indication of the permanent damage that a rock sample is experiencing throughout cyclic testing (Eberhardt et al., 1999). Accumulation of residual axial and

lateral strain during cyclic stages of each testing step is presented in Figure 4.16. What is striking in these plots is that the initial residual axial and lateral strains recorded for the second step of the test (step-2) are always greater than those of the first and third steps, regardless of loading conditions. The values for step-3 were also greater than those of step-1, i.e., $((\varepsilon_r)_{N=1})_{step-2} > ((\varepsilon_r)_{N=1})_{step-3} > ((\varepsilon_r)_{N=1})_{step-1}$. This result may be explained by the fact that residual permanent damage of the rock sample develops with the test step. The initial damage decreased from step-2 to step-3, which might be because of the hardening effect of the cyclic test after hundreds of cycles. In some loading conditions, when the applied load is not high enough for failure after a large number of cycles, the rock sample becomes difficult to damage. This could be because of the closure of some pre-existing microcracks or new microcracks nucleated at previous cyclic stages. On the other hand, closer analysis of these curves shows that the slope of the residual axial and lateral strain during step-2 is greater than that of step-1. However, the curves for step-3 become flat compared to those of the previous test steps ($\Delta\varepsilon_{r_{step-2}} > \Delta\varepsilon_{r_{step-1}} > \Delta\varepsilon_{r_{step-3}}$). Bar charts in each part of Figure 4.16 show the $\Delta\varepsilon_r$ of each test step. This also indicates that the development of permanent damage becomes slower as the number of cycles exceeds a specific value, which is not definite and depends on the stress level applied and other loading conditions. This behavior is the damage accumulation rate reduction due to cyclic loading. All granodiorite samples (G-1, G-3, G-4, and G-5) that did not fail after three steps of loading showed an increase in failure strength from 106% to 116% (Table 4.3). This effect was not observed for the sandstone samples because the applied stress levels were high enough to cause failure of the samples within the first or second test steps. It could be concluded that the stress level applied for a cyclic condition is of great importance since it may not only cause strength weakening but also lead to damage accumulation rate reduction and an increase in strength, which are in favor of loading capacity and stability issues. However, caution must be applied as this effect depends on the loading history, cyclic loading conditions, and rock type.

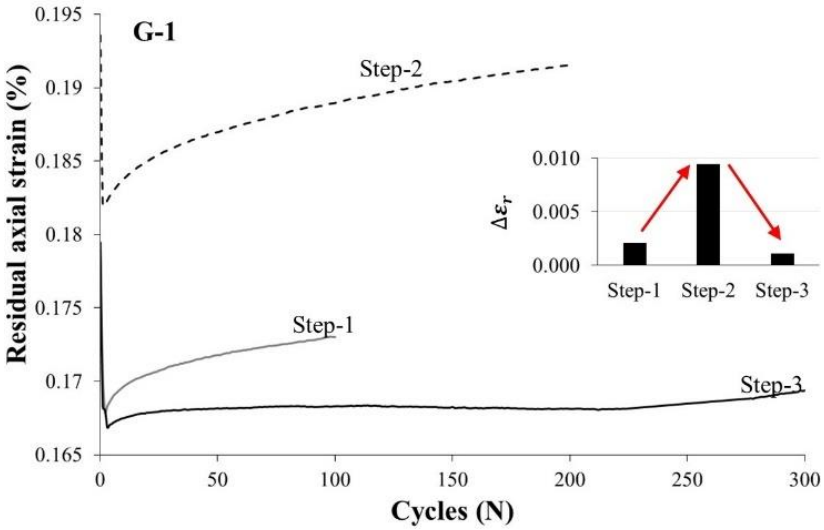

(a)

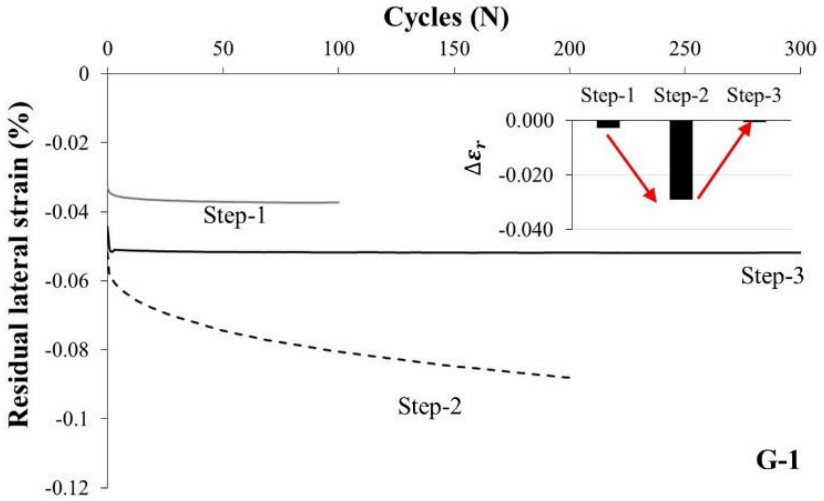

(b)

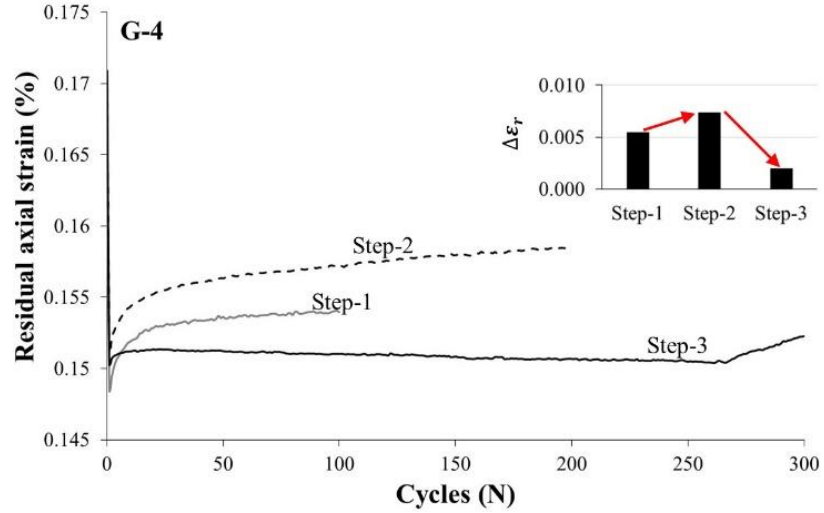

(c)

Figure 4.16 (continued on the next page).

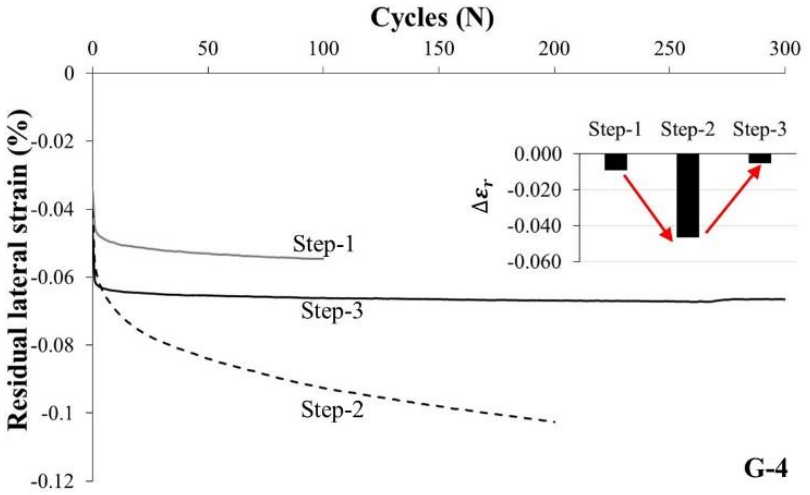

(d)

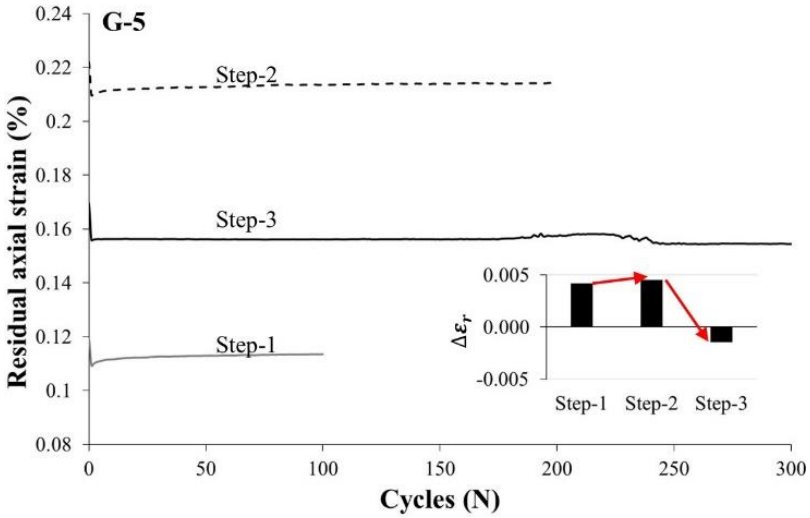

(e)

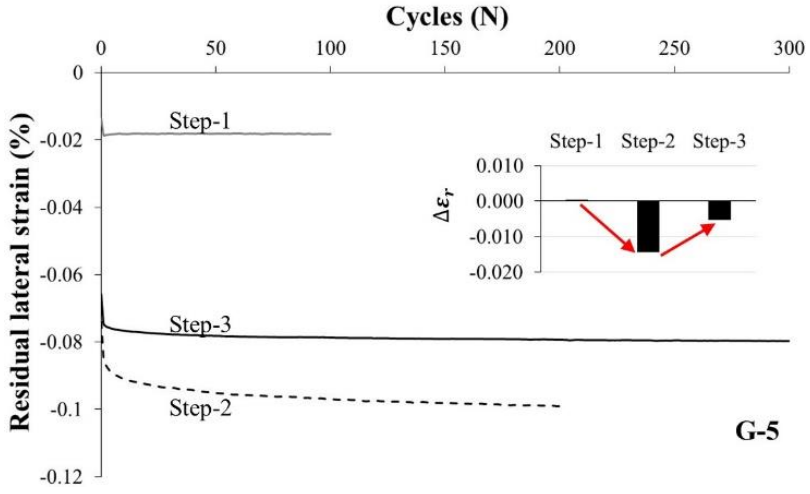

(f)

Figure 4.16 (continued from previous page). Comparison of the residual axial and lateral strains at each step of the test for granodiorite samples of (a and b) G-1, (c and d) G-4, and (e and f) G-5.

4.3.6. Monitoring of damage evolution by ultrasonic measurement results

Ultrasonic measurements were used for preliminary evaluation of the rock properties. This testing has been found to be very useful and precise, along with thin section analysis, for evaluation of the mechanical properties of rock samples (cf. chapter 2). Because wave travel time is directly affected by the internal microstructure of the rock sample, this testing was used for qualitative assessment of damage evolution after each step of the multi-stage cyclic tests, and to see how the cyclic fatigue process affects ultrasonic parameters. It should be mentioned that most samples were CT scanned before loading and after each step of the tests to check for internal cracking. Some samples were saturated with potassium chloride (KCL) doping for better detection of microcracks, however this technique was unsuccessful for this purpose.

The change in the compression P-wave and shear S-wave travel times (or velocities) could be related to damage evolution of the rock samples during the fatigue process. The P-wave and S-wave travel times of some samples were measured before each step of the multi-stage cyclic testing, according to ASTM D2845-08 and ISRM standards (ASTM, 2008a; Aydin, 2014). The P-wave travel time was measured along the axial direction of the samples (normal to the sample ends). The S-wave measurements were performed twice along the axial direction of the samples, termed as “In-Phase” and “Out-of-Phase” S-wave. For the In-Phase S-wave measurement, both transducers were parallel to each other, whereas for the Out-of-Phase S-wave measurement, one of the transducers, either transmitter or receiver, was rotated almost 90 degrees with respect to the other. The rotation makes a phase change of the first received main S-wave. The difference between the wave travel time or velocity recorded after each step of loading is an indication of the fracturing and damage evolution of a rock sample due to previous loading.

Figure 4.17 shows the P-wave velocities for representative samples before loading and after each step of loading. Comparing the P-wave velocities of samples before loading and after the first loading step (step-1) reveals that the P-wave velocities of all samples decreased after they underwent the first loading. A similar trend was also observed for the In-Phase S-wave velocities of both sandstone and granodiorite samples (Figure 4.18). This observation supports the fact that the rock samples accumulated

permanent damage after the first loading stage. Further analysis of these data showed that the reduction in P-wave velocity after the first loading step was 7% to 11% for sandstone and 11% to 14% for granodiorite. These findings indicate how the mechanical properties of hard rocks can be adversely affected by damage causing only a small amount of deformation induced by the fatigue process. Sandstone samples, on the other hand, experienced greater residual deformation, however, the effect of this fatigue damage on their mechanical properties was relatively low. This also agrees with the finding mentioned in Section 4.3.2 that the strength weakening of hard rocks under cyclic loading is more noticeable than that of soft rocks. It could be argued that the closure of pre-existing microcracks and initiation of new cracks along grain boundaries and finally grain detachment play a significant role in the deformation response of crystalline rocks, and this microcracking phenomenon can occur even at a stress level of 80% of UCS (as shown in these experiments). On the other hand, one can hypothesize that pore collapse and grain crushing of microstructurally uniform sandstone will govern its damage response and the applied stress level should be quite high for transgranular cracking leading to failure. Therefore, low-stress cyclic loading could cause damage evolution at individual boundaries of large and mineralogically different grains of hard rocks, whereas uniformly arranged grains with almost the same minerals as sandstone do not allow individual grain detachment unless microcracks initiate and coalesce across the grains themselves at high stress levels. This could explain why the damage evolution and strength degradation of hard rocks under cyclic loading is greater than that of soft rocks.

All sandstone samples failed during the first or second step of loading and ultrasonic parameters could not be obtained for them after the second step. However, P-wave velocities after step-2 of loading recorded for granodiorite samples increased in comparison with those of step-1. As shown in Figure 4.17a, Δv_0, which is the difference between velocity measured before loading and after step-1, is greater than Δv_1, which is the difference between velocity measured after step-1 and after step-2, for the granodiorite samples. Similarly, if $\Delta\varepsilon_0$ and $\Delta\varepsilon_1$ are defined as below:

$$\Delta\varepsilon_0 = ((\varepsilon_r)_{final})_{step-1} \tag{4.1}$$

$$\Delta\varepsilon_1 = ((\varepsilon_r)_{final})_{step-2} - ((\varepsilon_r)_{final})_{step-1} \tag{4.2}$$

where $((\varepsilon_r)_{final})_{step-1}$ and $((\varepsilon_r)_{final})_{step-2}$ are the residual strains of the sample at the end of loading step-1 and step-2, respectively, the $\Delta\varepsilon_0$ is greater than $\Delta\varepsilon_1$ for both axial and lateral strains. This is illustrated in Figure 4.19 for granodiorite samples that sustained step-2 of the cyclic loading.

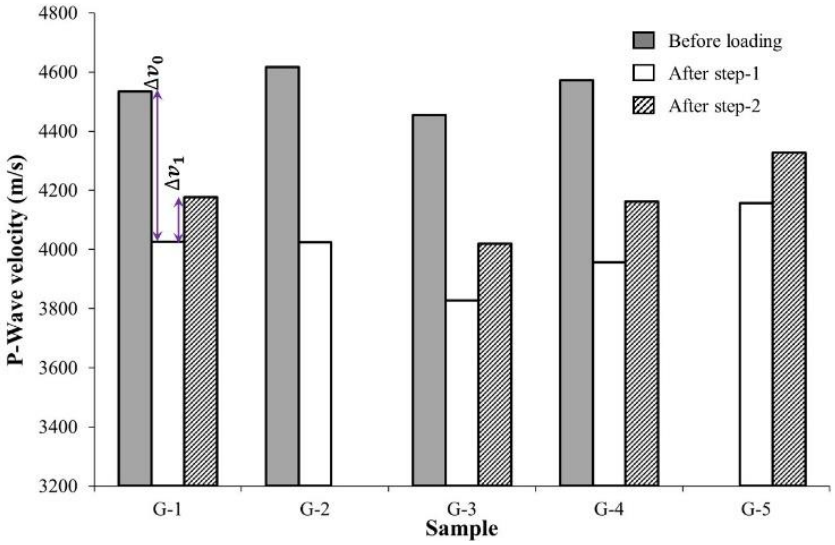

(a)

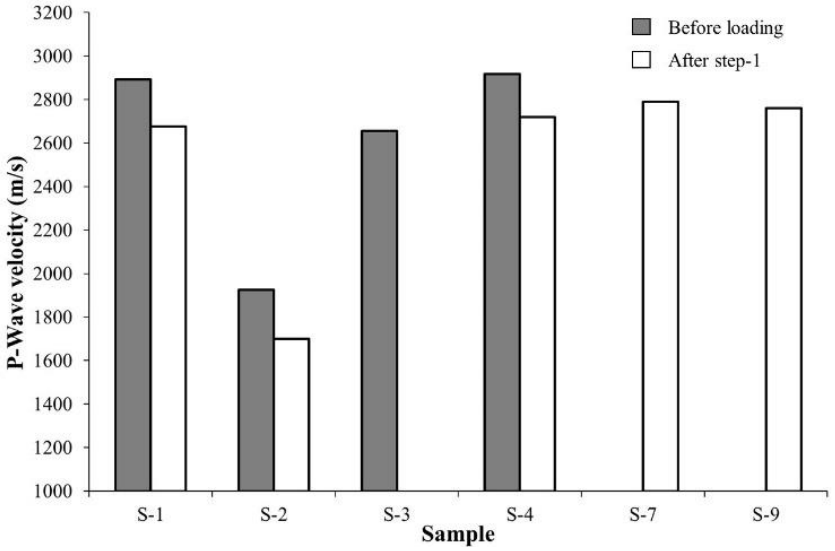

(b)

Figure 4.17. P-wave velocity recorded for some: (a) granodiorite samples, and (b) sandstone samples, before loading and after each step of loading.

Together these results provide important insights into the fatigue damage evolution of granodiorite samples. The first finding is that the permanent damage rock samples experienced during loading step-1 was greater than that experienced in the following

step. This indicates that permanent damage accumulates rapidly during the first cyclic stages followed by small increments during later steps. This result may be explained by the damage accumulation rate reduction because of cyclic loading discussed in previous sections. Another important finding is that the difference between $\Delta\varepsilon_0$ and $\Delta\varepsilon_1$ for axial strain is much greater than that of lateral strain. This also supports the fact that lateral strain develops faster than axial strain during cyclic loading because of the initiation and nucleation of microcracks aligned parallel to the loading direction. This is another indication of the relatively wider expansion of the stress–strain hysteresis loops for lateral strain discussed in Section 4.3.1 (cf. Figure 4.8).

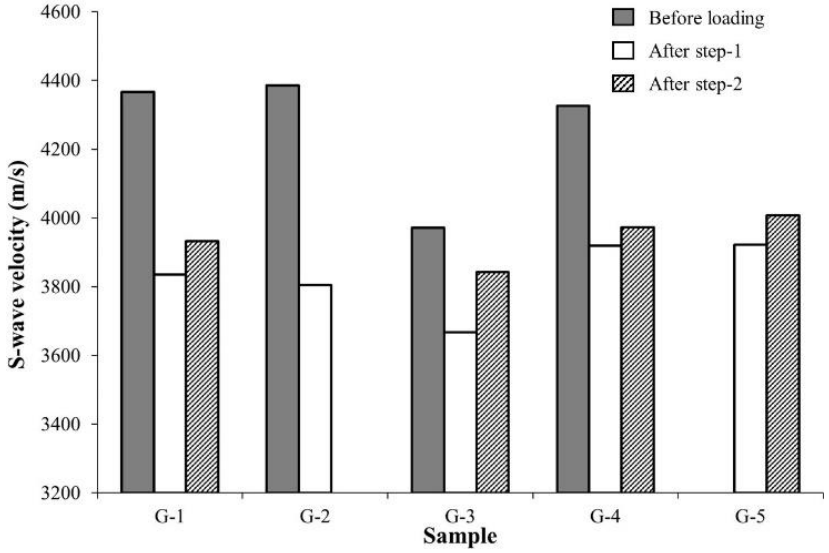

(a)

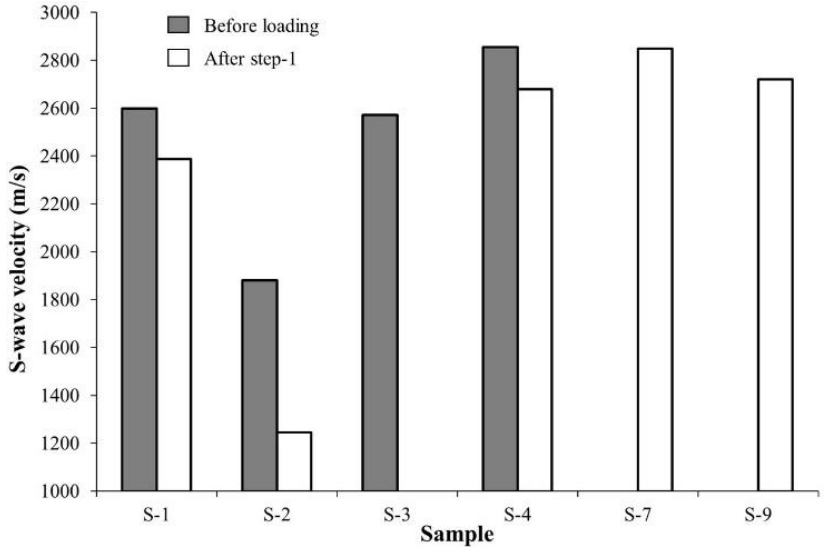

(b)

Figure 4.18. S-wave velocity recorded for some: (a) granodiorite samples, and (b) sandstone samples, before loading and after each step of loading.

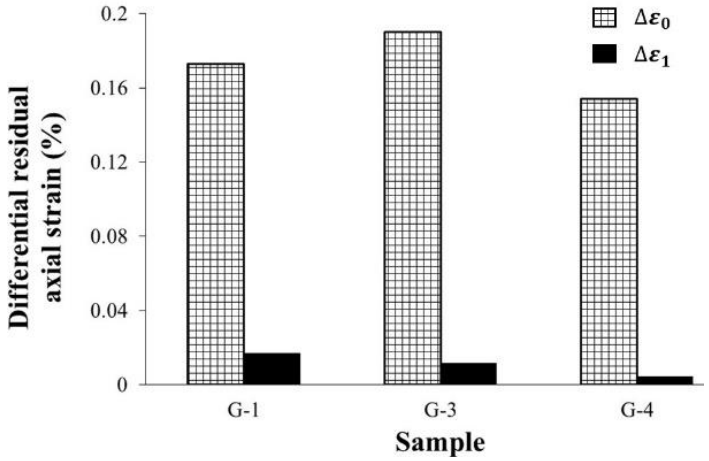

(a)

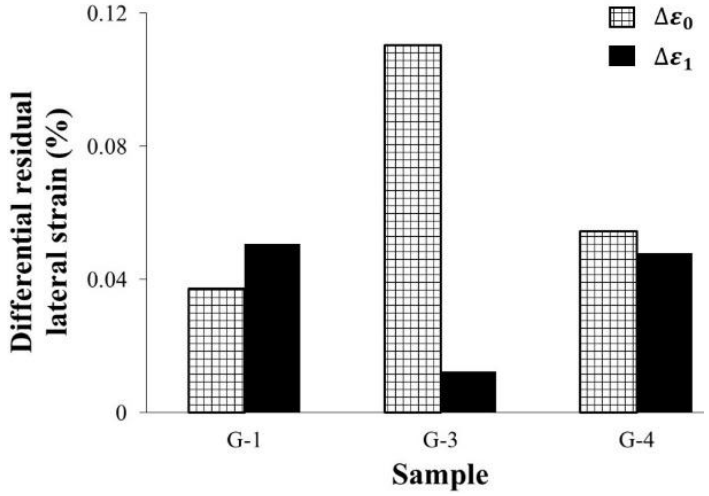

(b)

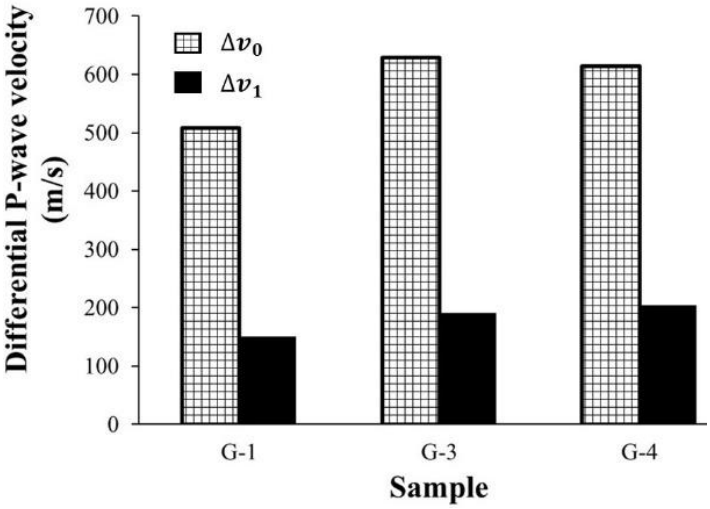

(c)

Figure 4.19. Bar charts of (a) differential residual axial strain, (b) differential residual lateral strain, and (c) differential P-wave velocity for three typical granodiorite samples.

4.3.7. Failure modes of tested samples

All materials are assumed to contain inherent defects leading to the occurrence of failure at stress levels lower than their theoretical strength (Gdoutos, 2005). Therefore, studying the failure mechanism of rocks at small scale may help in visualizing their damage at larger scales. Failure modes of rock materials are very complex because of mineralogical differences and heterogeneity of rock microstructure in nature, the presence of crack-like defects, and other environmental factors such as weathering degree, water content, and level and orientation of the applied stresses. A rock sample can fail at different modes depending on the loading conditions. Even under monotonic loading conditions, failure modes of a rock can be different depending on its strength (Basu et al., 2013). Several researchers have reported that the failure modes of rocks under cyclic loading conditions are different to those under monotonic conditions (Burdine, 1963; Guo et al., 2012; Royer-Carfagni & Salvatore, 2000; Taheri et al., 2016). More rock fragmentation and powdering, due to the local abrasion of grains, have been observed for rock samples under cyclic loading compared to monotonic conditions (Burdine, 1963; Guo et al., 2012; Liu et al., 2017; Royer-Carfagni & Salvatore, 2000). However, much uncertainty still exists around the failure mechanisms of rocks under cyclic fatigue conditions. Possible reasons for this uncertainty are that rocks fail at different modes depending on the rock microstructure itself, as mentioned above, and the effects of different cyclic loading conditions such as frequency and the level of stress applied.

Comparing the failure modes of sandstone and granodiorite samples investigated here showed that there is a clear difference between the failure modes of samples under cyclic and monotonic conditions. Figure 4.20 shows the typical failure modes of granodiorite samples. The failure modes of these samples under monotonic loading and cyclic loading with a higher frequency of 1.0 Hz are different to those under low-frequency cyclic loading. For sample G-7 tested under monotonic loading (Figure 4.20a), and G-1 and G-3 tested under cyclic loading with a frequency of 1.0 Hz (Figure 4.20b and Figure 4.20c), two shear cones developed from the central zone of the samples, ending their loaded end bases. However, fracturing of granodiorite samples under lower frequencies of 0.05 and 0.1 Hz occurred along a single shear plane inclined from the top corner to the bottom end of the sample accompanied by some other sub-

vertical crossed tensile bands (Figure 4.20d to Figure 4.20g). One possible explanation for this difference is that low-frequency cyclic loading allows initiation, nucleation, and localization of tensile cracks growing parallel to the loading axis during slow loading–unloading stages. This mechanism governs the damage evolution of granodiorite rock samples during the initial stages of cyclic loading, followed by shearing through a single plane throughout the entire length of the sample. On the other hand, under high-frequency cyclic loading, tensile cracks do not have enough time for development and propagation and final failure occurs along two shearing planes that join at the central zone of the sample. This failure mode was also observed for sample G-7 under monotonic loading.

A similar failure mode has also been reported by Royer-Carfagni and Salvatore (2000) for marble samples with an average UCS of about 100 MPa and loading frequency of about 0.017 Hz. Therefore, as shown herein, loading frequency is a key factor affecting the failure mechanism of this rock type. The failure modes observed for granodiorite samples under high-frequency cyclic loading are the same as those under monotonic conditions, whereas they are totally different under lower loading frequencies. Expansion of tensile cracks at low-frequency cyclic loading again clearly indicates a higher fatigue damage effect of cyclic loading at lower loading frequencies compared with higher loading frequencies as discussed in previous sections.

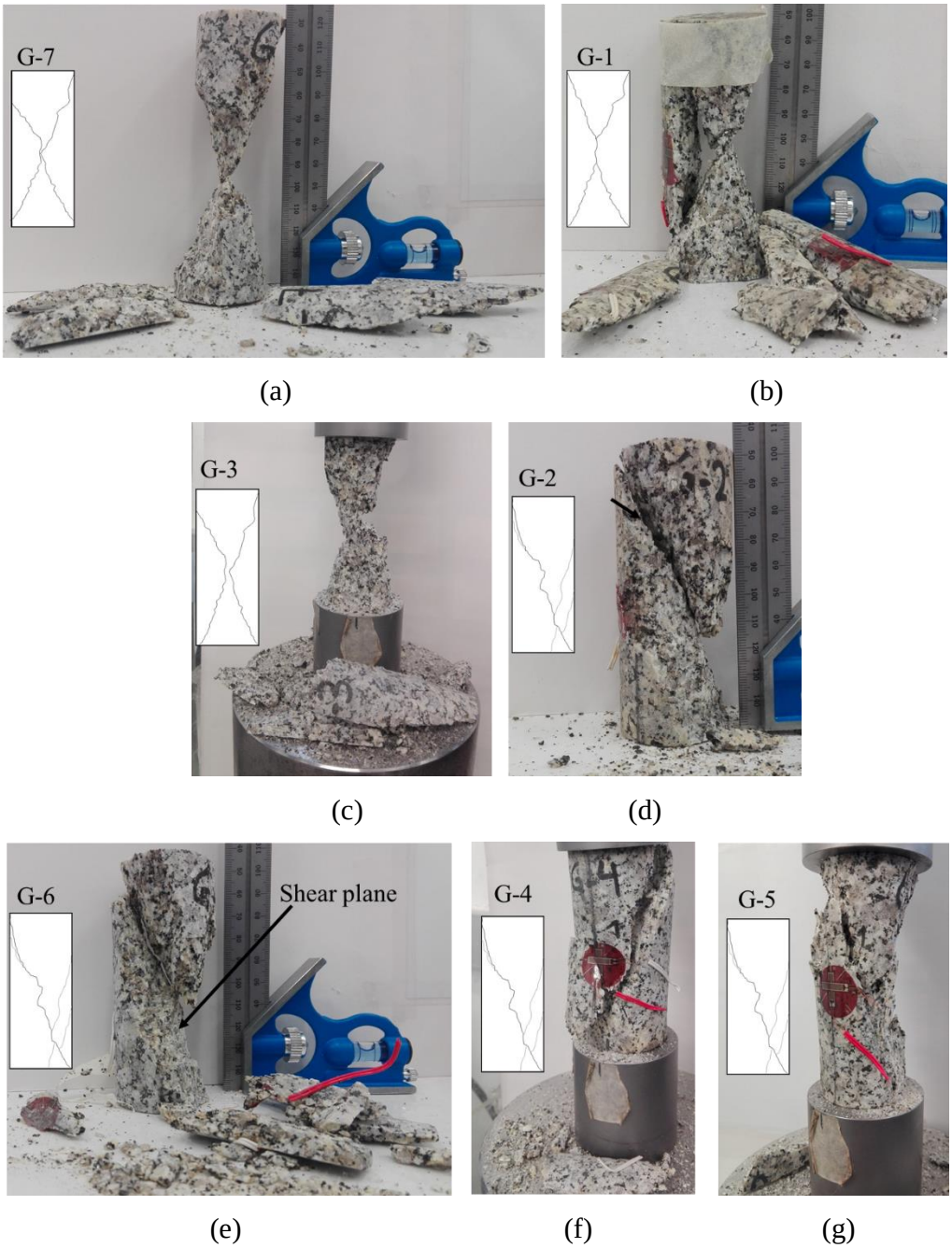

Figure 4.20. Failure modes of granodiorite samples of: (a) G-7 under monotonic loading, (b) G-1, and (c) G-3 under cyclic loading with f = 1 Hz, and (d) G-2, (e) G-6, and (f) G-4 under cyclic loading with f = 0.05 Hz, and (g) G-5 under cyclic loading with f = 0.1 Hz.

The failure modes of the sandstone samples after monotonic and cyclic tests are shown in Figure 4.21. Under uniaxial monotonic compression testing, axial splitting and shearing along a single plane have been reported to be two common failure modes of sandstone with UCS of less than 30 MPa and 30–60 MPa, respectively (Basu et al., 2013). Similarly, these two failure modes were observed for the sandstone samples which failed during monotonic loading or the first cycles of cyclic loading. Except for sample S-5, which failed at a lower stress level with axial splitting, all other samples subjected to monotonic loading (S-17) or step-1 of multi-stage cyclic loading (S-6, S-8, S-10, S-11, and S-14) failed along a single shear plane, regardless of the applied stress level and loading frequency. The only difference is that the shear plane is accompanied by more tensile splitting under cyclic loading than under monotonic loading (Figure 4.21e and Figure 4.21f). However, those samples that experienced pre-cyclic loading showed different failure modes. Sample S-4, which failed during the monotonic stage of the second step of multi-stage cyclic loading, showed the same single shear plane accompanied by another parallel shear band with a small opening (premature shear plane). Samples S-7 and S-9, which failed during the monotonic stage and after 117 cycles of step-2, respectively, showed a double plane shearing failure mode. Both S-4 and S-7 experienced pre-cyclic loading and failed just after the monotonic stage of step-2; their failure modes were a bit different, possibly because of the stress levels applied. The applied stress level on sample S-4 was 90% of UCS whereas sample S-7 was loaded with a stress level of 96% of UCS. The higher the applied stress level, the greater the fatigue effect. Therefore, it can be concluded that the failure mode of sandstone samples changes from axial splitting and shearing along a single plane under monotonic conditions to shearing along a single plane accompanied by axial tensile splitting under initial cycles of cyclic loading, and to double plane shearing for those samples that experienced cyclic loading with a large number of cycles. The failure modes of sandstone and granodiorite samples observed in the present study are summarized in Figure 4.22. The shear bands shown in this figure are tiny cracks propagated parallel to the main failure plane (shearing plane), whereas the tensile bands are sub-vertical cracks propagated parallel to the loading direction and crossed the shearing plane.

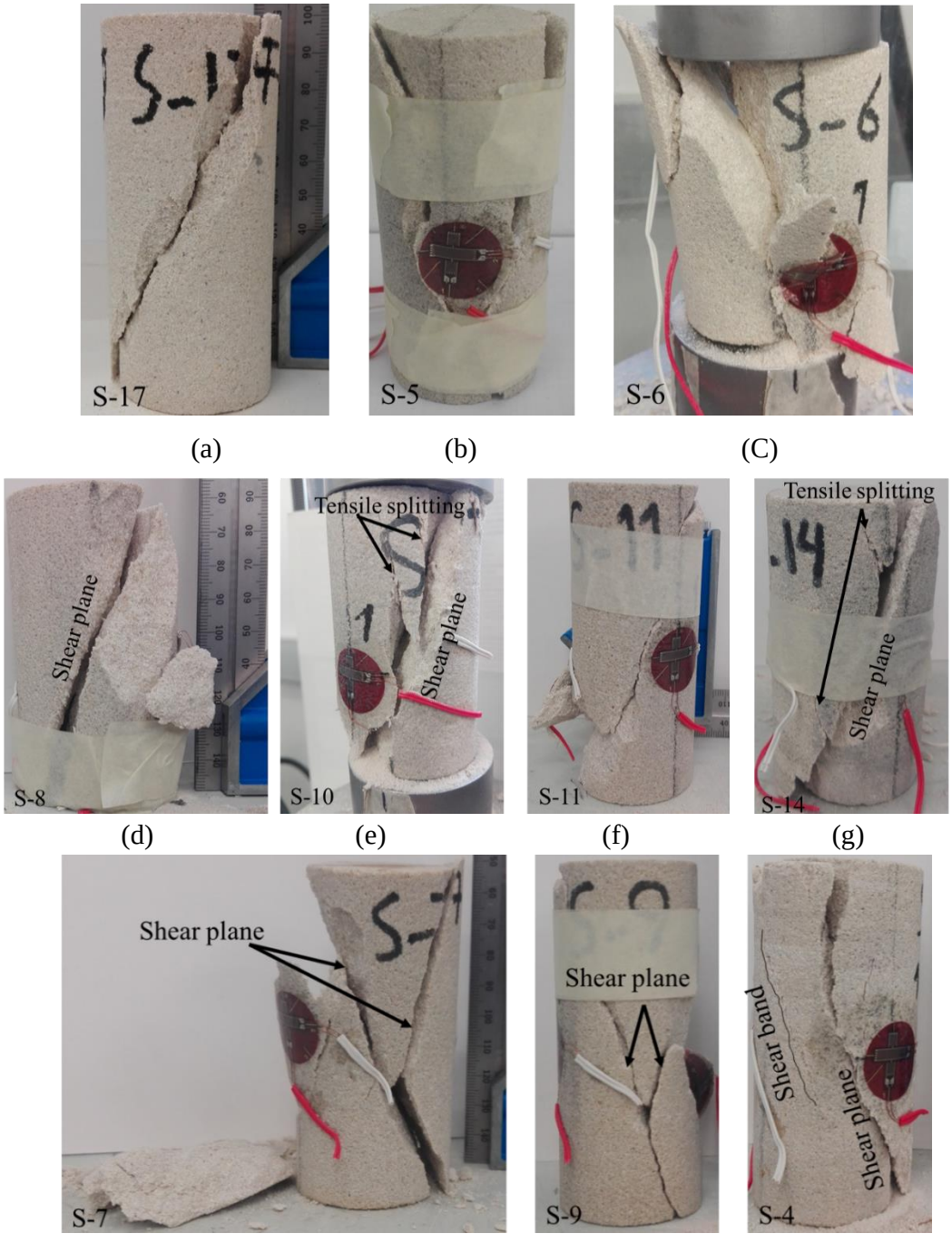

Figure 4.21. Failure modes of sandstone samples: (a) S-17, and (b) S-5, both failed at monotonic stage, and (c) S-6, (d) S-8, (e) S-10, and (f) S-11 failed during the first step of multi-stage cyclic loading with f = 0.05 Hz, and (g) S-14 failed during the first step of multi-stage cyclic loading with f = 1.0 Hz, and (h) S-7, and (i) S-9 both failed during the second step of multi-stage cyclic loading with f = 1.0 Hz, and (j) S-4 failed during the monotonic stage of the second step of multi-stage cyclic loading with f = 0.05 Hz.

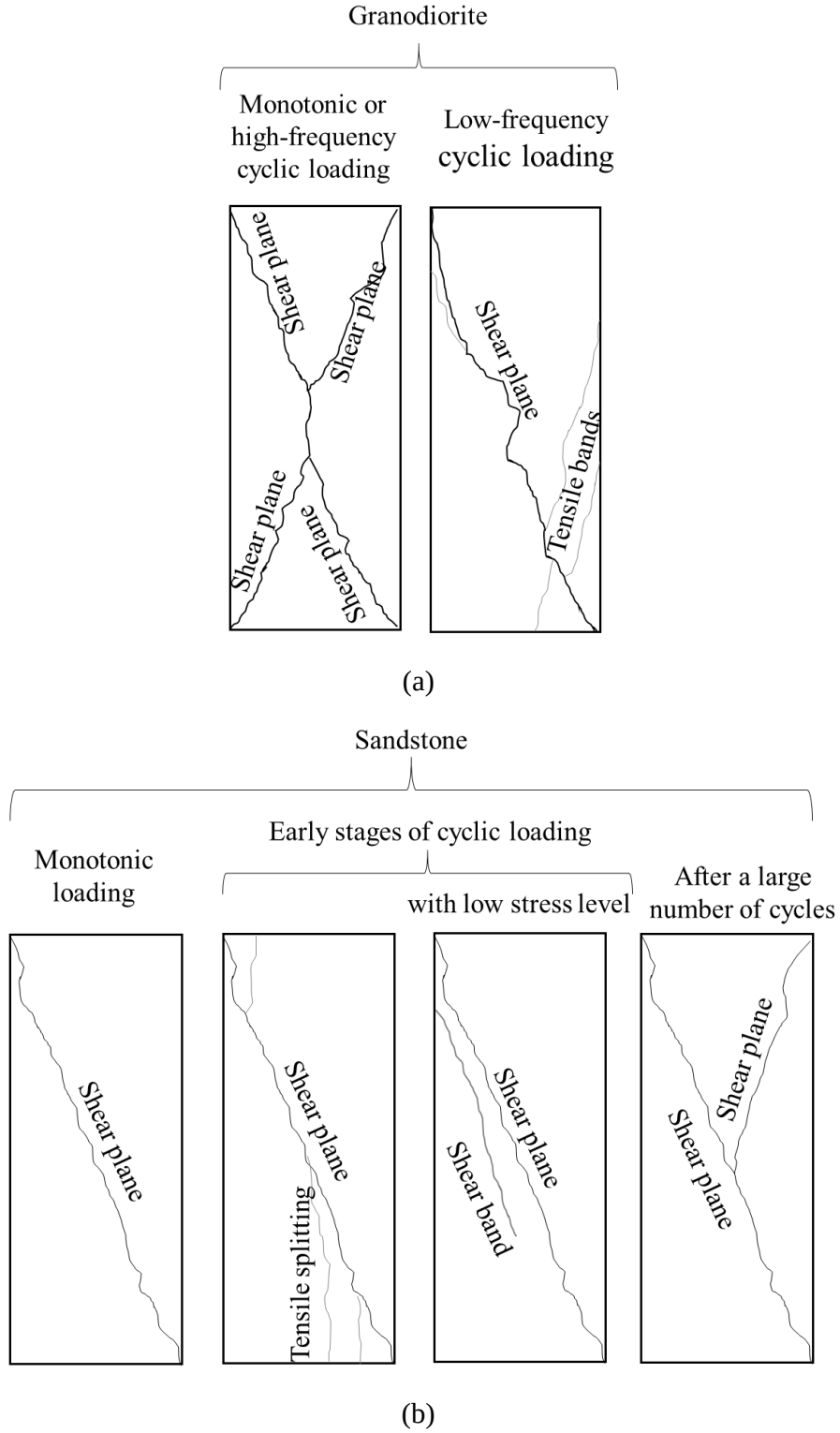

Figure 4.22. Failure modes of (a) granodiorite and (b) sandstone samples under monotonic and cyclic conditions.

4.4. Conclusions

The purpose of the current research was to explore the effect of cyclic loading on the deformation and strength of sandstone and granodiorite as representatives of granular and crystalline rocks. By conducting multi-stage cyclic loading, it has been found that the deformation of granodiorite and sandstone samples after each step of loading is greater than that of the previous steps. The increase in the axial and lateral strain of sandstone with each test step is greater than that of granodiorite. A similar result was also obtained for residual strain. This is caused by microstructural differences in these two rocks and the ductility behavior of the sandstone. The investigation of the stress–strain hysteresis loops of these two rock types also led to another interesting result. The stress–strain hysteresis loops of sandstone showed a clear three-phase development of loose–dense–loose during cyclic stages of the tests, compared to the cyclic loops developed in a dense–loose pattern (i.e. two-phase) for the hard rock of granodiorite. We also found that the expansion of the stress–strain hysteresis loops of lateral strain was wider than that of axial strain, which indicates greater damage of the samples in the axial direction. This behavior was also observed for residual lateral strain. The experiments also confirmed that the higher the maximum stress level and loading amplitude, the greater the axial and lateral strain, the shorter the fatigue life, and the faster the accumulation of residual strain and rock damage. Another important finding of this study is that sandstone, being a soft rock, showed greater fatigue limits compared to granodiorite which is a hard rock. By incorporating lots of data, it was found that the fatigue strength threshold of sandstone and granodiorite samples ranged from 75% to 90% and 65% to 80%, respectively. Investigation of the effect of loading frequency on fatigue response also showed that fatigue strength, fatigue life, and fatigue strain increase with loading frequency; however, residual permanent strain decreases as loading frequency increases. This finding indicates that residual and permanent damage develops faster at lower loading frequencies. Deformation analysis also revealed that some rocks may show damage accumulation rate reductions under cyclic loading, which greatly depends on the applied stress level and rock type. It was also found that damage propagation of rocks after fatigue processes can be well evaluated by ultrasonic measurement. The ultrasonic P-wave velocity of both granodiorite and sandstone samples decreased after the first step of loading because of the permanent damage

induced by cyclic loading. The reduction in P-wave velocity for granodiorite samples was greater than that of the sandstone samples. This is a new finding and specifies the greater susceptibility of the hard rock of granodiorite to permanent damage developed within its grain boundaries by the cyclic process.

Evaluation of fracturing of the samples after failure revealed that their failure modes under monotonic loading are different than those under cyclic loading. The failure mode of rocks under cyclic conditions seems to be controlled mainly by the loading frequency rather than by other loading factors, however this needs to be validated by further research. The granodiorite samples loaded under high-frequency cyclic conditions failed with double plane shearing mode, the same pattern as that under monotonic conditions. However, single plane shearing with tensile bands was the dominant failure mode observed under low-frequency cyclic loading. The failure modes of sandstone samples change from single plane shearing under monotonic conditions to single shearing with either tensile cracks or parallel shear band and double plane shearing under cyclic loading, which may vary depending on the loading parameters. The results of this study shed light on the mechanisms of rock failure under both cyclic and monotonic loading and will form a basis for further development of models describing the process of rock non-elastic deformation and fracturing.

Acknowledgements

The authors would like to thank both the Mining Research Institute of Western Australia (MRIWA) and Curtin University for their research scholarships awarded to the first author. The support of the departments of Mining and Metallurgical Engineering and Petroleum Engineering of the Western Australian School of Mines (WASM), Curtin University in providing laboratory equipment is gratefully acknowledged. We also highly appreciate the support from the Commonwealth Scientific and Industrial Research Organization (CSIRO) of Western Australia for the CT scanner.

References

ASTM. (2008a). ASTM D2845-08, Standard Test Method for Laboratory Determination of Pulse Velocities and Ultrasonic Elastic Constants of Rock (Withdrawn 2017). *ASTM International*. Retrieved from www.astm.org

ASTM. (2008b). *ASTM D4543-08, Standard Practices for Preparing Rock Core as Cylindrical Test Specimens and Verifying Conformance to Dimensional and Shape Tolerances*. Retrieved from https://doi.org/10.1520/D4543-08

Attewell, P. B., & Farmer, I. W. (1973). Fatigue behaviour of rock. *International Journal of Rock Mechanics and Mining Sciences & Geomechanics Abstracts*, *10*(1), 1–9. https://doi.org/https://doi.org/10.1016/0148-9062(73)90055-7

Aydin, A. (2014). Upgraded ISRM Suggested Method for Determining Sound Velocity by Ultrasonic Pulse Transmission Technique. *Rock Mechanics and Rock Engineering*, *47*(1), 255–259. https://doi.org/10.1007/s00603-013-0454-z

Bagde, M. N., & Petroš, V. (2005a). Fatigue properties of intact sandstone samples subjected to dynamic uniaxial cyclical loading. *International Journal of Rock Mechanics and Mining Sciences*, *42*(2), 237–250. https://doi.org/https://doi.org/10.1016/j.ijrmms.2004.08.008

Bagde, M. N., & Petroš, V. (2005b). The Effect of Machine Behaviour and Mechanical Properties of Intact Sandstone Under Static and Dynamic Uniaxial Cyclic Loading. *Rock Mechanics and Rock Engineering*, *38*(1), 59–67. https://doi.org/10.1007/s00603-004-0038-z

Bagde, M. N., & Petroš, V. (2005c). Waveform Effect on Fatigue Properties of Intact Sandstone in Uniaxial Cyclical Loading. *Rock Mechanics and Rock Engineering*, *38*(3), 169–196. https://doi.org/10.1007/s00603-005-0045-8

Bagde, M. N., & Petroš, V. (2009). Fatigue and dynamic energy behaviour of rock subjected to cyclical loading. *International Journal of Rock Mechanics and Mining Sciences*, *46*(1), 200–209. https://doi.org/https://doi.org/10.1016/j.ijrmms.2008.05.002

Basu, A., Mishra, D. A., & Roychowdhury, K. (2013). Rock failure modes under uniaxial compression, Brazilian, and point load tests. *Bulletin of Engineering*

Geology and the Environment, *72*(3), 457–475. https://doi.org/10.1007/s10064-013-0505-4

Bieniawski, Z. T., & Bernede, M. J. (1979). ISRM suggested methods for determining the uniaxial compressive strength and deformability of rock materials: Part 1. Suggested method for determining deformability of rock materials in uniaxial compression. *International Journal of Rock Mechanics and Mining Sciences & Geomechanics Abstracts*, *16*(2), 138–140. https://doi.org/https://doi.org/10.1016/0148-9062(79)91451-7

Brace, W. F., Paulding Jr., B. W., & Scholz, C. (1966). Dilatancy in the fracture of crystalline rocks. *Journal of Geophysical Research (1896-1977)*, *71*(16), 3939–3953. https://doi.org/10.1029/JZ071i016p03939

Burdine, N. T. (1963). Rock Failure Under Dynamic Loading Conditions. *Society of Petroleum Engineers Journal*, *3*(01), 1–8. https://doi.org/10.2118/481-PA

Cerfontaine, B., & Collin, F. (2018). Cyclic and Fatigue Behaviour of Rock Materials: Review, Interpretation and Research Perspectives. *Rock Mechanics and Rock Engineering*, *51*(2), 391–414. https://doi.org/10.1007/s00603-017-1337-5

Eberhardt, E., Stead, D., & Stimpson, B. (1999). Quantifying progressive pre-peak brittle fracture damage in rock during uniaxial compression. *International Journal of Rock Mechanics and Mining Sciences*, *36*(3), 361–380. https://doi.org/https://doi.org/10.1016/S0148-9062(99)00019-4

Fan, J., Chen, J., Jiang, D., Ren, S., & Wu, J. (2016). Fatigue properties of rock salt subjected to interval cyclic pressure. *International Journal of Fatigue*, *90*, 109–115. https://doi.org/https://doi.org/10.1016/j.ijfatigue.2016.04.021

Fuenkajorn, K., & Phueakphum, D. (2010). Effects of cyclic loading on mechanical properties of Maha Sarakham salt. *Engineering Geology*, *112*(1), 43–52. https://doi.org/https://doi.org/10.1016/j.enggeo.2010.01.002

Gdoutos, E. E. (2005). *Fracture Mechanics An Introduction* (2nd ed.). https://doi.org/https://doi.org/10.1007/1-4020-3153-X

Geranmayeh Vaneghi, R., Ferdosi, B., Okoth, A. D., & Kuek, B. (2018). Strength degradation of sandstone and granodiorite under uniaxial cyclic loading. *Journal of Rock Mechanics and Geotechnical Engineering*, *10*(1), 117–126.

https://doi.org/https://doi.org/10.1016/j.jrmge.2017.09.005

Gong, M., & Smith, I. (2003). Effect of Waveform and Loading Sequence on Low-Cycle Compressive Fatigue Life of Spruce. *Journal of Materials in Civil Engineering*, *15*(1), 93–99. https://doi.org/10.1061/(ASCE)0899-1561(2003)15:1(93)

Guo, Y., Yang, C., & Mao, H. (2012). Mechanical properties of Jintan mine rock salt under complex stress paths. *International Journal of Rock Mechanics and Mining Sciences*, *56*, 54–61. https://doi.org/https://doi.org/10.1016/j.ijrmms.2012.07.025

Haimson, B. C. (1978). Effect of Cyclic Loading on Rock. In M. Silver & D. Tiedemann (Eds.), *Dynamic Geotechnical Testing* (pp. 228–245). https://doi.org/10.1520/STP35679S

Hardy, H. R. (1970). Failure of geologic materials under low cycle fatigue. *Proc. 6th Can. Rock Mech. Symp., Montreal*, 33–47. Retrieved from https://ci.nii.ac.jp/naid/10006408402/en/

He, M., Li, N., Chen, Y., & Zhu, C. (2016). Strength and Fatigue Properties of Sandstone under Dynamic Cyclic Loading. *Shock and Vibration*, *2016*, 8. https://doi.org/https://doi.org/10.1155/2016/9458582

Ishizuka, Y., Abe, T., & Kodama, J. (1990). Fatigue Behaviour of Granite Under Cyclic Loading. *ISRM International Symposium*, p. 8. Retrieved from https://doi.org/

Kendrick, J. E., Smith, R., Sammonds, P., Meredith, P. G., Dainty, M., & Pallister, J. S. (2013). The influence of thermal and cyclic stressing on the strength of rocks from Mount St. Helens, Washington. *Bulletin of Volcanology*, *75*(7), 728. https://doi.org/10.1007/s00445-013-0728-z

Li, X., Gong, F., Tao, M., Dong, L., Du, K., Ma, C., … Yin, T. (2017). Failure mechanism and coupled static-dynamic loading theory in deep hard rock mining: A review. *Journal of Rock Mechanics and Geotechnical Engineering*, *9*(4), 767–782. https://doi.org/https://doi.org/10.1016/j.jrmge.2017.04.004

Liu, E., & He, S. (2012). Effects of cyclic dynamic loading on the mechanical properties of intact rock samples under confining pressure conditions. *Engineering Geology*, *125*, 81–91.

https://doi.org/http://dx.doi.org/10.1016/j.enggeo.2011.11.007

Liu, E., Huang, R., & He, S. (2012). Effects of Frequency on the Dynamic Properties of Intact Rock Samples Subjected to Cyclic Loading under Confining Pressure Conditions. *Rock Mechanics and Rock Engineering*, *45*(1), 89–102. https://doi.org/10.1007/s00603-011-0185-y

Liu, M., & Liu, E. (2017). Dynamic mechanical properties of artificial jointed rock samples subjected to cyclic triaxial loading. *International Journal of Rock Mechanics and Mining Sciences*, *98*, 54–66. https://doi.org/http://dx.doi.org/10.1016/j.ijrmms.2017.07.005

Liu, Y, Dai, F., Dong, L., Xu, N., & Feng, P. (2018). Experimental Investigation on the Fatigue Mechanical Properties of Intermittently Jointed Rock Models Under Cyclic Uniaxial Compression with Different Loading Parameters. *Rock Mechanics and Rock Engineering*, *51*(1), 47–68. https://doi.org/10.1007/s00603-017-1327-7

Liu, Yi, Dai, F., Fan, P., Xu, N., & Dong, L. (2017). Experimental Investigation of the Influence of Joint Geometric Configurations on the Mechanical Properties of Intermittent Jointed Rock Models Under Cyclic Uniaxial Compression. *Rock Mechanics and Rock Engineering*, *50*(6), 1453–1471. https://doi.org/10.1007/s00603-017-1190-6

Liu, Yi, Dai, F., Xu, N., Zhao, T., & Feng, P. (2018). Experimental and numerical investigation on the tensile fatigue properties of rocks using the cyclic flattened Brazilian disc method. *Soil Dynamics and Earthquake Engineering*, *105*, 68–82. https://doi.org/https://doi.org/10.1016/j.soildyn.2017.11.025

Liu, Yi, Dai, F., Zhao, T., & Xu, N. (2017). Numerical Investigation of the Dynamic Properties of Intermittent Jointed Rock Models Subjected to Cyclic Uniaxial Compression. *Rock Mechanics and Rock Engineering*, *50*(1), 89–112. https://doi.org/10.1007/s00603-016-1085-y

Ludovico-Marques, M., Chastre, C., & Vasconcelos, G. (2012). Modelling the compressive mechanical behaviour of granite and sandstone historical building stones. *Construction and Building Materials*, *28*(1), 372–381. https://doi.org/https://doi.org/10.1016/j.conbuildmat.2011.08.083

Ma, L., Liu, X., Wang, M., Xu, H., Hua, R., Fan, P., … Yi, Q. (2013). Experimental

investigation of the mechanical properties of rock salt under triaxial cyclic loading. *International Journal of Rock Mechanics and Mining Sciences*, *62*, 34–41. https://doi.org/http://dx.doi.org/10.1016/j.ijrmms.2013.04.003

Martin, C. D., & Chandler, N. A. (1994). The progressive fracture of Lac du Bonnet granite. *International Journal of Rock Mechanics and Mining Sciences & Geomechanics Abstracts*, *31*(6), 643–659. https://doi.org/https://doi.org/10.1016/0148-9062(94)90005-1

Momeni, A., Karakus, M., Khanlari, G. R., & Heidari, M. (2015). Effects of cyclic loading on the mechanical properties of a granite. *International Journal of Rock Mechanics and Mining Sciences*, *77*, 89–96. https://doi.org/http://dx.doi.org/10.1016/j.ijrmms.2015.03.029

Nejati, H. R., & Ghazvinian, A. (2014). Brittleness Effect on Rock Fatigue Damage Evolution. *Rock Mechanics and Rock Engineering*, *47*(5), 1839–1848. https://doi.org/10.1007/s00603-013-0486-4

Peng, J., & Yang, S.-Q. (2018). Comparison of Mechanical Behavior and Acoustic Emission Characteristics of Three Thermally-Damaged Rocks. *Energies* , Vol. 11. https://doi.org/10.3390/en11092350

Potyondy, D. O. (2012). The bonded-particle model as a tool for rock mechanics research and application: Current trends and future directions. *ISRM Regional Symposium - 7th Asian Rock Mechanics Symposium, ARMS 2012*, pp. 73–105. https://doi.org/10.1080/12269328.2014.998346

Rajaram, V. (1981). Mechanical Behavior of Granite Under Cyclic Compression. *International Conferences on Recent Advances in Geotechnical Earthquake Engineering and Soil Dynamics*, 11.

Ray, S. K., Sarkar, M., & Singh, T. N. (1999). Effect of cyclic loading and strain rate on the mechanical behaviour of sandstone. *International Journal of Rock Mechanics and Mining Sciences*, *36*(4), 543–549. https://doi.org/http://dx.doi.org/10.1016/S0148-9062(99)00016-9

Roberts, L. A., Buchholz, S. A., Mellegard, K. D., & Düsterloh, U. (2015). Cyclic Loading Effects on the Creep and Dilation of Salt Rock. *Rock Mechanics and Rock Engineering*, *48*(6), 2581–2590. https://doi.org/10.1007/s00603-015-0845-4

Royer-Carfagni, G., & Salvatore, W. (2000). The characterization of marble by cyclic compression loading: experimental results. *Mechanics of Cohesive-Frictional Materials*, *5*(7), 535–563. https://doi.org/10.1002/1099-1484(200010)5:7<535::AID-CFM102>3.0.CO;2-D

Schijve, J. (2008). *Fatigue of structures and materials* (2nd ed.). https://doi.org/10.1007/978-1-4020-6808-9

Scholz, C. H., & Koczynski, T. A. (1979). Dilatancy anisotropy and the response of rock to large cyclic loads. *Journal of Geophysical Research: Solid Earth*, *84*(B10), 5525–5534. https://doi.org/10.1029/JB084iB10p05525

Singh, S. K. (1989). Fatigue and strain hardening behaviour of graywacke from the flagstaff formation, New South Wales. *Engineering Geology*, *26*(2), 171–179. https://doi.org/http://dx.doi.org/10.1016/0013-7952(89)90005-7

Sun, B., Zhu, Z., Shi, C., & Luo, Z. (2017). Dynamic mechanical behavior and fatigue damage evolution of sandstone under cyclic loading. *International Journal of Rock Mechanics and Mining Sciences*, *94*, 82–89. https://doi.org/https://doi.org/10.1016/j.ijrmms.2017.03.003

Taheri, A, Royle, A., Yang, Z., & Zhao, Y. (2016). Study on variations of peak strength of a sandstone during cyclic loading. *Geomechanics and Geophysics for Geo-Energy and Geo-Resources*, *2*(1), 1–10. https://doi.org/10.1007/s40948-015-0017-8

Taheri, A, Yfantidis, N., Olivares, C., Connelly, B., & Bastian, T. (2016). *Experimental Study on Degradation of Mechanical Properties of Sandstone Under Different Cyclic Loadings BT - Experimental Study on Degradation of Mechanical Properties of Sandstone Under Different Cyclic Loadings*.

Taheri, Abbas, Hamzah, N., & Dai, Q. (2017). Degradation and improvement of mechanical properties of rock under triaxial compressive cyclic loading. *Japanese Geotechnical Society Special Publication*, *5*(2), 71–78. https://doi.org/10.3208/jgssp.v05.017

Tien, Y. M., Lee, D. H., & Juang, C. H. (1990). Strain, pore pressure and fatigue characteristics of sandstone under various load conditions. *International Journal of Rock Mechanics and Mining Sciences & Geomechanics Abstracts*, *27*(4), 283–289. https://doi.org/http://dx.doi.org/10.1016/0148-

9062(90)90530-F

Voznesenskii, A. S., Krasilov, M. N., Kutkin, Y. O., Tavostin, M. N., & Osipov, Y. V. (2017). Features of interrelations between acoustic quality factor and strength of rock salt during fatigue cyclic loadings. *International Journal of Fatigue*, *97*, 70–78. https://doi.org/https://doi.org/10.1016/j.ijfatigue.2016.12.027

Vutukiri, V. S., Lama, R. D., & Saluja, S. S. (1978). *Handbook on Mechanical Properties of Rocks (Series on Rocks and Soil Mechanics)*. Trans Technical Publications.

Wang, W., Wang, M., & Liu, X. (2016). Study on Mechanical Features of Brazilian Splitting Fatigue Tests of Salt Rock. *Advances in Civil Engineering*, *2016*(Article ID 5436240), 10. Retrieved from https://doi.org/10.1155/2016/5436240

Wang, Z., Li, S., Qiao, L., & Zhao, J. (2013). Fatigue Behavior of Granite Subjected to Cyclic Loading Under Triaxial Compression Condition. *Rock Mechanics and Rock Engineering*, *46*(6), 1603–1615. https://doi.org/10.1007/s00603-013-0387-6

Xiao, J.-Q., Ding, D.-X., Jiang, F.-L., & Xu, G. (2010). Fatigue damage variable and evolution of rock subjected to cyclic loading. *International Journal of Rock Mechanics and Mining Sciences*, *47*(3), 461–468. https://doi.org/http://dx.doi.org/10.1016/j.ijrmms.2009.11.003

Xiao, J.-Q., Ding, D.-X., Xu, G., & Jiang, F.-L. (2009). Inverted S-shaped model for nonlinear fatigue damage of rock. *International Journal of Rock Mechanics and Mining Sciences*, *46*(3), 643–648. https://doi.org/http://dx.doi.org/10.1016/j.ijrmms.2008.11.002

Xiao, J.-Q., Feng, X.-T., Ding, D.-X., & Jiang, F.-L. (2011). Investigation and modeling on fatigue damage evolution of rock as a function of logarithmic cycle. *International Journal for Numerical and Analytical Methods in Geomechanics*, *35*(10), 1127–1140. https://doi.org/10.1002/nag.946

Xiao, J., Ding, D., Xu, G., & Jiang, F. (2008). Waveform effect on quasi-dynamic loading condition and the mechanical properties of brittle materials. *International Journal of Rock Mechanics and Mining Sciences*, *45*(4), 621–

626. https://doi.org/http://dx.doi.org/10.1016/j.ijrmms.2007.07.025

Yamashita, S., Sugimoto, F., Imai, T., Namsrai, D., Yamauchi, M., & Kamoshida, N. (1999). The Relationship Between the Failure Process of the Creep Or Fatigue Test And of the Conventional Compression Test On Rock. *9th ISRM Congress*. Paris, France: International Society for Rock Mechanics and Rock Engineering.

Zhenyu, T., & Haihong, M. (1990). An experimental study and analysis of the behaviour of rock under cyclic loading. *International Journal of Rock Mechanics and Mining Sciences & Geomechanics Abstracts*, *27*(1), 51–56. https://doi.org/https://doi.org/10.1016/0148-9062(90)90008-P

Chapter 5

Fatigue damage response of typical crystalline and granular rocks to uniaxial cyclic compression[1]

[1] This chapter has been published as a journal article in *International Journal of Fatigue* as:

Geranmayeh Vaneghi R, Thoeni K, Dyskin A V, et al (2020) Fatigue damage response of typical crystalline and granular rocks to uniaxial cyclic compression. Int J Fatigue 138:105667. https://doi.org/https://doi.org/10.1016/j.ijfatigue.2020.105667.

ABSTRACT

The effect of cyclic loading on the fatigue life, deformation properties and damage mechanisms of two microstructurally different rock types is explored by conducting uniaxial monotonic and cyclic compression tests under different loading conditions. Results show greater damage effects of low-frequency cyclic loading on the crystalline rock than on the granular rock. The damage evolution is characterized by introducing a damage variable based on residual strain. The results also indicate that damage evolution in the axial direction is different from that in the lateral direction. The development of many tensile microcracks is the main response of rocks to cyclic loading conditions.

5.1. Introduction

Underground structures are usually subjected to cyclic loading conditions due to disturbances from repeated loading–unloading seismic activities such as injection or extraction of fluids into or from reservoirs (Fan, Chen, Jiang, Ren, & Wu, 2016; Roberts, Buchholz, Mellegard, & Düsterloh, 2015; Voznesenskii, Krasilov, Kutkin, Tavostin, & Osipov, 2017; Wang, Li, Qiao, & Zhao, 2013), man-made explosions (blasting) (Li et al., 2017), and natural earthquakes or even traffic (Haimson, 1978). Furthermore, mining-induced seismic events, which occur along pre-existing faults, can also lead to catastrophic rock failures such as rockburst (Kaiser & Cai, 2012) often occurring during deep hard rock mining. Rock damage in the form of bulking, ejection and rockfall (Figure 5.1) as a consequence of such events is unpredictable. Nevertheless, additional geotechnical considerations can be considered and precautions can be suggested. Development of these measures needs better understanding of the stress state in the rock as well as properly designed support. The cyclic or dynamic load is applied to rock mass which has already been in a state of in-situ stresses monotonically altered in the process of excavation. Therefore, a combination of static and cyclic stress states should be considered in analyzing the strength and deformation responses of rocks. The mechanism of cyclic fatigue of rocks is very complex and believed to be a combination of cyclic damage due to opening and closing of pre-existing cracks and further cracking due to progressive stress corrosion (Scholz & Koczynski, 1979). However, so far there is limited understanding as to how both

mechanisms may interact depending on rock microstructure, environmental conditions, and stress state (Cerfontaine & Collin, 2018; Scholz & Koczynski, 1979). Consequently, a better understanding of the damage responses of rocks under coupled static cyclic loading could be helpful in delivering well-engineered design of underground structures, which is crucial to the safety and profitability of mines (pillar stability in hard rock underground mining) and civil structures (bridges and tunnels), and longer durability of disc cutters for mechanized tunnel or shaft boring machines.

Over the past two decades, considerable effort has been put into studying the effects of cyclic loading on the mechanical behavior of rocks. These investigations have focused on the effect of this type of loading on the degradation of rock properties (Attewell & Farmer, 1973; Bagde & Petroš, 2005a), and changes in rock behavior caused by changes in conditions of stress cycles including applied stress level (Ma et al., 2013; Momeni et al., 2015; Ray et al., 1999), loading amplitude (Geranmayeh et al., 2018; He et al., 2016; Liu et al., 2018; Taheri et al., 2016), and loading frequency (Liu & He, 2012; Liu et al., 2012; Xiao et al., 2009). However, up to now, most research has only focused on a specific rock type without developing a systematic understanding of how different rock types behave under this particular loading type. Undoubtedly, soft or granular rocks behave differently as compared to hard or crystalline rocks under the same loading conditions and this difference matters in terms of deformation response and damage mechanisms, as two principles of rock behavior. Nevertheless, there is a lack of understanding of deformation and strength responses of microstructurally and mineralogically different rock types to cyclic loading under the same loading conditions.

In this work, comprehensive uniaxial monotonic and cyclic compression tests were conducted on intact sandstone and granite rock samples. These two rock types vary noticeably in terms of mineralogy, microstructure, and strength, and their fatigue behavior can be used to represent the fatigue responses of a wide range of rock types. The main objective of this study was to explore the differences in fatigue responses of these two typical rocks. The cyclic loading conditions, including loading stress level, amplitude, and frequency, were varied to see their effects on the parameters investigated. The aim was to draw robust conclusions on the effect of loading frequency on the fatigue life of crystalline and granular rocks. For this purpose, the stress level and amplitude of the cyclic load were normalized to the monotonic strength obtained, to investigate changes in the fatigue responses of these rocks related to differences in

their microstructures. Variations in fatigue life, axial strain, and differential residual strains of both rocks under different loading conditions are discussed. The mechanism of damage evolution in both axial and lateral directions, which had not been clear for rock materials, is investigated. A damage variable based on residual strain is defined to discuss the evolving damage of samples under different loading conditions. Finally, the failure modes of samples tested under both monotonic and different cyclic loading conditions are discussed with focus on the differences in the failure modes depending on the rock microstructure.

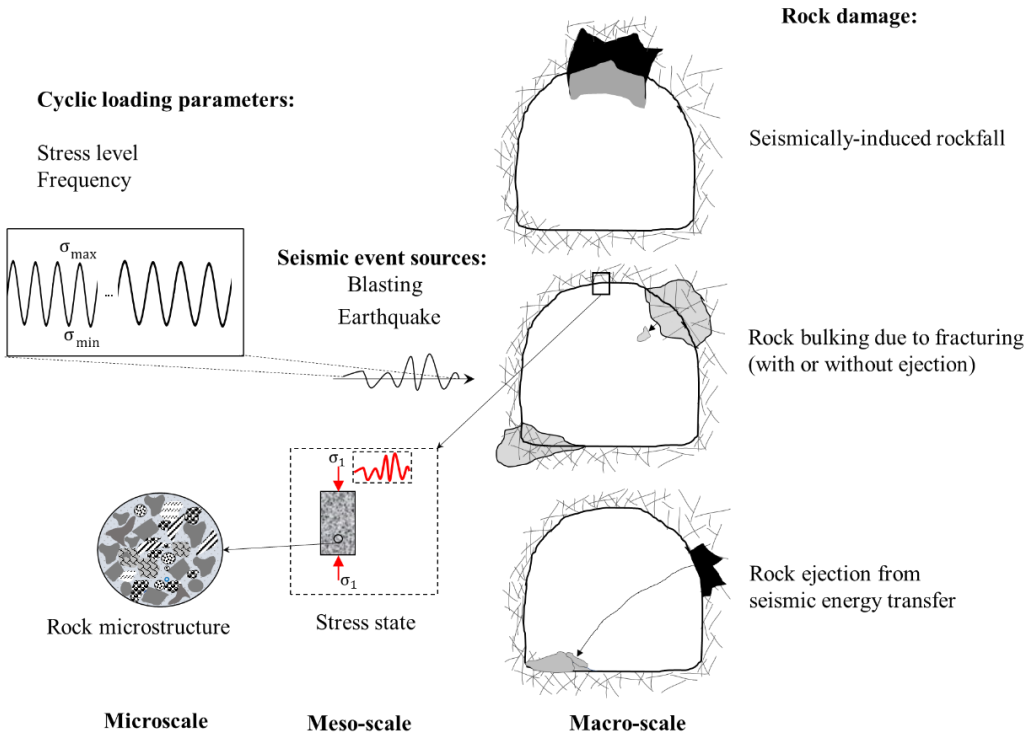

Figure 5.1. Schematic view of rock damage in mine galleries, induced by seismic events and affecting factors of the stress state and rock microstructures at different scales (rock types, rock microstructure, and loading parameters). $\boldsymbol{\sigma_1}$, $\boldsymbol{\sigma_{max}}$, and $\boldsymbol{\sigma_{min}}$ are the major principal stress applied on the rock, maximum, and minimum stress of the cyclic loading, respectively.

5.2. Experimental materials and test procedure

5.2.1. Rock samples and test device

Sandstone (S) as a granular rock, and granite (G) as a crystalline rock, are used as the two different rock types for this study. The sandstone samples, generally known as Hawkesbury sandstone, were taken from Mt White sandstone quarry, south of Somersby at Gosford, New South Wales, Australia. The granite samples are from another outcrop in this area. According to microscopic thin section analysis, the sandstone is fine-grained and well-sorted arenite with about 80% quartz minerals, and the granite is weakly altered with about 25% anhedral quartz (Figure 5.2). All samples were cored from the same block and prepared in a cylindrical shape with a length to diameter ratio of L/D >2 (ASTM, 2008b; Bieniawski & Bernede, 1979). Table 5.1 shows the mechanical and physical properties of the samples tested. Ultrasonic measurements and thin section analysis were used for initial evaluation of the rock properties (cf. Chapter 2). Isotropy of both sandstone and granite rock samples was confirmed by ultrasonic measurements conducted on oven-dried samples, along their longitudinal directions, according to which all determined P-wave velocities vary by less than 2% from their mean values (ASTM, 2008a; Aydin, 2014). All samples were dried in an oven before testing (ASTM, 2016b).

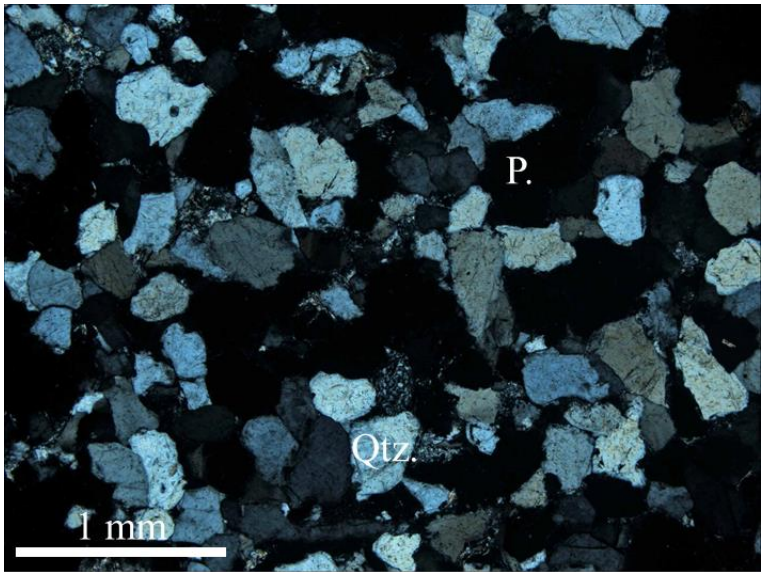

(a)

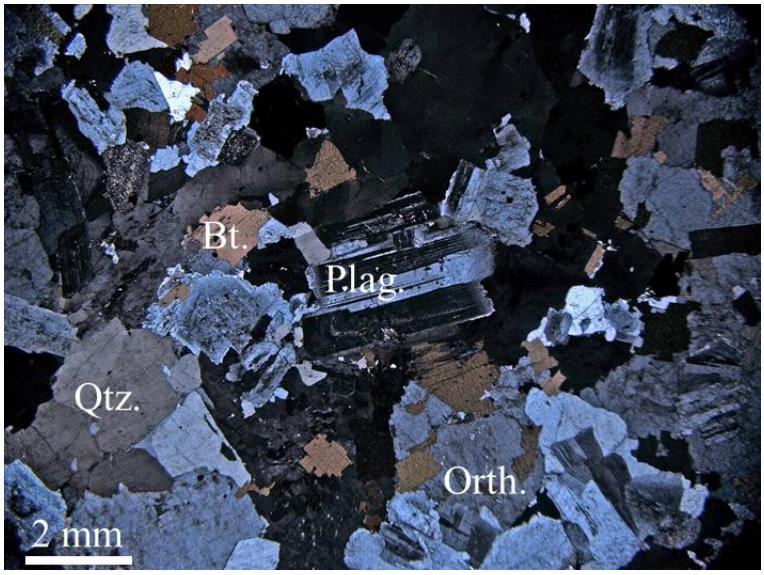

(b)

Figure 5.2. Microscopic thin section photomicrographs of (a) sandstone, and (b) granite in cross polarized light (XPL): Qtz., Plag., Orth., Bt., and P. stand for quartz, plagioclase, orthoclase, biotite, and intergranular porosity, respectively.

Table 5.1. Mechanical and physical properties of the samples tested.

Property	Sandstone	Granite
Mineral composition[a]	~75–80% sub-rounded to angular quartz, 5–7% clay and sericite in matrix, Rare grains of fine-grained, anhedral tourmaline, zircon and flakes of muscovite with associated fine opaques.	coarse-grained, leucocratic holocrystalline, ~20–30% quartz, ~20–30% orthoclase, ~10–20% subhedral, zoned plagioclase, ~10% medium-grained flakes of biotite, 10–30% other.
Grain size (mm) [a]	<1 mm	1–5 mm (50% of grains are >3 mm)
Intergranular porosity [a]	~25%	-
Dimensions L(mm) × D(mm): [b]	111.1× 54.1	130.0× 54.1
Density (kg/m^3) [b]	2205±11.2	2662±2.4
Water content (%) [b,c]	0.74±0.370	0.07±0.016
UCS (MPa) [d,e]	48.85±1.3	149.26±6.27
P-wave (m/s) [f]	2536±46	4302±134

[a]These results are determined from microscopic thin section analysis on two representative samples of each rock type (according to ISRM (1978)).

[b]61 sandstone samples and 54 granite samples were used to determine these average values.

[c]Water content was determined according to ASTM D2216 (ASTM, 2016b).

[d]The average Uniaxial Compression Strength (UCS) was determined from test results of 8 samples of each rock type (conducted according to ASTM D7012 and ISRM 1979 (ASTM, 2016a; Bieniawski & Bernede, 1979)).

[e]GCTS loading machine (UTC-1000) with 1000 kN compression loading capacity and 600–700 kN/mm stiffness.

[f]The average P-wave velocities are determined from ultrasonic measurements on 56 sandstone and 49 granite samples. A pair of V103-SM transducers from OLYMPUS with nominal element size and nominal frequency of 13 mm and 1.0 MHz, respectively, was used for ultrasonic measurements.

5.2.2. Test method

The experiments were designed to study differences in deformation and strength responses of sandstone and granite, as two different rocks in terms of strength and microstructure, at different cyclic loading conditions of maximum stress levels (σ_{max}), loading frequency (f), and peak to peak stress amplitudes (σ_{p-p}). Due to the larger dynamic effect of the sinusoidal waveform compared to the triangle ramp waveform (Bagde & Petroš, 2005b; Xiao et al., 2008; Zhenyu & Haihong, 1990), cyclic loading in the form of periodic sinusoidal waveforms was selected for these tests. Figure 5.3 shows the schematic loading path designed for this study in which samples were monotonically loaded up to a specified stress level and then subjected to the cyclic stage until failure. This stress path represents the natural stress regime given that the rocks are under coupled monotonic-cyclic loading conditions. The average UCS values obtained for both the sandstone and granite samples (cf. Table 5.1) were used to set up the starting stress level, peak to peak loading amplitude, and maximum stress level of the cyclic stage. Both sandstone and granite samples were tested under the same loading scenarios to achieve a meaningful comparison of their responses. The monotonic compression tests and monotonic stages of cyclic tests (i.e. pre-cyclic and post-cyclic stages) were conducted under a load-controlled mode at a loading rate of 0.1 MPa/s to allow for quasi-static loading conditions. Lateral and axial deformations of samples during tests were recorded by two 10 mm long rosette strain gauges attached in the middle and on the opposite sides of the samples. The resistance of the strain gauges is 120 Ω. The average of two strain gauge recordings was used for deformation analysis. The detailed cyclic loading paths are presented in Table 5.2. Each test was carried out 2–5 times to assure repeatability of the results. A few samples that did not fail during the cyclic loading (≤1080 cycles) were further monotonically loaded to failure (i.e. post-cyclic stage).

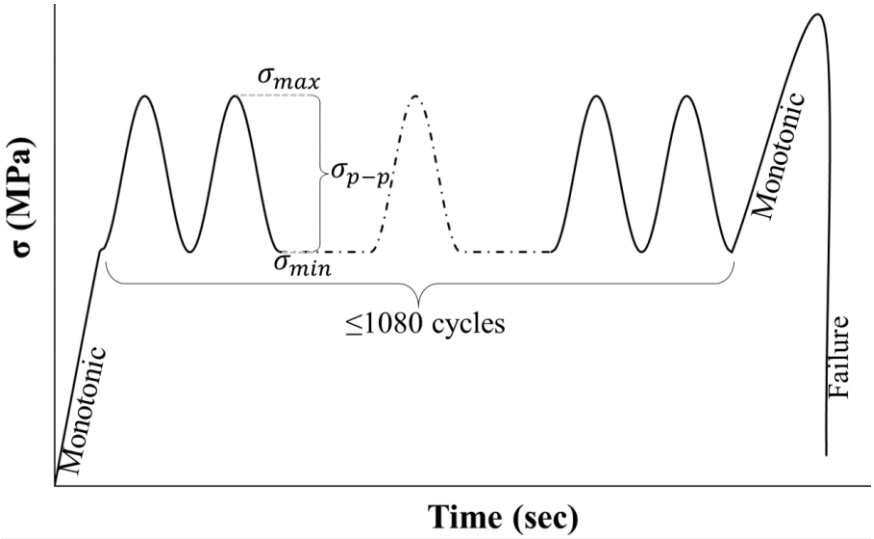

Figure 5.3. Schematics of the loading path used in the tests (a coupled monotonic-cyclic stress path).

Table 5.2. Parameters of the loading.

Loading path No.	Frequency (Hz)	σ_{max}/UCS (%)	σp-p/UCS (%)	Investigated factor			Number of samples tested	
				σ_{p-p}	σ_{max}	*f*	Sandstone	Granite
1	0.1	90	30	✓			5	5
2	0.1	90	35	✓			2	-
3	0.1	90	40	✓			3	-
4	0.1	90	50	✓	✓	✓	3	5
5	0.1	80	50		✓		5	4
6	0.1	70	50		✓		6	-
7	0.05	90	50			✓	2	5
8	0.5, 0.2*	90	50			✓	5, 1*	5

*One additional sandstone sample tested at 0.2 Hz.

5.3. Results and discussion

5.3.1. Fatigue life

Fatigue life was found to decrease with maximum stress level and loading amplitude and this reduction was more noticeable for granite samples, Figure 5.4. From the fitted curves in Figure 5.4a, it can be seen that the fatigue life of both sandstone and granite samples generally shows an exponential relation with the maximum stress level. It should be mentioned that the curve for the test data of granite is fitted on two data points of maximum stress levels since these samples did not fail after hundreds of cycles under a maximum stress of 80% of UCS and it would be meaningless to conduct tests at 70% of UCS. Therefore, the exponential curve fitted to these data points only gives a general trend and should be interpreted with caution. Figure 5.4a also shows that the fatigue strength threshold (i.e. the stress level at which a rock can sustain cyclic loading up to a large number of cycles without failure) of the granite samples tested in this study is greater than that of the sandstone samples. The fatigue strength threshold for the granite samples is around 80% of the peak uniaxial compression strength, whereas it does not exceed 70% of the UCS for the sandstone samples. However, the authors incorporated a large quantity of data from the literature in another investigation and showed that the fatigue strength threshold of soft rocks such as sandstone is generally greater than that of granite, as a hard rock (cf. chapter 4). The fatigue life of both sandstone and granite shows a small downward linear trend with loading amplitude, however, the granite samples sustained a larger number of loading cycles than the sandstone samples at the same loading amplitude (Figure 5.4b). This is more evident at higher loading amplitudes, indicating more susceptibility of sandstone to cyclic loading at higher loading amplitudes (>30% of UCS).

Turning now to the effect of loading frequency on fatigue life, it was found that the relationship between loading frequency and fatigue life was unclear for both rocks (Figure 5.4c). Incorporating these results with the results of previous studies indicates an increasing trend of fatigue life with loading frequency, especially at loading frequencies greater than 1 Hz (Haghgouei et al., 2018; He & Chen, 2016; Ishizuka et al., 1990; Liu et al., 2012; 2018; 2017; 2017; Ma et al., 2013; Momeni et al., 2015; chapter 4). This is shown in Figure 5.5, in which curves fitted to individual data points generally show an increasing trend in fatigue life with an increase in loading frequency,

regardless of cyclic loading conditions and test type. Therefore, it can be concluded that fatigue life increases with loading frequency for both rock types.

Re-plotting the data for fatigue life, presented in Figure 5.5, on a semi-logarithmic axis against the loading frequency (Figure 5.6) shows that fatigue life follows a linear and power relation with frequency for granular rocks (sandstone or rocks with similar strength) and hard/crystalline rocks (granite or rocks with similar strength), respectively. What stands out in this figure is the large damaging effect of low-frequency cyclic loading on both rock types. The rocks can withstand a smaller number of cycles at low loading frequencies than at high loading frequencies. This is more evident in the case of hard rocks (Figure 5.6b) which are more vulnerable to low-frequency cyclic loading. One possible explanation for this finding is that the slow loading process at low-frequency cyclic loading allows pre-existing or initiated microcracks along the grain boundaries to extend easily in a greater dilative manner which eventually results in a greater propagation of cracks and in turn greater damage. This dilative response is more evident for crystalline rocks, most probably because of preferred orientations of grain boundaries (i.e. pre-existing cracks) during mineralization. Therefore, it is evident that low-frequency seismic events have more damaging effects on all rock types and extra caution should be taken in designing rock structures when they are prone to this type of loading.

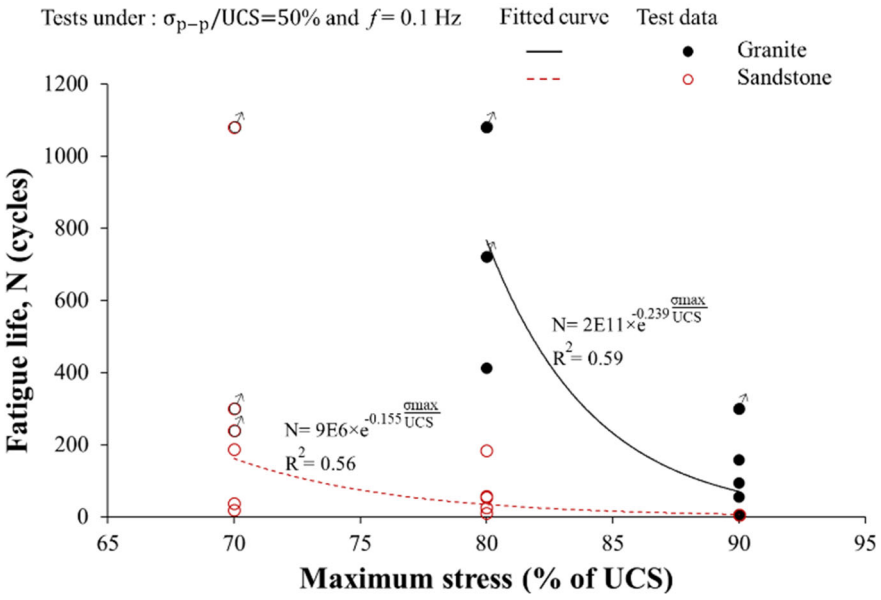

(a)

Figure 5.4 (continued on the next page).

Figure 5.4 (continued on the next page).

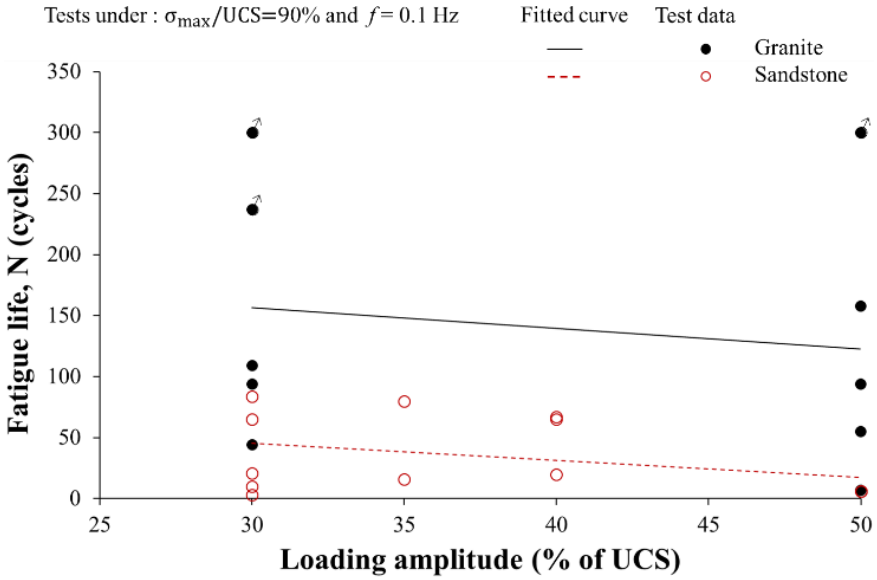

(b)

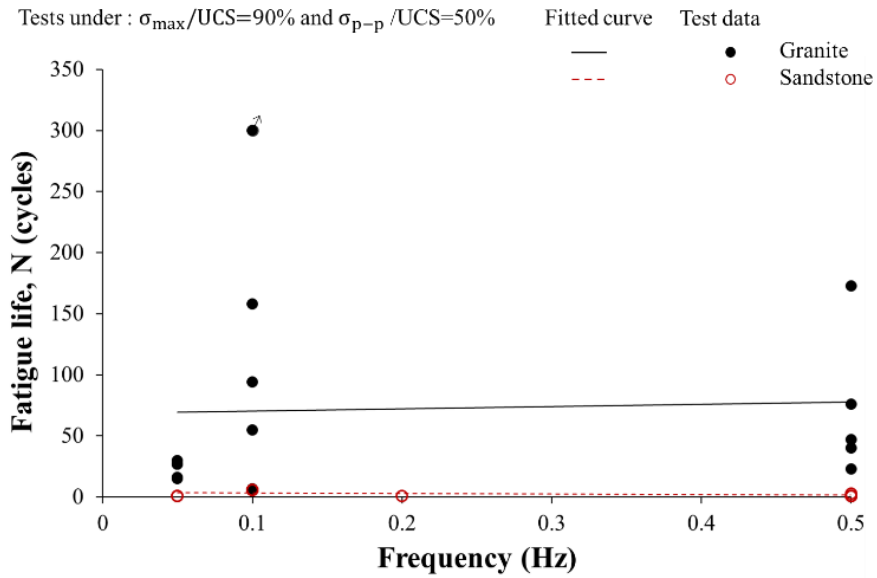

(c)

Figure 5.4 (continued from previous page). The relation between fatigue life and: (a) maximum stress level, (b) loading amplitude, and (c) loading frequency; data shown by arrows are for those samples that underwent post-cyclic loading, fitted curves are linear fittings.

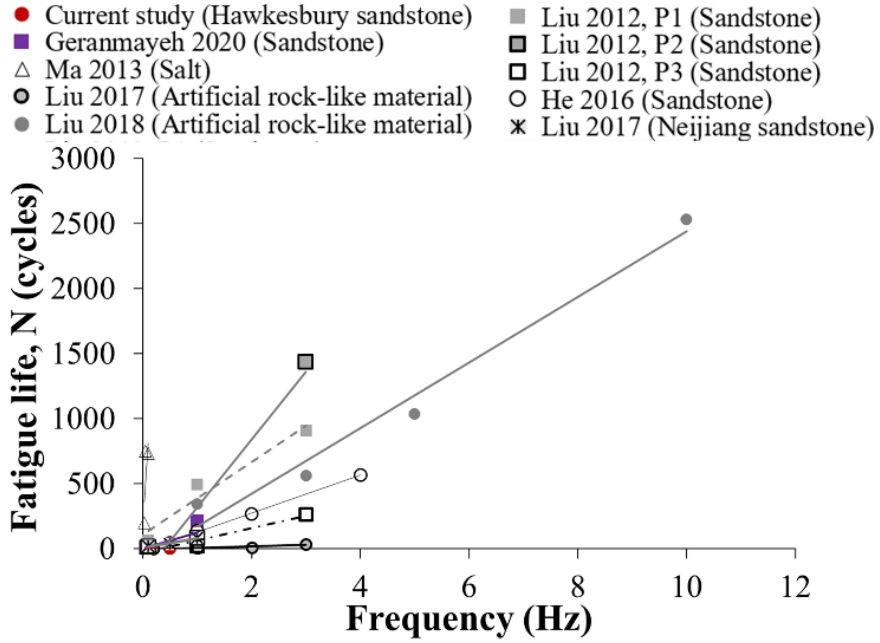

(a)

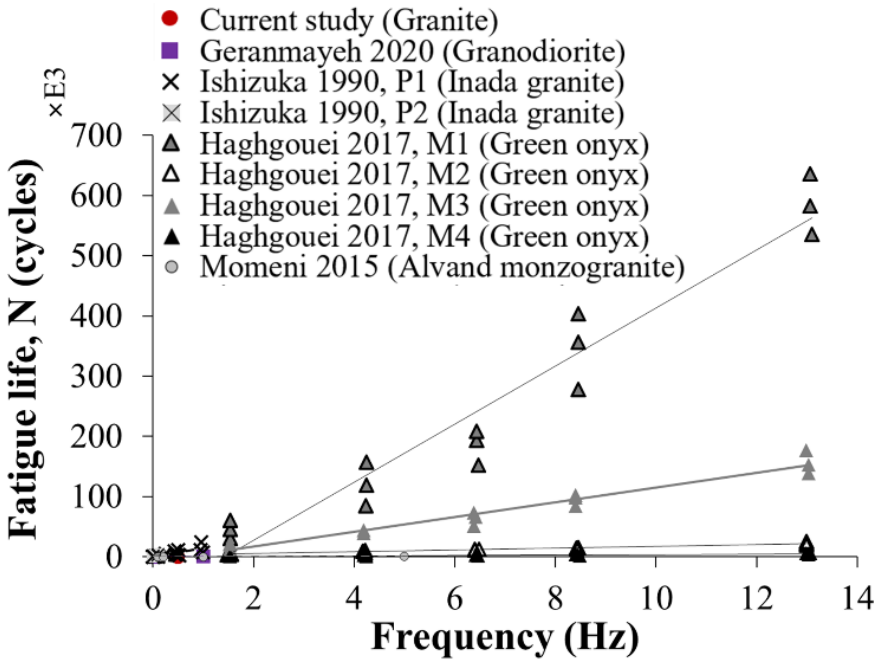

(b)

Figure 5.5. The increasing trend of fatigue life with loading frequency for: (a) soft rocks like sandstone, (b) hard rocks like granite; for notations shown on legends refer to references (Haghgouei et al., 2018; He & Chen, 2016; Ishizuka et al., 1990; Liu et al., 2012; 2018; 2017; 2017; Ma et al., 2013; Momeni et al., 2015; Geranmayeh 2020 refers to data in chapter 4).

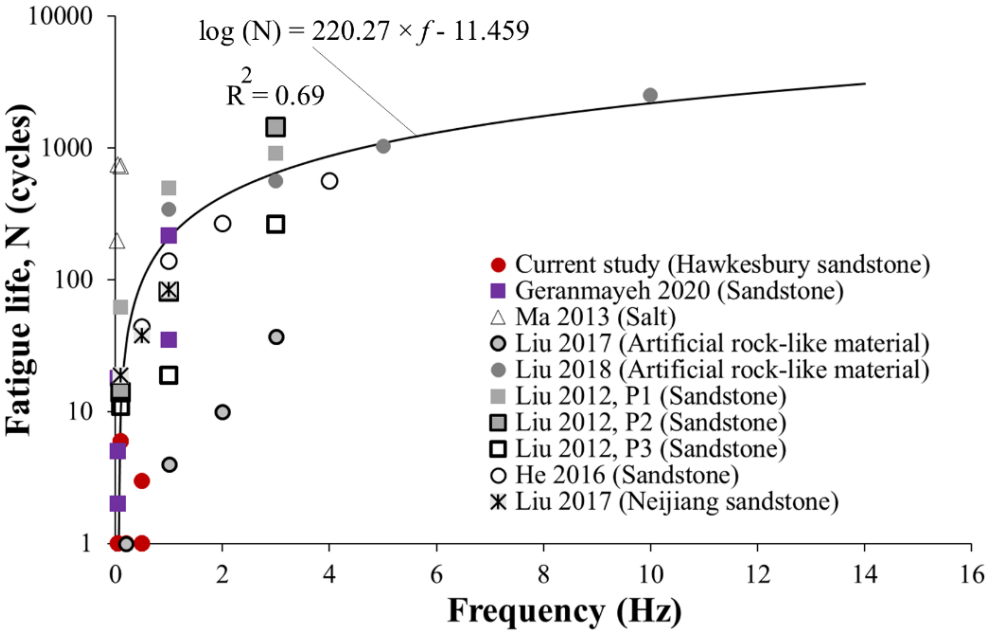

(a)

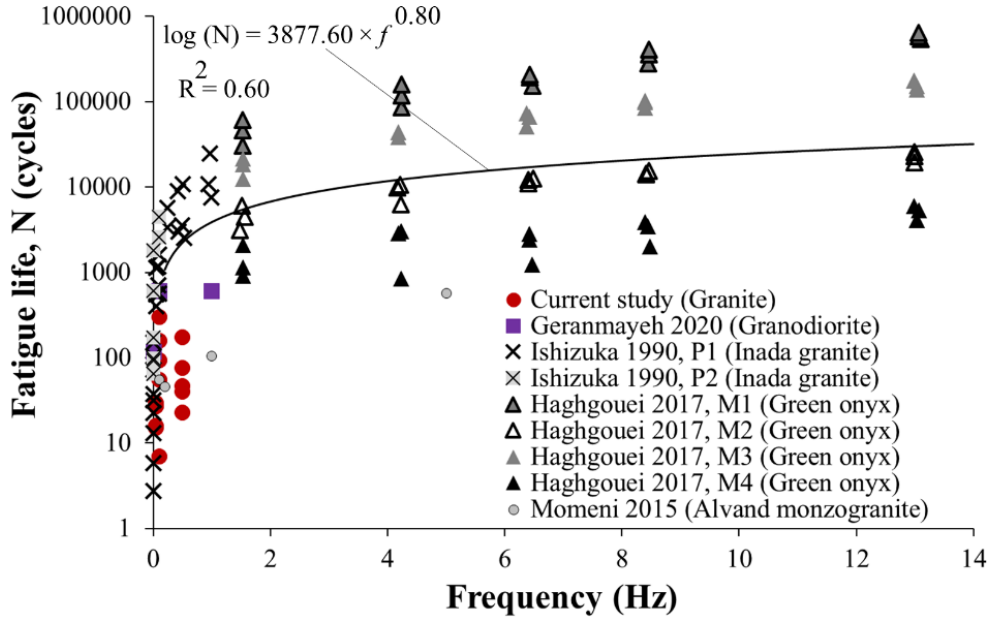

(b)

Figure 5.6. The relation between fatigue life and frequency of (a) soft rocks such as sandstone, (b) hard rocks such as granite; data obtained from the current study and the literature (Haghgouei et al., 2018; He & Chen, 2016; Ishizuka et al., 1990; Liu et al., 2012; 2018; 2017; 2017; Ma et al., 2013; Momeni et al., 2015; Geranmayeh 2020 refers to data in chapter 4).

5.3.2. Deformation response

The axial deformation response of the tested rock samples at the end of the cyclic stage, under different cyclic loading conditions, shows that there is a slight upward trend in the maximum axial strain at the end of the cyclic stage with the maximum stress level (Figure 5.7a). This trend is linked to the time period over which a sample is subjected to a stress level above the crack initiation stress threshold (σ_{ci}) and close to the crack damage stress threshold (σ_{cd}), which are around 40% and 80% of UCS, respectively (Martin & Chandler, 1994). At a higher maximum stress level, the time during which the sample is loaded around the crack damage stress threshold is longer than that under lower maximum stress levels. Therefore, the sample experiences more extensive crack growth during that time, which results in greater axial deformation. At a constant maximum stress level of 90% of UCS (around the crack damage stress threshold) the maximum axial strain of the cyclic stage is more or less independent of the loading amplitude (Figure 5.7b). The differential residual strains of both sandstone and granite samples, on the other hand, show a decreasing trend with loading amplitude, if the differential residual strains are defined as:

$$(\Delta\varepsilon_{r_i})_{ax.\ or\ lat.} = \left(\varepsilon_{r_{i=n}}\right)_{ax.\ or\ lat.} - (\varepsilon_{i=0})_{ax.\ or\ lat.} \quad (5.1)$$

where i is the number of cycle, $\varepsilon_{r_{i=n}}$ is the residual axial or lateral strain at the end of the current cycle (start of the loading of a cycle), $\varepsilon_{i=0}$ is the axial or lateral strain at the end of the monotonic stage (i.e. strain at the starting point of the first cycle), and ax. and lat. stand for axial and lateral, respectively.

The differential residual axial and lateral strains of both sandstone and granite at the end of the cyclic stage under higher loading amplitude (50% of UCS) were smaller than those under a lower loading amplitude of 30% of UCS (cf. fitted curves showing general trends in Figure 5.8). At high loading amplitudes, the sample was loaded for a shorter time at higher stress than under low loading amplitudes, under the same maximum stress level and loading frequency. Consequently, it resulted in relatively low strain before failure. The comparison of the differential residual strain of sandstone with that of granite shows that the differential residual strain in both axial and lateral directions for sandstone is greater than that of granite. Axial residual strain $\Delta\varepsilon_{r_{ax.}}$ for sandstone is mostly greater than 0.04% while it is less than 0.04% for granite samples

at the end of the cyclic stage. All granite samples failed at a differential residual lateral strain of less than or equal to –0.24% whereas the sandstone samples failed at a higher differential residual lateral strain. This behavior is related to the ductility of sandstone and brittle behavior of granite.

Turning now to variation in axial strain in the cyclic stage with loading frequency, this study found that axial strain at the end of the cyclic stage has no distinguishable relation with loading frequency for granite samples, whereas it decreases slightly with an increase in frequency for sandstone samples (Figure 5.7c). One possible explanation for this deformation response of sandstone is that in sandstone microcracks are produced at lower relative stress levels than in granite. Furthermore, the evolution of microcracks can easily occur at low loading frequencies because slow and gradual loading allows nucleation and development of existing and initiated microcracks before failure, resulting in greater deformation. In contrast, at higher loading frequencies microcracks do not have enough time to develop due to fast loading. Overall, a closer analysis of these curves shows that the deformation response of granite, as a brittle rock, is mostly affected by the maximum stress level rather than by any change in either loading amplitude or frequency. On the other hand, all cyclic loading conditions of maximum stress level, loading amplitude, and frequency can individually affect the deformation response of sandstone, as a ductile rock. This is a surprising result which may enhance our understanding of the deformation and fracturing response of hard or crystalline rocks and soft or granular rocks under fatigue.

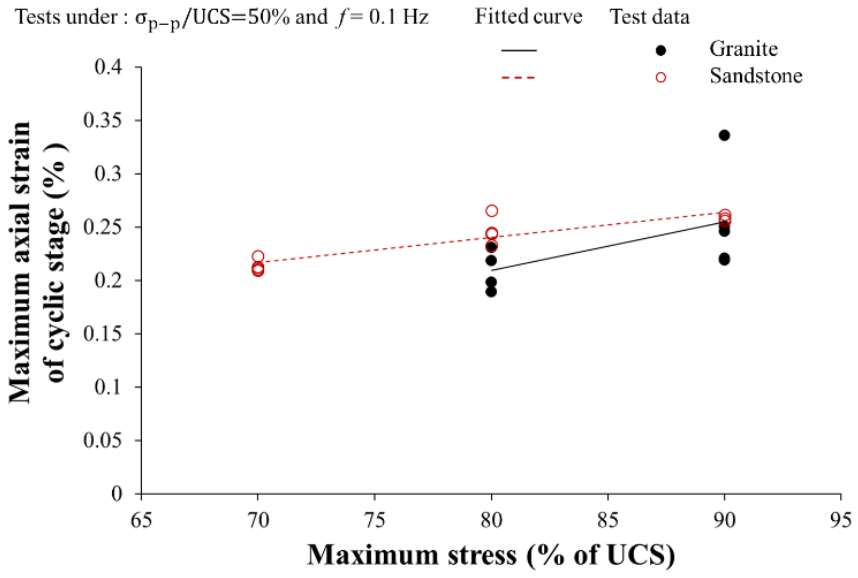

(a)

Figure 5.7 (continued on the next page).

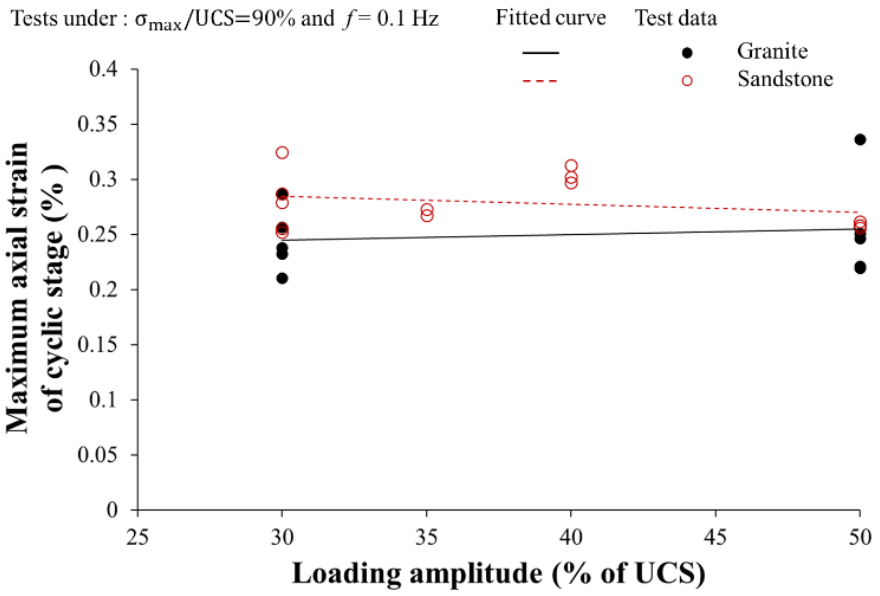

(b)

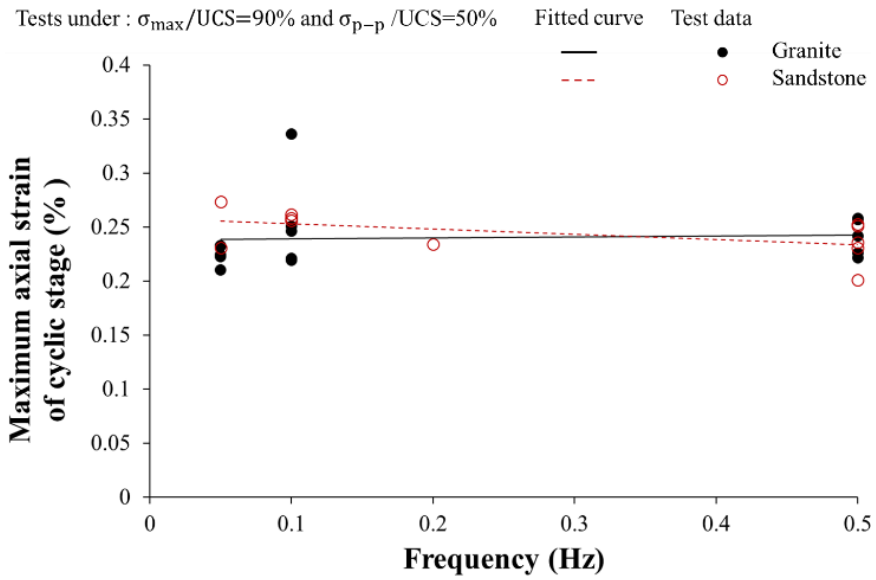

(c)

Figure 5.7 (continued from previous page). Maximum axial strain at the end of cyclic stage against: (a) maximum stress level, (b) loading amplitude, and (c) loading frequency, fitted curves are linear fittings.

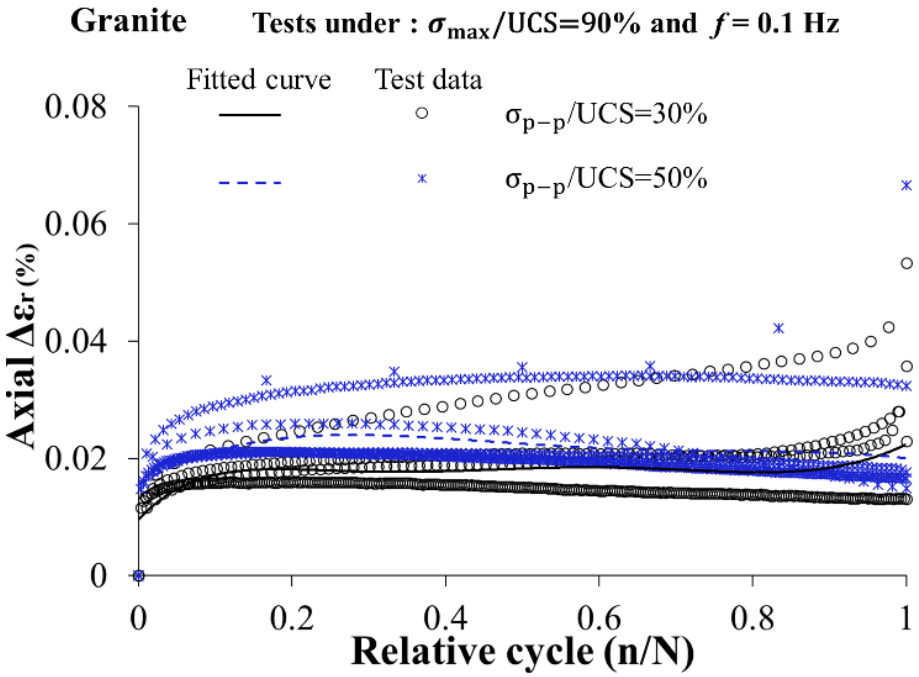

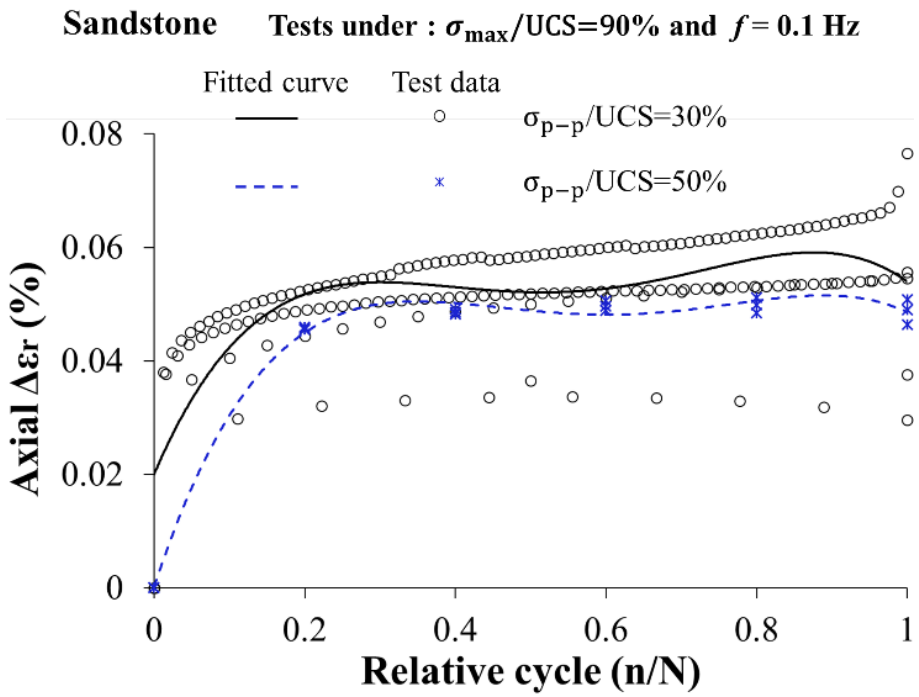

(a)

Figure 5.8 (continued on the next page).

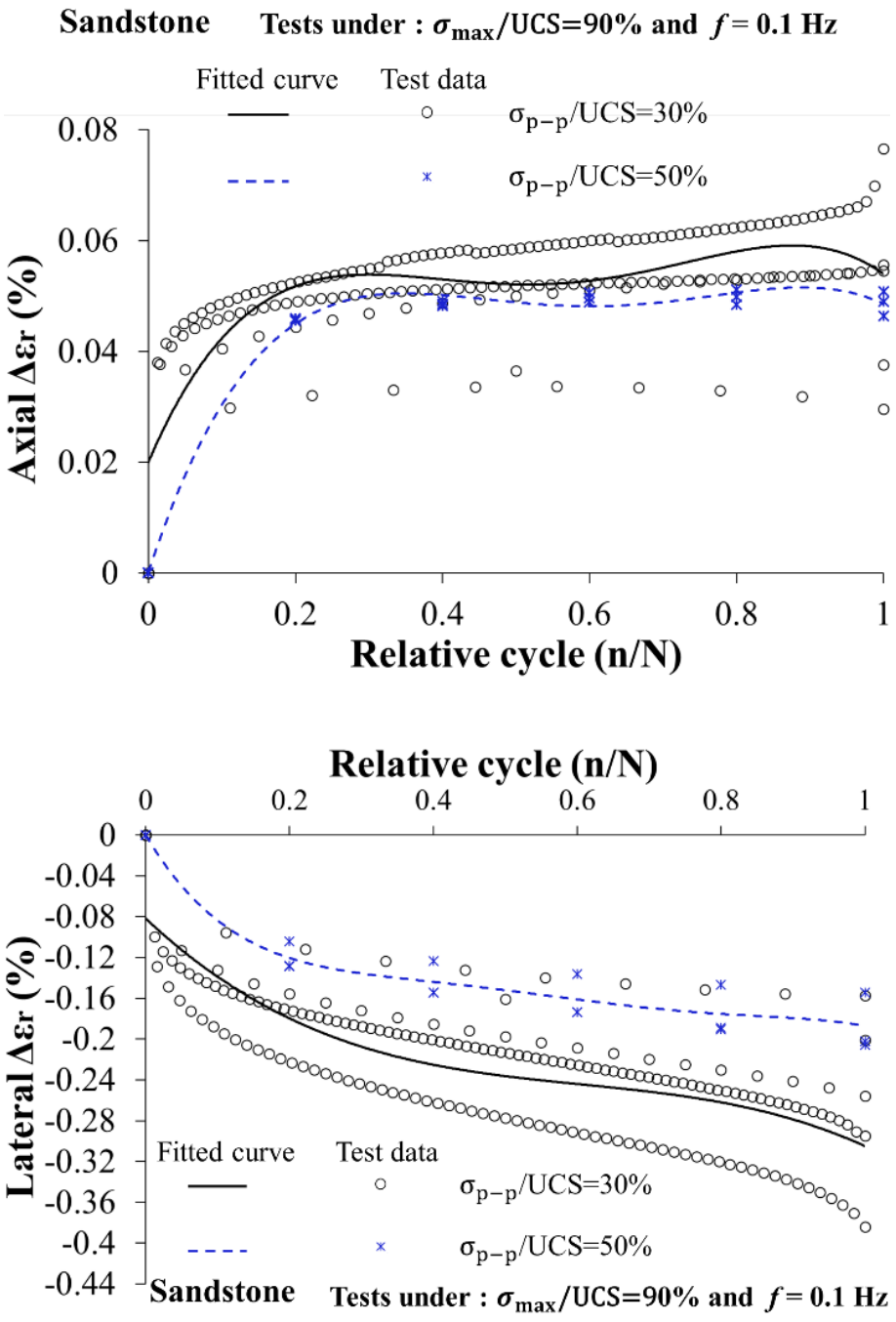

(b)

Figure 5.8 (continued from previous page). Variations in differential residual strain with the relative cycle number for sandstone and granite under different loading amplitudes: (a) axial strain; (b) lateral strain; N is the number of cycles at failure, fitted curves show the overall trends. All data starts at zero since differential residual strains at the starting point of the cyclic stage (i=0) are zero (refer to Eq. (5.1)).

5.3.3. Fatigue damage variable

Rock damage is associated with the development of microcracks (or cracks of a corresponding scale much smaller than the characteristic length of the load redistribution), due to irreversible destruction of bonds in rock microstructure (Eberhardt, 1998). Assessment of damage evolution during the fatigue process is of great importance since most rock properties are affected by microcracks evolving and propagating. Therefore, a damage variable is needed to quantify damage accumulation during the fatigue process. An appropriate damage variable should have a physical meaning to represent the degradation in the mechanical properties of rocks as loading proceeds. Previous studies used different variables for this purpose (Eberhardt et al., 1999; Liu & He, 2012; Qiu et al., 2014; Xiao et al., 2010; 2009; 2011).

Regardless of damage that occurred during the monotonic stage, any change in residual strain throughout the cyclic stage can be a good indication of fatigue damage accumulation. Therefore, the damage variable proposed in this study is defined as:

$$D_i = \Delta\varepsilon_{r_{i=n}}/\Delta\varepsilon_{r_{i=N}} \quad (5.2)$$

where D_i is the damage variable at cycle i, $\Delta\varepsilon_{r_{i=n}}$ is the differential residual strain (either axial or lateral) after n cycles, and $\Delta\varepsilon_{r_{i=N}}$ is the differential residual strain at failure. This damage variable has a physical meaning and represents damage evolution throughout the cyclic stage (the residual strains at the start of the cyclic stage are deducted from those measured in the target cycle). It is also helpful in analyzing the effect of cyclic loading conditions on the progress of the damage by focusing on the deformation response during the cyclic stage. This damage variable is different for axial and lateral strain and evolves from zero to one if the rock sample fails during the cyclic stage. As discussed in detail later, the damage variable may exceed one if other factors rather than mechanical cracking contribute to rock damage. The damage variable would be less than one if the sample fails during the post-cyclic stage, of which $\Delta\varepsilon_{r_{i=n}}$ is taken as maximum strain during the cyclic stage. The axial and lateral damage accumulation of sandstone and granite under different loading amplitudes is illustrated in Figure 5.9. It is apparent from this figure that damage, especially lateral damage, usually develops in a three-phase process for both sandstone and granite, in which it accumulates rapidly during the initial cycles, phase I, followed by a steadily increasing trend in phase II,

and eventually a sharp accumulation during the final cycles, phase III. Phase I corresponds to rapid damage accumulation during the initial cycles due to the activation of weak microcracks (either existing or initiated during the monotonic stage of the loading). Then crack accumulation and propagation becomes steady and the damage evolution occurs in a steady trend throughout the later stage, which corresponds to phase II. Eventually, cracks reach the unstable stage of their growth and damage accumulation accelerates again approaching failure; this is phase III. This resembles the three stages of creep deformation. Nevertheless, the trend of the damage variables may sometimes only show two phases, depending on the stress level and other conditions.

The proposed variables are capable of describing damage evolution at different loading conditions. The fitted curves show that the axial and lateral damage of both sandstone and granite samples under loading amplitude of 50% of UCS is greater than under loading amplitude of 30% of UCS. This result is independent of the rock type and indicates the greater fatigue damage effect of high-amplitude cyclic loading. The fitted curves in Figure 5.9 also show that axial damage of both sandstone and granite samples at high loading amplitudes occurs during the initial stage, whereas lateral damage evolves gradually throughout the test and follows the three-phase development form. The axial damage variables for both granite and sandstone samples tested at a high loading amplitude of 50% of UCS and a high maximum stress level of 90% of UCS increase sharply to a value greater than one during the initial phase then decrease gradually to one during the final cycles. This two-phase trend, which occurs for tests at higher amplitudes and higher stress levels, is very complex and most probably related to stress corrosion and/or rock dilatancy. Stress corrosion, as the most prevalent mechanism of damage evolution in a creep test dominating at a high maximum stress level and low loading amplitude, cannot easily be distinguished from fatigue damage, which is the main process at high stress amplitude and low maximum stress level (Cerfontaine & Collin, 2018; Scholz & Koczynski, 1979). Stress corrosion cracking is mainly induced by a change in the environment of cracks (chemical constituents) and temperature (Anderson & Grew, 1977), however anisotropy of the microstructures of minerals and grains and their preferred orientations can also induce this cracking phenomenon (Scholz & Koczynski, 1979). Stress corrosion is associated with low-frequency events such as earthquakes, where this phenomenon is crucial and should be considered more precisely (Anderson & Grew, 1977; Cerfontaine & Collin, 2018;

Scholz & Koczynski, 1979). It can be argued that stress corrosion also contributed to the axial damage of the samples because all of the following factors, which are believed to be the main contributing characteristics of this process, existed in the tests:

1. Stress state: stress corrosion is a probable phenomenon at high-stress or low-frequency loading. All tests which showed this trend correspond to high stress levels. On the other hand, the loading frequency was also low. Therefore, this mechanism most probably contributed to the subcritical cracking of these samples. It should be noted that the influence of this mechanism was reinforced by a higher loading amplitude, when the maximum stress level was fixed.
2. Tensile stress: stress corrosion is usually due to tensile stress concentration, most likely localized at the tips of pre-existing cracks or newly initiated cracks, which progressively branches into other microcracks (i.e. more tensile stress localizations), throughout the test.
3. Environmental conditions: since all samples were tested after oven drying, the water content could not be an environmental condition resulting in stress corrosion. Changes in room temperature are not of concern since all samples were kept in a sealed box. However, changes in the temperature of the samples themselves during testing could occur since crack working can increase the temperature of the crack environment (crack tips or grain boundaries).
4. Anisotropy in the grain boundaries and microstructures of both rock types reinforces stress corrosion. This mechanism is more significant in granite with more heterogeneous grain materials in different sizes and orientations.

The greater lateral damage and its gradual increasing growth can be explained by the fact that samples expand laterally during the loading stage of a loading–unloading cycle due to the detachment of grains and opening of pre-existing microcracks along the loading direction (the dilatancy). Partial closure of such axial microcracks happens during the next unloading stage. However, tensile stress localized at the tips of microcracks allows their propagation if it exceeds the tensile strength of the rock. Tensile stress at tips of microcracks at higher loading amplitudes is relatively higher than under low loading amplitudes because of a higher unloading stress level. Accordingly, branching and propagation of axial microcracks would be more dominant, which subsequently results in higher lateral expansion continuously throughout the test or, in other words, greater axial splitting. Therefore, lateral damage

is higher due to the weakening of rock samples under high-amplitude cyclic loading. However, the weakening of rock samples under low loading amplitudes is controlled by both lateral and axial damage. From the curves in Figure 5.9, it can also be seen that the proportion of the second phase of lateral damage development (phase II) of sandstone to the whole process of its fatigue is relatively smaller than that for granite samples. The second phase of lateral damage development for granite samples accounts for about 60–70% of the fatigue process, whereas most of the fatigue damage of sandstone samples occurs during 30% of its fatigue process (Figure 5.9).

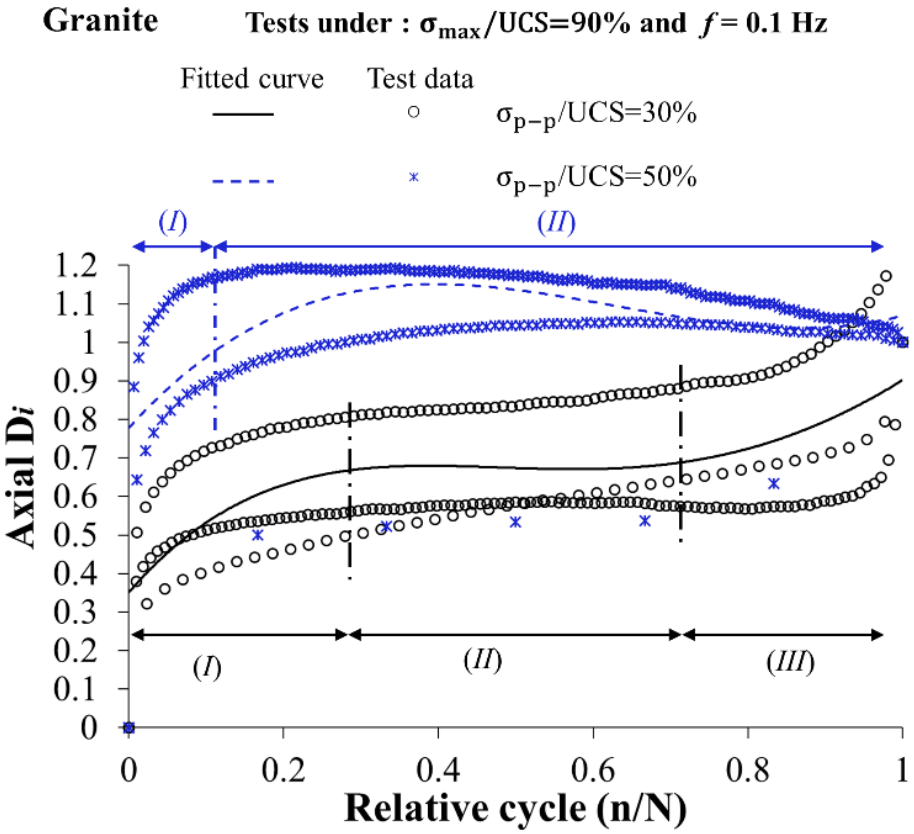

Figure 5.9 (continued on the next page).

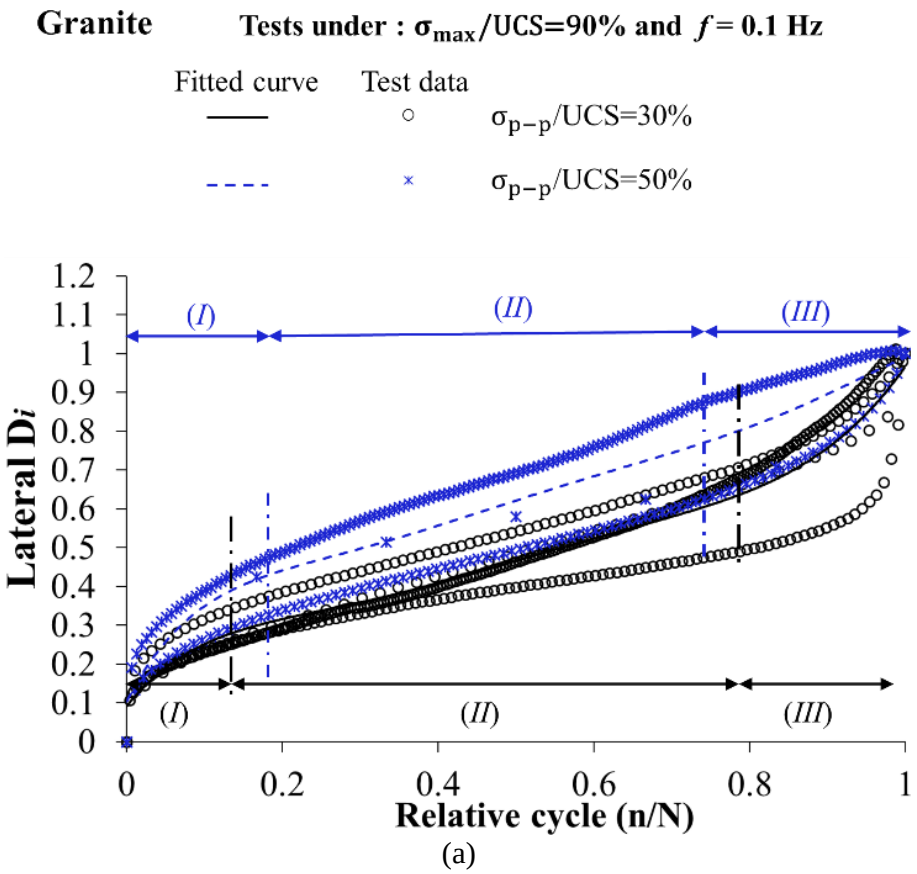

(a)

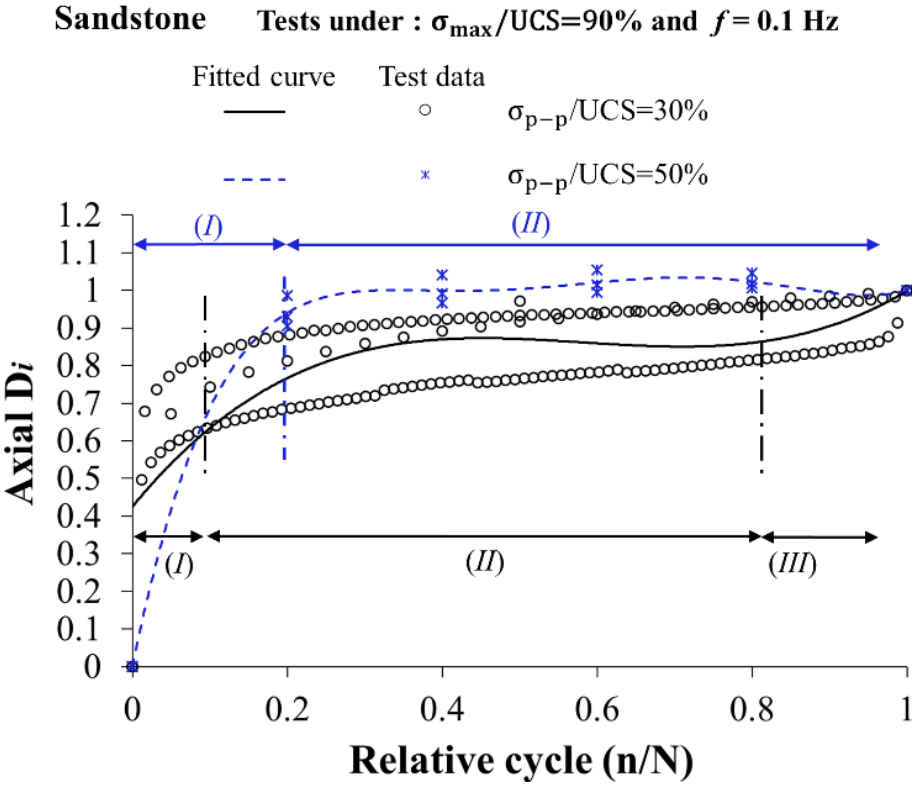

Figure 5.9 (continued on the next page).

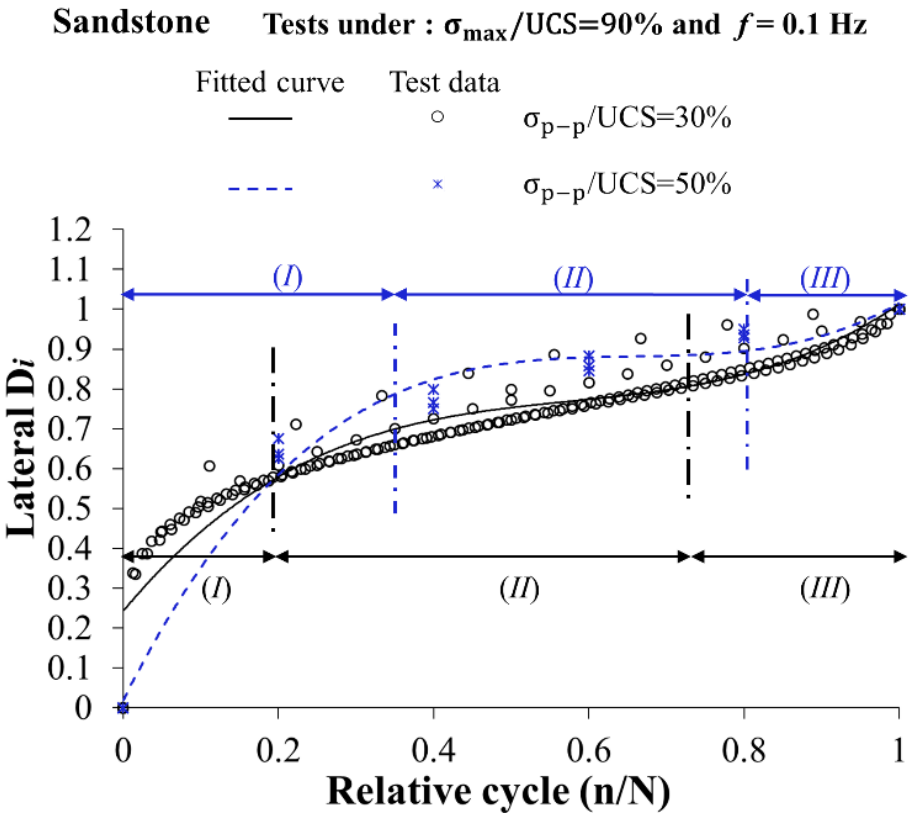

(b)

Figure 5.9 (continued from previous pages). The variations in axial and lateral fatigue damage variables of (a) granite, and (b) sandstone samples under different loading amplitudes; vertical dotted lines indicate the boundaries between the identified phases, the fitted curves show the overall trends. All data start at zero since the damage variable is taken as zero at the starting point of the cyclic stage, i.e. i=0 (refer to Eq. (5.2)).

As well as the loading amplitude, the maximum stress level greatly affects the damage evolution of both rock types. The greater the maximum stress level, the greater the damage evolution of rocks in both axial and lateral directions (Figure 5.10). The permanent axial damage of samples under a low maximum stress level is less than 30% of its total damage which indicates the greater dependency of axial damage on the stress level applied. From the fitted curves in Figure 5.10, we can also see that the proportion of the first phase of damage development to the whole fatigue process increases as the maximum stress level increases, especially for the axial damage variable. In other words, this finding reveals that rocks under a high cyclic stress regime experience most fatigue damage during the initial cycles. The axial damage variable greater than one

(cf. Figure 5.10) for both sandstone and granite samples can be explained by stress corrosion, which was discussed in the previous paragraphs.

The effect of loading frequency on fatigue damage is very complex and there is no clear relation between the defined damage variable and frequency (Figure 5.11). The difference between the damage evolutions of granite samples under different loading frequencies ranging from 0.05 to 0.5 Hz is hardly distinguishable. However, the first phase of the damage evolution for the samples loaded under 0.05 Hz is noticeable during the initial cycles, which may be an indication of the greater damage effect of low-frequency cyclic loading.

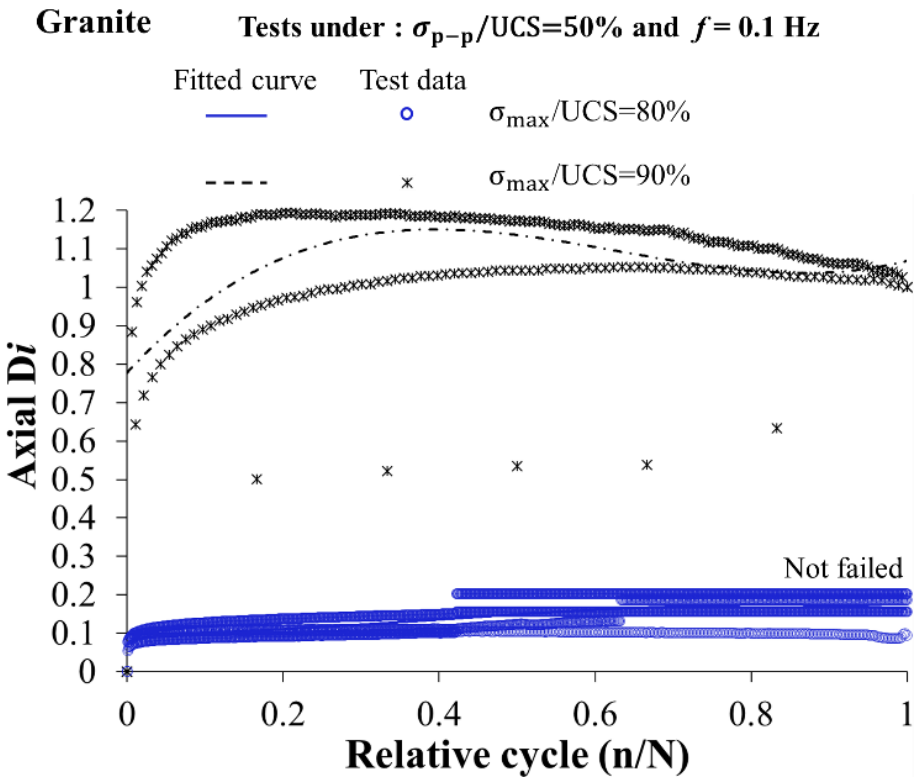

Figure 5.10 (continued on the next page).

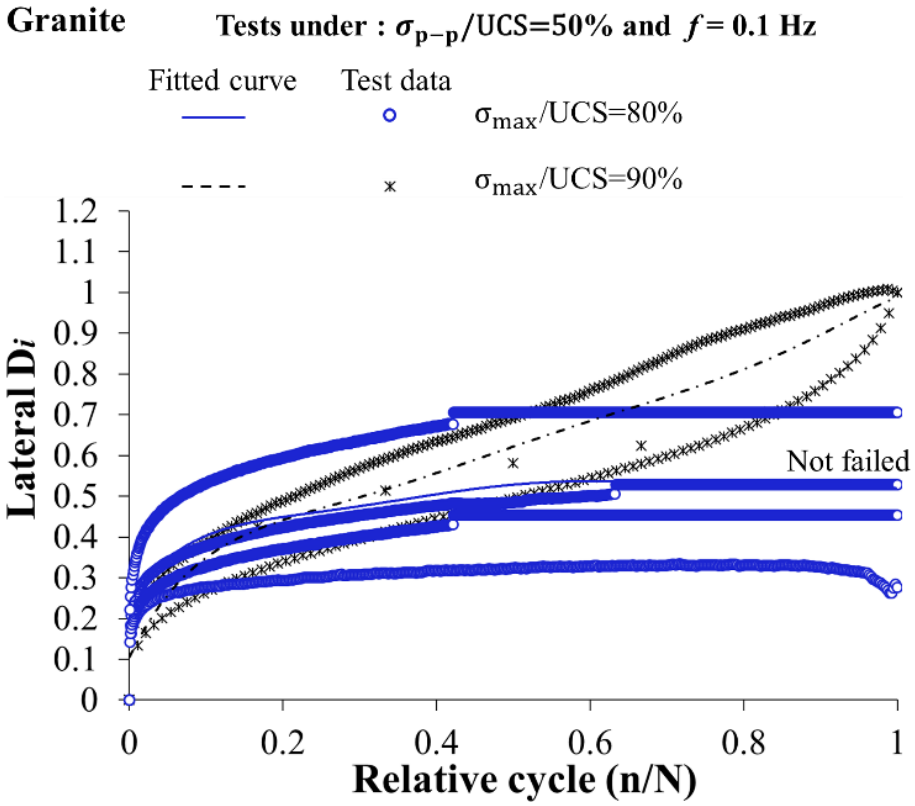

(a)

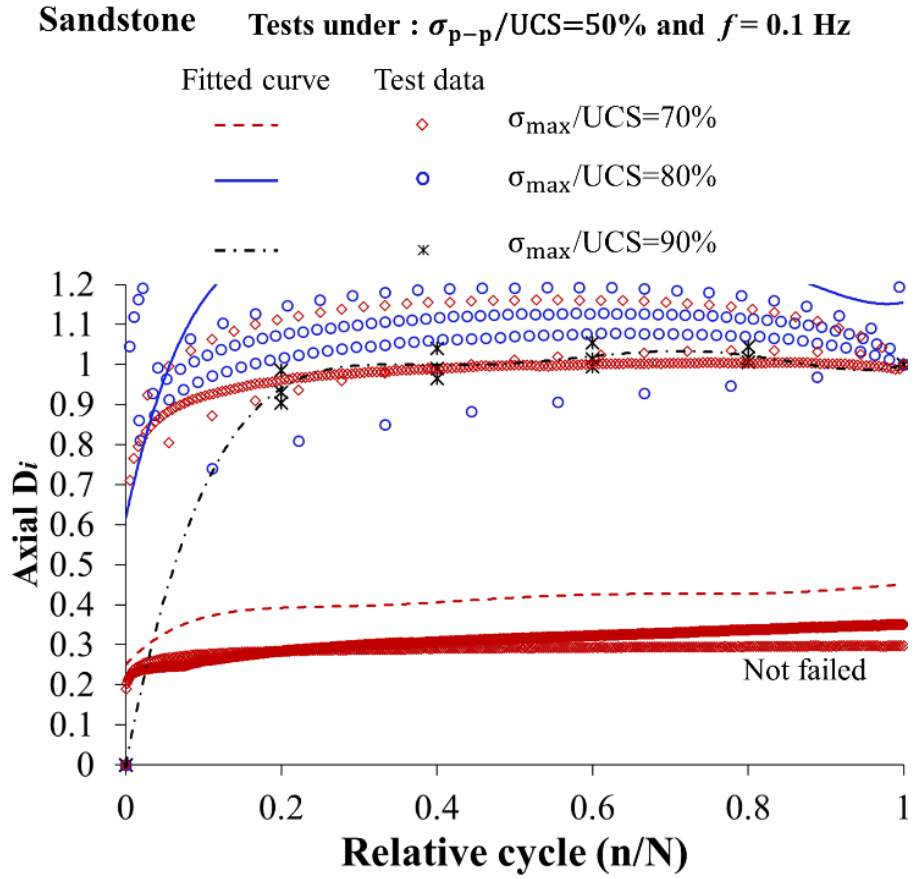

Figure 5.10 (continued on the next page).

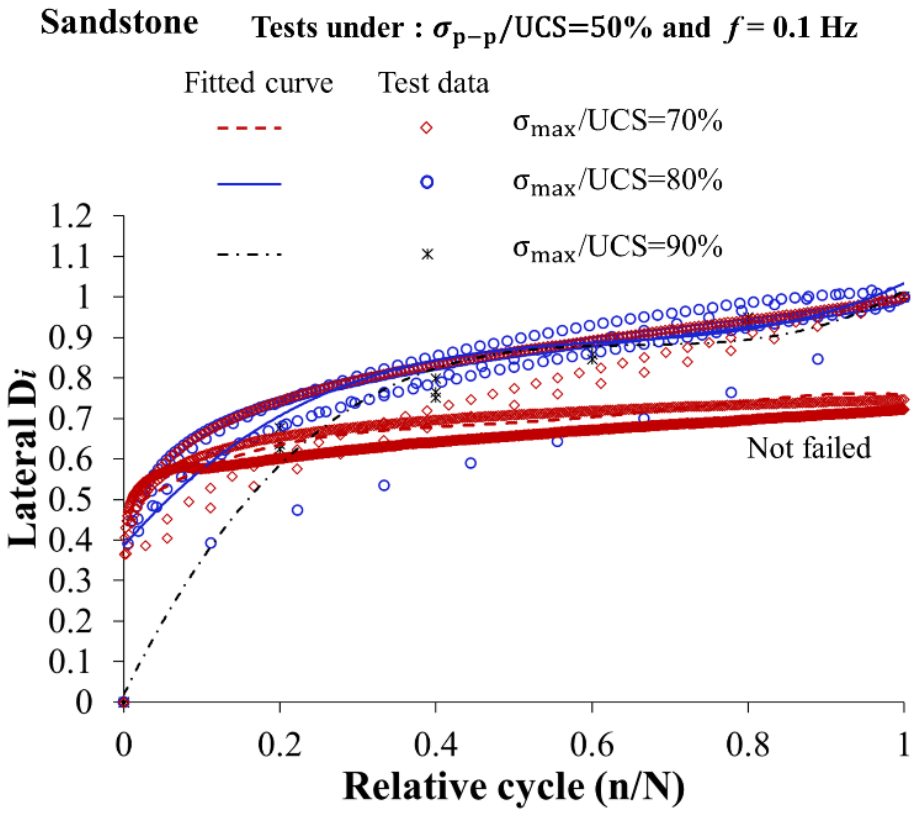

(b)

Figure 5.10 (continued from previous page). The variations in axial and lateral fatigue damage variables of (a) granite, and (b) sandstone samples under different maximum stress levels; data above 1.2 for axial damage of sandstone samples are not shown to be consistent with the scale of the vertical axis of other plots, the fitted curves show the overall trends. All data start at zero since the damage variable is taken as zero at the starting point of the cyclic stage, i.e. i=0 (refer to Eq. (5.2)).

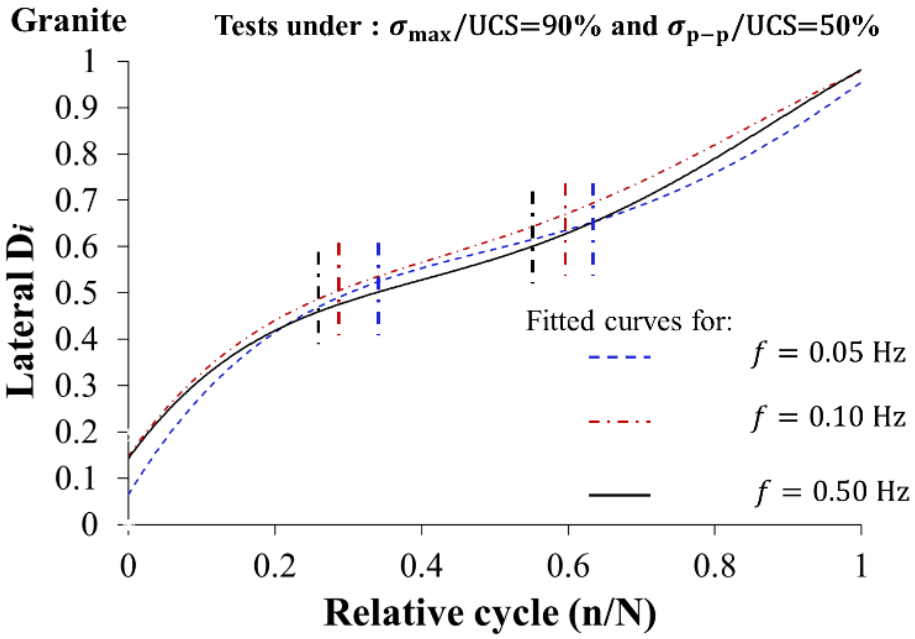

Figure 5.11. Lateral fatigue damage variable of granite under different frequencies; dotted vertical lines indicate the boundaries between the identified phases for each curve, fitted curves show the overall trends.

5.3.4. Failure modes of tested samples

Fracture mechanics originated from experiments carried out by Griffith on glass (Griffith & Taylor, 1921), in which he found that the strength of materials is lower than their theoretical strength and is affected by many factors including loading conditions, microstructure, crack size, and material properties (Gdoutos, 2005). Studying how materials fracture is very useful in figuring out how crack-like initial defects, which are assumed to exist in all solid materials, lead to their failure and affect the load-bearing capacity of structures. Observation of fracture patterns and failure mechanisms may help in analyzing stress distributions and the deformation response of rock in experiments; however, it could also be used as a basis for building theoretical damage models at different scales. The failure mode of rocks is mostly governed by their strength and microstructures. The failure mechanism of compact rocks such as granite, with very little porosity, is different to that of porous rocks such as sandstone with granular microstructures, merely due to the difference in their microstructures, even if all other conditions are kept identical (Basu et al., 2013). The failure mechanism of rock under cyclic loading conditions is more complex than under monotonic conditions and depends on many factors. It has been found that fracturing under cyclic conditions

is accompanied by more fragmentation and powdering of rock grains in failed surfaces (Burdine, 1963; Liu et al., 2017; Royer-Carfagni & Salvatore, 2000), however, the difference between failure mechanisms of rocks under monotonic and cyclic conditions is beyond this understanding and greatly depends on loading conditions (cf. chapter 4).

Hard rocks fail abruptly without prior warning at a particular stress level. This is a simple definition of brittle fracturing. Figure 5.12 illustrates typical and representative failure modes of tested granite and sandstone samples after uniaxial monotonic and cyclic compression tests. As can be seen, the failure mode of granite samples under monotonic loading is associated with two shear fractures inclined at an angle of less than 45° to the loading direction. These two shear planes developed in a cone shape from the loaded ends to the middle of the sample. Some tensile microcracks originate mostly across the shear planes in response to induced local tensile stresses, however, the shearing phenomenon is the main fracturing mode of granite under monotonic conditions. The failure modes of those samples that did not fail during the cyclic stage are similar to those under monotonic conditions (cf. sample 25 in Figure 5.12, for instance). The only difference is that the shearing planes of the samples that failed at the post-cyclic stage were accompanied by more tensile microcracks. This observation indicates that cyclic loading induces more tensile stress localizations around the grain boundaries or pre-existing defects of rock, leading to the nucleation and propagation of tensile cracks parallel to the axial loading. The failure modes of these samples under cyclic compression are certainly different and governed by shearing through a single plane throughout the entire length of the sample accompanied by more parallel axial cracks close to each other (making narrow straps of fractured rocks, herein called tensile bands). The effect of cyclic loading conditions on fracturing can be easily distinguished from the observed failure modes. Under the same maximum stress level and loading frequency, the aperture of tensile microcracks increases with an increase in loading amplitude (cf. granite samples 12 and 21 in Figure 5.12). This leads to greater dilation and lateral expansion of the samples at high loading amplitudes, which was discussed in Section 5.3.3. Similarly, at a constant loading amplitude and maximum stress level, the single shear plane is accompanied by relatively more tensile bands of greater length and aperture at lower loading frequencies than under high loading frequencies (cf. granite samples 21 and 13 in Figure 5.12). Slow loading–unloading at low loading frequencies facilitates the initiation, nucleation, opening, and localization of tensile cracks growing parallel or at a small angle to the loading direction. However,

the failure modes of granite samples under a higher loading frequency (here 0.5 Hz) are similar to those under monotonic conditions. Rapid loading–unloading at high loading frequencies does not allow for tensile stress localization at grain boundaries or existing flaws, which resulted in shearing along two inclined planes with occasional axial splitting.

As can be seen in Figure 5.12, the failure modes of sandstone samples after uniaxial cyclic and monotonic compression tests are very similar. All samples tested under monotonic conditions failed along a single shear plane, accompanied by tensile splitting which propagated parallel to the loading direction and crossed the shearing plane (cf. sandstone sample 5 in Figure 5.12). A very similar failure mode was observed for those samples that did not fail after hundreds of cycles then underwent the post-cyclic stage before failure (cf. sandstone sample 41 in Figure 5.12). One could speculate that the stress levels applied to these samples were not high enough to induce tensile stress localization, which is essential for grain detachment and intergranular cracking as the main mechanisms of failure in granular materials. Therefore, they failed in a very similar pattern to that under monotonic conditions. Under constant loading amplitude and frequency, as the maximum stress level increases, the shearing plane is accompanied by more axial splitting. Under the maximum stress level of 80% of UCS (cf. sandstone sample 23 in Figure 5.12), the extension and branching of axial cracks were obvious. However, as the maximum stress level increases to 90% of UCS (cf. sandstone sample 52 in Figure 5.12), the shear plane is accompanied by another premature shear plane, creating a shear band caused by either coalescence of large numbers of tiny tensile microcracks or grain compression itself. However, this shear band merged with the main shear plane in the middle of the sample and did not extend throughout the whole section of the sample. The loading amplitude also affects the failure mode of sandstone under cyclic conditions. The failure of samples tested under a higher loading amplitude occurred along a shear band rather than on a single shear plane (cf. sandstone samples 21 and 52 in Figure 5.12). Differences between failure modes of sandstone samples under different loading frequencies are very difficult to distinguish. Sandstone samples tested under a low loading frequency of 0.05 Hz failed along a single shear plane, whereas samples tested under higher loading frequencies of 0.1 and 0.5 Hz failed along a shear band.

Monotonic loading	Cyclic/fatigue loading σ_{max} / UCS (%) $\sigma_{p\text{-}p}$ / UCS (%) *f* (Hz)					
	90 30 0.1	70 50 0.1	80 50 0.1	90 50 0.1	90 50 0.05	90 50 0.5

Granite

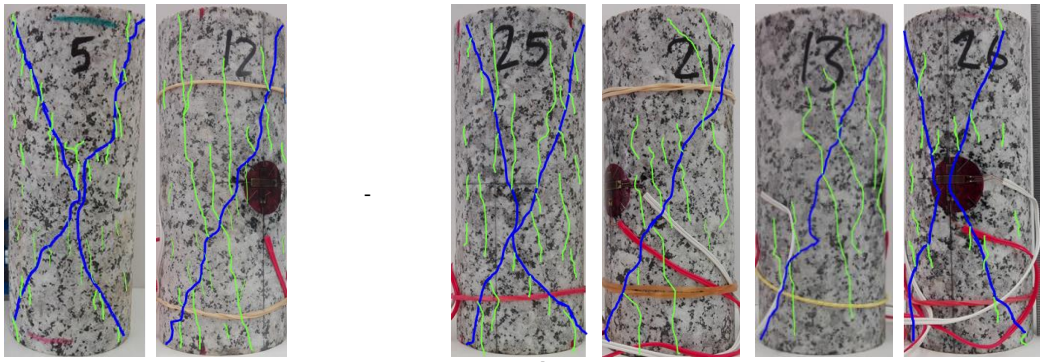

Post-cyclic

Sandstone

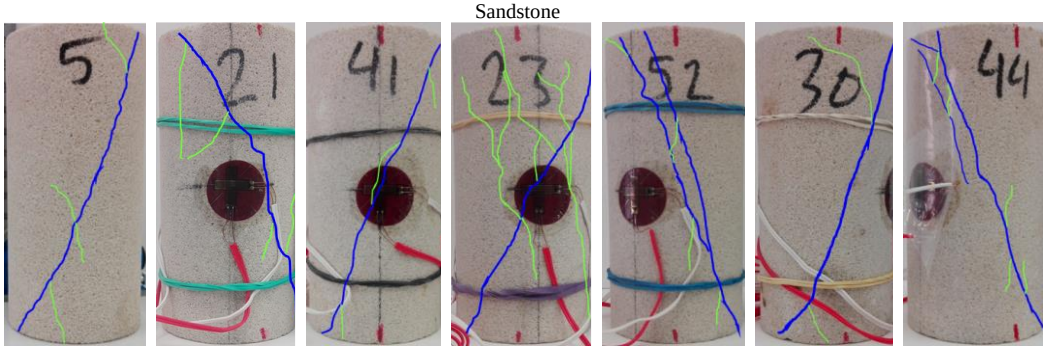

Post-cyclic

Figure 5.12. Failure modes of granite and sandstone samples under uniaxial monotonic and cyclic compression tests; blue line represents shear fracturing and green line is the tensile cracking.

Taken together, these observations indicate that tensile cracking is an indication of the fatigue process in both granular and crystalline rocks. However, this tendency is more evident in coarse-grained granite. This supports the previous understanding of rock fracture mechanism, that fine-grained rocks show less axial splitting than coarse-grained rocks(Wawersik & Fairhurst, 1970). Moreover, the failure mode may vary depending on the cyclic loading conditions. The effect of an increase in the stress amplitude of cycles becomes visible in more widening and extension of tensile cracks in crystalline rocks and more widening of the shear plane accompanied by another premature shear plane in granular rocks. As the maximum stress level of cyclic loading increases, more tensile cracks that usually form tensile bands propagate in both types

of rock, however, these tensile cracks finally form a shear band in sandstone and a single shear plane in granite before failure. An increase in extension and aperture of tensile cracks is the result of a reduction in loading frequency in crystalline granite. On the other hand, they fail in a similar mode of monotonic conditions when the loading frequency exceeds a specific value. The failure modes of sandstone, however, did not show a clear relation with loading frequency.

5.4. Conclusions

This study characterizes the difference in damage responses of two mineralogically and microstructurally different rock types under the fatigue process. Test data obtained from uniaxial cyclic compression tests conducted on samples of both rock types show a greater susceptibility of tested samples to low-frequency cyclic loading, especially granite as a crystalline/hard rock. Both rock types show low deformation before fatigue failure under a higher amplitude of cyclic loading. However, analyzing the proposed damage variable indicates greater damage evolution of both rock types under higher loading amplitudes. Test data also show that the lower the frequency of load variation, the bigger the fatigue deformation. By incorporating plenty of data from the literature with the results of these tests, this study showed that high-frequency loading is more favorable to fatigue mechanisms since the fatigue life of rock samples increased with loading frequency.

The damage evolution of both rocks shows three-phase or two-phase development. We also found that this damage evolution response is surprisingly different for axial and lateral damage and depends on the loading conditions. The duration of each phase of the damage evolution relative to the whole fatigue process depends on the cyclic loading conditions. We found that the damage evolution of rocks under higher loading amplitudes is mostly seen in the lateral expansion which evolves gradually throughout the fatigue process. Axial damage of both rocks under higher loading amplitudes and higher maximum stress levels occurs during initial cycles and the rock damage during later cycles is mainly induced by lateral expansion because of tensile stress localization. This finding suggests using lateral confinement to contain the lateral expansion and consequently fatigue damage. Stress corrosion (static fatigue) is also inferred as another mechanism interacting with fatigue damage of rocks in high-stress fatigue; however, it is still a gray area and needs to be verified by more experiments and observations.

The evaluation of failure modes of the samples revealed different failure mechanisms depending on the loading conditions. More tensile fracturing was found to be the main indication of the fatigue effect on failure modes of both crystalline and granular rocks. The effect of loading amplitude and frequency on the failure mode of granite is reflected in tensile cracking. The lower the loading frequency and the higher the loading amplitude, the bigger the opening and extension of tensile microcracks, which finally form tensile bands crossing the shear planes. For sandstone samples, as loading amplitude increases, tensile fractures create other shear bands merged with the main shearing plane, leading to the failure of the sample. We also found that granite samples tend to fail in a fracturing mode similar to that under monotonic conditions at higher loading frequencies. The effect of loading frequency on the failure mode of sandstone, on the other hand, is very complex and difficult to distinguish.

The results of this study improve our understanding of the damage evolution and non-linear deformation responses of hard rocks and soft rocks under cyclic loading, which is essential to monitor, predict and whenever possible control rock damage evolution both in the natural environment and in mining excavations.

Acknowledgements

The financial support provided by the Mining Research Institute of Western Australia (MRIWA) project M474 and Curtin University is gratefully acknowledged by the authors. We also would like to thank the department of Mining and Metallurgical Engineering and Petroleum Engineering of the Western Australian School of Mines (WASM), Curtin University, for the laboratory equipment. Finally, a very special thank you to Karin Hosking who provided professional copyediting assistance.

References

Anderson, O. L., & Grew, P. C. (1977). Stress corrosion theory of crack propagation with applications to geophysics. *Reviews of Geophysics*, *15*(1), 77–104. https://doi.org/10.1029/RG015i001p00077

ASTM. (2008a). ASTM D2845-08, Standard Test Method for Laboratory Determination of Pulse Velocities and Ultrasonic Elastic Constants of Rock (Withdrawn 2017). *ASTM International*. Retrieved from www.astm.org

ASTM. (2008b). *ASTM D4543-08, Standard Practices for Preparing Rock Core as Cylindrical Test Specimens and Verifying Conformance to Dimensional and Shape Tolerances*. Retrieved from https://doi.org/10.1520/D4543-08

ASTM. (2016a). *ASTM Standard Test Methods for Compressive Strength and Elastic Moduli of Intact Rock Core Specimens under Varying States of Stress and Temperatures*.

ASTM. (2016b). *ASTM Standard Test Methods for Laboratory Determination of Water (Moisture) Content of Soil and Rock by Mass*.

Attewell, P. B., & Farmer, I. W. (1973). Fatigue behaviour of rock. *International Journal of Rock Mechanics and Mining Sciences & Geomechanics Abstracts*, *10*(1), 1–9. https://doi.org/https://doi.org/10.1016/0148-9062(73)90055-7

Aydin, A. (2014). Upgraded ISRM Suggested Method for Determining Sound Velocity by Ultrasonic Pulse Transmission Technique. *Rock Mechanics and Rock Engineering*, *47*(1), 255–259. https://doi.org/10.1007/s00603-013-0454-z

Bagde, M. N., & Petroš, V. (2005a). Fatigue properties of intact sandstone samples subjected to dynamic uniaxial cyclical loading. *International Journal of Rock Mechanics and Mining Sciences*, *42*(2), 237–250. https://doi.org/https://doi.org/10.1016/j.ijrmms.2004.08.008

Bagde, M. N., & Petroš, V. (2005b). Waveform Effect on Fatigue Properties of Intact Sandstone in Uniaxial Cyclical Loading. *Rock Mechanics and Rock Engineering*, *38*(3), 169–196. https://doi.org/10.1007/s00603-005-0045-8

Basu, A., Mishra, D. A., & Roychowdhury, K. (2013). Rock failure modes under uniaxial compression, Brazilian, and point load tests. *Bulletin of Engineering Geology and the Environment*, *72*(3), 457–475.

https://doi.org/10.1007/s10064-013-0505-4

Bieniawski, Z. T., & Bernede, M. J. (1979). ISRM suggested methods for determining the uniaxial compressive strength and deformability of rock materials: Part 1. Suggested method for determining deformability of rock materials in uniaxial compression. *International Journal of Rock Mechanics and Mining Sciences & Geomechanics Abstracts*, *16*(2), 138–140. https://doi.org/https://doi.org/10.1016/0148-9062(79)91451-7

Burdine, N. T. (1963). Rock Failure Under Dynamic Loading Conditions. *Society of Petroleum Engineers Journal*, *3*(01), 1–8. https://doi.org/10.2118/481-PA

Cerfontaine, B., & Collin, F. (2018). Cyclic and Fatigue Behaviour of Rock Materials: Review, Interpretation and Research Perspectives. *Rock Mechanics and Rock Engineering*, *51*(2), 391–414. https://doi.org/10.1007/s00603-017-1337-5

Eberhardt, E. B. (1998). *Brittle rock fracture and progressive damage in uniaxial compression* (University of Saskatchewan). Retrieved from http://hdl.handle.net/10388/etd-10212004-001228

Eberhardt, E., Stead, D., & Stimpson, B. (1999). Quantifying progressive pre-peak brittle fracture damage in rock during uniaxial compression. *International Journal of Rock Mechanics and Mining Sciences*, *36*(3), 361–380. https://doi.org/https://doi.org/10.1016/S0148-9062(99)00019-4

Fan, J., Chen, J., Jiang, D., Ren, S., & Wu, J. (2016). Fatigue properties of rock salt subjected to interval cyclic pressure. *International Journal of Fatigue*, *90*, 109–115. https://doi.org/https://doi.org/10.1016/j.ijfatigue.2016.04.021

Gdoutos, E. E. (2005). *Fracture Mechanics An Introduction* (2nd ed.). https://doi.org/https://doi.org/10.1007/1-4020-3153-X

Geranmayeh Vaneghi, R., Ferdosi, B., Okoth, A. D., & Kuek, B. (2018). Strength degradation of sandstone and granodiorite under uniaxial cyclic loading. *Journal of Rock Mechanics and Geotechnical Engineering*, *10*(1). https://doi.org/10.1016/j.jrmge.2017.09.005

Griffith, A. A., & Taylor, G. I. (1921). VI. The phenomena of rupture and flow in solids. *Philosophical Transactions of the Royal Society of London. Series A, Containing Papers of a Mathematical or Physical Character*, *221*(582–593),

163–198. https://doi.org/10.1098/rsta.1921.0006

Haghgouei, H., Hashemolhosseini, H., Baghbanan, A., & Jamali, S. (2018). The Effect of Loading Frequency on Fatigue Life of Green onyx under Fully Reversed Loading. *Experimental Techniques*, *42*(1), 105–113. https://doi.org/10.1007/s40799-017-0226-x

Haimson, B. C. (1978). Effect of Cyclic Loading on Rock. In M. Silver & D. Tiedemann (Eds.), *Dynamic Geotechnical Testing* (pp. 228–245). https://doi.org/10.1520/STP35679S

He Ning;, M. L., & chen Caihui, Y. Z. (2016). Strength and Fatigue Properties of Sandstone under Dynamic Cyclic Loading. *Shock and Vibration*, *2016*, 8. https://doi.org/https://doi.org/10.1155/2016/9458582

Ishizuka, Y., Abe, T., & Kodama, J. (1990). Fatigue Behaviour of Granite Under Cyclic Loading. *ISRM International Symposium*, p. 8. Retrieved from https://doi.org/

ISRM. (1978). ISRM suggested method for petrographic description of rocks. *International Journal of Rock Mechanics and Mining Sciences & Geomechanics Abstracts*, *15*(2), 43–45. https://doi.org/https://doi.org/10.1016/0148-9062(78)91676-5

Kaiser, P. K., & Cai, M. (2012). Design of rock support system under rockburst condition. *Journal of Rock Mechanics and Geotechnical Engineering*, *4*(3), 215–227. https://doi.org/https://doi.org/10.3724/SP.J.1235.2012.00215

Li, X., Gong, F., Tao, M., Dong, L., Du, K., Ma, C., … Yin, T. (2017). Failure mechanism and coupled static-dynamic loading theory in deep hard rock mining: A review. *Journal of Rock Mechanics and Geotechnical Engineering*, *9*(4), 767–782. https://doi.org/https://doi.org/10.1016/j.jrmge.2017.04.004

Liu, E., & He, S. (2012). Effects of cyclic dynamic loading on the mechanical properties of intact rock samples under confining pressure conditions. *Engineering Geology*, *125*, 81–91. https://doi.org/http://dx.doi.org/10.1016/j.enggeo.2011.11.007

Liu, E., Huang, R., & He, S. (2012). Effects of Frequency on the Dynamic Properties of Intact Rock Samples Subjected to Cyclic Loading under Confining Pressure Conditions. *Rock Mechanics and Rock Engineering*, *45*(1),

89–102. https://doi.org/10.1007/s00603-011-0185-y

Liu, Y, Dai, F., Dong, L., Xu, N., & Feng, P. (2018). Experimental Investigation on the Fatigue Mechanical Properties of Intermittently Jointed Rock Models Under Cyclic Uniaxial Compression with Different Loading Parameters. *Rock Mechanics and Rock Engineering*, *51*(1), 47–68. https://doi.org/10.1007/s00603-017-1327-7

Liu, Yi, Dai, F., Xu, N., & Zhao, T. (2017). Cyclic flattened Brazilian disc tests for measuring the tensile fatigue properties of brittle rocks. *Review of Scientific Instruments*, *88*(8), 83902. https://doi.org/10.1063/1.4995656

Liu, Yi, Dai, F., Zhao, T., & Xu, N. (2017). Numerical Investigation of the Dynamic Properties of Intermittent Jointed Rock Models Subjected to Cyclic Uniaxial Compression. *Rock Mechanics and Rock Engineering*, *50*(1), 89–112. https://doi.org/10.1007/s00603-016-1085-y

Ma, L., Liu, X., Wang, M., Xu, H., Hua, R., Fan, P., … Yi, Q. (2013). Experimental investigation of the mechanical properties of rock salt under triaxial cyclic loading. *International Journal of Rock Mechanics and Mining Sciences*, *62*, 34–41. https://doi.org/http://dx.doi.org/10.1016/j.ijrmms.2013.04.003

Martin, C. D., & Chandler, N. A. (1994). The progressive fracture of Lac du Bonnet granite. *International Journal of Rock Mechanics and Mining Sciences & Geomechanics Abstracts*, *31*(6), 643–659. https://doi.org/https://doi.org/10.1016/0148-9062(94)90005-1

Momeni, A., Karakus, M., Khanlari, G. R., & Heidari, M. (2015). Effects of cyclic loading on the mechanical properties of a granite. *International Journal of Rock Mechanics and Mining Sciences*, *77*, 89–96. https://doi.org/http://dx.doi.org/10.1016/j.ijrmms.2015.03.029

Qiu, S.-L., Feng, X.-T., Xiao, J.-Q., & Zhang, C.-Q. (2014). An Experimental Study on the Pre-Peak Unloading Damage Evolution of Marble. *Rock Mechanics and Rock Engineering*, *47*(2), 401–419. https://doi.org/10.1007/s00603-013-0394-7

Ray, S. K., Sarkar, M., & Singh, T. N. (1999). Effect of cyclic loading and strain rate on the mechanical behaviour of sandstone. *International Journal of Rock Mechanics and Mining Sciences*, *36*(4), 543–549.

https://doi.org/http://dx.doi.org/10.1016/S0148-9062(99)00016-9

Roberts, L. A., Buchholz, S. A., Mellegard, K. D., & Düsterloh, U. (2015). Cyclic Loading Effects on the Creep and Dilation of Salt Rock. *Rock Mechanics and Rock Engineering*, *48*(6), 2581–2590. https://doi.org/10.1007/s00603-015-0845-4

Royer-Carfagni, G., & Salvatore, W. (2000). The characterization of marble by cyclic compression loading: experimental results. *Mechanics of Cohesive-Frictional Materials*, *5*(7), 535–563. https://doi.org/10.1002/1099-1484(200010)5:7<535::AID-CFM102>3.0.CO;2-D

Scholz, C. H., & Koczynski, T. A. (1979). Dilatancy anisotropy and the response of rock to large cyclic loads. *Journal of Geophysical Research: Solid Earth*, *84*(B10), 5525–5534. https://doi.org/10.1029/JB084iB10p05525

Taheri, A., Royle, A., Yang, Z., & Zhao, Y. (2016). Study on variations of peak strength of a sandstone during cyclic loading. *Geomechanics and Geophysics for Geo-Energy and Geo-Resources*, *2*(1), 1–10. https://doi.org/10.1007/s40948-015-0017-8

Voznesenskii, A. S., Krasilov, M. N., Kutkin, Y. O., Tavostin, M. N., & Osipov, Y. V. (2017). Features of interrelations between acoustic quality factor and strength of rock salt during fatigue cyclic loadings. *International Journal of Fatigue*, *97*, 70–78. https://doi.org/https://doi.org/10.1016/j.ijfatigue.2016.12.027

Wang, Z., Li, S., Qiao, L., & Zhao, J. (2013). Fatigue Behavior of Granite Subjected to Cyclic Loading Under Triaxial Compression Condition. *Rock Mechanics and Rock Engineering*, *46*(6), 1603–1615. https://doi.org/10.1007/s00603-013-0387-6

Wawersik, W. R., & Fairhurst, C. (1970). A study of brittle rock fracture in laboratory compression experiments. *International Journal of Rock Mechanics and Mining Sciences & Geomechanics Abstracts*, *7*(5), 561–575. https://doi.org/https://doi.org/10.1016/0148-9062(70)90007-0

Xiao, J.-Q., Ding, D.-X., Jiang, F.-L., & Xu, G. (2010). Fatigue damage variable and evolution of rock subjected to cyclic loading. *International Journal of Rock Mechanics and Mining Sciences*, *47*(3), 461–468.

https://doi.org/http://dx.doi.org/10.1016/j.ijrmms.2009.11.003

Xiao, J.-Q., Ding, D.-X., Xu, G., & Jiang, F.-L. (2009). Inverted S-shaped model for nonlinear fatigue damage of rock. *International Journal of Rock Mechanics and Mining Sciences*, *46*(3), 643–648. https://doi.org/http://dx.doi.org/10.1016/j.ijrmms.2008.11.002

Xiao, J.-Q., Feng, X.-T., Ding, D.-X., & Jiang, F.-L. (2011). Investigation and modeling on fatigue damage evolution of rock as a function of logarithmic cycle. *International Journal for Numerical and Analytical Methods in Geomechanics*, *35*(10), 1127–1140. https://doi.org/10.1002/nag.946

Xiao, J., Ding, D., Xu, G., & Jiang, F. (2008). Waveform effect on quasi-dynamic loading condition and the mechanical properties of brittle materials. *International Journal of Rock Mechanics and Mining Sciences*, *45*(4), 621–626. https://doi.org/http://dx.doi.org/10.1016/j.ijrmms.2007.07.025

Zhenyu, T., & Haihong, M. (1990). An experimental study and analysis of the behaviour of rock under cyclic loading. *International Journal of Rock Mechanics and Mining Sciences & Geomechanics Abstracts*, *27*(1), 51–56. https://doi.org/https://doi.org/10.1016/0148-9062(90)90008-P

Chapter 6

Conclusions and recommendations

6.1. Conclusions

The main objective of this research was to explore the damage responses of rocks to cyclic/fatigue loading. The research focused on experimental studies to investigate important subjects related to cyclic/fatigue loading under different loading scenarios. This final chapter describes the conclusions of this study and some promising avenues for further research in this area. The following conclusions were reached in the present investigation:

Valid rock testing

Rock samples need to be examined and inspected properly before conducting any experimental tests. Rock engineers or experimentalists must not rely merely on visual inspection and should implement other techniques for appropriate categorization of a set of real samples. It was found that P-wave velocity measurements are a quick and straightforward method for the initial assessment and categorization of rock samples in order to minimize the effects of variabilities from inherent characteristics of rock samples on the test results obtained. CT scanning was also found to be an appropriate tool for detection of visually invisible microcracks detected by neither ultrasonic measurements nor thin section analysis. It is suggested that CT scanning and ultrasonic measurements be conducted on rock samples before testing to a provide better pre-assessment of rock samples. These techniques could be included in the relevant standards in the field of rock mechanics.

This research discussed the sources of variabilities in test results of rocks. Among them, shape deviation as sample-based variability and equipment precision as machine-based variability were found to be hidden factors, often not seen but considerably affecting laboratory test results. Hence, accurate preparation of samples and regular testing/calibration of machines need to be considered.

Fatigue strength and fatigue life

Based on the test results obtained, this research strongly proved that the fatigue life and fatigue strength of both rock types decrease with the amplitude and maximum level of cyclically applied stress. On the other hand, fatigue life and fatigue strength showed an upward trend with loading frequency. The reduction in fatigue life with increases in the

maximum stress level of cyclic loading is more remarkable for the crystalline granite/granodiorite rock. It was also found that sandstone samples sustained a lower number of stress cycles than granodiorite samples under the same loading amplitude, indicating that sandstone is more prone to weakening at higher stress amplitudes than the granodiorite samples. The research also found that loading amplitude, generally, has stronger fatigue damage effects on rocks than maximum stress levels. Therefore, bigger mitigation and protection measures should be considered in the geotechnical design of structures under a lower maximum stress levels with higher loading amplitudes, than under high-stressed cyclic conditions but with low fluctuations in the loading-unloading amplitude.

The most significant finding to emerge from this investigation is that the fatigue strength threshold of a rock depends highly on its fabric and the heterogeneity of its microstructure. Crystalline or hard rocks showed lower fatigue strength thresholds than granular or soft rocks. The thresholds were found to be 0.65 to 0.80 of the monotonic peak strength for the granite/granodiorite and 0.75 to 0.90 for the sandstone. This indicates a greater susceptibility of hard or crystalline rocks to fatigue loading than soft or granular rocks. Generally, a fatigue strength threshold of 0.80 should be considered for both rock types when loading-unloading is predicted to be repeated for fewer than 100 cycles.

Loading history

It was demonstrated that the effect of the previous loading history on the damage progress can be investigated by specific loading paths. In this study, the stepped cyclic loading and multi-stage cyclic loading paths were shown to be capable of presenting the effect of loading history on progressive damage in the rock. It was shown that when a rock experienced any level of stress, despite it being less than the fatigue strength threshold at previous loading stages, shorter fatigue life, a lower fatigue strength and greater deformation are obtained. This was more noticeable in the sandstone than in the granodiorite, reflecting the ductility behavior of sandstone. However, the effect of loading history on rock damage greatly depends on the stress level and other loading conditions the rock has previously experienced.

Stress–strain behavior

The results of this study revealed that crystalline/brittle rocks showed a different pattern for stress–strain hysteresis loops compared to granular/ductile rocks. The stress–strain hysteresis loops for granite/granodiorite generally showed a dense–loose pattern (i.e. two-phase) of development throughout the cyclic/fatigue process, especially in the axial direction; whereas it was a three-phase pattern of loose–dense–loose for the sandstone. However, it should be noted that the trend of stress–strain hysteresis loops may vary in axial or lateral directions and depend on the loading conditions. Comparing stress–strain hysteresis loops in axial and lateral directions also showed greater extension and a higher overall slope of hysteresis loops of the stress–lateral strain than those of the stress–axial strain. This result was more obvious for the sandstone, which is an indication of the microstructural differences and the greater number of dilatant microcracks in the fine-grained granular sandstone, than in the large-grained crystalline granite/granodiorite. The greater rate of increase in the lateral strain than the axial strain for both rock types addresses the main damage mechanism of these rocks under cyclic/fatigue conditions. It was also observed that the higher the loading amplitude, the wider the stress–strain hysteresis loops, indicating an increased damage effect of high-amplitude cyclic loadings.

The maximum axial and lateral strains and the differential residual axial and lateral strains at the end of the cyclic stage showed an upward trend with the maximum stress level, independent of the rock type, whereas they showed a slightly decreasing trend with increases in the stress amplitude, especially for the sandstone. This response, which is more noticeable at higher maximum stress levels, is related to the length of time a sample spent loaded under high levels of stress. As the maximum stress level was fixed at a higher level close to or above the crack damage stress threshold, this effect of loading amplitude on the deformation response of rocks was more noticeable. The amplitude and maximum level of the applied stress also affect the accumulation of both axial and lateral deformations at different stages of the fatigue process. The results showed that higher maximum stress levels resulted in a relatively higher accumulation of deformations during the second phase of fatigue development. The effect of loading frequency on the fatigue deformation of crystalline/hard rocks was found to be uncertain and the obtained test data did not show a distinguishable relationship between them. On the other hand, the axial strain of the cyclic stage for the granular rock of sandstone showed a decreasing trend with increased loading frequency.

Fatigue damage response

The damage analysis in this study revealed that all cyclic conditions of maximum stress level, loading amplitude and frequency individually affect the damage evolution of sandstone, as a granular rock. However, fatigue damage in granite/granodiorite, as a brittle crystalline rock, is mostly governed by maximum stress levels rather than other conditions of stress cycles. It was also observed that fatigue damage in both crystalline and granular rocks increased with the maximum stress level and loading amplitude. The fatigue damage progress of both rocks under high-amplitude stress cycles was found to be controlled by gradually evolving lateral damage due to tensile stress localization. On the other hand, both axial and lateral damage contributed to the fatigue damage of rocks under low-amplitude stress cycles. The axial damage of both rocks under high amplitude and maximum levels of stress cycles occurred during initial cycles, which indicates that fatigue damage in the axial direction probably interacts with another mechanism, potentially stress corrosion.

It was also demonstrated that the microstructure of rock plays an important role in fatigue damage. Low-stress cyclic loading could damage individual grain boundaries of crystalline rocks, leading to fatigue damage evolution, whereas the applied stress should be high enough for individual grain detachment of granular rocks.

The evolution of both axial and lateral damage of sandstone and granite became slower at higher loading frequencies. Therefore, the current research highlights the greater damage effect of low-frequency cyclic loading on both rock types. This effect was more evident for crystalline/hard rocks, indicating that these rock types are more susceptible to low-frequency cyclic loading.

The ultrasonic P-wave velocity measurements and a damage variable defined based on the differential residual strains were shown to be capable of describing the damage evolution throughout the cyclic/fatigue process.

The study also complements the understanding of the hardening response that rocks may show under the cyclic fatigue process, depending on the loading history, cyclic loading conditions, and rock type. The reduction in the damage accumulation rate, i.e. a hardening effect, was observed for some rock samples, indicating that some rocks may not only become gradually weaker under this kind of loading, but also become gradually less likely to fail, which greatly depends on the applied stress level.

Failure mechanism

The main difference between the failure mechanisms of rocks under monotonic and cyclic conditions is local cracks, which are more dominant under cyclic loading conditions. The current research provides evidence that the propagation of tensile microcracks, as a result of tensile stress localization around grain boundaries or pre-existing cracks, is the main response of both rock types to cyclic/fatigue loading. This is the main reason for the strength degradation of rocks under cyclic conditions, compared to the monotonic strength. Crystalline rocks showed a greater tendency to tensile cracking under the fatigue/cyclic process, compared to granular rocks. This is empirical evidence confirming that the fatigue strength threshold of a crystalline rock is less than that of a granular rock.

The research also provides strong evidence that both rock types may fail in different modes depending on the cyclic loading conditions. The effect of loading frequency on the damage mechanisms of both rock types reflects itself in initiation, branching, elongation, or opening of more tensile microcracks, especially in crystalline rocks. On the other hand, the effect of loading frequency on the failure modes of sandstone is hard to distinguish. Low-frequency cyclic loading was found to have a more damaging effect on both rocks. However, the failure modes of both rock types tend to be similar to those under monotonic conditions, when the loading frequency exceeds a specific value which is not definite. The failure modes of both sandstone and granite/granodiorite are affected by amplitude and maximum level of cyclic stress. An increase in the extensions and apertures of tensile cracks, which finally led to the creation of tensile bands and in turn to a single shear plane in high-stressed conditions in granite/granodiorite as crystalline rock and a premature shear plane propagated along the main shear plane in sandstone as granular rock, was observed.

Rock heterogeneity

The clear variability in cyclic responses of crystalline and granular rocks is a direct consequence of heterogeneity at a microscale, i.e. fabric, grain size, porosity, and initial defects. The research provides evidence of how the fatigue life, fatigue strength, deformation, damage response, and failure modes of crystalline and granular rocks differ from each other under cyclic/fatigue processes due to heterogeneity in their microstructures. Heterogeneity in rock microstructure, as an inherent source of variability, created another dimension to all variabilities, contributing to change in the mechanical

response of a heterogeneous rock sample. The study shows how stress corrosion, as a hidden mechanism in rock damage under high-stressed cyclic conditions, is more effective when the rock is more heterogeneous in terms of mineralogy, grain size, and preferred orientation of mineralization.

6.2. Contribution to the current state of knowledge

The findings from this experimental study not only complement those of earlier investigations but also make several important contributions to the current state of knowledge in the field of rock fatigue:

- The research demonstrates that improving the quality of rock testing and better pre-assessment of rock samples and equipment before testing are of benefit in reducing the scatter of test results. This will lead to optimizing the number of laboratory tests required to determine the mechanical properties of intact rocks, with a satisfactory level of confidence.

- The study is the first comprehensive investigation comparing the strength and damage responses of two different crystalline and granular rocks under cyclic/fatigue processes. The findings obtained from the fatigue strength analysis provide insights for a better understanding of the time-dependent behavior of hard/crystalline/brittle and soft/granular/ductile rocks. The Cyclic Allowable Maximum Stress Levels (CAMSL) which were determined for both rock types would be of benefit for design purposes, not only in experimental studies but also in practical applications. Prior to this study it was difficult to make judgments about how the strength and deformation responses of granular and crystalline rocks would differ when subjected to cyclic/fatigue loading.

- The insights gained from the study of failure mechanisms of both crystalline and granular rock under cyclic and monotonic conditions may be of benefit for further development of models describing the process of nonlinear rock deformation. The findings provide a new understanding of all mechanisms contributing to the evolving damage of these rock types under loading-unloading processes.

- The study provides the first assessment of fatigue damage evolution using the result of ultrasonic measurements carried out on rock samples. This investigation also

appears to be the first study providing evidence of how ultrasonic measurements are of benefit in rock categorization.

- The results of this experimental study contribute to existing knowledge of rock fatigue by providing more evidence about the effects of different cyclic loading conditions such as stress amplitude, maximum stress level, and frequency on the deformation and strength responses of rocks. The effect of each individual loading condition was analyzed separately and compared to the others considering the microstructural differences of tested rock types.

6.3. Recommendations for future research

The research conducted provides the following insights for future research:

- The current research highlighted that the relevant standards for rock sample preparation and testing procedures should be revised to consider the effects of sample shape deviation, especially end flatness, loading machine performance, and the design and setup considerations of spherical seats. Detailed suggestions for further research avenues in this area are provided in Section 2.7.

- Further experiments, using a broader range of rocks with different fabrics, grain sizes, and microstructures, could shed more light on the fatigue responses of rocks and variation due to rock inhomogeneity.

- In the current study, it was not possible to implement continuous ultrasonic measurements along with the loading cycles. A continuous measurement of P-wave velocity, cycle after cycle, could provide more definitive evidence about the damage evolution of rocks under cyclic/fatigue processes.

- Continuous Acoustic Emission (AE) monitoring would also be beneficial in detection of crack development, types of cracks, and stress thresholds at which the cracks initiate and propagate in an unstable manner during loading. The current study was unable to implement AE, however this technique, which has already been used in several research, could shed more light on the fatigue damage mechanisms of hard/crystalline or soft / granular rocks.

- Further experimental investigations with primary focus on comparing the effects of loading amplitude and maximum stress levels on the strength degradation of rocks

might be of benefit to validate the novel research in which loading amplitude was shown to have a stronger damage effect on rocks than maximum stress levels during the cyclic stage.

- The fatigue mechanism under high-stressed cyclic conditions and high loading frequencies is complex. Studying the interaction of the main fatigue damage mechanism with stress corrosion to find out which of these two mechanisms cause rock failure would be another interesting research area. All experiments were conducted under loading frequencies of less than 1 Hz. Further experiments under higher loading frequencies would be of benefit to deeply explore the effect of high-frequency cyclic loading on rock damage and fatigue parameters and to distinguish it from creep behavior, which is a likely mechanism at higher loading frequencies.

- The major limitation of the current study is the lack of numerical simulation to validate the failure modes and other results obtained through experimental investigations. Numerical modeling using discrete element methods would be highly valuable to better understand and validate the differences in fatigue/cyclic damage responses of these rocks due to their inhomogeneities and microstructural differences.

- Development of a new constitutive law to reproduce the cyclic behavior of these rocks, especially the accumulation of residual/permanent deformations with the number of cycles, is another direction for further research. Such physical models could reproduce different features of crystalline and granular rocks under cyclic loading, such as differences in stress–strain development depending on cyclic load, strength degradation, and accumulation of differential residual strain obtained through experiments.

Appendix A

Summary of researches related to the rock fatigue behaviour[1]

[1] Modified after (Cerfontaine & Collin, 2018)

APPENIDIX A

Reference	**Material**	**Frequency, rate**	**Type**	**N $_{max}$**	**Fatigue Limit**	**Loading form**
Grover et al., (1950)	Limestone	–	UCT	–	0.65	Constant
Burdine (1963)	Sandstone	15–50 Hz	UCT, TCT	1×10^6	0.74	Constant
Haimson and Kim (1971)	Marble	2–4 Hz	UCT	1×10^6	0.75	Constant
Attewell and Farme (1973)	Limestone	0.3–20 Hz	UCT	4.1×10^4	–	Constant
Brown and Hudson (1973)	Gypsum plaster	0.5–2 Hz	UCT	1.4×10^4	–	Constant
Scholz and Kranz (1974)	Granite	1×10^{-5} /s	UCT	2×10^1	–	Constant
Haimson (1978)	Tennessee marble, Indiana limestone, Berea sandstone. Westerly granite	1 Hz	UCT, TCT, UTT	2×10^6	0.6-0.8	Constant
Scholz and Koczynski (1979)	Westerly granite, Diabase	1 MPa/s	TCT	3.2×10^3	–	Constant
Rajaram (Rajaram, 1981)	Westerly granite	1 Hz	UCT, TCT	1×10^6	0.73	Constant
Singh (1989)	Sandstone	1 Hz	UCT	1×10^4	0.87	Constant
Ishizuka et al., (1990)	Inada Granite	0.00025-1.0 Hz	UCT, TCT	4×10^4	0.76-0.85	Constant
Tien et al., (1990)	Sandstone	0.1–1 Hz	TCT	1×10^3	–	Constant
Zhenyu and Haihong (1990)	Sandstone, marble	0.0019–0.005 Hz	UCT	3×10^2	0.85-0.97	Constant, Ramp
Li et al., (1992)	Sandstone	0.5 Hz	Brz.	3×10^4	–	Constant
Rao and Ramana (1992)	Granite	–	UCT	2.4×10^1	–	Damage
Martin and Chandler (1994)	Granite	0.75 MPa/s	UCT, TCT	–	–	Damage
Celestino et al., (1995)	Granite	7 kN/min	Brz.	2.3×10^1	–	Constant
Eberhardt et al., (1999)	Granite	0.25 MPa/s	UCT	–	–	Damage
Yamashita et al., (1999)	Tuff, sandstone, marble, granite	1 Hz	UCT	1×10^6	0.55–0.80	Constant
Royer-Carfagni and Salvatore (2000)	Marble	1–2 MPa/s	UCT	1.8×10^2	–	Constant
Ray et al., (1999)	Sandstone	2.5×10^1/s	UCT	1×10^4	0.65	Constant
Cattaneo and Labuz (2001)	Marble	–	FLx.	–	–	Damage
Lavrov (2001)	Limestone	–	UCT, Brz.	–	–	Damage
Li et al., (2001)	gypsum	0.2, 2, 21 Hz	UCT	–	–	Damage
Gatelier et al., (2002)	Sandstone	0.025–0.2 Hz	UCT, TCT	–	–	Damage
Li et al., (2003)	Sandstone	2–20 Hz	UCT	–	–	Damage
Akesson et al., (2004)	Granite	4 Hz	UCT	3.5×10^4	0.6	Constant
Ko (2005)	Gypsum	0.5 Hz	UCT	4×10^3	–	Constant
Bagde and Petroš (2005)	Sandstone	0.1–1–10 Hz	UCT	–	–	Ramp
Zhang et al., (2008)	Reconstituted	0.02, 2, 1 Hz	UCT	–	–	Constant
Heap and Faulkner (2008)	Westerly granite	2.5 MPa/min	UCT	–	–	Damage
Mitchell and Faulkner (2008)	Granite, granodiorite	3.3×10^{-4} Hz	TCT	1×10^1	–	Constant
Jiang et al., (2009)	Sandstone	100.9 kN/min	UCT	–	–	Constant
Xiao et al., (2009)	Granite	0.2 Hz	UCT	–	–	Constant

Reference	**Material**	**Frequency, rate**	**Type**	**N max**	**Fatigue Limit**	**Loading form**
Heap et al., (2009)	Basalt	7.0×10^{-6} /s	UCT	–	–	Damage
Heap et al., (2010)	Basalt, sandstone, granite	7.0×10^{-6} /s	TCT	–	–	Damage
Xiao et al., (2010)	Granite	0.2 Hz	UCT	3×10^3	–	Constant
Fuenkajorn and Phueakphum (2010)	Salt	0.001–0.03 Hz	TCT	1×10^3	–	Constant
Chen et al., (2011)	Westerly Granite	0.1 Hz	UCT	43×10^3	–	Constant
Xiao et al., (2011)	Granite	0.2 Hz	UCT	1×10^3	–	Constant
Liu et al., (2011)	Sandstone	1 Hz, 60 kN/min	TCT	6.2×10^2	–	Constant
Erarslan and Williams (2012b)	Brisbane Tuff	1 Hz	Brz.	1×10^5	0.7	Constant, Ramp
Erarslan and Williams (2012a)	Brisbane Tuff	1 Hz	Brz.	2.9×10^3	–	Ramp
Liu et al., (2012)	Sandstone	0.1, 1.0, 3 Hz, 60 kN/min	TCT	14.3×10^2	–	Constant
Liu and He (2012)	Sandstone	1 Hz	TCT	6.2×10^2	–	Constant
Guo et al., (2012)	Salt	1 Hz	UCT	1.5×10^4	0.75	Constant
David et al., (2012)	Sandstone, granite	2×10^{-6} /s	UCT	–	–	Damage
Wang et al., (2013)	Granite	50 N/s	TCT	–	–	Damage
Ma et al., (2013)	Salt	0.025 –0.1 Hz	TCT	8.5×10^2	–	Constant
Song et al., (2013)	Salt	0.36–10 kN/s	UCT	6×10^2	0.75	Constant
Trippetta et al., (2013)	Evaporites	7×10^{-6} /s	UCT	–	–	Damage
Faoro et al., (2013)	Granite, basalt	5×10^{-6} m/s	TCT	–	–	Damage
Kendrick et al., (2013)	Volcanic	1×10^{-5} /s	UCT	–	–	Damage
Bastian et al., (2014)	Sandstone	1–6 mm/min	UCT, TCT	1×10^2	–	Constant
Erarslan et al., (2014)	Brisbane Tuff	–	Brz.	8×10^5	0.68	Constant, Ramp
Nejati and Ghazvinian (2014)	Marble,sandstone, limestone	1 Hz	Brz.	3×10^3	0.6 / 0.7 / 0.8	Constant
Le et al., (2014)	Sandstone	1 Hz	FLx.	5.5×10^3	–	Constant
Liu et al., (2014)	Salt	1 Hz	UCT	–	–	Damage
Pola et al., (2014)	Lava, pyroclastic, tuff, ignimbrite	4 mm/h	UCT	–	–	Damage
Ni (2014)	Granite	0.01–1 Hz	UCT	–	–	Constant
Qiu et al., (2014)	Marble	0.25 MPa/s	TCT			Damage
Shi et al., (2014)	Mudstone	1.0 - 10 Hz	TCT	5×10^5	–	Constant
Momeni et al., (2015)	Granite	0.1–5 Hz	UCT	2.4×10^3	–	Constant
Voznesenskii et al., (2015)	Limestone, gabbro, marble	–	UCT	2×10^2	–	Constant
Yang et al., (2015)	Sandstone	0.08 mm/min	TCT	–	–	Damage
Schaefer et al., (2015)	Basalt	10^{-5} /s	UCT	–	–	Damage
Roberts et al., (2015)	Salt	–	TCT	–	–	Constant

APPENIDIX A

Reference	**Material**	**Frequency, rate**	**Type**	**N $_{max}$**	**Fatigue Limit**	**Loading form**
Voznesenskii et al., (2016)	Gypsum	–	UCT	1×10^2	–	Constant
Taheri et al., (2016)	Sandstone	5 mm/min	TCT	2.2×10^3	0.94	Constant, Damage
Taheri et al., (2016)	Sandstone	2 mm/min	TCT	2.68×10^2	–	Constant
Ghamgosar and Erarslan (2016)	Tuff	1–5 Hz	Brz.	–	–	Ramp, Damage
Erarslan (2016)	Tuff	–	Brz.	–	–	Constant, Ramp
Wang et al., (2016)	Salt	1 Hz	Brz.	5.2×10^3	–	Damage
Fan et al., (2016)	Salt	2 kN/s	UCT	9×10^1	–	Interval
Jiang et al., (2016)	Salt	2 kN/s	UCT	6×10^1	–	Interval
Song et al., (2016)	Sandstone	0.12 mm/min	UCT	–	–	Damage
Meng et al., (2016)	Sandstone	0.5–4 kN/s	UCT	–	–	Damage
Karakus et al., (2016)	Sandstone	–	UCT	1×10^4	–	Constant
Liu et al., (2016)	Mudstone, siltstone	5 mm/min	UCT	–	–	Damage
Hu et al., (2016)	Sandstone	0.1 Hz	UCT	6×10^1	–	Constant
Fan et al., (2017)	Salt	2 kN/s	UCT	9×10^1	–	Interval
Jobli et al., (2017)	Granite	1 Hz	UCT	1×10^2	–	Constant
Yang et al., (2017)	Marble	0.02 mm/s	TCT	–	–	Damage
Wang et al., (2017)	Sandstone	–	TCT	–	–	Damage
Ghamgosar et al., (2017)	Tuff/monzonite	1, 5 Hz	Brz.	–	–	Ramp
Voznesenskii et al., (2017)	Salt	10^{-4} –2 mm/min	UCT	1×10^2	–	Constant
Liu et al., (2017)	Sandstone	0.1, 0.5, 1.0 Hz	Brz.	8.5×10^1	–	Constant
Liu et al., (2017)	Artificial	1 Hz	TCT	4.65×10^4	–	Constant
Liu et al., (2017)	Artificial	0.01–20 Hz	UCT	1.2×10^3	–	Constant
Liu et al., (2017)	Artificial	0.1, 0.2, 1.0, 3.0 Hz	UCT	4.4×10^1		Constant
Jamali Zavareh et al., (2017)	Gabbro, onyx, limestone	5 Hz	B.	$> 1 \times 10^6$	0.4–0.6	Constant
Munoz and Taheri (2017)	Sandstone	0.18×10^{-4} /s	UCT	–	–	Damage
Ma et al., (2017)	Salt	0.025 –0.1 Hz	TCT	–	–	Constant
Rukhaiyar and Samadhiya (2018)	Limestone	0.05 - 0.4 kN/s	UCT	2.0×10^1	0.9	Damage, Constant
Su et al., (2018)	Granodiorite	0.2 - 3.0 Hz	True TCT	–	–	Constant
Sun et al., (2017)	Sandstone	–	TCT	–	–	Constant
Liu et al., (2018)	Artificial	1 Hz	UCT	2.4×10^3	–	Constant
Liu et al., (2018)	Sandstone	0.5 - 1.5 kN/s	D.S.	5.0×10^2	–	Constant
Liu et al., (2018)	Artificial	1.0–10 Hz	UCT	2.5×10^3	–	Constant

Reference	**Material**	**Frequency, rate**	**Type**	**N max**	**Fatigue Limit**	**Loading form**
Liu et al., (2018)	Artificial	–	UCT	–	–	Variable
Meng et al., (2018)	Sandstone	0.5–4 kN/s	UCT	–	–	Damage
Ning et al., (2018)	Coal	0.002 mm/s	TCT	–	–	Damage
Zhou et al., (2019)	Beishan granite	0.05 MPa/s	TCT	1.4×10^1	–	Damage
Peng et al., (2019)	Sandstone	0.1 Hz, 0.02%/min	TCT	2.4×10^2	–	Constant
Peng et al., (2019)	Sandstone	0.1, 0.3, 0.5 Hz, 0.02%/min	TCT	2.4×10^2	–	Constant

Note: UCT, TCT, UTT, Flx., Brz., B., and D.S. stand for Uniaxial compression test, Triaxial compression test, Uniaxial tension test, Flexion, Brazilian, Bending, and Direct shear, respectively.

Interval mode is when a time interval is imposed between cycles at a constant amplitude and without changing the load level.

References

Akesson, U., Hansson, J., & Stigh, J. (2004). Characterisation of microcracks in the Bohus granite, western Sweden, caused by uniaxial cyclic loading. *Engineering Geology*, *72*(1), 131–142. https://doi.org/https://doi.org/10.1016/j.enggeo.2003.07.001

Attewell, P. B., & Farmer, I. W. (1973). Fatigue behaviour of rock. *International Journal of Rock Mechanics and Mining Sciences & Geomechanics Abstracts*, *10*(1), 1–9. https://doi.org/https://doi.org/10.1016/0148-9062(73)90055-7

Bagde, M. N., & Petroš, V. (2005). Fatigue properties of intact sandstone samples subjected to dynamic uniaxial cyclical loading. *International Journal of Rock Mechanics and Mining Sciences*, *42*(2), 237–250. https://doi.org/https://doi.org/10.1016/j.ijrmms.2004.08.008

Bastian, T. J., Connelly, B. J., Olivares, C. S., Yfantidis, N., & Taheri, A. (2014). Progressive damage of Hawkesbury sandstone subjected to systematic cyclic loading. *Mining Education Australia – Research Projects Review*.

Brown, E. T., & Hudson, J. A. (1973). Fatigue failure characteristics of some models of jointed rock. *Earthquake Engineering & Structural Dynamics*, *2*(4), 379–386. https://doi.org/10.1002/eqe.4290020407

Burdine, N. T. (1963). Rock Failure Under Dynamic Loading Conditions. *Society of Petroleum Engineers Journal*, *3*(01), 1–8. https://doi.org/10.2118/481-PA

Celestino, T. B., Bortolucci, A. A., & Nobrega, C. A. (1995). *Determination of rock fracture toughness under creep and fatigue*. American Rock Mechanics Association.

Cerfontaine, B., & Collin, F. (2018). Cyclic and Fatigue Behaviour of Rock Materials: Review, Interpretation and Research Perspectives. *Rock Mechanics and Rock Engineering*, *51*(2), 391–414. https://doi.org/10.1007/s00603-017-1337-5

Chen, Y., Watanabe, K., Kusuda, H., Kusaka, E., & Mabuchi, M. (2011). Crack growth in Westerly granite during a cyclic loading test. *Engineering Geology*, *117*(3), 189–197. https://doi.org/https://doi.org/10.1016/j.enggeo.2010.10.017

David, E. C., Brantut, N., Schubnel, A., & Zimmerman, R. W. (2012). Sliding crack model for nonlinearity and hysteresis in the uniaxial stress–strain curve of rock. *International Journal of Rock Mechanics and Mining Sciences*, *52*, 9–17. https://doi.org/https://doi.org/10.1016/j.ijrmms.2012.02.001

Eberhardt, E., Stead, D., & Stimpson, B. (1999). Quantifying progressive pre-peak brittle fracture damage in rock during uniaxial compression. *International Journal of Rock Mechanics and Mining Sciences*, *36*(3), 361–380. https://doi.org/https://doi.org/10.1016/S0148-9062(99)00019-4

Erarslan, N, Alehossein, H., & Williams, D. J. (2014). Tensile Fracture Strength of Brisbane Tuff by Static and Cyclic Loading Tests. *Rock Mechanics and Rock Engineering*, *47*(4), 1135–1151. https://doi.org/10.1007/s00603-013-0469-5

Erarslan, N, & Williams, D. J. (2012a). Investigating the Effect of Cyclic Loading on the Indirect Tensile Strength of Rocks. *Rock Mechanics and Rock Engineering*, *45*(3), 327–340. https://doi.org/10.1007/s00603-011-0209-7

Erarslan, N, & Williams, D. J. (2012b). Mechanism of rock fatigue damage in terms of fracturing modes. *International Journal of Fatigue*, *43*, 76–89. https://doi.org/https://doi.org/10.1016/j.ijfatigue.2012.02.008

Erarslan, Nazife. (2016). Microstructural investigation of subcritical crack propagation and Fracture Process Zone (FPZ) by the reduction of rock fracture toughness under cyclic loading. *Engineering Geology*, *208*, 181–190. https://doi.org/https://doi.org/10.1016/j.enggeo.2016.04.035

Fan, J., Chen, J., Jiang, D., Chemenda, A., Chen, J., & Ambre, J. (2017). Discontinuous cyclic loading tests of salt with acoustic emission monitoring. *International Journal of Fatigue*, *94*, 140–144. https://doi.org/https://doi.org/10.1016/j.ijfatigue.2016.09.016

Fan, J., Chen, J., Jiang, D., Ren, S., & Wu, J. (2016). Fatigue properties of rock salt subjected to interval cyclic pressure. *International Journal of Fatigue*, *90*, 109–115. https://doi.org/https://doi.org/10.1016/j.ijfatigue.2016.04.021

Faoro, I., Vinciguerra, S., Marone, C., Elsworth, D., & Schubnel, A. (2013). Linking permeability to crack density evolution in thermally stressed rocks under cyclic loading. *Geophysical Research Letters*, *40*(11), 2590–2595. https://doi.org/10.1002/grl.50436

Fuenkajorn, K., & Phueakphum, D. (2010). Effects of cyclic loading on mechanical properties of Maha Sarakham salt. *Engineering Geology*, *112*(1), 43–52. https://doi.org/https://doi.org/10.1016/j.enggeo.2010.01.002

Gatelier, N., Pellet, F., & Loret, B. (2002). Mechanical damage of an anisotropic porous rock in cyclic triaxial tests. *International Journal of Rock Mechanics and Mining Sciences*, *39*(3), 335–354. https://doi.org/https://doi.org/10.1016/S1365-

1609(02)00029-1

Ghamgosar, M., & Erarslan, N. (2016). Experimental and Numerical Studies on Development of Fracture Process Zone (FPZ) in Rocks under Cyclic and Static Loadings. *Rock Mechanics and Rock Engineering*, *49*(3), 893–908. https://doi.org/10.1007/s00603-015-0793-z

Ghamgosar, M., Erarslan, N., & Williams, D. J. (2017). Experimental Investigation of Fracture Process Zone in Rocks Damaged Under Cyclic Loadings. *Experimental Mechanics*, *57*(1), 97–113. https://doi.org/10.1007/s11340-016-0216-4

Grover, H., Dehlinger, P., & McClure, G. (1950). *Investigation of fatigue characteristics of rocks*.

Guo, Y., Yang, C., & Mao, H. (2012). Mechanical properties of Jintan mine rock salt under complex stress paths. *International Journal of Rock Mechanics and Mining Sciences*, *56*, 54–61. https://doi.org/https://doi.org/10.1016/j.ijrmms.2012.07.025

Haimson, B. C. (1978). Effect of Cyclic Loading on Rock. In M. Silver & D. Tiedemann (Eds.), *Dynamic Geotechnical Testing* (pp. 228–245). https://doi.org/10.1520/STP35679S

Haimson, B., & Kim, C. (1971). Mechanical behaviour of rock under cyclic fatigue. *Proceedings of the 13th Symposium on Rock Mechanics*, 845–863. New York: ASCE.

Heap, M. J., & Faulkner, D. R. (2008). Quantifying the evolution of static elastic properties as crystalline rock approaches failure. *International Journal of Rock Mechanics and Mining Sciences*, *45*(4), 564–573. https://doi.org/https://doi.org/10.1016/j.ijrmms.2007.07.018

Heap, M. J., Faulkner, D. R., Meredith, P. G., & Vinciguerra, S. (2010). Elastic moduli evolution and accompanying stress changes with increasing crack damage: implications for stress changes around fault zones and volcanoes during deformation. *Geophysical Journal International*, *183*(1), 225–236. Retrieved from http://dx.doi.org/10.1111/j.1365-246X.2010.04726.x

Heap, M. J., Vinciguerra, S., & Meredith, P. G. (2009). The evolution of elastic moduli with increasing crack damage during cyclic stressing of a basalt from Mt. Etna volcano. *Tectonophysics*, *471*(1), 153–160. https://doi.org/https://doi.org/10.1016/j.tecto.2008.10.004

Hu, Y., Deng, H., Wang, W., Wang, Z., Zhang, X., & Assefa, E. (2016). Influence of

Moisture Content and Stress Cyclic Loading Amplitude on the Dynamic Characteristics of Sandstone. *Electronic Journal of Geotechnical Engineering*, *21*(16), 5167–5182.

Ishizuka, Y., Abe, T., & Kodama, J. (1990). Fatigue Behaviour of Granite Under Cyclic Loading. *ISRM International Symposium*, p. 8. Retrieved from https://doi.org/

Jamali, S., Hashemolhosseini, H., Baghbanan, A., Khoshkam, M., & Haghgouei, H. (2017). Evaluating Fatigue in Crystalline Intact Rocks under Completely Reversed Loading. *Geotechnical Testing Journal*, *40*(5), 789–797. https://doi.org/10.1520/GTJ20160250

Jiang, D., Fan, J., Chen, J., Li, L., & Cui, Y. (2016). A mechanism of fatigue in salt under discontinuous cycle loading. *International Journal of Rock Mechanics and Mining Sciences*, *86*, 255–260. https://doi.org/http://dx.doi.org/10.1016/j.ijrmms.2016.05.004

Jiang, X., Shu-chun, L., Yun-qi, T., Xiao-jun, T., & Xin, W. (2009). Acoustic emission characteristic during rock fatigue damage and failure. *Procedia Earth and Planetary Science*, *1*(1), 556–559. https://doi.org/https://doi.org/10.1016/j.proeps.2009.09.088

Jobli, A. F., Noor, M. J. M., Tawie, R., Hampden, A. Z., & Julai, N. N. (2017). Uniaxial compressive strength of Malaysian weathered granite due to cyclic loading. *ARPN Journal of Engineering and Applied Sciences*, *12*(14), 4298–4301.

Karakus, M., Akdag, S., & Bruning, T. (2016). Rock Fatigue Damage Assessment by Acoustic Emission. *International Conference on Geomechanics, Geo-Energy and Geo-Resources*.

Kendrick, J. E., Smith, R., Sammonds, P., Meredith, P. G., Dainty, M., & Pallister, J. S. (2013). The influence of thermal and cyclic stressing on the strength of rocks from Mount St. Helens, Washington. *Bulletin of Volcanology*, *75*(7), 728. https://doi.org/10.1007/s00445-013-0728-z

Ko, T. Y. (2005). *Crack coalescence in rock-like material under cycling loading* (Massachusetts Institute of Technology). Retrieved from http://hdl.handle.net/1721.1/30195

Lavrov, A. (2001). Kaiser effect observation in brittle rock cyclically loaded with different loading rates. *Mechanics of Materials*, *33*(11), 669–677.

https://doi.org/https://doi.org/10.1016/S0167-6636(01)00081-3

Le, J.-L., Manning, J., & Labuz, J. F. (2014). Scaling of fatigue crack growth in rock. *International Journal of Rock Mechanics and Mining Sciences*, *72*, 71–79. https://doi.org/https://doi.org/10.1016/j.ijrmms.2014.08.015

Li, G., Moelle, K. H. R., & Lewis, J. A. (1992). Fatigue crack growth in brittle sandstones. *International Journal of Rock Mechanics and Mining Sciences & Geomechanics Abstracts*, *29*(5), 469–477. https://doi.org/http://dx.doi.org/10.1016/0148-9062(92)92631-L

Li, N, Chen, W., Zhang, P., & Swoboda, G. (2001). The mechanical properties and a fatigue-damage model for jointed rock masses subjected to dynamic cyclical loading. *International Journal of Rock Mechanics and Mining Sciences*, *38*(7), 1071–1079. https://doi.org/http://dx.doi.org/10.1016/S1365-1609(01)00058-2

Li, Ning, Zhang, P., Chen, Y., & Swoboda, G. (2003). Fatigue properties of cracked, saturated and frozen sandstone samples under cyclic loading. *International Journal of Rock Mechanics and Mining Sciences*, *40*(1), 145–150. https://doi.org/http://dx.doi.org/10.1016/S1365-1609(02)00111-9

Liu, Enlong, & He, S. (2012). Effects of cyclic dynamic loading on the mechanical properties of intact rock samples under confining pressure conditions. *Engineering Geology*, *125*, 81–91. https://doi.org/http://dx.doi.org/10.1016/j.enggeo.2011.11.007

Liu, EnLong, He, S., Xue, X., & Xu, J. (2011). Dynamic Properties of Intact Rock Samples Subjected to Cyclic Loading under Confining Pressure Conditions. *Rock Mechanics and Rock Engineering*, *44*(5), 629–634. https://doi.org/10.1007/s00603-011-0151-8

Liu, Enlong, Huang, R., & He, S. (2012). Effects of Frequency on the Dynamic Properties of Intact Rock Samples Subjected to Cyclic Loading under Confining Pressure Conditions. *Rock Mechanics and Rock Engineering*, *45*(1), 89–102. https://doi.org/10.1007/s00603-011-0185-y

Liu, J., Xie, H., Hou, Z., Yang, C., & Chen, L. (2014). Damage evolution of rock salt under cyclic loading in unixial tests. *Acta Geotechnica*, *9*(1), 153–160. https://doi.org/10.1007/s11440-013-0236-5

Liu, M., & Liu, E. (2017). Dynamic mechanical properties of artificial jointed rock samples subjected to cyclic triaxial loading. *International Journal of Rock Mechanics and Mining Sciences*, *98*, 54–66.

https://doi.org/http://dx.doi.org/10.1016/j.ijrmms.2017.07.005

Liu, X. R., Kou, M. M., Lu, Y. M., & Liu, Y. Q. (2018). An experimental investigation on the shear mechanism of fatigue damage in rock joints under pre-peak cyclic loading condition. *International Journal of Fatigue*, *106*, 175–184. https://doi.org/https://doi.org/10.1016/j.ijfatigue.2017.10.007

Liu, X. S., Ning, J. G., Tan, Y. L., & Gu, Q. H. (2016). Damage constitutive model based on energy dissipation for intact rock subjected to cyclic loading. *International Journal of Rock Mechanics and Mining Sciences*, *85*, 27–32. https://doi.org/http://dx.doi.org/10.1016/j.ijrmms.2016.03.003

Liu, Y, Dai, F., Dong, L., Xu, N., & Feng, P. (2018). Experimental Investigation on the Fatigue Mechanical Properties of Intermittently Jointed Rock Models Under Cyclic Uniaxial Compression with Different Loading Parameters. *Rock Mechanics and Rock Engineering*, *51*(1), 47–68. https://doi.org/10.1007/s00603-017-1327-7

Liu, Yi, & Dai, F. (2018). A damage constitutive model for intermittent jointed rocks under cyclic uniaxial compression. *International Journal of Rock Mechanics and Mining Sciences*, *103*, 289–301. https://doi.org/https://doi.org/10.1016/j.ijrmms.2018.01.046

Liu, Yi, Dai, F., Fan, P., Xu, N., & Dong, L. (2017). Experimental Investigation of the Influence of Joint Geometric Configurations on the Mechanical Properties of Intermittent Jointed Rock Models Under Cyclic Uniaxial Compression. *Rock Mechanics and Rock Engineering*, *50*(6), 1453–1471. https://doi.org/10.1007/s00603-017-1190-6

Liu, Yi, Dai, F., Feng, P., & Xu, N. (2018). Mechanical behavior of intermittent jointed rocks under random cyclic compression with different loading parameters. *Soil Dynamics and Earthquake Engineering*, *113*, 12–24. https://doi.org/https://doi.org/10.1016/j.soildyn.2018.05.030

Liu, Yi, Dai, F., Xu, N., & Zhao, T. (2017). Cyclic flattened Brazilian disc tests for measuring the tensile fatigue properties of brittle rocks. *Review of Scientific Instruments*, *88*(8), 83902. https://doi.org/10.1063/1.4995656

Liu, Yi, Dai, F., Zhao, T., & Xu, N. (2017). Numerical Investigation of the Dynamic Properties of Intermittent Jointed Rock Models Subjected to Cyclic Uniaxial Compression. *Rock Mechanics and Rock Engineering*, *50*(1), 89–112. https://doi.org/10.1007/s00603-016-1085-y

Ma, Lin-jian, Liu, X., Wang, M., Xu, H., Hua, R., Fan, P., … Yi, Q. (2013). Experimental investigation of the mechanical properties of rock salt under triaxial cyclic loading. *International Journal of Rock Mechanics and Mining Sciences*, *62*, 34–41. https://doi.org/http://dx.doi.org/10.1016/j.ijrmms.2013.04.003

Ma, Linjian, Wang, M., Zhang, N., Fan, P., & Li, J. (2017). A Variable-Parameter Creep Damage Model Incorporating the Effects of Loading Frequency for Rock Salt and Its Application in a Bedded Storage Cavern. *Rock Mechanics and Rock Engineering*, *50*(9), 2495–2509. https://doi.org/10.1007/s00603-017-1236-9

Martin, C. D., & Chandler, N. A. (1994). The progressive fracture of Lac du Bonnet granite. *International Journal of Rock Mechanics and Mining Sciences & Geomechanics Abstracts*, *31*(6), 643–659. https://doi.org/https://doi.org/10.1016/0148-9062(94)90005-1

Meng, Q., Zhang, M., Han, L., Pu, H., & Chen, Y. (2018). Acoustic Emission Characteristics of Red Sandstone Specimens Under Uniaxial Cyclic Loading and Unloading Compression. *Rock Mechanics and Rock Engineering*, *51*(4), 969–988. https://doi.org/10.1007/s00603-017-1389-6

Meng, Q., Zhang, M., Han, L., Pu, H., & Nie, T. (2016). Effects of Acoustic Emission and Energy Evolution of Rock Specimens Under the Uniaxial Cyclic Loading and Unloading Compression. *Rock Mechanics and Rock Engineering*, *49*(10), 3873–3886. https://doi.org/10.1007/s00603-016-1077-y

Mitchell, T. M., & Faulkner, D. R. (2008). Experimental measurements of permeability evolution during triaxial compression of initially intact crystalline rocks and implications for fluid flow in fault zones. *Journal of Geophysical Research: Solid Earth*, *113*(B11). https://doi.org/10.1029/2008JB005588

Momeni, A., Karakus, M., Khanlari, G. R., & Heidari, M. (2015). Effects of cyclic loading on the mechanical properties of a granite. *International Journal of Rock Mechanics and Mining Sciences*, *77*, 89–96. https://doi.org/http://dx.doi.org/10.1016/j.ijrmms.2015.03.029

Munoz, H., & Taheri, A. (2017). Local Damage and Progressive Localisation in Porous Sandstone During Cyclic Loading. *Rock Mechanics and Rock Engineering*, *50*(12), 3253–3259. https://doi.org/10.1007/s00603-017-1298-8

Nejati, H. R., & Ghazvinian, A. (2014). Brittleness Effect on Rock Fatigue Damage Evolution. *Rock Mechanics and Rock Engineering*, *47*(5), 1839–1848. https://doi.org/10.1007/s00603-013-0486-4

Ni, X. H. (2014). Failure Characteristic of Granite under Cyclic Loading with Different Frequencies. *Applied Mechanics and Materials*, *638–640*, 1967–1970. Retrieved from https://doi.org/10.4028/www.scientific.net/amm.638-640.1967

Ning, J., Wang, J., Jiang, J., Hu, S., Jiang, L., & Liu, X. (2018). Estimation of Crack Initiation and Propagation Thresholds of Confined Brittle Coal Specimens Based on Energy Dissipation Theory. *Rock Mechanics and Rock Engineering*, *51*(1), 119–134. https://doi.org/10.1007/s00603-017-1317-9

Peng, K., Zhou, J., Zou, Q., & Song, X. (2019). Effect of loading frequency on the deformation behaviours of sandstones subjected to cyclic loads and its underlying mechanism. *International Journal of Fatigue*, 105349. https://doi.org/https://doi.org/10.1016/j.ijfatigue.2019.105349

Peng, K., Zhou, J., Zou, Q., & Yan, F. (2019). Deformation characteristics of sandstones during cyclic loading and unloading with varying lower limits of stress under different confining pressures. *International Journal of Fatigue*, *127*, 82–100. https://doi.org/https://doi.org/10.1016/j.ijfatigue.2019.06.007

Pola, A., Crosta, G. B., Fusi, N., & Castellanza, R. (2014). General characterization of the mechanical behaviour of different volcanic rocks with respect to alteration. *Engineering Geology*, *169*, 1–13. https://doi.org/https://doi.org/10.1016/j.enggeo.2013.11.011

Qiu, S.-L., Feng, X.-T., Xiao, J.-Q., & Zhang, C.-Q. (2014). An Experimental Study on the Pre-Peak Unloading Damage Evolution of Marble. *Rock Mechanics and Rock Engineering*, *47*(2), 401–419. https://doi.org/10.1007/s00603-013-0394-7

Rajaram, V. (1981). Mechanical Behavior of Granite Under Cyclic Compression. *International Conferences on Recent Advances in Geotechnical Earthquake Engineering and Soil Dynamics*, 11.

Rao, M. V. M. S., & Ramana, Y. V. (1992). A study of progressive failure of rock under cyclic loading by ultrasonic and AE monitoring techniques. *Rock Mechanics and Rock Engineering*, *25*(4), 237–251. https://doi.org/10.1007/BF01041806

Ray, S. K., Sarkar, M., & Singh, T. N. (1999). Effect of cyclic loading and strain rate on the mechanical behaviour of sandstone. *International Journal of Rock Mechanics and Mining Sciences*, *36*(4), 543–549. https://doi.org/http://dx.doi.org/10.1016/S0148-9062(99)00016-9

Roberts, L. A., Buchholz, S. A., Mellegard, K. D., & Düsterloh, U. (2015). Cyclic

Loading Effects on the Creep and Dilation of Salt Rock. *Rock Mechanics and Rock Engineering*, *48*(6), 2581–2590. https://doi.org/10.1007/s00603-015-0845-4

Royer-Carfagni, G., & Salvatore, W. (2000). The characterization of marble by cyclic compression loading: experimental results. *Mechanics of Cohesive-Frictional Materials*, *5*(7), 535–563. https://doi.org/10.1002/1099-1484(200010)5:7<535::AID-CFM102>3.0.CO;2-D

Rukhaiyar, S., & Samadhiya, N. K. (2018). Strength Behavior of Rocks Under Cyclic Loading. *Indian Geotechnical Journal*, *48*(1), 176–187. https://doi.org/10.1007/s40098-017-0238-6

Sara, C., & F., L. J. (2001). Damage of Marble from Cyclic Loading. *Journal of Materials in Civil Engineering*, *13*(6), 459–465. https://doi.org/10.1061/(ASCE)0899-1561(2001)13:6(459)

Schaefer, L. N., Kendrick, J. E., Oommen, T., Lavallée, Y., & Chigna, G. (2015). Geomechanical rock properties of a basaltic volcano . *Frontiers in Earth Science* , Vol. 3, p. 29. Retrieved from https://www.frontiersin.org/article/10.3389/feart.2015.00029

Scholz, C. H., & Koczynski, T. A. (1979). Dilatancy anisotropy and the response of rock to large cyclic loads. *Journal of Geophysical Research: Solid Earth*, *84*(B10), 5525–5534. https://doi.org/10.1029/JB084iB10p05525

Scholz, C. H., & Kranz, R. (1974). Notes on dilatancy recovery. *Journal of Geophysical Research (1896-1977)*, *79*(14), 2132–2135. https://doi.org/10.1029/JB079i014p02132

Shi, C., Ding, Z., Lei, M., & Peng, L. (2014). Accumulated Deformation Behavior and Computational Model of Water-Rich Mudstone Under Cyclic Loading. *Rock Mechanics and Rock Engineering*, *47*(4), 1485–1491. https://doi.org/10.1007/s00603-013-0427-2

Singh, S. K. (1989). Fatigue and strain hardening behaviour of graywacke from the flagstaff formation, New South Wales. *Engineering Geology*, *26*(2), 171–179. https://doi.org/http://dx.doi.org/10.1016/0013-7952(89)90005-7

Song, H., Zhang, H., Fu, D., & Zhang, Q. (2016). Experimental analysis and characterization of damage evolution in rock under cyclic loading. *International Journal of Rock Mechanics and Mining Sciences*, *88*, 157–164. https://doi.org/http://dx.doi.org/10.1016/j.ijrmms.2016.07.015

Song, R., Yue-ming, B., Jing-Peng, Z., De-yi, J., & Chun-he, Y. (2013). Experimental investigation of the fatigue properties of salt rock. *International Journal of Rock Mechanics and Mining Sciences*, *64*, 68–72. https://doi.org/http://dx.doi.org/10.1016/j.ijrmms.2013.08.023

Su, G., Hu, L., Feng, X., Yan, L., Zhang, G., Yan, S., … Yan, Z. (2018). True Triaxial Experimental Study of Rockbursts Induced By Ramp and Cyclic Dynamic Disturbances. *Rock Mechanics and Rock Engineering*, *51*(4), 1027–1045. https://doi.org/10.1007/s00603-017-1384-y

Sun, B., Zhu, Z., Shi, C., & Luo, Z. (2017). Dynamic mechanical behavior and fatigue damage evolution of sandstone under cyclic loading. *International Journal of Rock Mechanics and Mining Sciences*, *94*, 82–89. https://doi.org/https://doi.org/10.1016/j.ijrmms.2017.03.003

Taheri, A., Royle, A., Yang, Z., & Zhao, Y. (2016). Study on variations of peak strength of a sandstone during cyclic loading. *Geomechanics and Geophysics for Geo-Energy and Geo-Resources*, *2*(1), 1–10. https://doi.org/10.1007/s40948-015-0017-8

Taheri, A., Yfantidis, N., Olivares, C., Connelly, B., & Bastian, T. (2016). *Experimental Study on Degradation of Mechanical Properties of Sandstone Under Different Cyclic Loadings BT - Experimental Study on Degradation of Mechanical Properties of Sandstone Under Different Cyclic Loadings*.

Tien, Y. M., Lee, D. H., & Juang, C. H. (1990). Strain, pore pressure and fatigue characteristics of sandstone under various load conditions. *International Journal of Rock Mechanics and Mining Sciences & Geomechanics Abstracts*, *27*(4), 283–289. https://doi.org/http://dx.doi.org/10.1016/0148-9062(90)90530-F

Trippetta, F., Collettini, C., Meredith, P. G., & Vinciguerra, S. (2013). Evolution of the elastic moduli of seismogenic Triassic Evaporites subjected to cyclic stressing. *Tectonophysics*, *592*, 67–79. https://doi.org/https://doi.org/10.1016/j.tecto.2013.02.011

Voznesenskii, Aleksandr S, Kutkin, Y. O., Krasilov, M. N., & Komissarov, A. A. (2015). Predicting fatigue strength of rocks by its interrelation with the acoustic quality factor. *International Journal of Fatigue*, *77*, 194–198. https://doi.org/https://doi.org/10.1016/j.ijfatigue.2015.02.012

Voznesenskii, Aleksandr Sergeevich, Krasilov, M. N., Kutkin, Y. O., Tavostin, M. N., & Osipov, Y. V. (2017). Features of interrelations between acoustic quality factor

and strength of rock salt during fatigue cyclic loadings. *International Journal of Fatigue*, *97*, 70–78. https://doi.org/https://doi.org/10.1016/j.ijfatigue.2016.12.027

Voznesenskii, Aleksandr Sergeevitch, Kutkin, Y. O., Krasilov, M. N., & Komissarov, A. A. (2016). The influence of the stress state type and scale factor on the relationship between the acoustic quality factor and the residual strength of gypsum rocks in fatigue tests. *International Journal of Fatigue*, *84*, 53–58. https://doi.org/https://doi.org/10.1016/j.ijfatigue.2015.11.016

Wang, H. L., Xu, W. Y., Cai, M., Xiang, Z. P., & Kong, Q. (2017). Gas Permeability and Porosity Evolution of a Porous Sandstone Under Repeated Loading and Unloading Conditions. *Rock Mechanics and Rock Engineering*, *50*(8), 2071–2083. https://doi.org/10.1007/s00603-017-1215-1

Wang, W., Wang, M., & Liu, X. (2016). Study on Mechanical Features of Brazilian Splitting Fatigue Tests of Salt Rock. *Advances in Civil Engineering*, *2016*(Article ID 5436240), 10. Retrieved from https://doi.org/10.1155/2016/5436240

Wang, Z., Li, S., Qiao, L., & Zhao, J. (2013). Fatigue Behavior of Granite Subjected to Cyclic Loading Under Triaxial Compression Condition. *Rock Mechanics and Rock Engineering*, *46*(6), 1603–1615. https://doi.org/10.1007/s00603-013-0387-6

Xiao, J.-Q., Ding, D.-X., Jiang, F.-L., & Xu, G. (2010). Fatigue damage variable and evolution of rock subjected to cyclic loading. *International Journal of Rock Mechanics and Mining Sciences*, *47*(3), 461–468. https://doi.org/http://dx.doi.org/10.1016/j.ijrmms.2009.11.003

Xiao, J.-Q., Ding, D.-X., Xu, G., & Jiang, F.-L. (2009). Inverted S-shaped model for nonlinear fatigue damage of rock. *International Journal of Rock Mechanics and Mining Sciences*, *46*(3), 643–648. https://doi.org/http://dx.doi.org/10.1016/j.ijrmms.2008.11.002

Xiao, J.-Q., Feng, X.-T., Ding, D.-X., & Jiang, F.-L. (2011). Investigation and modeling on fatigue damage evolution of rock as a function of logarithmic cycle. *International Journal for Numerical and Analytical Methods in Geomechanics*, *35*(10), 1127–1140. https://doi.org/10.1002/nag.946

Yamashita, S., Sugimoto, F., Imai, T., Namsrai, D., Yamauchi, M., & Kamoshida, N. (1999). The Relationship Between the Failure Process of the Creep Or Fatigue Test And of the Conventional Compression Test On Rock. *9th ISRM Congress*.

Paris, France: International Society for Rock Mechanics and Rock Engineering.

Yang, S.-Q., Ranjith, P. G., Huang, Y.-H., Yin, P.-F., Jing, H.-W., Gui, Y.-L., & Yu, Q.-L. (2015). Experimental investigation on mechanical damage characteristics of sandstone under triaxial cyclic loading. *Geophysical Journal International*, *201*(2), 662–682. https://doi.org/10.1093/gji/ggv023

Yang, S.-Q., Tian, W.-L., & Ranjith, P. G. (2017). Experimental Investigation on Deformation Failure Characteristics of Crystalline Marble Under Triaxial Cyclic Loading. *Rock Mechanics and Rock Engineering*, *50*(11), 2871–2889. https://doi.org/10.1007/s00603-017-1262-7

Zhang, P., Xu, J., & Li, N. (2008). Fatigue properties analysis of cracked rock based on fracture evolution process. *Journal of Central South University of Technology*, *15*(1), 95–99. https://doi.org/10.1007/s11771-008-0019-6

Zhenyu, T., & Haihong, M. (1990). An experimental study and analysis of the behaviour of rock under cyclic loading. *International Journal of Rock Mechanics and Mining Sciences & Geomechanics Abstracts*, *27*(1), 51–56. https://doi.org/https://doi.org/10.1016/0148-9062(90)90008-P

Zhou, H. W., Wang, Z. H., Wang, C. S., & Liu, J. F. (2019). On Acoustic Emission and Post-peak Energy Evolution in Beishan Granite Under Cyclic Loading. *Rock Mechanics and Rock Engineering*, *52*(1), 283–288. https://doi.org/10.1007/s00603-018-1614-y

Appendix B

Declarations of Authorship

DECLARATION OF AUTHORSHIP

I, Rashid Geranmayeh Vaneghi, contributed:

80% of the design, analysis and authoring the paper entitled “Strength degradation of sandstone and granodiorite under uniaxial cyclic loading”. Achola D. Okoth and Barnabas Kuek both conducted the tests with me and under my supervision. Dr. Behnam Ferdosi assisted with test design and supervision of the study and reviewed the paper.

Rashid Geranmayeh Vaneghi

Date: 13/11/2019

I, as a Co-Author, endorse that this level of contribution by the candidate indicated above is appropriate.

Achola D. OkothDate:

14/11/2019

Barnabas Kuek

18/11/2019

DECLARATION OF AUTHORSHIP

I, Rashid Geranmayeh Vaneghi, contributed:

- 80% of the design, analysis of the study and authoring the paper entitled "*Sources of variability in laboratory rock test results*". S. E. Saberhosseini assisted with the numerical analysis. M. Sarmadivaleh assisted with the design, CT scanning of samples, supervision of the study, and reviewed the paper. A. V. Dyskin and K. Thoeni assisted with the analysis, supervision of the study, and critically reviewed the paper. M. Sharifzadeh reviewed the paper.

Rashid Geranmayeh Vaneghi

Date:
10/06/2020

I, as a Co-Author, endorse that this level of contribution by the candidate indicated above is appropriate.

Dr. Mohammad Sarmadivaleh
Supervisor and Co-author — 11/06/2020

Prof. Arcady V. Dyskin
A/ supervisor and Co-author — 15/06/2020

Dr. Klaus Thoeni
A/ supervisor and Co-author — 12/06/2020

Dr. Mostafa Sharifzadeh
Co-supervisor and Co-author

Seyed Erfan Saberhosseini
Co-author — 12/06/2020

DECLARATION OF AUTHORSHIP

I, Rashid Geranmayeh Vaneghi, contributed:

- 85% of the design, analysis of the study and authoring the paper entitled "*Strength and damage response of sandstone and granodiorite under different loading conditions of multi-stage uniaxial cyclic compression*". M. Sarmadivaleh assisted with the design, CT scanning of samples, supervision of the study, and reviewed the paper. A. V. Dyskin and K. Thoeni assisted with the analysis, the supervision of the study and reviewed the paper. M. Sharifzadeh assisted with the supervision of the study and reviewed the paper.
- 85% of the design, analysis of the study and authoring the paper entitled "*Fatigue damage response of typical crystalline and granular rocks to uniaxial cyclic compression*". M. Sarmadivaleh assisted with the design, CT scanning of samples, supervision of the study, and reviewed the paper. K. Thoeni assisted with the test design, analysis, the supervision of the study and reviewed the paper. A. V. Dyskin assisted with the analysis, the supervision of the study and reviewed the paper. M. Sharifzadeh assisted with the supervision of the study and reviewed the paper.

Rashid Geranmayeh Vaneghi

Date:
10/06/2020

I, as a Co-Author, endorse that this level of contribution by the candidate indicated above is appropriate.

Dr. Mohammad Sarmadivaleh
Supervisor and Co-author

11/06/2020

Prof. Arcady V. Dyskin
A/ supervisor and Co-author

15/06/2020

Dr. Klaus Thoeni
A/ supervisor and Co-author

12/06/2020

Dr. Mostafa Sharifzadeh
Co-supervisor and Co-author

Appendix C

Copyright Licenses

Paper 2:

Copyright: Journal of Rock Mechanics and Geotechnical Engineering is completely Open Access journal with the included article: Rashid Geranmayeh Vaneghi, Behnam Ferdosi, Achola D. Okoth, Barnabas Kuek, (2018). Strength degradation of sandstone and granodiorite under uniaxial cyclic loading. Journal of Rock Mechanics and Geotechnical Engineering freely reproduced completely with no copyright infringements as a part of this thesis by the first author. See https://creativecommons.org/licenses/by-nc-nd/4.0/ for more information if necessary.

Paper 3:

As an original author of an ASCE journal article or proceedings paper, you are permitted to reuse your own content (including figures and tables) for another ASCE or non-ASCE publication (including your thesis), provided it does not account for more than 25% of the new work.

Authors may post the final draft of their work on open, unrestricted Internet sites or deposit it in an institutional repository when the draft contains a link to the bibliographic record of the published version in the ASCE Library or Civil Engineering Database. "Final draft" means the version submitted to ASCE after peer review and prior to copyediting or other ASCE production activities; it does not include the copyedited version, the page proof, or a PDF of the published version.

https://ascelibrary.org/page/informationforasceauthorsreusingyourownmaterial

Paper 4:

Appendix D

Paper 2

Journal of Rock Mechanics and Geotechnical Engineering 10 (2018) 117–126

Contents lists available at ScienceDirect

Journal of Rock Mechanics and Geotechnical Engineering

journal homepage: www.rockgeotech.org

Full Length Article

Strength degradation of sandstone and granodiorite under uniaxial cyclic loading

Rashid Geranmayeh Vaneghi*, Behnam Ferdosi, Achola D. Okoth, Barnabas Kuek

Department of Mining Engineering and Metallurgical Engineering, Western Australian School of Mines (WASM), Curtin University, Kalgoorlie, Australia

ARTICLE INFO

Article history:
Received 29 June 2017
Received in revised form
14 September 2017
Accepted 17 September 2017
Available online 26 December 2017

Keywords:
Rock fatigue
Cyclic loading
Strength degradation
Fatigue life

ABSTRACT

Change in mechanical properties of rocks under static loading has been widely studied and documented. However, the response of rocks to cyclic loads is still a much-debated topic. Fatigue is the phenomenon when rocks under cyclic loading fail at much lower strength as compared to those subjected to the monotonic loading conditions. A few selected cored granodiorite and sandstone specimens have been subjected to uniaxial cyclic compression tests to obtain the unconfined fatigue strength and life. This study seeks to examine the effects of cyclic loading conditions, loading amplitude and applied stress level on the fatigue life of sandstone, as a soft rock, and granodiorite, as a hard rock, under uniaxial compression test. One aim of this study is to determine which of the loading conditions has a stronger effect on rock fatigue response. The fatigue response of hard rocks and soft rocks is also compared. It is shown that the loading amplitude is the most important factor affecting the cyclic response of the tested rocks. The more the loading amplitude, the shorter the fatigue life, and the greater the strength degradation. The granodiorite specimens showed more strength degradation compared to the sandstone specimens when subjected to cyclic loading. It is shown that failure modes of specimens under cyclic loadings are different from those under static loadings. More local cracks were observed under cyclic loadings especially for granodiorite rock specimens.

1. Introduction

In situ rock is basically subjected to monotonic and cyclic or dynamic loadings. A proper and detailed understanding of how the mechanical properties of rock change when subjected to different loading scenarios is required for the safe and proper design and construction of civil, mining and geotechnical engineering structures such as underground openings, tunnels, rock pillars, foundations and for better understanding of other related operations such as drilling and blasting. Cyclic loadings are generated by seismic events, earthquakes, blasting, repetitive loadings and explosions which affect either surface or underground rock structures (Fig. 1). As shown in Fig. 1, the stability of an underground excavation (openings like tunnels, galleries, caverns and shafts) is not only controlled by rock microstructures, geological features and in situ stress state, but also by the type of loading which could be static or dynamic. The period of cyclic loading, its frequency and stress level are important factors which govern the influence of cyclic loading on a rock body. Hence, the mechanical properties of rock under cyclic or dynamic loading should be different from those under static loading condition.

It has been widely acknowledged that a rock structure subjected to cyclic loading often fails prior to reaching its designed stress level or bearing capacity of its static uniaxial compressive strength (UCS). The mechanism is widely referred to as “fatigue” (Eberhardt et al., 1998). Fundamental rock structures, as mentioned above, are often subjected to cyclic loadings and their mechanical strengths experience degradation along with the loading period. Therefore, the effects of cyclic loading on stability and serviceability of rock structures cannot be neglected.

From the literature review, it was found that some researchers focused on the variation and degradation of intact or jointed rock properties under uniaxial and triaxial cyclic loadings and some others investigated the fatigue damage mechanism. It was first reported by Burdine (1963) that the pore pressure and confinement affected the cyclic response of sandstone, and rock fatigue strength decreased and increased at high pore pressure and confinement,

* Corresponding author.
E-mail address: r.geranmayeh@postgrad.curtin.edu.au (R. Geranmayeh Vaneghi).
Peer review under responsibility of Institute of Rock and Soil Mechanics, Chinese Academy of Sciences.

https://doi.org/10.1016/j.jrmge.2017.09.005

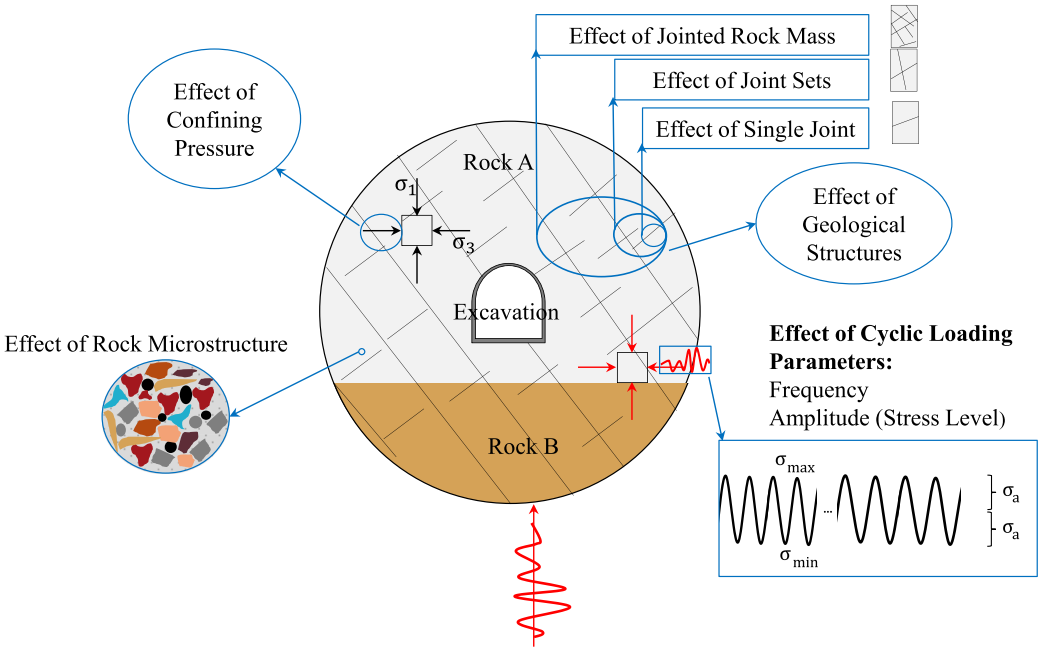

Fig. 1. Typical schematic view of rock cyclic problems and their important factors in underground excavation design as well as other common influencing factors. σ_1 and σ_3 are the major and minor principal stresses, respectively; and σ_{min}, σ_{max}, and σ_a are the minimum stress, maximum stress, and loading amplitude stress levels, respectively, during a cyclic loading.

respectively. Attewell and Farmer (1973) also examined the strength degradation of concrete, mortar and rock under cyclic loading. They revealed that the fatigue strengths of their tested materials decreased up to 50–70% compared to the static strength. Prost (1988) investigated the effect of pre-existing joints in Pikes Peak granite and Dakota sandstone on the crack initiation and propagation under compression-tension cyclic loading. He reported that the rocks generally failed at low number of cycles when loaded under higher stress levels and loading amplitudes. Macro tests conducted by Singh (1989) also concluded that cyclic loadings led to progressive weakening of rocks and in particular showed that there was a remarkable drop in the UCS of rocks following cyclic loading.

Tao and Mo (1990) attempted to correlate the experimental data of fatigue life to the mechanical properties of a rock specimen. They developed a constitutive equation to explain the stress–strain curves for cyclic loading. However, there is no single validated rule to describe the cyclic loading behavior of a rock. The equation developed by Tao and Mo (1990) only gives a best fit under given conditions.

The effects of cyclic loading and strain rate on the uniaxial strength of sandstone were studied by Ray et al. (1999). They reported that the degradation of rock strength is noticeable at higher maximum stress levels. According to their results, the axial failure strain was also relatively higher at higher stress levels.

Bagde and Petroš (2005a) reported that the fatigue strength and Young's modulus of sandstone decreased and increased, respectively, with the loading frequency. Bagde and Petroš (2005b) reported that the loading machine showed sensitivity to high loading amplitude applied at high loading frequency, and found that the real applied loading amplitude was remarkably lower than the target loading amplitude. Bagde and Petroš (2005c) also revealed that the cyclic dynamic responses are different under different loading waveforms and loading rates. The sine waveform was found to have a stronger dynamic effect than a ramp (triangle) waveform. It was reported that damage accumulates most rapidly under square waveforms (Gong and Smith, 2003); however, it is purely of academic interest. Because the loading rate of a square waveform is theoretically infinite in a quarter of a cycle, its dynamic effect is similar to an impact load (Xiao et al., 2008). The effects of loading amplitude and frequency on the strength degradation and deformation behavior of rocks under uniaxial cyclic compression were also studied by Bagde and Petroš (2009). They reported that the microstructure, texture and quartz content of the rock specimens affect the fatigue strength and cyclic dynamic response. It was found that the microfracturing is the main cause of fatigue failure.

Different damage variables used to examine the damage evolution under cyclic loading were discussed by Xiao et al. (2009, 2010). When the permanent strain was plotted against the number of cycles, it was observed that the three-stage inverted S-shaped model is well capable of describing the whole process of fatigue damage development. The curve can be divided into three phases. The shape of the curve is dependent on the rock properties and magnitude of stress applied to the rock. The three phases may be associated with the three stages that a crack undergoes, i.e. crack initiation, stable propagation and unstable propagation (Xiao et al., 2009). Bastian et al. (2014) conducted uniaxial and triaxial cyclic compressive tests on Hawkesbury sandstone to examine the variation in its mechanical properties under cyclic loading conditions. Rapid evolution of damage was observed as unloading initiation stress and unloading amplitude increased. The variations of mechanical parameters and failure mechanism of Lac du Bonnet granite under uniaxial cyclic loading were discussed by Ghazvinian (2015). He described the relationship between the critical stress thresholds (crack initiation and crack damage thresholds) and the fatigue damage pattern during the cyclic process. Taheri et al. (2016) also studied the change in mechanical properties of the Hawkesbury sandstone during various cyclic loading conditions using uniaxial and triaxial compression tests. They reported that the unstable crack propagation was observed at approximately 65% of the cumulative axial strain.

To date, most of previous works attempted to evaluate the change in mechanical properties of rocks under different cyclic

loading conditions. Few studies, however, have addressed the question: Which of the maximum stress level and loading amplitude has a stronger cyclic effect? Moreover, the cyclic response of soft rocks and hard rocks is not fully understood. As mentioned previously, the fatigue behavior of hard rocks such as granodiorite and soft rocks such as sandstone, which are very common rocks in most rock structures, was always of great importance. The cyclic behaviors of these two kinds of rocks under constant frequency but with varying loading stress amplitude and stress level are presented in this study.

2. Experimental set-up

2.1. Rock specimens

Among the intrusive rocks, granite and granodiorite are the most common and frequently encountered ones in most underground mining activities. In addition, as a result of the high strength of granitic rock, it is also widely used in the construction industry. Sandstone is also bedrock for rock structures and its behavior is different from a hard rock like granodiorite. The rock specimens were obtained from sandstone and Gosford granite/granodiorite outcrops quarry in New South Wales, Australia. Petrographic thin section analysis shows that granodiorite is weakly altered coarse-grained leucocratic holocrystalline and it contains anhedral quartz (20–30%), orthoclase (~20%), subhedral, zoned plagioclase (20–30%) and medium-grained flakes biotite (~10%). Sandstone is fine-grained and well-sorted and dominated by sub-rounded to angular quartz (~80%). The matrix material consisting of clay and sericite accounts for around 10% of the specimen. The intergranular porosity of this sandstone is approximately 10%. Photographs of the analyzed specimens from these two rock types in cross polarized light (XPL) are shown in Fig. 2. The typical specimens of granodiorite and sandstone are shown in Fig. 3. The densities of tested sandstone and granodiorite specimens were 2204 kg/m^3 and 2524 kg/m^3, respectively.

Specimens were available in two sizes: regular-size with diameter of about 54 mm and height of 131 mm and small-size with diameter of 42 mm and height of 102 mm. Seven (five small-size and two regular-size) specimens of granodiorite and seven (four small-size and three regular-size) of sandstone were tested to determine their UCS values. The sandstone specimens were oven-dried for 24 h so as to eliminate any moisture present therein. Since the average water content was determined to be very low (equal to 0.3%), the effect of water content on the obtained results was neglected.

2.2. Equipment

The tests were done using a GCTS uniaxial testing system UCT 1000, as shown in Fig. 4. The machine is fitted with a computer-controlled axial actuator and can load a specimen by controlling the loading rate or strain rate. The UCT 1000 is capable of performing both dynamic and static tests, and the data obtained from the tests are collected automatically using PC-based software.

The specimens were loaded using a servo-controlled loading machine. The linear variable differential transformers (LVDTs) were used for simultaneous readings of axial, radial and volumetric strains. UCS values for all specimens were recorded for analysis.

2.3. Methodology

Some laboratory tests have been performed through use of uniaxial cyclic loading to investigate the mechanical fatigue behaviors of the tested rocks. The granodiorite and sandstone specimens, used for cyclic loading, were in the same size as those used for monotonic uniaxial compression loadings.

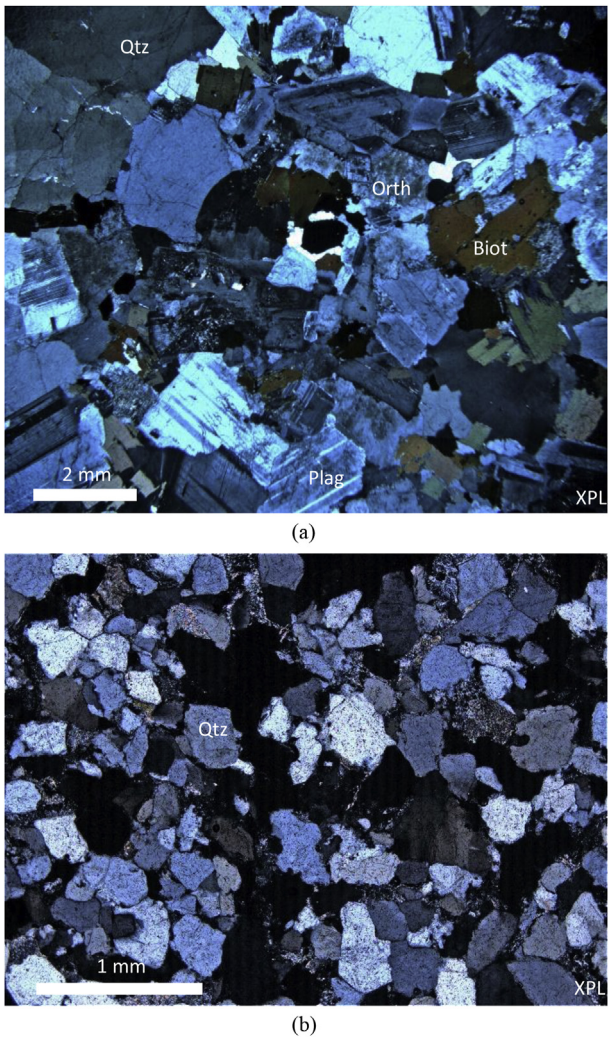

Fig. 2. Photomicrographs of (a) granodiorite and (b) sandstone in XPL. Qtz, Plag, Orth and Biot stand for quartz, plagioclase, orthoclase and biotite, respectively.

Uniaxial monotonic compression tests were conducted on both rock types. The average UCS for the tested specimens was used as the guiding maximum possible strength of the rock and to define the maximum stress level of cyclic loading. Table 1 shows the average UCS for regular- and small-size granodiorite and sandstone specimens. The stress–strain curves of uniaxial tests on small-size specimens are illustrated in Fig. 5.

The uniaxial cyclic tests were carried out in a stress control mode. The loading waveform was sine waveform which has already been found to have a stronger dynamic effect than a ramp (triangle) waveform (Bagde and Petroš, 2005c). The loading amplitudes were varied yet frequency was kept constant at 1 Hz. Two types of cyclic loadings were considered in these uniaxial cyclic tests. These two types were constant mean stress level or constant cyclic loading (CCL), and increasing mean stress level or stepped cyclic loading (SCL). The cyclic loading path with respect to time is illustrated schematically in Fig. 6.

The CCL was designed to examine the effects of loading amplitude and the maximum stress level on fatigue strength. The regular-size specimens were tested under a CCL condition while the testing for the small-size specimens was done in a SCL manner.

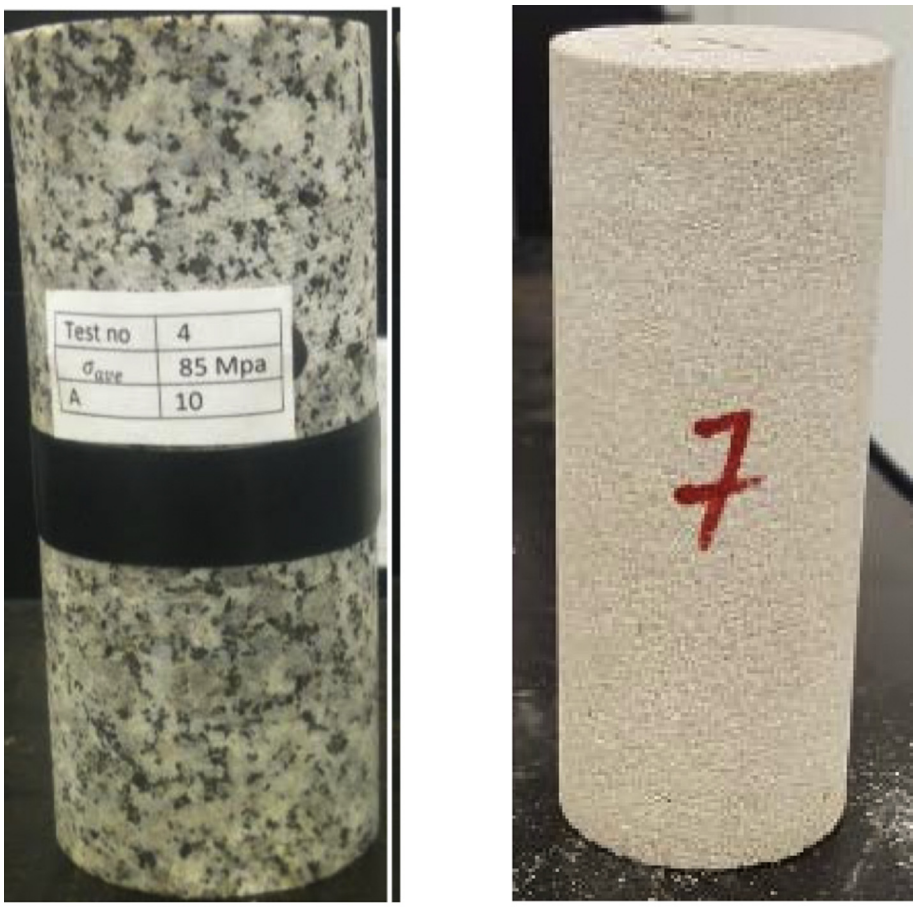

Fig. 3. Typical specimens of (a) granodiorite and (b) sandstone before testing.

Under SCL conditions, the loading amplitude was kept constant whereas the maximum stress level was increased step by step. These tests were designed to find the fatigue stress of the tested rocks and to explore the effect of maximum stress level on the fatigue strength. For the SCL tests, the initial mean stress was set and the specimen was loaded at a set amplitude for a specific time *t*. If no failure occurred, the mean stress was raised and the amplitude was kept constant and again the loading was done for another period of time *t*. This stepwise increase of mean stress was done up to the failure point. The maximum stress level was set as 75–90% of static strength (UCS) for the granodiorite specimens and 85–97% of UCS for the sandstone specimens. The amplitude stresses were set as 3–8 MPa and 5–10 MPa in cyclic tests conducted on sandstone and granodiorite specimens, respectively. The specimen was axially loaded up to the mean stress level (the average of the maximum and minimum stress levels, σ_{mean}) in the load control mode with loading rates of approximately 1 kN/s and 0.23 kN/s for regular- and small-size sandstone specimens and 3.3 kN/s and 0.23 kN/s for regular- and small-size granodiorite specimens, respectively. Since the results of the cyclic tests on regular specimens were somewhat scattered, the loading rate on small-size specimens was set relatively low. However, for the cyclic tests, it was attempted to set the loading rate of the initial loading to be the same as that of the uniaxial monotonic tests.

3. Results and discussion

The effects of the maximum stress level and loading amplitude on fatigue life and strength degradation of the tested rocks were investigated by uniaxial cyclic tests. As mentioned earlier, two types of cyclic loadings with constant mean stress level, named CCL, and increasing mean stress level cyclic loading, named SCL, were considered in these tests. Table 2 shows the experimental scheme and obtained results of uniaxial compression cyclic tests for both granodiorite and sandstone specimens. It is noteworthy that some specimens (St.-R-9, G-R-3 and G-R-4) were reloaded when they did not fail after a large number of cycles during the first loading path of CCL tests. Therefore, the results for specimens St.-R-10, G-R-5 and G-R-6 were used to analyze the effect of cyclic loading history on their fatigue response. Although these three specimens were loaded at a higher mean stress level for the second time, they were put into the CCL category.

Characteristics of all SCL paths are detailed in Table 3. As can be seen, in all SCL, the loading amplitudes (σ_α) were constant yet the mean stress levels were varied. According to this table, the mean stress level and loading amplitude of specimen St.-S-5, for instance, were set to 34.5 MPa and 3 MPa, respectively, for the first step. Then the specimen would be loaded for up to 30 min (1800 cycles). If it did not fail, the test would continue for another 1800 cycles within the second step in which the mean stress level would be increased to 37 MPa under the same loading amplitude (3 MPa). This procedure would be continued up to the failure point of the specimen.

Fig. 7 shows the stress–strain curves for the cyclic tests carried out on regular- and small-size specimens of granodiorite and sandstone. As displayed in Fig. 7a, the sandstone specimens St.-R-5, St.-R-6, St.-R-8 and St.-R-10 failed at 30.92 MPa, 30.89 MPa, 32.84 MPa and 33.84 MPa, respectively. Fig. 7b also presents that specimens St.-S-5, St.-S-6 and St.-S-7, which were loaded under

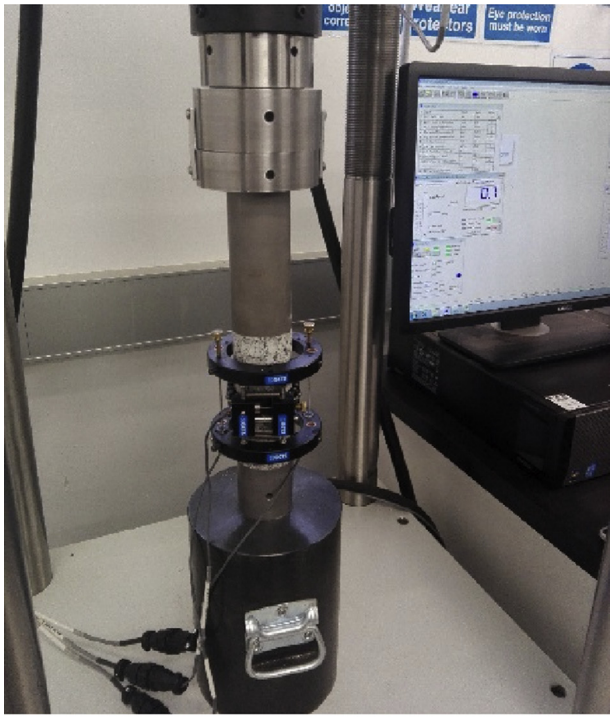

(a)

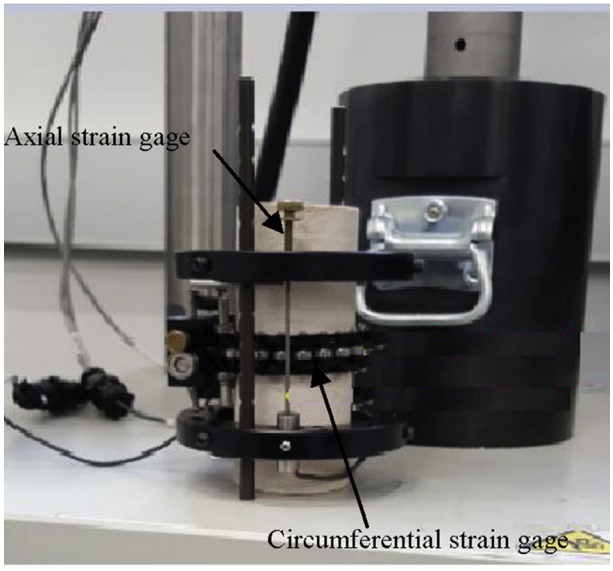

(b)

Fig. 4. (a) Machine set-up and (b) LVDTs configuration to measure the axial and radial deformations.

3 MPa, 5 MPa and 6 MPa, failed at 39.47 MPa, 38.03 MPa and 35.69 MPa, respectively. The greater the loading amplitude, the lower the fatigue strength. The regular-size granodiorite specimens G-R-5, G-R-6 and G-R-7 failed at 85.09 MPa, 102.4 MPa and 93.11 MPa, respectively (Fig. 7c). The small-size granodiorite specimens (G-S-6 and G-S-7), as illustrated in Fig. 7d, failed at 83.33 MPa and 79.4 MPa, respectively. These two specimens failed at the first step of SCL even though it was planned to load them under different stress levels during the fatigue process. The results are explained in detail in the following sections.

Table 1
Average UCS of small- and regular-size granodiorite and sandstone specimens.

Rock type	Specimen No.[a]	UCS (MPa)	Average UCS (MPa)
Sandstone	St.-R-1	35.6	36.2
	St.-R-2	35.3	
	St.-R-3	37.6	
	St.-S-1	43.76	44
	St.-S-2	52.11[b]	
	St.-S-3	45.21	
	St.-S-4	42.95	
Granodiorite	G-R-1	116.71	120
	G-R-2	123.25	
	G-S-1	86.7	105.1
	G-S-2	103	
	G-S-3	124.6	
	G-S-4	103.3	
	G-S-5	107.7	

[a] St.: sandstone; G: granodiorite; R: regular-size specimen; S: small-size specimen.
[b] This specimen was not considered in the calculation of average UCS, since its strength seems to be quite different from the approximate strength values obtained for the three specimens.

3.1. Effect of maximum stress level

The analysis of fatigue behavior of specimens as well as strength characteristics under various maximum stress levels has been carried out. In Table 2, the maximum stress levels were inadequate to influence the fatigue behavior of some rock specimens, either for granodiorite or sandstone.

As can be found in Table 2, the sandstone specimens St.-R-4 and St.-R-9 did not fail even after a large number of cycles when they

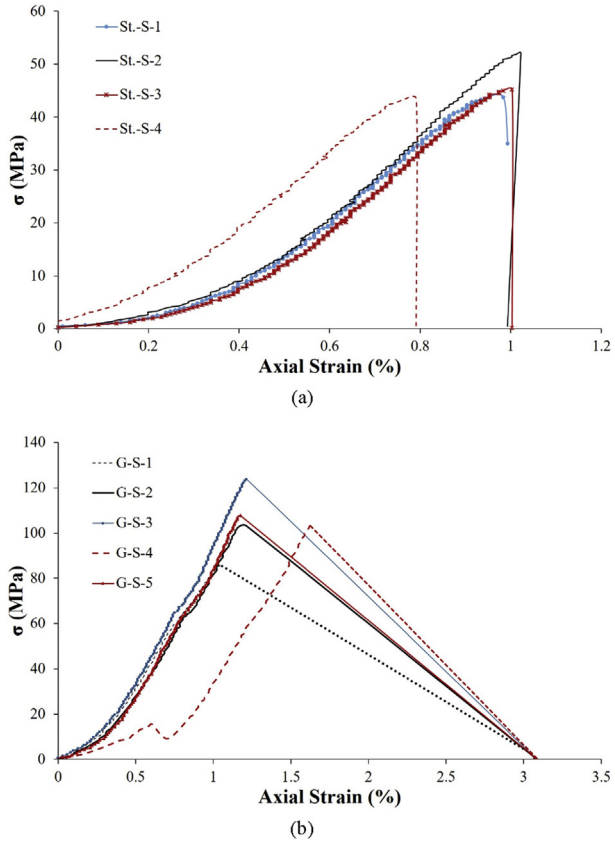

Fig. 5. Stress–strain curves for monotonic uniaxial compression tests conducted on small-size (a) sandstone and (b) granodiorite specimens.

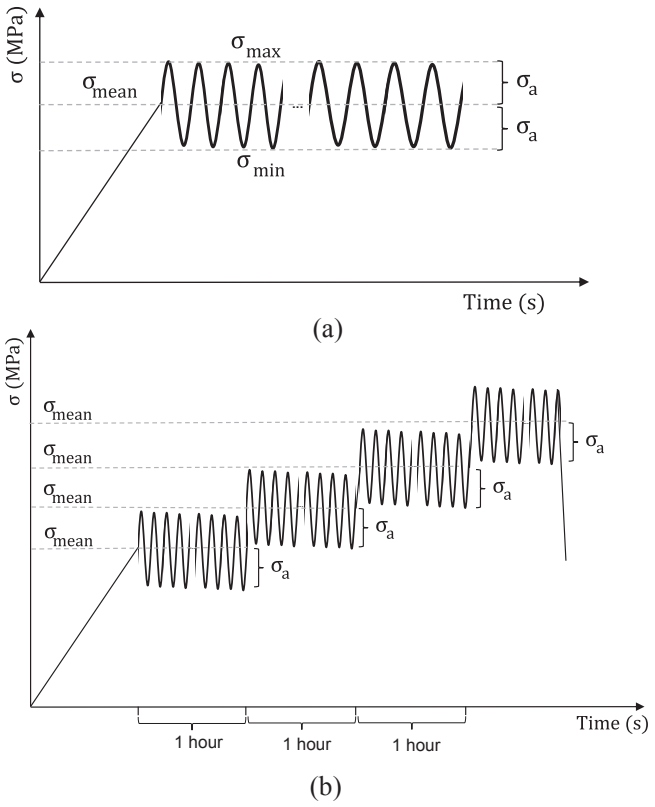

Fig. 6. Schematic illustration of cyclic loading path with (a) CCL and (b) SCL.

were loaded under the maximum stress levels of 30 MPa (83.3% of UCS) and 32 MPa (88.8% of UCS), respectively. This was also observed during the cyclic tests on small-size sandstone specimens, St.-S-5 and St.-S-6, under the maximum stress levels of 85.2% of UCS (37.5 MPa) during the first step of SCL path. As the maximum stress level exceeded 90% of UCS, all sandstone specimens failed and fatigue life decreased as well. The specimens St.-S-5 and St.-S-6, as can be seen in Table 2, yielded when the applied maximum stress level increased to 91% of UCS (40 MPa) during the second step of SCL. The effect of the maximum stress level on strength degradation of specimens St.-R-5 and St.-R-8 was more noticeable. They failed just after 65 cycles and 71 cycles (shorter fatigue life), respectively, since they were loaded under a higher maximum stress level of 94.4% of UCS (34 MPa).

Comparing the results of specimens St.-R-4 and St.-S-6 with that of St.-R-5, under the same loading amplitude of 5 MPa, it can be seen that the fatigue life of specimens decreased as the maximum stress level increased. The specimen St.-R-5 failed after 65 cycles under a maximum stress level of 34 MPa (94.4% of UCS), whereas both specimens St.-R-4 and St.-S-6 did not fail under the maximum stress of 83.3% and 85.2% of UCS, respectively, even after a large number of cycles.

A similar result was also obtained for granodiorite specimens. Specimens G-R-3 and G-R-4 did not fail after 1 h (about 3600 cycles) and 2 h (about 7200 cycles) of loading under the maximum stress levels of 90 MPa (75% of UCS) and 94 MPa (78.3% of UCS), respectively, however, they failed when the maximum stress levels increased to 82.5% and 88.3% of UCS (results of G-R-5 and G-R-6), respectively. The fatigue life and strength (σ_f) of specimen G-S-7 under a maximum stress level of 85 MPa (81% of UCS) were compared with those of G-R-5 and G-R-6 under higher maximum stress levels of 99 MPa and 106 MPa (82.5% and 88.3% of UCS), respectively. It was found that the loading history had a great effect on cyclic response even though the loading amplitude was equal to 10 MPa for all specimens. Since G-R-5 and G-R-6 failed under a larger number of cycles compared to G-S-7, the strain-hardening behavior is clear, because they have already been loaded under cyclic conditions and experienced the fatigue process. As can be seen, specimen G-R-6, which had already been loaded under the maximum stress level of 78.3% of UCS, failed after 217 cycles, while specimen G-R-5, which had already experienced loading under a maximum stress level of 75% of UCS, failed after 313 cycles. Thus it can be stated that when a rock experienced a higher loading level at previous loading stages, yet less than the fatigue stress threshold, a shorter fatigue life would be resulted in.

A similar finding was also reported by other researchers. According to Singh (1989) and Momeni et al. (2015), the rock material tends to fail at a low number of cycles and has a shorter fatigue life as the maximum stress level increases (Fig. 8). As can be seen in Fig. 8, when the maximum stress level exceeded 90% of monotonic compressive strengths of granodiorite and graywacke, they failed at a number of cycles less than 200. Whereas when the graywacke, for instance, was loaded at 88% of UCS, it sustained more than 6000 cycles. It can be concluded that every rock material has a strength threshold, named as fatigue strength, and the rock fails at a low

Table 2
Experimental scheme of uniaxial compression cyclic tests for both granodiorite and sandstone specimens.

Rock type	Specimen No.	Loading type	σ_{min} (MPa)	σ_{mean} (MPa)	σ_{max} (MPa)	σ_{max}/UCS (%)	σ_a (MPa)	σ_f (MPa)	σ_f/UCS (%)	Number of cycles	Remarks
Sandstone	St.-R-4	CCL	20	25	30	83.3	5				Not failed after 2 h
	St.-R-5		24	29	34	94.4	5	30.92	85.9	65	
	St.-R-6		26	29	32	88.8	3	30.89	85.8	12	
	St.-R-7		18	26	34	94.4	8				Failed before cyclic loading starts
	St.-R-8		18	26	34	94.4	8	32.84	91	71	
	St.-R-9		20	26	32	88.8	6				Not failed after 2 h
	St.-R-10		24	29	35	97.2	6	33.84	94	449	Continued on specimen St.-R-9
	St.S-5	SCL	31.5	34.5	37.5	85.2	3	39.47	89.7	2153	Failed on the second step
	St.-S-6		27.5	32.5	37.5	85.2	5	38.03	86.4	1930	Failed on the second step
	St.S-7		25.5	31.5	37.5	85.2	6	35.69	81.1	470	Failed on the first step
Granodiorite	G-R-3	CCL	80	85	90	75	5				Not failed after 1 h
	G-R-4		84	89	94	78.3	5				Not failed after 2 h
	G-R-5		79	89	99	82.5	10	85.09	71	331	Continued on specimen G-R-3
	G-R-6		86	96	106	88.3	10	102.4	85.3	217	Continued on specimen G-R-4
	G-R-7		81.5	89	96.5	80.41	7.5	93.11	77.6	7	
	G-S-6	SCL	70	77.5	85	81	7.5	83.33	79.3	9	Failed on the first step
	G-S-7		65	75	85	81	10	79.4	75.6	191	Failed on the first step

Note: σ_f is the fatigue strength.

Table 3
Detail of loading path for specimens loaded under SCL tests.

Rock type	Specimen No.	Step	σ_{mean} (MPa)	σ_a (MPa)	Loading sequence
Sandstone	St.S-5	1	34.5	3	Loading for 30 min. If no failure, increase mean stress to 37 MPa
		2	37		Loading for 30 min. If no failure, increase mean stress to 39 MPa
		3	39		Loading for 30 min. If no failure, increase mean stress to 41 MPa
		4	41		Loading for 30 min. If no failure, stop test
	St.S-6	1	32.5	5	Loading for 30 min. If no failure, increase mean stress to 35 MPa
		2	35		Loading for 30 min. If no failure, increase mean stress to 37 MPa
		3	37		Loading for 30 min. If no failure, increase mean stress to 39 MPa
		4	39		Loading for 30 min. If no failure, stop test
	St.-S-7	1	31.5	6	Loading for 30 min. If no failure, increase mean stress to 34 MPa
		2	34		Loading for 30 min. If no failure, increase mean stress to 36 MPa
		3	36		Loading for 30 min. If no failure, increase mean stress to 38 MPa
		4	38		Loading for 30 min. If no failure, stop test
Granodiorite	G-S-6	1	77.5	7.5	Loading for 1 h. If no failure, increase mean stress to 82.5 MPa
		2	82.5		Loading for 1 h. If no failure, increase mean stress to 87.5 MPa
		3	87.5		Loading for 1 h. If no failure, increase mean stress to 92.5 MPa
		4	92.5		Loading for 1 h. If no failure, increase mean stress to 122.5 MPa
		5	112.5		Loading for 1 h. If no failure, stop the test
	G-S-7	1	75	10	Loading for 1 h. If no failure, increase mean stress to 80 MPa
		2	80		Loading for 1 h. If no failure, increase mean stress to 85 MPa
		3	85		Loading for 1 h. If no failure, increase mean stress to 90 MPa
		4	90		Loading for 1 h. If no failure, increase mean stress to 110 MPa
		5	110		Loading for 1 h. If no failure, stop the test

number of cycles when the maximum stress level is more than this threshold, if other testing conditions remain constant. Thus the maximum applied stress level is of great importance in assessing the mechanical parameters of rock and design of any structure which will be operated under a cyclic loading condition.

3.2. Effect of loading amplitude

Amplitude is a key factor when analyzing the cyclic loading, as it is an indicator of how much the maximum and minimum stresses vary from the mean stress and it also determines the values

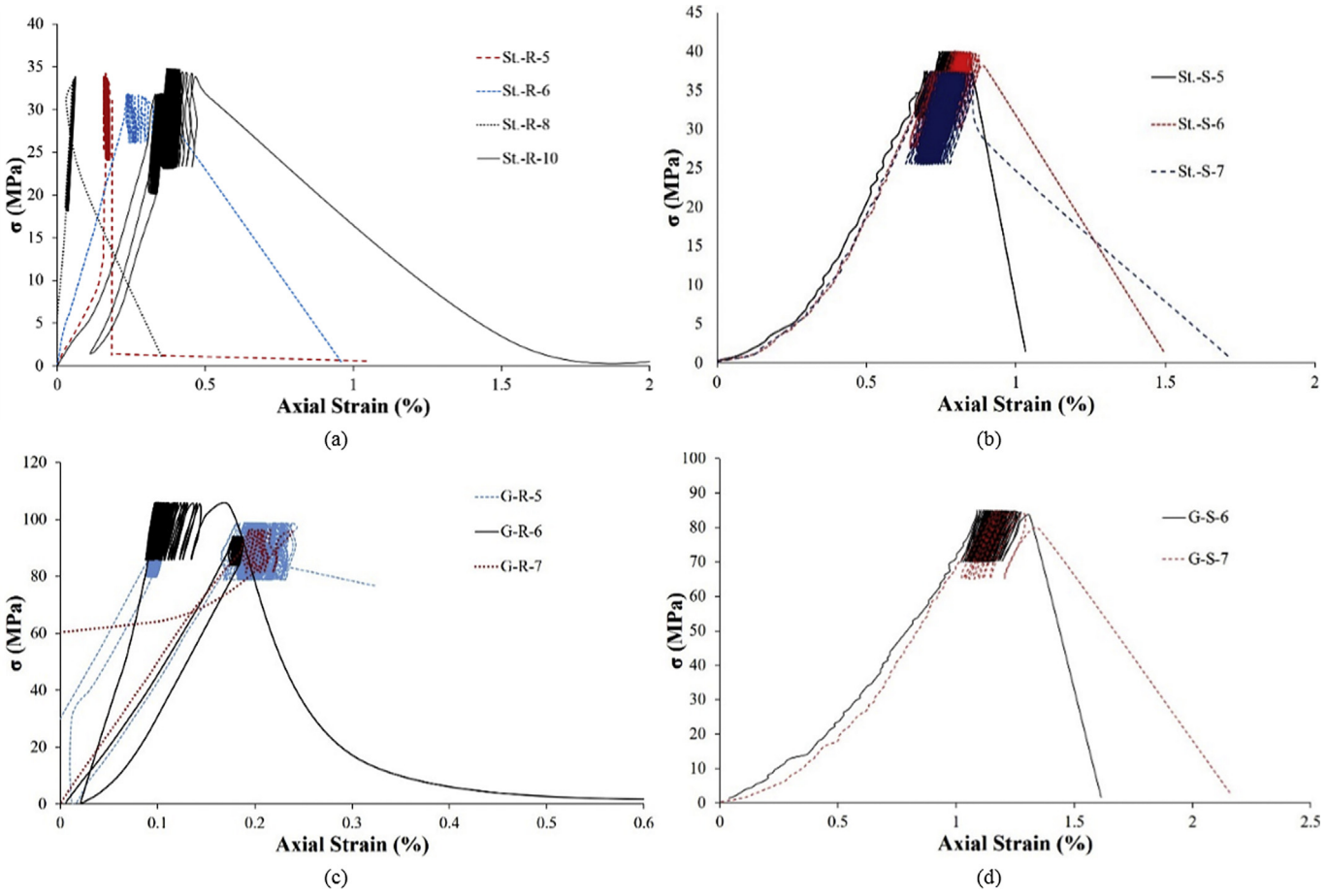

Fig. 7. Stress–strain curves for uniaxial cyclic tests conducted on (a) regular- and (b) small-size sandstone specimens, and (c) regular- and (d) small-size granodiorite specimens.

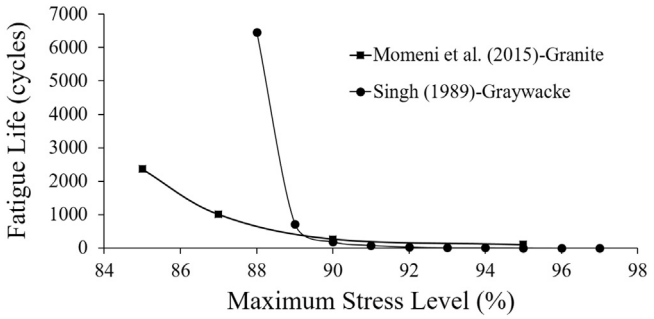

Fig. 8. Effect of the maximum stress level on fatigue life of granodiorite and graywacke. Data obtained from Singh (1989) and Momeni et al. (2015) under loading frequency of 1 Hz.

expected for the maximum stress reached. Even with a slightly lower initial loading stress, the specimens subjected to higher magnitudes of amplitude failed sooner than those under low amplitudes.

Comparing the fatigue life and strength of small-size sandstone specimens, St.-S-5 and St.-S-6, under the same maximum stress level, it is clear that the fatigue life and strength of sandstone decreased as the loading amplitude increased from 3 MPa to 5 MPa. Specimen St.-S-5 with loading amplitude of 3 MPa failed after 2153 cycles during the second stage of SCL when the maximum stress level was 40 MPa. Specimen St.-S-6, whereas, with loading amplitude of 5 MPa, failed after 1930 cycles during the second stage of SCL when the maximum stress level was 40 MPa. The fatigue strength of specimen St.-S-6 loaded under a higher loading amplitude was 38.03 MPa (86.4% of UCS), lower than that of specimen St.-S-5, which was 39.47 MPa (89.7% of UCS).

Comparing the fatigue life and strength of specimen St.-S-7 with those of specimens St.-S-5 and St.-S-6, it suggests that the effect of loading amplitude is stronger than that of the maximum stress level. Specimen St.-S-7 loaded under a maximum stress level of 85.2% of UCS with higher loading amplitude of 6 MPa failed during the first step of SCL, after just 470 cycles (shorter fatigue life) and lower fatigue stress (81.1% of UCS) compared to St.-S-5 and St.-S-6 that did not fail during the first step (at the same maximum stress level of 85.2% of UCS). These two specimens failed during the second stage when the maximum stress level increased to 91% of UCS. Thus it can be concluded that the rock would more easily yield at a lower maximum stress level with higher loading amplitude than at a high maximum stress level with low loading amplitude. This finding, however, needs to be validated by more experimental data. The importance of loading amplitude has also been stated by Attewell and Farmer (1973) when they compared the cyclic response of rocks under different loading amplitudes and frequencies. They believed that failure of rock occurs more easily at low-frequency dynamic stress with higher amplitude than at high-frequency dynamic stress with low loading amplitude.

As can be found in Table 2, if the fatigue strengths of granodiorite specimens G-S-6 and G-S-7 are compared, the fatigue strength of G-S-6 with loading amplitude of 7.5 MPa was 83.33 MPa (79.3% of UCS) compared to that of 79.4 MPa (75.6% of UCS) for G-S-7 with higher loading amplitude of 10 MPa.

The effect of loading amplitude on fatigue life was also reported by Singh (1989), He et al. (2016) and Taheri et al. (2016). The more the loading amplitude, the shorter the fatigue life. As shown in Fig. 9, the graywacke specimens sustained 10,189 cycles under loading amplitude of 50 MPa, while they failed at 287 cycles when the loading amplitude increased to 83 MPa (Singh, 1989). As illustrated in this figure, this trend was also reported by He et al. (2016) and Taheri et al. (2016) for their tested sandstone specimens. The sandstone specimens were loaded more than 100 cycles under loading amplitude of 40 MPa, whereas they failed just after 2 cycles as the loading amplitude increased to 47 MPa (Taheri et al., 2016). The sandstone specimens tested by He et al. (2016) showed a similar result. Specimens sustained loading up to 233 cycles when the loading amplitude was less than 10 MPa, while they failed after 20 cycles when the loading amplitude was more than 60 cycles.

3.3. Fatigue strength

The fatigue strength of the tested rocks can be determined from the results discussed above. As previously mentioned, each type of rock has a strength threshold at which it can sustain loading under a large number of cycles if the loading level is less than this threshold. According to Table 2 and based on the discussion in previous sections, the fatigue strengths of sandstone and granodiorite specimens can be taken as 90% and 80% of their UCS values, respectively. Thus the fatigue strengths of regular- and small-size sandstone specimens are 32 MPa and 40 MPa, respectively. These amounts were found equal to be 96 MPa and 85 MPa for regular- and small-size granodiorite, respectively.

Based on the fatigue strengths of sandstone and granodiorite, it can be concluded that the fatigue strength of hard rocks is relatively lower than that of soft rocks. Thus the brittle rocks are more prone to be weakened under cyclic loading than ductile rocks. The more brittle the rock, the more the strength degradation, and the less the fatigue strength.

3.4. Failure modes of the tested rock specimens

Damage mechanism was always an interesting topic to figure out how solid materials fail by fracturing and cracking. Identifying crack development through laboratory tests would improve our understanding of the real failure process in practice (Eberhardt, 1998). The failure modes of the tested sandstone and granodiorite specimens are presented in Fig. 10. As can be seen in this figure, there were more fractured planes observed on both sandstone and granodiorite specimens after cyclic loading compared to static loading tests. The main shearing plane (named 1) is accompanied by axial tensile cracks (named 2) for both specimens under cyclic loading. More tensile splitting cracks were observed under a cyclic loading condition. Since the granodiorite rock is more brittle, there was more powder on the fracture planes after the cyclic tests, which is an indication of fatigue failure. This pattern was also observed by Wang et al. (2013). Similar failure modes for sandstone specimens under triaxial monotonic and cyclic tests were also reported by Liu et al. (2011, 2012) and Yang et al. (2015).

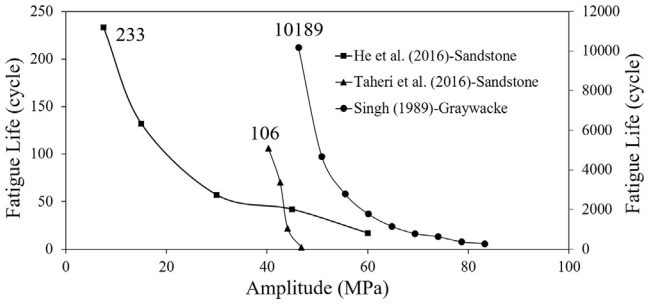

Fig. 9. Effect of loading amplitude on fatigue life of rock material under cyclic loading. Data obtained from Singh (1989), He et al. (2016) and Taheri et al. (2016).

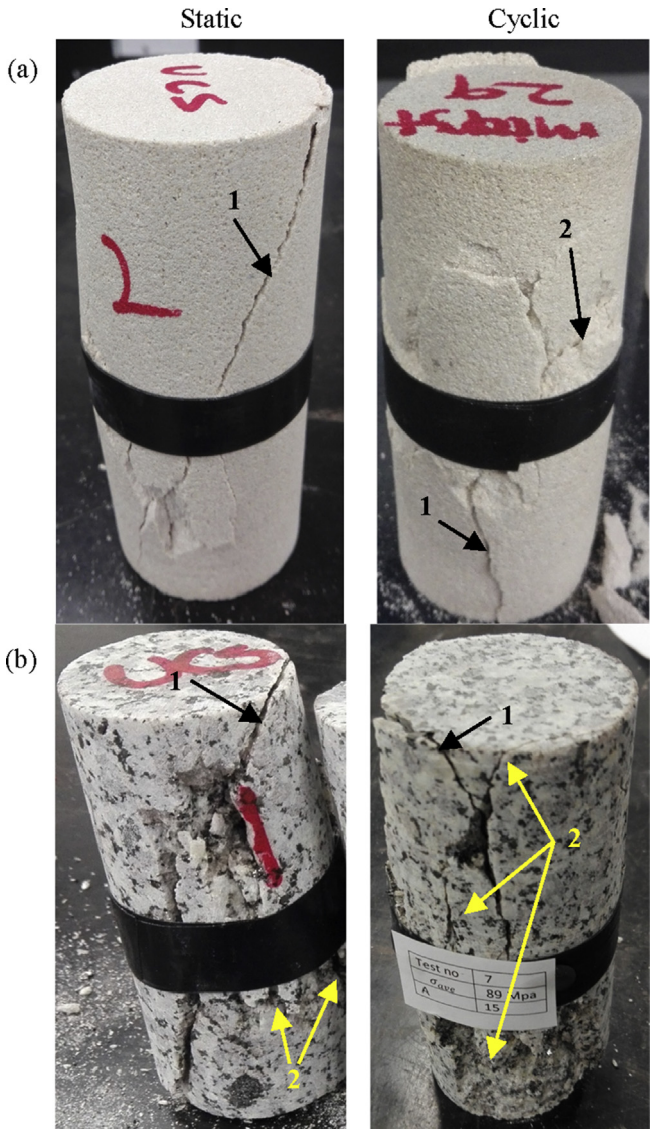

Fig. 10. Failure modes of tested (a) sandstone and (b) granodiorite specimens under static and cyclic loadings. Cracks named 1 are shearing cracks and the ones named 2 are axial tensile cracks.

3.5. Rock nonhomogeneity and response to cyclic loadings

During laboratory testing of granodiorite and sandstone specimens subjected to uniaxial cyclic loadings, there were some disparities observed in the fatigue failure of rock specimens. Some specimens developed immediate failure and premature yielding though the loading amplitude was minimal and the maximum stresses were not significantly high. However, a few specimens have shown no yielding or axial strain and lateral strain as a result of dynamic deformation failure. One significant observation noted is that fatigue characteristics are dependent on geological condition, in situ stress and depth of core extraction as well as chemical composition of the rock microstructure formation. The unlikely variability in cyclic failure is an obvious heterogeneity of the rock specimens due to changes in in situ stress distribution, which might have altered the mechanical properties of the intact rock, i.e. strength, deformability and especially permeability initiated due to development of network of stress relief cracks. These conditions could have created stress corrosion phenomena and plenty of weakening mechanical actions, i.e. weak strain bonds around the crack tips thus facilitating crack propagation at lower stress levels.

Moreover, the perceived nonhomogeneity is a result of micro-scale heterogeneity of the rock specimens. It is believed that the presence of microstructures has created an additional dimension on the nonhomogeneous specimen. There is room for expansion of one or more individual micro-fractures into cleavage fractures (splitting/extension mode) and a dramatic drop of load-bearing capacity to abrupt failure.

4. Conclusions

The main objectives for this study were to investigate the effects of loading amplitude and stress on the mechanical properties of sandstone and granodiorite and to understand how the cyclic response differs from soft rock of sandstone to hard rock of granodiorite. From the conducted tests and obtained results, the following conclusions were drawn:

(1) The increasing mean stress level tests (SCL path) provides a decent way to not only explore the effect of the maximum stress level and loading amplitude on cyclic response of rocks but also to investigate the effect of loading history on their fatigue behavior.
(2) The fatigue life decreased with an increase in the maximum stress level if the cyclic loading amplitude remained constant.
(3) The decreases in the fatigue life and strength were evident with increasing loading amplitude.
(4) The effect of loading amplitude is stronger than that of the maximum stress level. The rock would more easily yield at a lower maximum stress level with higher loading amplitude than at high maximum stress level with lower loading amplitude.
(5) The fatigue strength of hard/brittle rocks seems to be less than that of soft/ductile rocks. The more brittle the rock, the more the strength degradation, and the less the fatigue strength.
(6) It is observed that more local cracks are formed after cyclic loading tests compared to static loading tests.

Further experimental work, however, is required to be carried out to validate that the loading amplitude has more cyclic effect than the maximum stress level. Different rock types are suggested to be tested under cyclic loading to precisely explore the difference between fatigue response of hard rocks and soft rocks. It would also be interesting to assess the effects of rock fabric and its heterogeneity on the fatigue response.

Conflicts of interest

The authors wish to confirm that there are no known conflicts of interest associated with this publication and there has been no significant financial support for this work that could have influenced its outcome.

Acknowledgments

We would like to express our sincere gratitude to Department of Mining Engineering and Metallurgical Engineering of Western Australian School of Mines (WASM), Curtin University for the provided laboratory equipment at Geomechanics Laboratory, Mining Research Institute of Western Australia (MRIWA) for the financial support and also special appreciation to Dr. Takahiro Funatsu for his technical support to undertake the laboratory tests.

References

Attewell PB, Farmer IW. Fatigue behaviour of rock. International Journal of Rock Mechanics and Mining Sciences & Geomechanics Abstracts 1973;10(1):1–9.

Bagde MN, Petroš V. Fatigue properties of intact sandstone samples subjected to dynamic uniaxial cyclical loading. International Journal of Rock Mechanics and Mining Sciences 2005a;42(2):237–50.

Bagde MN, Petroš V. The effect of machine behaviour and mechanical properties of intact sandstone under static and dynamic uniaxial cyclic loading. Rock Mechanics and Rock Engineering 2005b;38(1):59–67.

Bagde MN, Petroš V. Waveform effect on fatigue properties of intact sandstone in uniaxial cyclical loading. Rock Mechanics and Rock Engineering 2005c;38(3):169–96.

Bagde MN, Petroš V. Fatigue and dynamic energy behaviour of rock subjected to cyclical loading. International Journal of Rock Mechanics and Mining Sciences 2009;46(1):200–9.

Bastian T, Connelly B, Lazo Olivares C, Yfantidis N, Taheri A. Progressive damage of Hawkesbury sandstone subjected to systematic cyclic loading. Journal of Research Projects Review 2014;3(1):7–14.

Burdine NT. Rock failure under dynamic loading conditions. Society of Petroleum Engineers Journal 1963;3(1). https://doi.org/10.2118/481-PA.

Eberhardt E. Brittle rock fracture and progressive damage in uniaxial compression. PhD Thesis. Saskatoon, Canada: University of Saskatchewan; 1998.

Eberhardt E, Stead D, Stimpson B, Read RS. Identifying crack initiation and propagation thresholds in brittle rock. Canadian Geotechnical Journal 1998;35(2):222–33.

Ghazvinian E. Fracture initiation and propagation in low porosity crystalline rocks: implications for excavation damage zone (EDZ) mechanics. PhD Thesis. Kingston, Ontario, Canada: Queen's University; 2015.

Gong M, Smith I. Effect of waveform and loading sequence on low-cycle compressive fatigue life of spruce. Journal of Materials in Civil Engineering 2003;15(1):93–9.

He MM, Li N, Chen YS, Zhu CH. Strength and fatigue properties of sandstone under dynamic cyclic loading. Shock and Vibration 2016. https://doi.org/10.1155/2016/9458582.

Liu EL, He SM, Xue XH, Xu J. Dynamic properties of intact rock samples subjected to cyclic loading under confining pressure conditions. Rock Mechanics and Rock Engineering 2011;44(5):629–34.

Liu EL, Huang RQ, He SM. Effects of frequency on the dynamic properties of intact rock samples subjected to cyclic loading under confining pressure conditions. Rock Mechanics and Rock Engineering 2012;45(1):89–102.

Momeni A, Karakus M, Khanlari GR, Heidari M. Effects of cyclic loading on the mechanical properties of a granite. International Journal of Rock Mechanics and Mining Sciences 2015;77:89–96.

Prost GL. Jointing at rock contacts in cyclic loading. International Journal of Rock Mechanics and Mining Sciences & Geomechanics Abstracts 1988;25(5):263–72.

Ray SK, Sarkar M, Singh TN. Effect of cyclic loading and strain rate on the mechanical behaviour of sandstone. International Journal of Rock Mechanics and Mining Sciences 1999;36(4):543–9.

Singh SK. Fatigue and strain hardening behaviour of graywacke from the flagstaff formation, New South Wales. Engineering Geology 1989;26(2):171–9.

Taheri A, Yfantidis N, Olivares C, Connelly B, Bastian T. Experimental study on degradation of mechanical properties of sandstone under different cyclic loadings. Geotechnical Testing Journal 2016;39(4):673–87.

Tao ZY, Mo HH. An experimental study and analysis of the behaviour of rock under cyclic loading. International Journal of Rock Mechanics and Mining Sciences & Geomechanics Abstracts 1990;27(1):51–6.

Wang Z, Li S, Qiao L, Zhao J. Fatigue behavior of granite subjected to cyclic loading under triaxial compression condition. Rock Mechanics and Rock Engineering 2013;46(6):1603–15.

Xiao JQ, Ding DX, Jiang FL, Xu G. Fatigue damage variable and evolution of rock subjected to cyclic loading. International Journal of Rock Mechanics and Mining Sciences 2010;47(3):461–8.

Xiao JQ, Ding DX, Xu G, Jiang FL. Waveform effect on quasi-dynamic loading condition and the mechanical properties of brittle materials. International Journal of Rock Mechanics and Mining Sciences 2008;45(4):621–6.

Xiao JQ, Ding DX, Xu G, Jiang FL. Inverted S-shaped model for nonlinear fatigue damage of rock. International Journal of Rock Mechanics and Mining Sciences 2009;46(3):643–8.

Yang SQ, Ranjith PG, Huang YH, Yin PF, Jing HW, Gui YL, Yu QL. Experimental investigation on mechanical damage characteristics of sandstone under triaxial cyclic loading. Geophysical Journal International 2015;201(2):662–82.

Every reasonable effort has been made to acknowledge the owners of copyright material. I would be pleased to hear from any copyright owner who has been omitted or incorrectly acknowledged.